# INFORMATION TO USERS

This manuscript has been reproduced from the microfilm master. UMI films the text directly from the original or copy submitted. Thus, some thesis and dissertation copies are in typewriter face, while others may be from any type of computer printer.

The quality of this reproduction is dependent upon the quality of the copy submitted. Broken or indistinct print, colored or poor quality illustrations and photographs, print bleedthrough, substandard margins, and improper alignment can adversely affect reproduction.

In the unlikely event that the author did not send UMI a complete manuscript and there are missing pages, these will be noted. Also, if unauthorized copyright material had to be removed, a note will indicate the deletion.

Oversize materials (e.g., maps, drawings, charts) are reproduced by sectioning the original, beginning at the upper left-hand corner and continuing from left to right in equal sections with small overlaps. Each original is also photographed in one exposure and is included in reduced form at the back of the book.

Photographs included in the original manuscript have been reproduced xerographically in this copy. Higher quality 6" x 9" black and white photographic prints are available for any photographs or illustrations appearing in this copy for an additional charge. Contact UMI directly to order.

UMI

A Bell & Howell Information Company
300 North Zeeb Road, Ann Arbor, MI 48106-1346 USA
313/761-4700 800/521-0600

# STUDIES OF FORCED-DISSIPATIVE TURBULENCE IN MODEL HYDRODYNAMICS

ALEXEI V. CHEKHLOV

A DISSERTATION
PRESENTED TO THE FACULTY
OF PRINCETON UNIVERSITY
IN CANDIDACY FOR THE DEGREE
OF DOCTOR OF PHILOSOPHY

RECOMMENDED FOR ACCEPTANCE
BY THE PROGRAM IN
APPLIED AND COMPUTATIONAL MATHEMATICS

MAY, 1995

You have attained the age of reason, Mathiew, you have attained the age of reason, or you ought to have done so...

*Jean-Paul Sartre*, "The Age of Reason"

# ABSTRACT

This thesis focuses upon the large-scale and long-time statistical properties of several forced-dissipative fluid dynamical systems, including: (i) the one-dimensional Burgers equation, (ii) a model one-dimensional equation without Galilean invariance, and the two-dimensional Navier-Stokes system with (vi) and without (iii) effects of differential rotation in the $\beta$-plane approximation. It is shown that a certain large-scale forcing in the Burgers equation results in statistical properties which are remarkably close to those of three-dimensional fully developed turbulence. The corresponding probability distribution function of velocity differences possesses nontrivial algebraic tails due to the effects of shock waves, thus leading to a biscaling behavior of the velocity structure functions. A phenomenological theory describing the experimental findings is proposed. Experimental results are compared with predictions of the one-loop renormalized perturbation expansion. It is demonstrated that cubic nonlinearity in a one-dimensional Burgers-like system which violates Galilean invariance allows efficient analytical treatment using the Renormalization Group (RG) and the $\epsilon$-expansion methods, unlike its Burgers counterpart. The corresponding fixed-point critical behavior is studied in detail using a finite-step RG transformation. For the two-dimensional Navier-Stokes system, it is shown that a two-parametric eddy viscosity in the inverse energy transfer regime is in excellent agreement with predictions based upon the RG theory, as well as other closure models. This result yields a new strategy of large-eddy simulation of two-dimensional turbulent flows which was successfully tested in a wide range of flow parameters. Effects of differential rotation are shown to strongly alter the large-scale properties of forced two-dimensional turbulence. The directional energy spectrum at very long times is found to be essentially anisotropic with two scaling laws; one similar to Kolmogorov $k^{-5/3}$-law and the other – to Rhines $k^{-5}$-law. Practical applications of our results are discussed.

# Contents

# List of Figures

# Preface

This thesis is composed of a collection of results obtained for several simplified problems which may be referred to as *fluid turbulence models*. Some of them are as "simple" as Burgers equation, others are more complicated and, hopefully, more realistic in describing real-life turbulence properties. Among the main tools of this study is numerical computation, which otherwise may be called *direct numerical simulation* (DNS) of the equations of motions involved. One of the major theoretical tools employed is the *dynamic renormalization group* theory (RG) coupled with the $\epsilon$-*expansion*, by analogy with similar methods used in the theory of critical phenomena. In some places, to fill in gaps between subjects, we will use other theoretical tools borrowed from classical and geophysical fluid dynamics, statistical physics, kinetic theory, probability theory and others. Our style of convincing the reader will remain at a physical level of rigor throughout the thesis, as is normally done in the physical turbulence literature. In most cases, the validity of important conclusions is verified via comparison of their consequences with the results of DNS. Our general goal or, philosophically, what we mean by solving a problem, is to find the *large-scale, long-time statistical behavior* of the considered forced-dissipative system. The models include different types of nonlinearity, scalings of the force, numbers of spatial dimensions, effects of differential rotation. More specifically, the following models are considered:

- One-dimensional forced-dissipative Burgers equation;
- One-dimensional forced-dissipative equation which does not possess Galilean invariance and with cubic nonlinearity of the mKdV-type;

- Two-dimensional forced-dissipative Navier-Stokes equation;
- Two-dimensional forced-dissipative Navier-Stokes equation with effects of differential rotation in the $\beta$-plane approximation;

The original results we obtain here can be briefly outlined as follows:

1. It is shown that solutions to the one-dimensional forced-dissipative Burgers equation may display properties close to Kolmogorov turbulence, in contrast to what was believed previously. For negative velocity gradients it is found that the probability distribution functions have algebraic tails, leading to nontrivial biscaling behavior of velocity structure functions.

2. Near-equilibrium statistical properties of a cubically nonlinear Galilean noninvariant equation of the mKdV-type are studied using finite-step dynamic RG theory and the $\epsilon$-expansion. It is found that the system displays a phase transition at the thermal equilibrium point from Gaussian to non-Gaussian behavior.

3. For the isotropic Navier-Stokes equations, it is shown that a two-parametric eddy viscosity, first introduced by R. Kraichnan, accurately describes results of DNS and agrees well with the corresponding predictions based on RG theory.

4. For the case of $\beta$-plane turbulence the shape of the anisotropic, differential rotation-induced energy spectrum is not limited to the $k \geq k_\beta$ region, as was previously believed. Effects of $\beta$ appear across Fourier-space and for $k < k_\beta$ the energy spectrum has a two-slope form, with Rhines $k^{-5}$ scaling along the $\pm\pi/2$-directions and Kolmogorov $k^{-5/3}$ scaling in other directions.

5. On the basis of result 3 above, a *large eddy simulation* (LES) strategy is proposed for the two-dimensional Navier-Stokes equations and successfully tested across a wide range of parameters.

Some of these results are included in the publications [11, 12, 9, 10, 24, 83].

This thesis does not claim to provide a complete treatment of the problems discussed and the results presented here in most cases should be followed by a more

thorough analysis, especially for the case of result (1) above and applications for the case of result (4) above. In fact, results contained in [11, 12] have stimulated more deep theoretical studies of the proposed problem by other research groups, which hopefully will lead to some fruitful collaboration. Also, the LES strategy proposed in [83] may be followed by applications to *global circulation geophysical models* of the ocean and atmosphere. Investigation of the cutoff-dependent eddy viscosities [9, 83] for more complicated problems than isotropic ones, e.g., problems which include effects of differential rotation, is also very promising.

The work presented in this thesis was done during the period 1993–1995 while the author had the honor to be a post-general graduate student in the Program in Applied and Computational Mathematics at Princeton University under the supervision of Prof. S. A. Orszag. Steve was the one who actually gave me the opportunity to continue my education and pursue a scientific career, for which I am deeply in debt to him. It is also a great pleasure to acknowledge assistance from different persons with whom I interacted closely while working. Among them are Victor Yakhot, Ilya Staroselsky, Semion Sukoriansky and Boris Galperin. Scientific collaboration with these persons eventually has led to personal friendships the importance of which is hard to overestimate. My wholehearted thanks to them and all others who have helped me in establishing as a scientist.

Also I wish to acknowledge stimulating discussions with V. Yakhot, A. Migdal, and Ya. Sinai of the material contained in Chapter 1. For the results contained in Chapter 3, I would like to thank E. Jackson for his valuable help with some programming issues and R. Kraichnan, who kindly provided his original numerical data for the two-parametric eddy viscosity.

Special thanks are due to B. Galperin and Department of Marine Sciences of the University of South Florida for inviting me to be their guest in December, 1994. Mexico Bay shore was a very nice place to work in the middle of winter.

Going back in time, I would like to extend my sincere gratitude and respect to Prof. N. A. Inogamov from the Landau Institute for Theoretical Physics, who convinced me at the proper time how beautiful and exciting physics, and, particularly, fluid

dynamics, may be. It was my very good luck to meet him while I was looking for an undergraduate thesis advisor back in 1987.

I also must mention my parents: my father, Valerii I. Chekhlov, who by his personal example taught me the ability to think, one of the best human qualities; and my mother, Liudmila V. Chekhlova, who gave me so much of herself at all times. Without such parents, being frank to myself, I would have never achieved anything substantial in life.

Finally, I would like to thank Prof. Mark Nelkin from the Physics Department at New York University and Levich Institute, City College of New York, and Prof. Ioannis G. Kevrekidis from the Program in Applied and Computational Mathematics and the Department of Chemical Engineering at Princeton University for being readers of my thesis and for providing many constructive comments regarding the style and scientific content of my work. I would also like to thank Eric Jackson for having so kindly assisted in improving my writing in the preliminary versions of the thesis.

# Chapter 1

# The Forced-Dissipative Burgers Equation

It has long been believed that solutions to Burgers equation are not a good model of hydrodynamic turbulence. For example, J. M. Burgers, in the Introduction to his well-known book [8], wrote:

> It has come forward that the phenomena pictured by the solutions of this equation are far removed from hydrodynamic turbulence. The equation can be considered as referring to motions in an infinitely compressible medium, without pressure, and there is nothing in the system which deals with shear or with vortex motion. Certain correlation problems can be studied and show analogies with correlation problems in hydrodynamic turbulence. But the statistical problems connected with the solutions of the equation refer to features which depend upon the randomness of the initial conditions. It appears that in the limiting case of infinitely small viscosity, the algorithm used in the solution of the equation acts as a kind of 'selector', which transmits certain details of the initial data to the solution, while eliminating other details (...). There is no mechanism for mixing features of the initial data and thereby generating new randomness.

One of the first authors to write extensively on the Burgers equation was Prof. E. Hopf – indeed, in some literature Burgers equation is even called the Burgers-Hopf equation. Prof. Hopf in his paper [30] on the subject wrote:

> We doubt that Burgers equation fully illustrates the statistics of free turbulence. Kolmogoroff's idea about the probability distribution of the turbulent fluctuations in the small is essentially concerned with the velocity differences, not the velocities themselves. Equation (...) is too simple a model to display chance fluctuations of these differences.

This is certainly true about the Cauchy problem for the unforced Burgers equation with random initial data. But this does not mean that the same statements apply to a statistical ensemble of steady-states in the forced-dissipative case.

In this Chapter we will pose and numerically solve a problem which possesses a wide range of properties which are commonly attributed to real-life three-dimensional turbulence. The problem of the forced-dissipative Burgers equation with a power-law force self-correlation function raises a variety of simultaneous issues to be studied. Results for some of them, those involving the greatest theoretical interest, are considered in some detail here. Among them are: a case leading to Kolmogorovian properties of turbulence in one dimension, where the exponent of the force self-correlation function $y = 1$ (for a full definition of $y$, see below); a case with a steeper forcing scaling law, with $y = 3/2$; and a case with large-scale forcing (the limiting case, when the power law degenerates into a $\delta$-function). Experimentation in all these cases is quite "theoretical", because no direct counterparts to these phenomena may be found in real life, and, therefore, no natural experiments are possible. However, there exists a growing theoretical interest in such experiments because, as we will demonstrate below, these systems may and in some cases do show properties very close to those in much more complicated three-dimensional turbulent systems. Numerical experimentation, which is now possible due to the wide availability of powerful computational facilities, should naturally come first in such situations, followed by slower, but, of course, more fundamental and "reliable" theoretical studies. In the case of the problems raised here a variety of theoretical studies in our and other scientific groups

has been initiated. There is a hope that soon the problem considered here will obtain analytical treatment, leading to new understanding of Kolmogorovian properties [34, 35] and intermittency effects for pressure-free turbulence in one and, possibly, even in three dimensions. Although there exist some very important astrophysical applications for Burgers-like systems, it is also hoped that these results will have some impact on real-life fluid turbulence. In this regard, such aspects as the importance of the stirring force and the pressure term in dimensions higher than one still require investigation.

Section 1.1 below, which deals with general properties of Kolmogorov turbulence for Burgers equation, is based on the paper [11]. Section 1.2 describes in more detail the statistical properties of the solution obtained in Section 1.1 through a variety of probability distribution functions. Analytical studies currently in progress [62, 92] (to be published later) use this information extensively. New nontrivial behavior of the probability distribution functions is discovered, which illustrate effects of coherent structures in the turbulent flow. Some of these results are included in [12]. The case of large-scale forcing was to some extent studied in the previous literature and in Section 1.3 we also present some results for this case which are in qualitative agreement with the previous studies. Section 1.4 gives some new results for the case $y = 3/2$ which exemplify the fact that one-loop RG predictions in the finite $\epsilon = 3 + y$ case are not necessarily correct. Finally, Section 1.5 reviews basic qualitative features of the Renormalization Group approach applied to hydrodynamic problems and provides its application to the $d$-dimensional irrotational forced-dissipative Burgers equation.

## 1.1 Kolmogorov Turbulence in the Random-Force-Driven Burgers Equation

From a theoretical viewpoint, one of the most challenging features of strong hydrodynamic turbulence is the interplay between an almost Gaussian random background and coherent ordered structures responsible for deviations from Gaussian statistics. Although coherent structures have been visualized in three-dimensional flows as sheets

or tubes of high vorticity [66], little is known about their analytic structure, stability and, as a consequence, about their relevance to turbulence dynamics. For a recent review of experimental and numerical results in three-dimensional turbulence, see [56]. In two-dimensional systems, the role of coherent structures is much better understood: The flow can be decomposed into two components, a background field having close to Gaussian statistics and coherent, extremely stable point vortices, responsible for strongly non-Gaussian features of the flow [74, 75]. Still, the analytic structure of such vortices and the distributions of their sizes and strengths are not yet understood and this is one of the reasons why a full statistical theory of two-dimensional turbulence does not yet exist.

The analytic properties of the one-dimensional Burgers equation [8, 41, 21]

$$\frac{\partial v}{\partial t} + \frac{1}{2}\frac{\partial v^2}{\partial x} = \nu_0 \frac{\partial^2 v}{\partial x^2}, \tag{1.1}$$

subject to initial and boundary conditions, are understood rather well: the flow is dominated by shocks, leading to an energy spectrum $E(k) \propto k^{-2}$ [8]. The same energy spectrum exponent is obtained on the basis of the so-called $\beta$-model of intermittency, applied to the one-dimensional case [22]. Moreover, in some cases, the Burgers equation has a stationary solution. For example, if $v = -U$ and $v = U$ at $x = \infty$ and $-\infty$ respectively, then $U(x) = -U \tanh[x\,U/(2\,\nu_0)]$, which describes a single shock of width $l \approx \nu_0/U$. In this particular solution, "fluid" particles, created at the boundaries, are carried towards the center of the shock where they disappear. Shock formation is the most significant dynamic property of the Burgers equation; shocks have been studied in systems decaying from specific initial conditions and in systems driven by large-scale random noise [68, 67, 65]. In the latter case, the energy spectrum is $E(k) \propto k^{-2}$ and all velocity structure functions $S_{2n}(r) = \overline{[u(x+r) - u(x)]^{2n}}$ scale as $S_{2n}(r) \propto r^1$, characteristic of the shocks. Some closure studies of this problem may be found, for example, in [37].

A totally different result is found in a system governed by (1.1) driven by a white-in-time random force $f(x,t)$ defined by its correlation function

$$\overline{f(k,\omega)f(k',\omega')} = 2\,(2\pi)^2\, D_0\, k^{-y}\delta(k+k')\delta(\omega+\omega') \tag{1.2}$$

with $y = -2$ corresponding to thermal equilibrium. Here, in the limit $k \to 0$ and $\omega \to 0$ the two-point velocity correlation function is given by

$$C(k,\omega) = \int\int \frac{\overline{v(k,\omega)\, v(k',\omega')}}{2} \frac{d\omega'}{2\pi} \frac{dk'}{2\pi} \propto k^{-\alpha} F(\frac{\omega}{k^z}) \tag{1.3}$$

with $\alpha = z = 3/2$ corresponding to $E(k)$=const. Both the exponents $z$ and $\alpha$ may be evaluated using theories based on one-loop renormalized perturbation expansions [16, 95, 50] and have been confirmed by numerical experiments [95]. Examples of applying the *replica trick* to this problem may be found in [32, 97, 28]. In this case, the small-scale forcing was strong enough to prevent formation of shocks and the $k^{-2}$-energy spectrum. In recent papers [84, 20], it was shown that computation of second loops for the $y = -2$ case does not invalidate the results of the one-loop approximation.

Here we are interested in an intermediate case of a system governed by (1.1) with a forcing function added to the right side defined by the relation (1.2) with $y = 1$. This case is extremely interesting because it corresponds to "almost" constant energy flux $\Pi(k)$ in wavenumber space: $\Pi(k) \propto \log(k/k_0)$, where $k_0$ is the inverse of the largest allowed scale in the system. Since the analytic structure of (1.1) resembles that of the Navier-Stokes equations, the Kolmogorov argument leading to $E(k) \propto k^{-5/3}$ can be applied at least on a superficial level. However, in this case the process of generation of the Kolmogorov spectrum must compete with the natural tendency of the solutions to Burgers equation to form coherent shocks, thus leading to interesting dynamics.

We investigate fluctuations generated by equation (1.1) with a hyperviscous dissipation term $\nu_0 (-1)^{p+1} \partial^{2p} v/\partial x^{2p}$ and driven by a random force $f(x,t)$. Numerical results, shown below, correspond to $p = 6$, which has been chosen empirically to produce a sufficiently sharp ultra-violet energy spectrum fall-off. The effect of the hyperviscous dissipation on solutions of Burgers equation has been studied in a recent paper [6] and we will not dwell upon this issue here. We will just mention that its use is dictated by the desire to have as wide a universal range as possible and is based on the assumption that universal infra-red properties should not depend on the type of dissipation chosen. To simulate (1.2), the random force has been assigned in Fourier space as: $f(k,t) = A_f/\sqrt{\delta t}\ |k|^{-y/2}\ \sigma_k$, where $\sigma_k$ is a Gaussian random

function with $\overline{|\sigma_k|^2} = 1$ and $\delta t$ is the time-step. The force cut-off $k_c$ is chosen well inside the dissipation range of the energy spectrum. In the case $p = 1$ the dissipation scale is, according to the relation given above, $l_d \approx \nu_0/U_0$, where $U_0$ is the velocity of the most energetic shock in the system. The spatial discretization is based on the Fourier-Galerkin pseudospectral method with the nonlinear term computed using the conservative form and a de-aliasing procedure based on the 2/3-rule. The temporal discretization includes two second-order schemes: a Runge-Kutta scheme for restarting and a stiffly-stable Adams-type scheme described in [33] for serial computations. The spectral resolution used is 12288 including the aliased modes. Other parameters are chosen to be: $\nu_0 = 9.0 \times 10^{-40}$, $\delta t = 5.0 \times 10^{-5}$, and $A_f = 1.4142 \times 10^{-3}$. It was carefully verified that this set of parameters does lead to strong coupling in the inertial range $10 \leq k \leq 600$, such that the viscous term in the energy equation derived from (1.1) is negligibly small compared with the corresponding nonlinear term.

The results of numerical experiments are presented in Figs. $1.1 - 1.6$. Integration was performed for approximately $11\,\tau_{to}$, where $\tau_{to} = \pi/V_{rms} \approx 100$ is the large eddy turnover time. After approximately $0.5\,\tau_{to}$ a statistically steady-state is achieved. In Fig. 1.1 we plot two successive realizations of the velocity field in this steady-state. One can see the typical saw-tooth structures, characteristic of the dynamical system governed by Burgers equation. In our case, however, they are superimposed on a random velocity field. It was noticed that the system spends most of its time in a state where there are only a few (three – four) large-amplitude shocks and many small-amplitude ones. However processes leading to the creation of a single strong shock and its later breakdown into several smaller ones constantly take place. The time-evolution of the total energy in the system $E(t)$ demonstrates strong (with an amplitude of more than 100% of the average energy) fluctuations, characteristic of the instability of the large-scale structures (see Fig. 1.2). The time-averaged energy spectrum $E(k,t)$ $[E(t) = \int E(k,t)dk]$, presented in Fig. 1.3, is well approximated by the Kolmogorov law: $E(k) \propto k^{-\beta}$ with $\beta = 5/3 \pm 0.02$. The error bars were estimated in the following way: various values of the parameter $\beta$ were used to plot the compensated energy spectrum $e(k) = k^{\beta}E(k)$ and only values of the exponent $\beta$

for which $e(k)$ was within the experimental noise in the entire interval $10 < k < 600$ were chosen as satisfactory. The velocity structure functions $S_{2n}(r)$ are shown in Fig. 1.4 for various values of $n$. From Fig. 1.4 we see that for all $n$ higher than two $S_{2n}(r) \propto r^{\beta_{2n}}$ with $\beta_{2n} \approx 0.91$, indicating that these correlation functions are dominated by coherent shocks. We were not able to detect logarithmic corrections to the energy spectrum $E(k)$. However, the fact that high-order moments, presented in Fig. 1.4, are characterized by exponents close to, but not exactly equal to unity indicates that logarithmic contributions cannot be ruled out. One remarkable result is related to the dissipation rate correlation function presented in Fig. 1.5, G(r)=$\overline{\epsilon(x+r)\epsilon(x)} \propto r^{-\mu}$, with an intermittency exponent $\mu \approx 0.25 \pm 0.05$ measured inside the universal range $0.01 \leq r \leq 0.63$. Note that the dissipation rate correlation function is defined in physical space and, since $\epsilon(x)$ is nonlinear in $v(x)$, the 2/3-rule de-aliasing procedure was also used for its computation. The value of the dissipation rate exponent $\mu$ so obtained is close to that observed in experiments on three-dimensional turbulence: $\mu = 0.25 \pm 0.05$, see [77], and its general shape resembles the model shape of $G(r)$ proposed for three-dimensional turbulence in [55]. We would like to emphasize that in the present work the dissipation rate $\epsilon(x) = \nu_0 (\partial^p v/\partial x^p)^2$ with $p = 6$ strongly differs from the normal viscosity case with $p = 1$. The fact that the exponent $\mu$ obtained in this work is close to one observed in real-life turbulence provides an indication that the correlation function of the dissipation rate for inertial range values of the displacement $r$ is independent of the structure of the dissipation range. A similar conclusion was reached in recent numerical experiments of three-dimensional turbulence [5]. As one can see from Fig. 1.5, the accuracy of the exponent $\mu$ is not as good as that of the exponent in the expression for the energy spectrum. In addition, to assess the importance of the result, the role of the hyperviscosity in the dissipation rate correlation function must be investigated further.

Important information about the dynamics of a nonlinear system can be extracted from the correlation function defined by (1.3). In a scale-invariant regime, according to theories based on one-loop renormalized perturbation expansions [16, 95, 50] (we

will elaborate on these and other one-loop formulas in Section 1.6 below)

$$C(k,\omega) = \frac{D_0\, k^{-1}}{\omega^2 + \nu^2(k,\omega=0)\, k^4}, \tag{1.4}$$

where $\nu(k,\omega=0) \approx [3\,D_0/(4\pi)]^{1/3}\, k^{-4/3}$, corresponding to $z = 2/3$ and $\alpha = -7/3$ in (1.3). The frequency dependence of the effective viscosity $\nu(k,\omega)$ is neglected in the relation (1.4). This is done because it is assumed that the dynamics of inertial range modes $v(k,\omega)$ is dominated by "distant interactions" with modes $v(q,\Omega)$ with $|k| \ll |q|$ and can be described by a $k$-dependent eddy-viscosity. It is clear that this approximation cannot be valid when we are interested in the behavior of the most powerful large-scale structures because of the strong interaction between them that leads to the shock instabilities we observe here. The energy spectrum derived from (1.4) is [58, 16]: $E(k) = 2\int C(k,\omega) d\,\omega/(2\pi)^2 = [D_0^2/(6\,\pi^2)]^{1/3}\, k^{-5/3}$. The energy flux in wavenumber space can be expressed in terms of the amplitude of the force correlation function $D_0$ as follows: $\Pi(k) = \Pi(k_0) + D_0 \log(k/k_0)$. Then, the value of the "Kolmogorov" constant is: $C_K = \{[\Pi(k) - \Pi(k_0)]\,/\log(k/k_0)\}^{-2/3}\, k^{5/3} E(k) = [1/(6\,\pi^2)]^{1/3}$. The numerical value $C_K \approx 0.257$ is quite close to the results of numerical simulation, see Fig. 1.3. Some discrepancy in the Kolmogorov constant may be explained by the fact that this theory does not give a small coupling constant and higher-order corrections may change the value of the theoretical prediction. But the fact that the result of one-loop prediction correctly reproduces even the order of magnitude is quite remarkable. As in many other cases, understanding of the reasons for good agreement between the theory, based on a one-loop renormalized perturbation expansion, and experimental data, remains a major challenge.

The computational procedure for the evaluation of $C(k,\omega)$ is as follows. Starting from some initial moment $t = t_0$ in a statistically steady state, the solution $v(k,t)$ is stored at times $t_j = t_0 + T\,j/M$, where $T = 100$ is chosen to be of the order of $\tau_{to}$. Then, at $t = t_M$, the solution $v(k,\omega)$ is found via a discrete Fourier transform. Repeating this procedure in time, and assuming each realization of $v(k,\omega)$ to be independent of the others, which certainly is only an approximation, one can compute $C(k,\omega)$ as an average over such realizations. Memory limitations forced us to keep

only the first 200 wavenumbers and to limit ourselves to $M = 3000$. The results of these computations of $C(k,\omega)$, presented in Fig. 1.6, can be compared with the prediction (1.4). The relation (1.4) was derived neglecting the infra-red divergences resulting in transport of small-scale fluctuations by the large-scale coherent structures. This kinematic interaction ("sweeping effect") can be accounted for by a Doppler shift $\omega \to \omega + kV$ in (1.4), where $V$ is the characteristic velocity of the large scale structures. It is of major interest whether $C(k,\omega)$ is described by (1.4) or not and whether $V$ is zero or not. If the sweeping effect is present in the long-time behavior then there are three possible scaling regimes of $C(k,\omega)$ as $\omega \to 0+$: $C(k,\omega) \propto k^{-1}$ if $k \ll (\omega^3/D_0)^{1/2}$, $C(k,\omega) \propto k^{-7/3}$ if $(\omega^3/D_0)^{1/2} \ll k \ll D_0/V^3$, and $C(k,\omega) \propto k^{-3}$ if $k \gg D_0/V^3$. It is clear from Fig. 1.6 that the theoretical prediction (1.4) is surprisingly accurate in the limit of both large and small frequencies $\omega$. Only in a narrow intermediate range of wavenumbers such that $\omega \approx \nu(k,\omega=0)\,k^2$, does prediction (1.4) fail. The flattening of $C(k,\omega)$ observed in this interval indicates that the scaling function $F(x)$ in (1.3) is a decreasing function of $x$ when $x \approx 1$. The quantitative agreement between theory and simulations in the limit of large wavenumbers $k$ shows that the "sweeping velocity" $V$ is small. This may be a consequence of the fact that the large-scale shocks are almost steady. We would also like to note that the accuracy of our $C(k,\omega)$ computation may not be easily increased because of computer resource limits. The above result leads to an interesting possibility: Infra-red divergences present in the theory are not summed up into a mere transfer of small-scale fluctuations by the large-scale structures, but are reflected in the creation of a large-scale condensate state, which in this case has the very simple physical meaning of a collection of strong shocks moving with a very small velocity $V$. Derivation of an equation of motion describing the dynamics of coherent shocks is an important and interesting problem and will be the subject of future work.

The above results, obtained in a simple one-dimensional system, are surprisingly similar to results of experimental investigations of real-life three-dimensional turbulence. In the one-dimensional case, however, the dynamics and geometrical structure of the turbulence building blocks are well understood and a cascade process is readily

envisioned as a coagulation of weak, wide shocks (shock width and amplitude are related as $l \approx \nu_0/U$) into ever stronger, narrower structures until dissipation takes over. Moreover, the total dissipation rate in an interval of length $r$ is prescribed and is equal to $\epsilon_r \propto \log\ (r\,U_0/\nu_0)$. Given these simplifications, one may hope that a full Kolmogorov-type theory of turbulence in the one-dimensional Burgers equation is not out of reach.

## 1.2 Kolmogorov Turbulence in the Random-Force-Driven Burgers Equation: Anomalous Scaling and Probability Density Functions

In the previous Section (see, also [11]), we have shown that investigation of the velocity structure functions $S_n(r) = \overline{[u(x+r)-u(x)]^n} \equiv \overline{(\Delta u)^n}$, with integer $n$, revealed strong deviations from the Kolmogorov picture of turbulence: all moments $S_{n>3}(r) \propto r^{\xi_n}$, with $\xi_n \approx 1$, characteristic of strong shocks. Thus, the system governed by $(1.1)-(1.2)$ shows both "normal" (Kolmogorov) and anomalous scalings with the latter dominated by coherent structures (shocks). In this Section, we are interested in the details of the probability density functions (PDFs) characterizing the fluctuations generated by $(1.1)-(1.2)$ and in the role the structures play in the determination of shape of the PDFs. Most of these results are included in [12]. The probability density $\mathcal{P}(\Delta u, r)$ is defined such that $\mathcal{P}(X,r)\,dX$ is the probability to find a velocity difference $\Delta u = u(x+r)-u(x)$ within the interval $(X, X+dX)$ for infinitesimally small $dX$.

As we have already mentioned above, the most prominent feature of Burgers equation is a tendency to create shocks and, consequently, to increase the negative velocity differences $\Delta u < 0$ and decrease the positive ones $\Delta u > 0$ [8]. Thus, strong asymmetry of the curve $\mathcal{P}(\Delta u, r)$ is expected. The two-point PDF $\mathcal{P}(\Delta u, r)$ was measured for a set of separations $r$ covering a variety of scales in the system in the following way. The range of variation of the velocity difference, $-5 < \Delta u/u_{rms} < 5$,

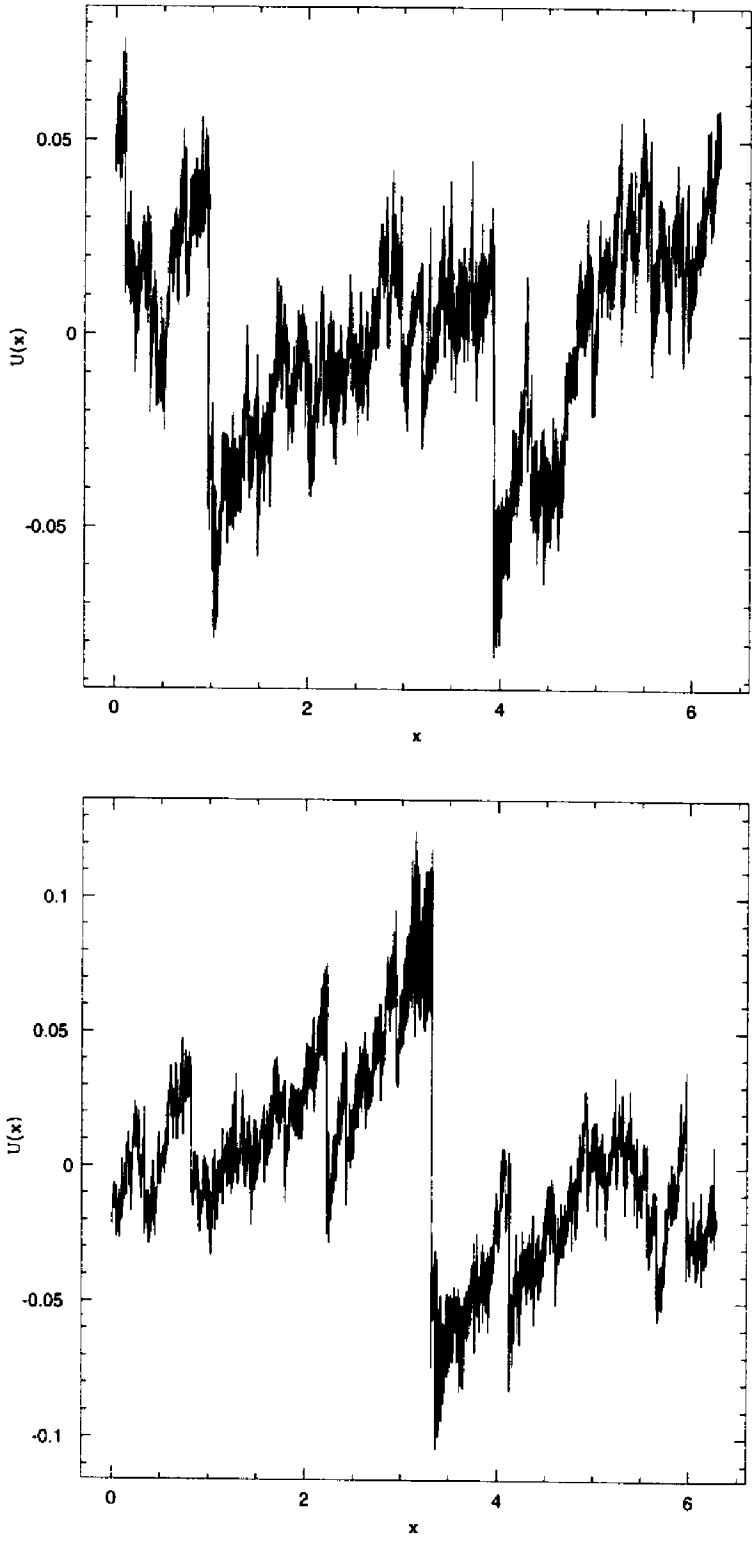


Figure 1.1: Solutions $v(x,t)$ at times $t = 90.0$ (upper) and $t = 213.5$ (lower).

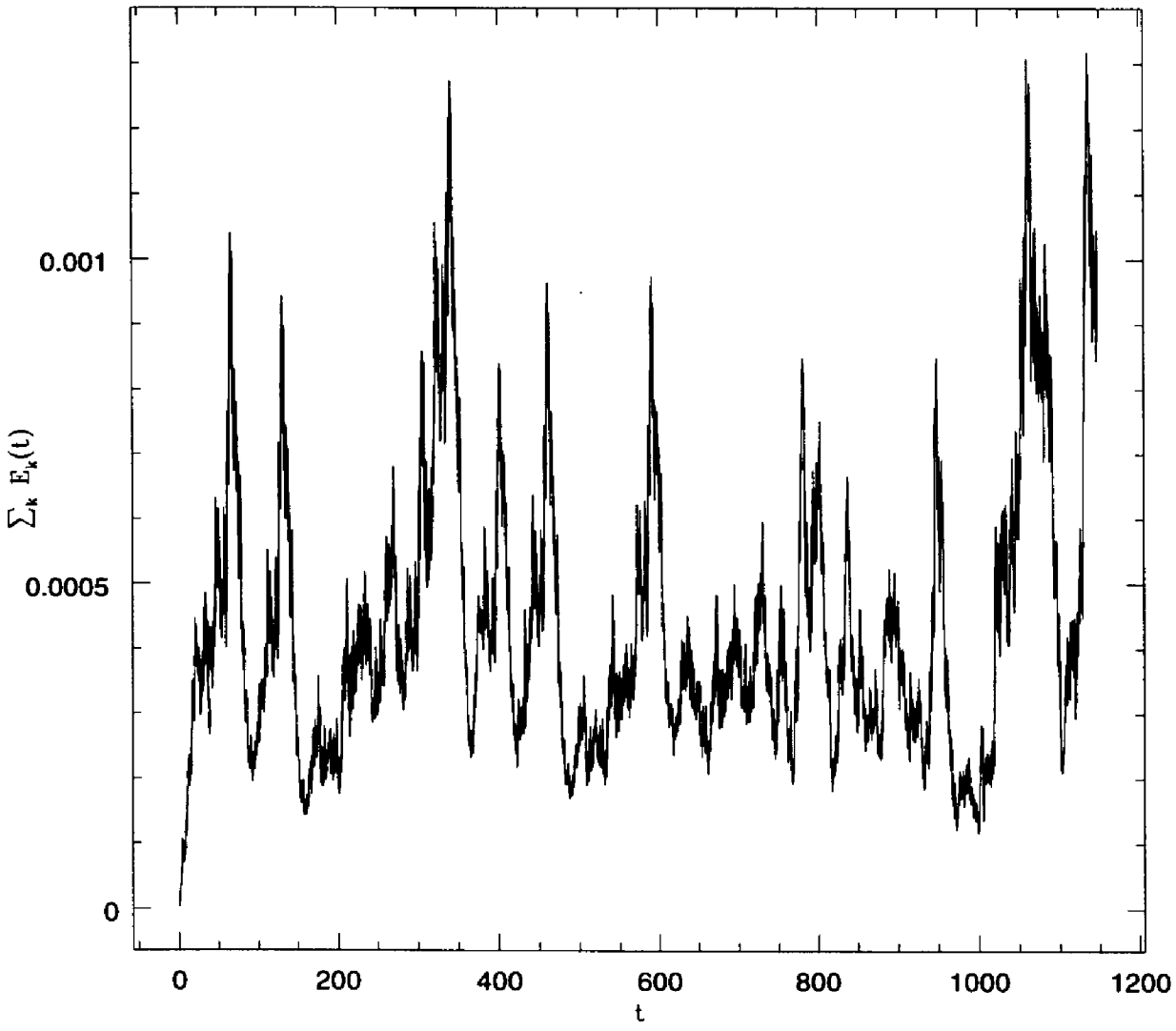


Figure 1.2: Time-evolution of the total energy $E(t)$.

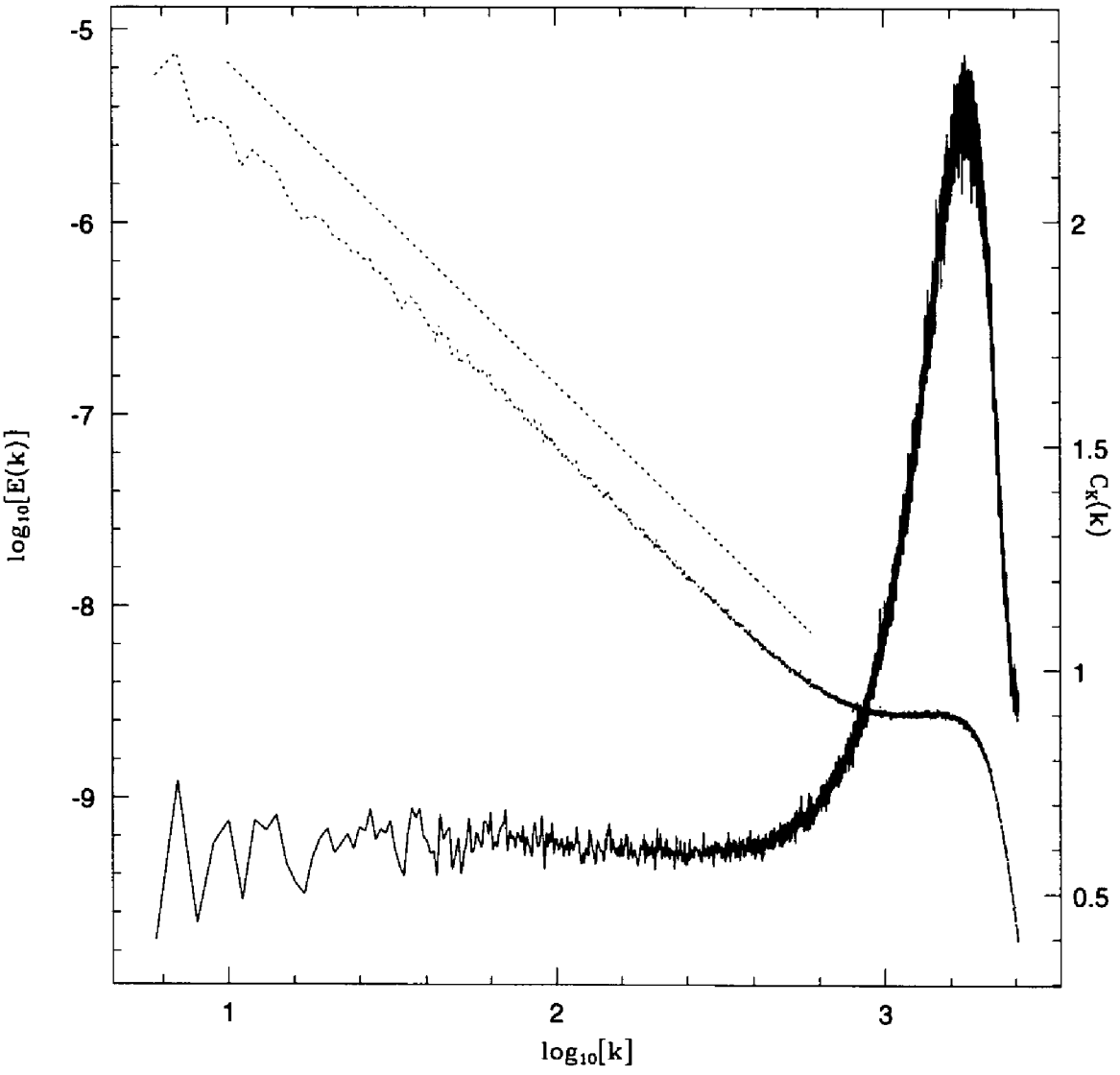


Figure 1.3: The dotted curve here represents the energy spectrum $E(k)$ (left axis), and the straight line above it has the exact slope $-5/3$. The solid curve is the compensated energy spectrum $C_K$ defined in the text (right axis).

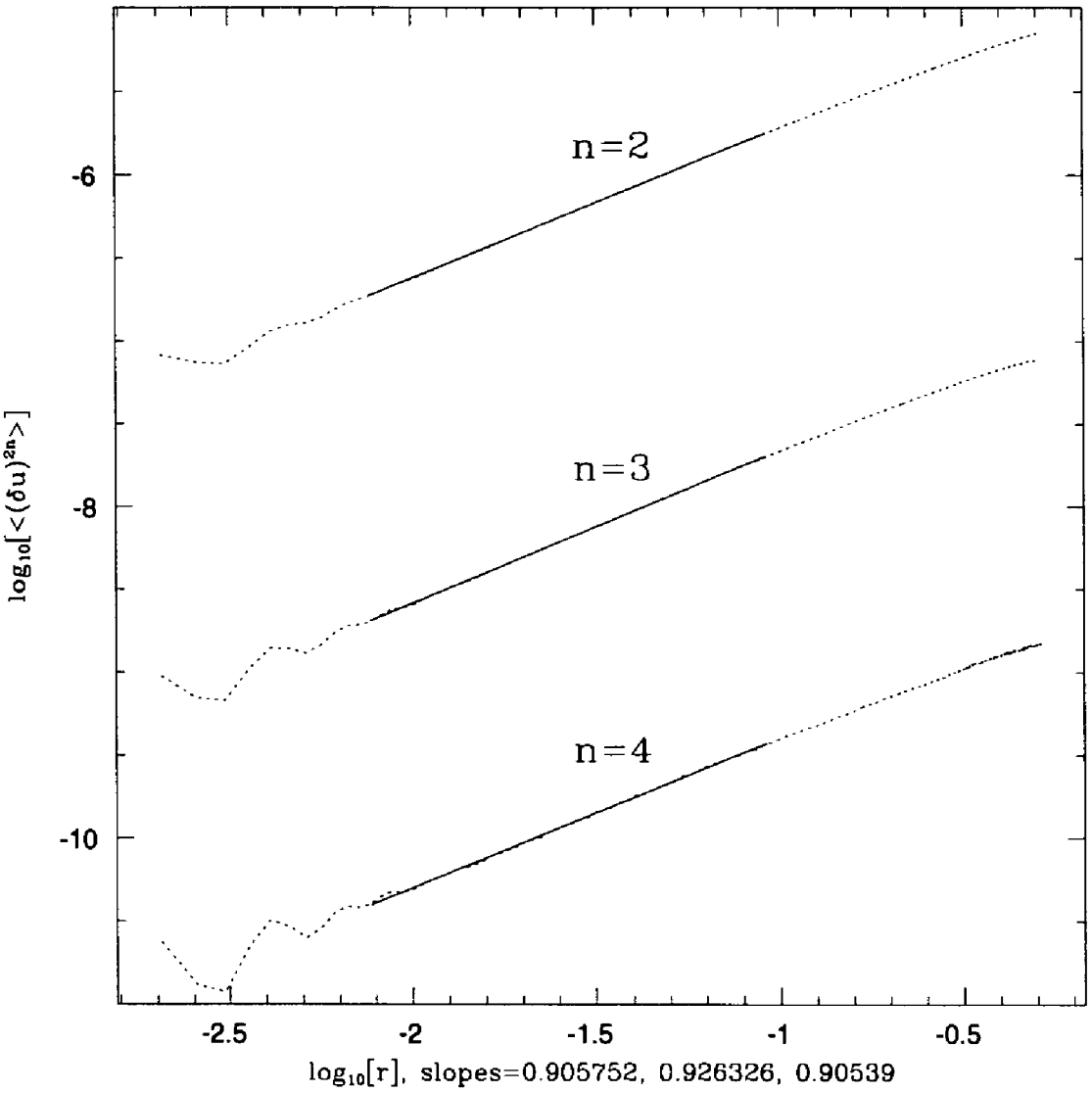


Figure 1.4: Velocity structure functions $\overline{(v(x+r)-v(x))^{2n}}$ for $n = 2, 3, 4$ (dotted curves) with linear least-squares fits (solid lines).

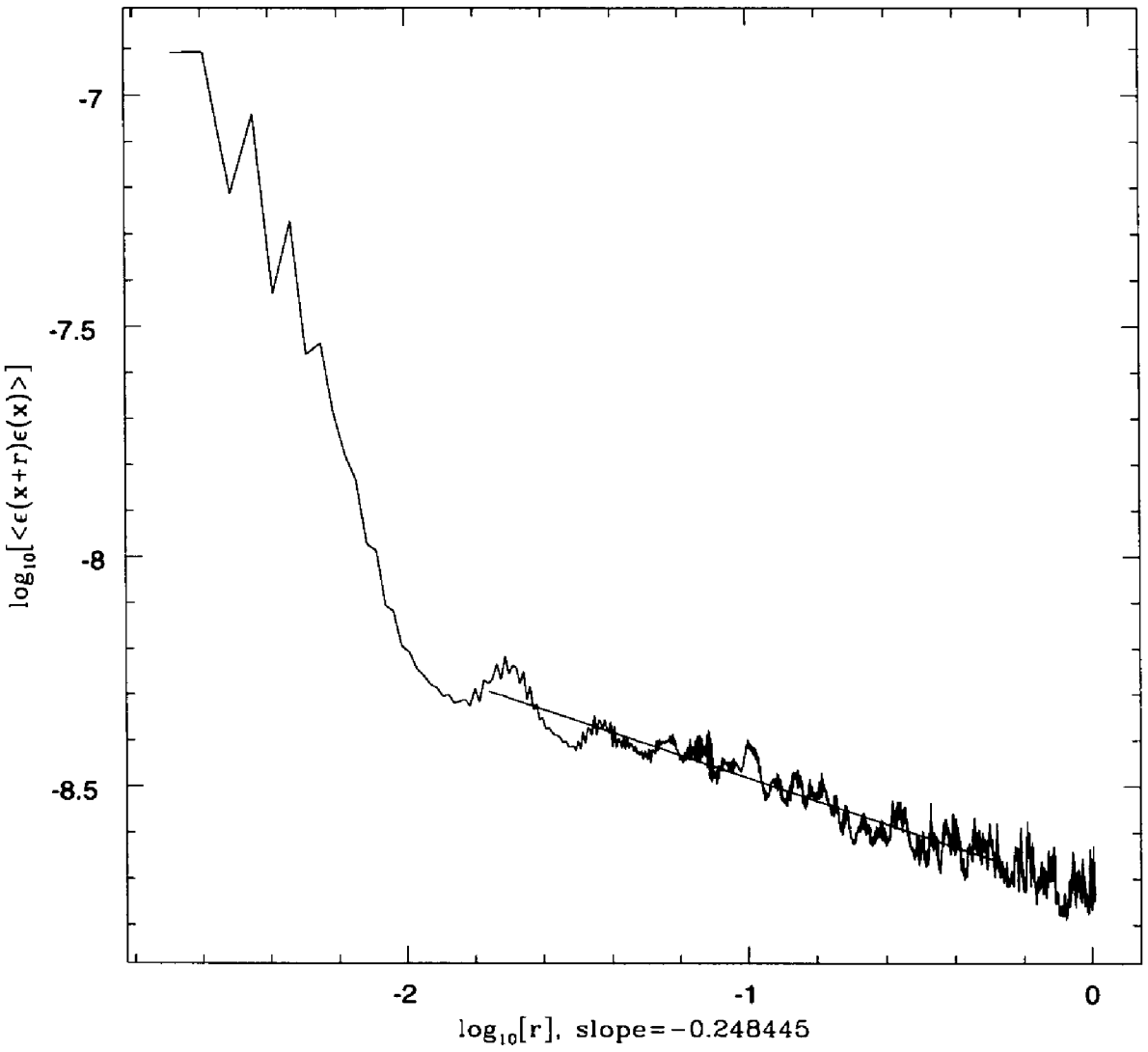


Figure 1.5: Energy dissipation correlation function $\overline{\epsilon(x+r)\,\epsilon(x)}$ with linear least-squares fit, giving the intermittency exponent $\mu = 0.25 \pm 0.05$.

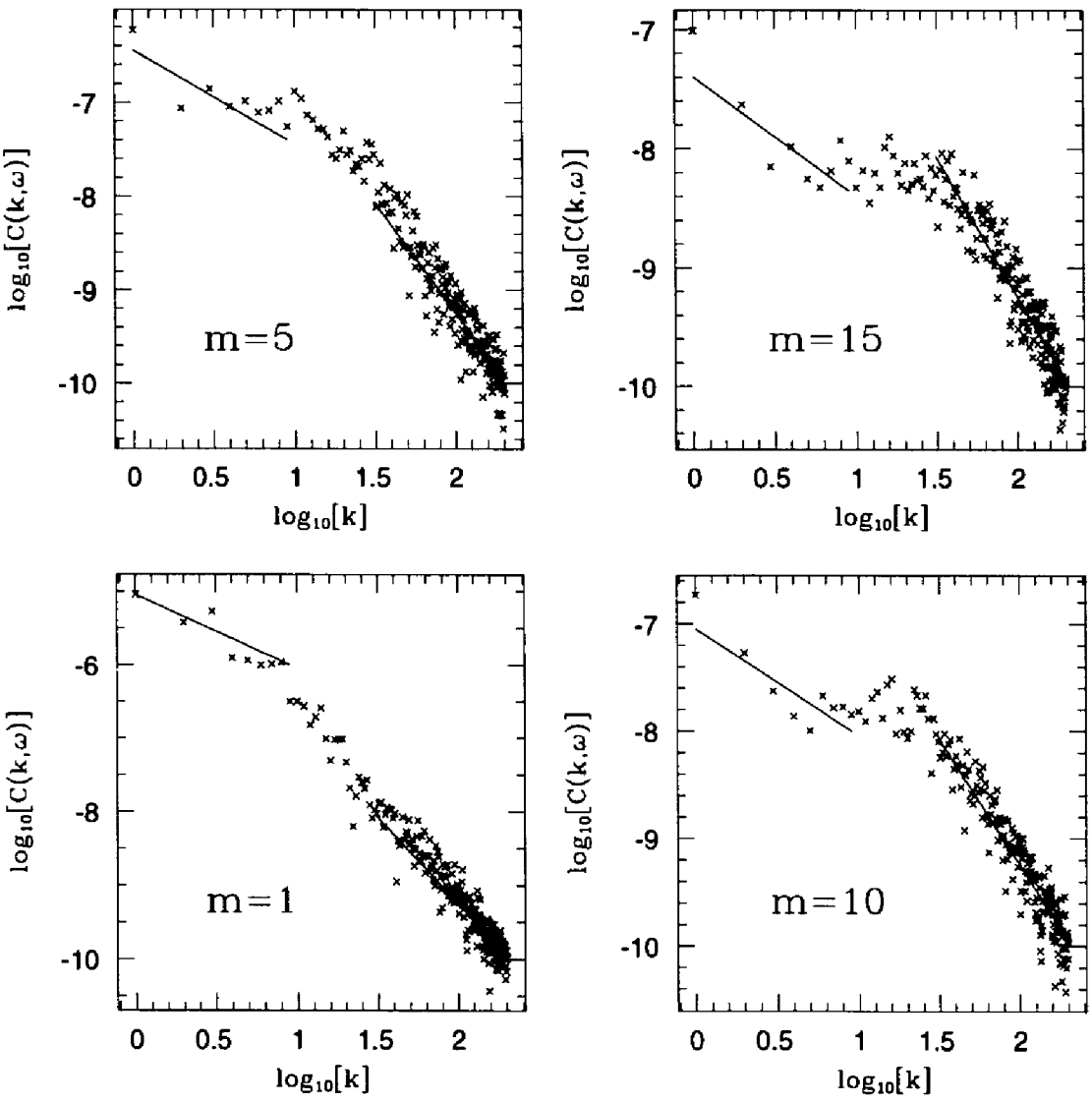


Figure 1.6: Points denote the self-correlation function of the solution $C(k,\omega)$ for fixed frequencies $\omega = 2\pi m/\tau$ with $m = 1$, $m = 5$, $m = 10$, $m = 15$ and $\tau = 100.05$. Solid lines denote the corresponding asymptotic behavior of the one-loop prediction given by (1.4).

was divided into $10^4$ bins. The data were collected during a time longer than 10 large eddy turnover times (corresponding to $O(10^7)$ time-steps) and were distributed among the appropriate bins to generate a histogram. Fig. 1.7 presents $\mathcal{P}(\Delta u, r)$ for the inertial range separations $r/dx = 200, 250, 300, 350, 400$, where $dx = 2\pi/12288$ is the mesh size. It follows from (1.1)−(1.2) that $\overline{(\Delta u)^3} \propto r \log r$; that is why this PDF has a shifted maximum at approximately $\phi = (\Delta u)/R^{1/3} \approx 0.5$. Here the function $R(r)$, defined as $R(r) = \int_{y=0}^{r} \overline{[f(x+y) - f(x)]^2}\, dy$, was also directly measured. The PDF $\mathcal{P}(\Delta u, r)$ for $r/dx = 200$ within the universal range, is shown in Fig. 1.8 on a logarithmic-linear scale. It follows from the analysis of the data that

$$\mathcal{P}(\Delta u, r) \propto (\Delta u)^{-q}, \quad \text{for} \quad \Delta u \ll 0, \tag{1.5}$$

with $q \approx 4$ and

$$\mathcal{P}(\Delta u, r) \propto e^{-\alpha \frac{(\Delta u)^3}{r}}, \quad \text{for} \quad \Delta u \gg 0, \tag{1.6}$$

with a constant $\alpha \approx 1/9$. This result is highly nontrivial because the observed algebraic decay of the PDF $\mathcal{P}(\Delta u, r)$ as $\Delta u \to -\infty$ leads to divergence of the moments $S_n(r)$ for $n > 3$ for the inviscid case. However, in the viscous problem with $\nu_0 \neq 0$ the occurrence of shocks with an amplitude $\Delta u > U_0 \approx L\sqrt{D_0/\nu_0}$ is highly improbable and one can expect the PDF $\mathcal{P}(\Delta u)$ to decrease sharply for $\Delta u > U_0$. This is sufficient for the existence of all moments $S_n(r)$. The single-point PDF is presented in Fig. 1.9. One can observe the measured $\mathcal{P}(u)$ together with the best Gaussian fit $\mathcal{P}(u) \propto e^{-\gamma u^2/u_{rms}^2}$, with $\gamma \approx 1/4$. However, deviations from gaussianity are noticeable for $3 < |u/u_{rms}| < 0.5$.

Let us make a note about the function $R(r)$ mentioned above. This function is of principal importance in the theory of probability density functions [62, 92] currently in progress. Formal computation of the $R(r)$ for the $y = 1$ case, similarly to how it is done in [54], diverges if viscosity is exactly equal to zero. At the same time, introduction of the ultra-violet cut-off wavenumber $k_d$, which is associated with the viscous dissipation, leads to the finiteness of this function and asymptotic behavior: $R(r) \propto -r \log(r\, k_d)$, as is possible to show. This emphasizes once again the importance of infinitecimal viscosity in this problem.

To develop a phenomenological theory we assume that the flow can be represented as a superposition of coherent and random components. The coherent contribution is visualized as a "gas of shocks" and a single structure (shock) can be approximated by the exact tanh-solution of the unforced problem [8]. In particular, let us assume that solution for the normal (not the hyper-) viscosity case has the form

$$u(x,t) = -\sum_{i=0}^{N} U_i \tanh\left[\frac{(x-a_i)\,U_i}{2\nu_0}\right] + \phi(x). \tag{1.7}$$

The first contribution to the right side of (1.7) describes the "gas of shocks", whereas the second represents the effects unaccounted for by the first term. Here $a_i$ and $U_i$ denote the coordinates of the centers of the shocks and the shock amplitudes respectively. It will become clear below that the detailed shape of the shock assumed in (1.7) is unimportant. The most essential feature of the tanh-solution (1.7) is that the shock width $l_i \approx \nu_0/U_i$, which means that, the stronger the shock, the more narrow it is.

The argument presented below is based on the assumption that energy dissipation takes place exclusively inside the shocks. Then the mean dissipation rate $\bar{\epsilon} = \nu_0 \overline{(\partial u/\partial x)^2}$ in an interval of length $r$ is

$$\bar{\epsilon}_r = \frac{1}{4\,r\,\nu_0}\int_{x=0}^{r} dx \sum_{i,j=0}^{N} \frac{U_i^2\,U_j^2}{\cosh^2 Y_i \cosh^2 Y_j}, \tag{1.8}$$

where we denote $Y_i = (x-a_i)\,U_i/(2\nu_0)$. The main contribution to the sum comes from the strong and narrow shocks, and therefore we can neglect the nondiagonal terms with $i \neq j$. Assuming the density of the shocks to be $r$-independent we have

$$\bar{\epsilon}_r \propto \sum_{i=0}^{N} \frac{U_i^3}{r} \approx \frac{\overline{U^3}}{r}. \tag{1.9}$$

Another way to derive this is to take the integral in (1.8) exactly and consider its asymptotic behavior for $\nu_0/U_i \ll r \ll L$, which makes sense if the viscosity is small enough. One may deduce then, that under this condition, integral in fact will not depend on the specific value of $r$.

On the other hand, it can be directly shown from (1.1) – (1.2) that

$$\bar{\epsilon}_r = D_0\, ln\left(\frac{r\,U_0}{\nu_0}\right). \tag{1.10}$$

Introducing the probability density $\mathcal{P}(U,r)$ to find a shock with amplitude $U$ in an interval of length $r$, we obtain from the last two relations

$$\int_{r^x}^{U_0} U^3\,\mathcal{P}(U,r)\,dU \propto D_0\,r\,ln\left(\frac{r\,U_0}{\nu_0}\right), \tag{1.11}$$

from which we readily establish the form of $\mathcal{P}(U,r)$

$$\mathcal{P}(U,r) \propto \frac{D_0\,r}{U^4}. \tag{1.12}$$

Since $\mathcal{P}(U,r) = \mathcal{P}(U)\,r/L$ where $L$ denotes the system size, the relation (1.12) establishes the probability density $\mathcal{P}(U) \propto U^{-4}$ of finding a shock of amplitude $U$. Note that $r/L$ is the probability to find a shock center within the interval of length $r$. The physical meaning of the lower integration limit in (1.11) and the value of the exponent $x$ will be discussed in what follows. Formula (1.12) is a consequence of relations (1.9) and (1.10), and is valid in the logarithmic case when the forcing function is defined by (1.2). It is only in this case that we can establish the form of the PDF.

The goal of a statistical theory is to calculate the energy spectrum and correlation functions of velocity differences $S_n(r)$. The structure functions $S_n(r)$ are very important since they measure local spatial inhomogeneity and order in the system. For example, if $u(x,t) = const$, all $S_n(r) = 0$. In the case of a single shock of amplitude $U$, evaluation of $S_n(r)$ is very simple: The velocity differences are zero everywhere, unless the single shock is situated between the points separated by the distance $r$. For these points: $u(x+r) - u(x) = U$ and $S_n(r) = U^n\,r/L$. In this case the energy spectrum $E(k) = \overline{|u(k)|^2}/2$, which is the Fourier transform of $S_2(r)$, is readily evaluated to give $E(k) \propto k^{-2}$ [8]. In the forced problem considered in this work, the situation is not so simple since we are dealing with many shocks of various strengths and amplitudes. Still, knowledge of $\mathcal{P}(U)$ enables us to evaluate the structure functions $S_n(r)$. Let us choose an interval of length $r$ and consider shocks with widths $l < r$ and $l > r$ separately. Using (1.12) we obtain

$$S_n(r) = \int_{U(r)}^{U_0} U^n\,\mathcal{P}(U,r)\,dU \propto \frac{r}{L}\int_{U(r)}^{U_0} U^n\,\mathcal{P}(U)\,dU, \tag{1.13}$$

where $U_0$ is the amplitude of the strongest and narrowest shock in the system. The lower integration limit $U(r)$ accounts for contributions coming from wide "typical"

structures with $l \approx r$. A simple calculation shows that the weakest shocks with $l \gg r$ do not contribute to the correlation functions. The above expression can be evaluated in the following way: Let us assume that $U(r) \propto r^x$, where $x$ is a yet unknown exponent. The physics behind this expression is very clear: The spatial inhomogeneity on the scale $r$ is represented as an effective "dressed" shock of amplitude $U(r) \propto r^x$. This construction, consistent with the concept of effective (eddy) viscosity, yields $U(r) \approx \sqrt{S_2(r)}$. Then, the exponent $x$ may be found from the condition

$$S_2(r) \propto r^{2x} = r \int_{r^x}^{U_0} U^{-2}\, dU \propto r^{1-x}, \tag{1.14}$$

which leads to $x = 1/3$. Equation (1.14) is obtained in a way similar to the semi-dynamical dimensional considerations which are the basis of the Kolmogorov theory of turbulence, which gives: $S_2(r) = O(r^{2/3})$. However, unlike the Kolmogorov theory, the above relation, when combined with (1.12) and (1.13), gives the anomalous scaling of the higher-order moments. Indeed, it follows from (1.12) – (1.13) that all moments $S_n(r)$ with $n > 3$ are completely determined by the upper cut-off in (1.13)

$$S_n(r) = r \int_{r^x}^{U_0} U^{n-4}\, dU = r\, \frac{U_0^{n-3}}{n-3}, \quad \forall\, n > 3\,, \tag{1.15}$$

which is in excellent quantitative agreement with the outcome of [11]. Using the expressions above, we can calculate all $S_n(r)$ for small positive $n$

$$S_n(r) \propto r^{\frac{n}{3}}, \quad \forall\, 0 \le n \le 3\,, \tag{1.16}$$

as in the Kolmogorov theory of turbulence [34, 35]. Thus, the anomalous scaling of the velocity structure functions $S_n(r)$ appears only for $n > 3$. The prediction (1.15) has been tested in [11]. It has been shown that $S_{2n}(r) \propto r^{\xi_{2n}}$ with $\xi_{2n} \approx 0.91$ for $n > 2$, indicating that these correlation functions are dominated by coherent shocks. The results of the measurements of the structure functions $S_n$ with $n = 1/3, 2/3, \ldots, 6/3$, presented on Fig. 1.10, are in good agreement with the scaling law (1.16).

Fig. 1.11 presents the PDF of the shock amplitudes. The problem of the shock location was solved in the following simple but reliable way. At each spatial point $x$ the local gradient of the solution $u'(x)$ was measured. Then, if $u'(x) \ge 0$, it was

assumed that this point $x$ is outside of a shock, otherwise $x$ lies inside of a shock. Once inside a shock, one can march in $x$ until the gradient becomes zero, and thus the boundaries of the shock may be located. Note that the shock amplitude obtained in this way has been corrected to exclude the Gibbs phenomenon typical in spectral approximations of discontinuous functions. To reduce the statistical noise in $\mathcal{P}(U)$ in Fig. 1.11, a simple smoothing procedure was applied: $\mathcal{P}(U)$ was averaged over eight surrounding values. The result presented in Fig. 1.11 demonstrates that

$$\mathcal{P}(U) \propto U^{-4} \tag{1.17}$$

for all $|U/U_{rms}| > 0.5$. The fact that $\mathcal{P}(\Delta u) \approx \mathcal{P}(U)$ when $\Delta u < 0$ tells us that in this range $\mathcal{P}(\Delta u)$ is dominated by the well-separated shocks. This confirms the main assumption of the phenomenological theory presented above. It follows from Figs. 1.7, 1.10 that the PDF obeys a simple scaling: $\mathcal{P}(\Delta u, r) = P(\Delta u/R^{1/3})$ and that the anomaly in the high-order moments results only from the slow (algebraic) decrease of the probability density in the interval $\Delta u < 0$. As was pointed out above, in this case one expects a cut-off at some $\Delta u \approx U_0$.

## 1.3 The Large-Scale Forcing Case

The problem involving a force concentrated only at the largest scales in the system has attracted some scientific attention [8, 68, 37]. Despite this, and also despite the fact that most of the quantitative features of the solution are more or less known, this problem remains unresolved in the rigorous sense: a satisfactory analytical solution has not been yet found.

Burgers himself [8] believed that this problem leads to an exactly constant energy flux in wavenumber space from the largest to the smallest scales, down to the dissipative. Primarily from numerical experiments [87] and from such approximate theories as closure [37], the following properties of the solution are believed to be true: energy spectrum scaling is $k^{-2}$; moments of velocity differences $\overline{U^n}$ scale as $r^1$ [87] for high enough $n$; the solution in physical space $u(x,t)$ consists of countable number of shock waves and smooth ramp regions [8]: shocks move in the positive $x$-direction and tend

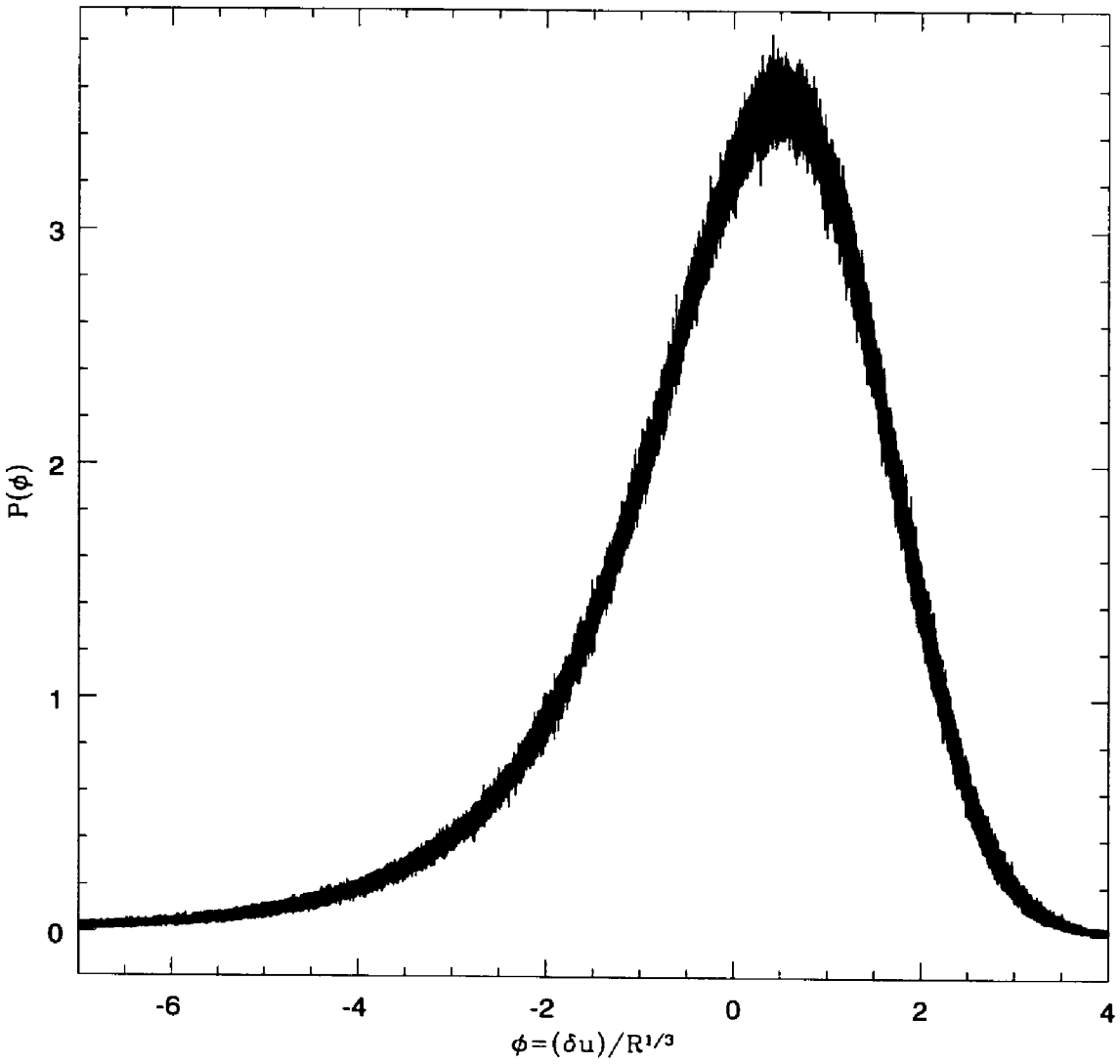


Figure 1.7: Two-point PDF $\mathcal{P}(\Delta u, r) = P(\Delta u/R^{1/3})$ for separations $r/dx = 200$, 250, 300, 350, 400 within the universal range. The collapse of various curves supports the choice of the scaling variable $\phi = (\Delta u)/R^{1/3}$.

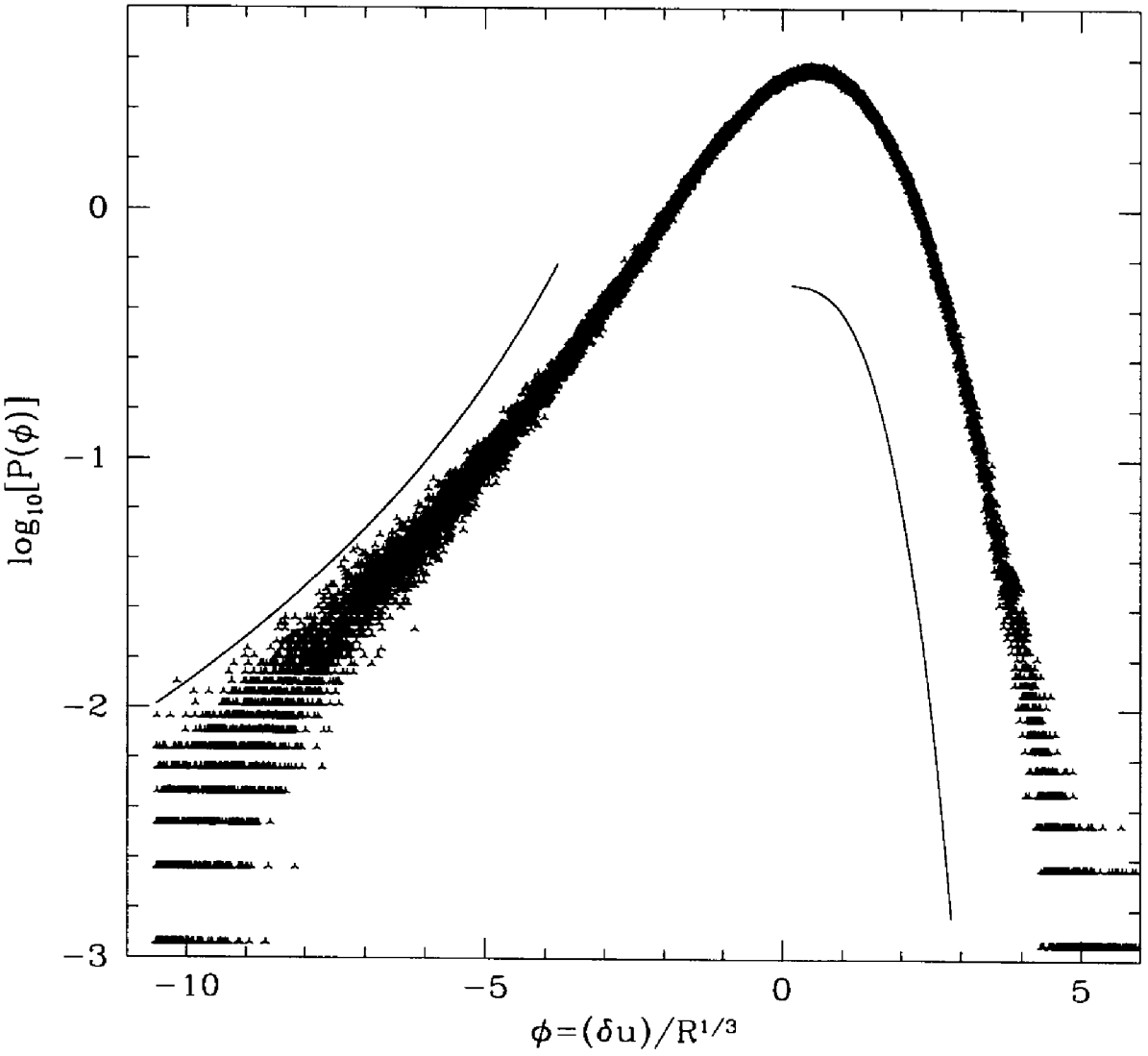


Figure 1.8: Two-point PDF $\mathcal{P}(\Delta u, r)$ for $r/dx = 200$ on a logarithmic-linear scale. Solid lines correspond to the relations $(\Delta u)^{-4}$ and $e^{-(\Delta u)^3/(9R)}$ discussed in the text.

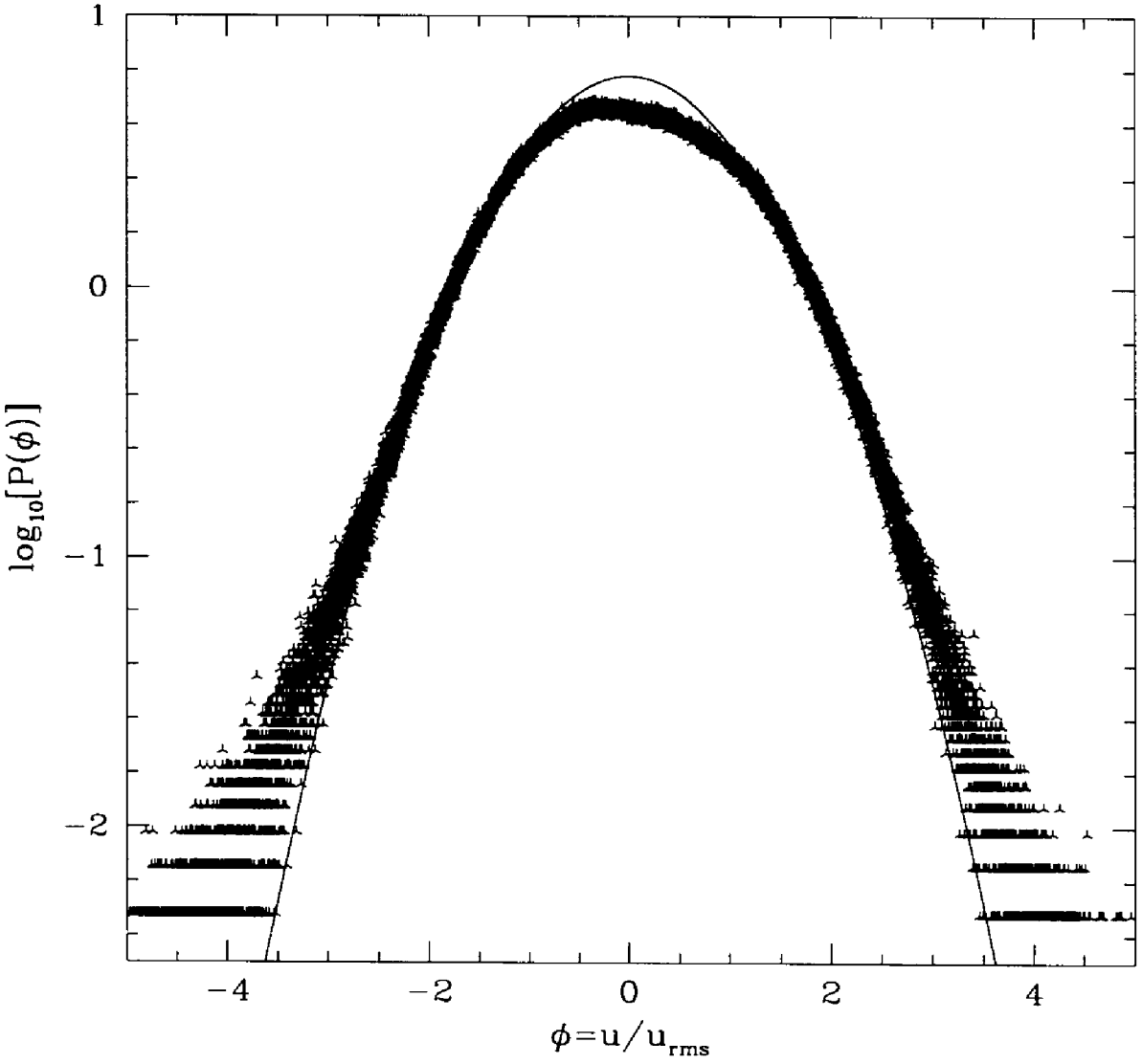


Figure 1.9: Single-point PDF $\mathcal{P}(u)$ with the Gaussian fit $e^{-u^2/(4u_{rms}^2)}$.

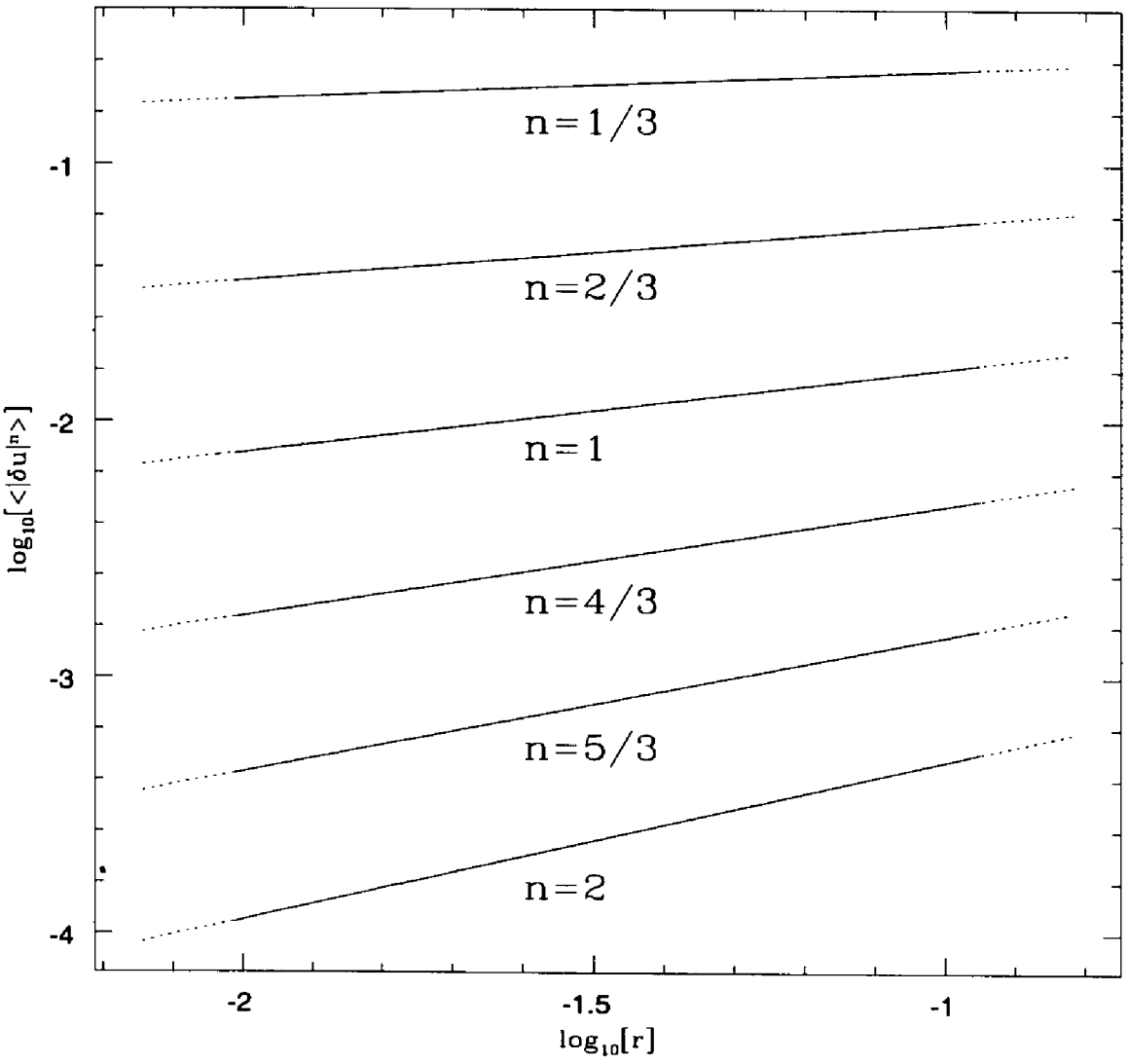


Figure 1.10: Velocity structure functions $\overline{|\Delta u|^n}$ for noninteger values $n = 1/3, 2/3, \ldots, 6/3$ (dotted curves). Slopes of the linear least square fits (solid lines) from top to bottom: 0.111, 0.222, 0.330, 0.433, 0.531, 0.620, respectively.

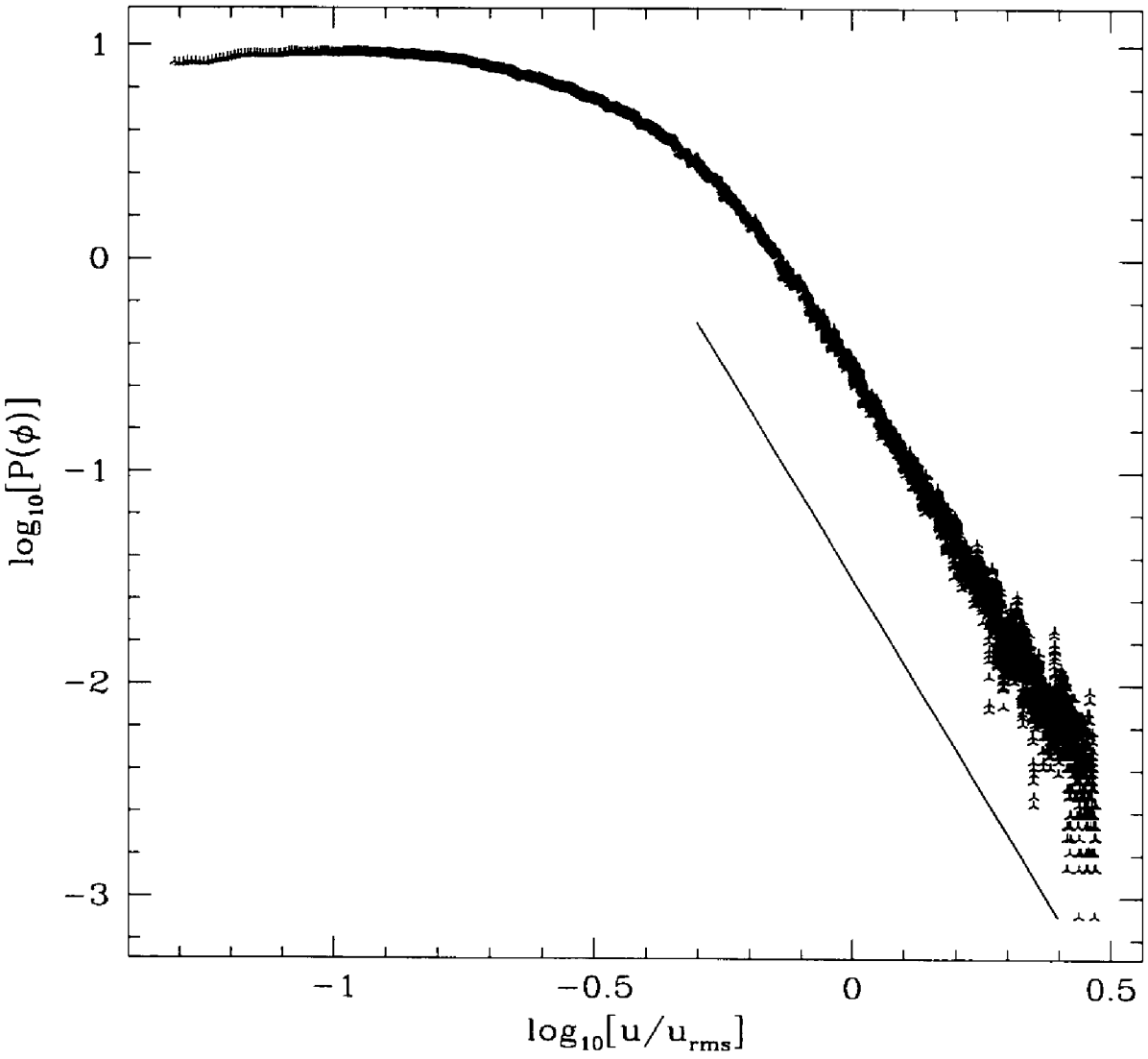


Figure 1.11: PDF of shock amplitudes, $\mathcal{P}(U)$, on a logarithmic-logarithmic scale (points). The slope of the solid line is $-4$.

to coalesce. Some rigorous results, although somewhat distant from being physically transparent and useful, may be found in [67].

Here we briefly present results of a simulation with the following parameter values: spectral resolution 12288, hyperviscosity with $\nu_0 = 9 \times 10^{-40}$ and $p = 6$, and time-step $\tau = 5 \times 10^{-5}$; the run was continued for over three-four large eddy turnover times.

We do observe that the energy flux in Fourier space is nearly constant, see Fig. 1.12; the exponent of the energy spectrum is $-2$ with good accuracy, as may be seen in Fig. 1.13. The total energy, similar to $y = 1$ case, exhibits large-amplitude fluctuations, corresponding to interactions of the largest shocks, see Fig. 1.14. A notable feature of the physical space solution, depicted in Fig. 1.15, is a finite and small number of shocks. Due to the fact that the force here affects only the amplitudes of harmonics with the longest wavelengths (in this particular run the force was nonzero for the first 10 wavenumbers $k$ only), shocks are created rather slowly, through the gradual steepening of initially smooth negative gradients. This is in contrast to the $y = 1$ case, where shocks could be created almost at once through the introduction of sharp gradients at small scales directly by the force.

Velocity differences presented in Fig. 1.16 confirm the previously noted fact that all the moments $\overline{U^n} \propto r^1$ for all $n \geq 1$ and are determined by shocks (viscous cutoff), leading to "maximal intermittency" effects in this case compared with all the $y < 2$ cases.

## 1.4 A Force With a Steeper Scaling Law

The particular case $y = 3/2$ has special importance. As we will demonstrate below, the one-loop renormalization group (RG) approximation gives the following prediction for the energy spectrum exponent $\nu_E(y) = 1 - 2\epsilon/3$ for $y > -2$ and $\nu_E(y) = 0$ for all $y \leq -2$, where $\epsilon = 3 + y$. This theory thus proposes a "phase transition" at $y = -2$, leading to a jump in the energy exponent at the transition point and corresponding jumps in some other exponents (of the RG eddy viscosity, for example). Let us emphasize that this is true under the condition that RG "works" in this case. It is

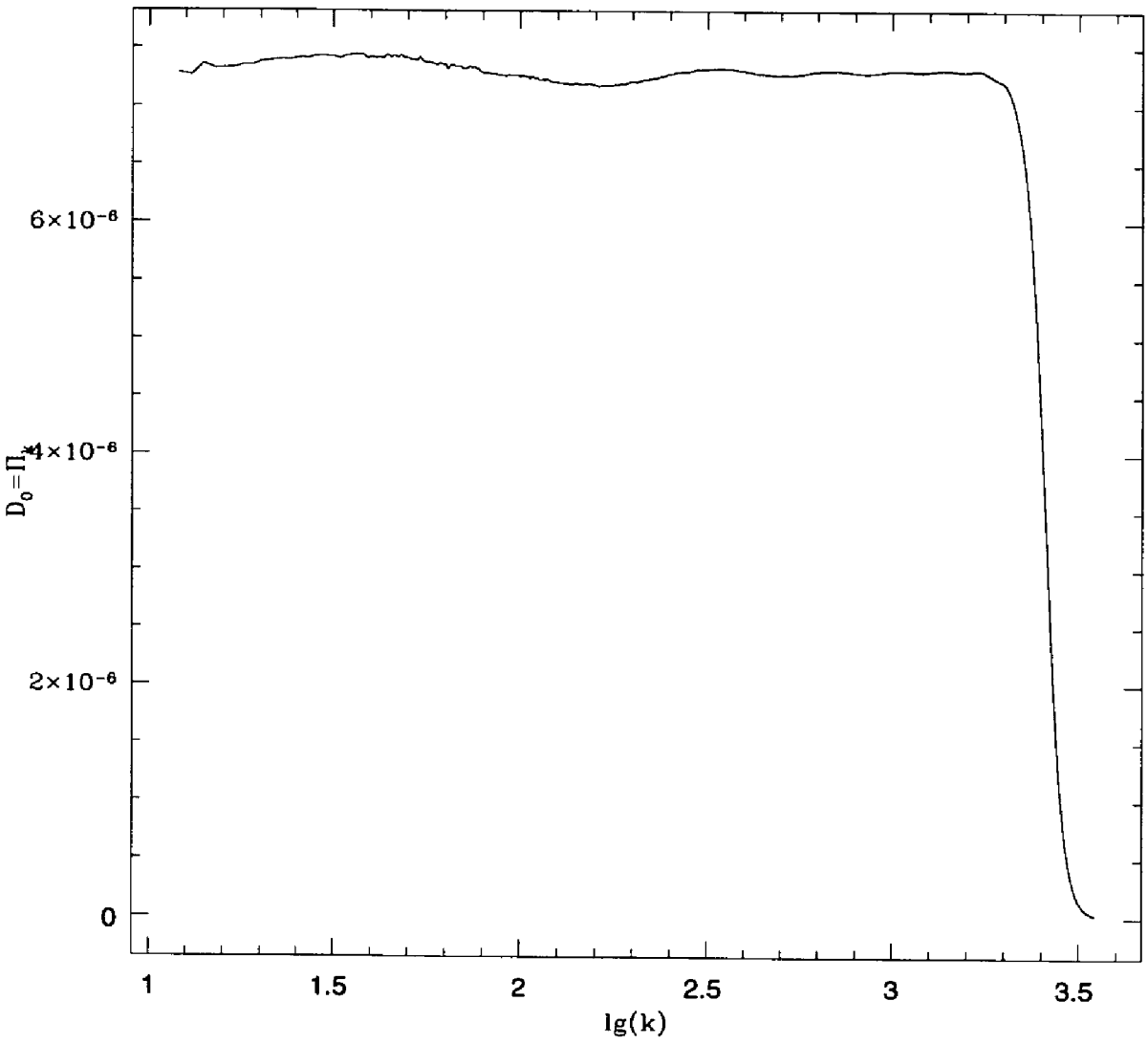


Figure 1.12: Energy flux in the large-scale forcing case; $k \leq 10$ are not shown because they inject energy in the system.

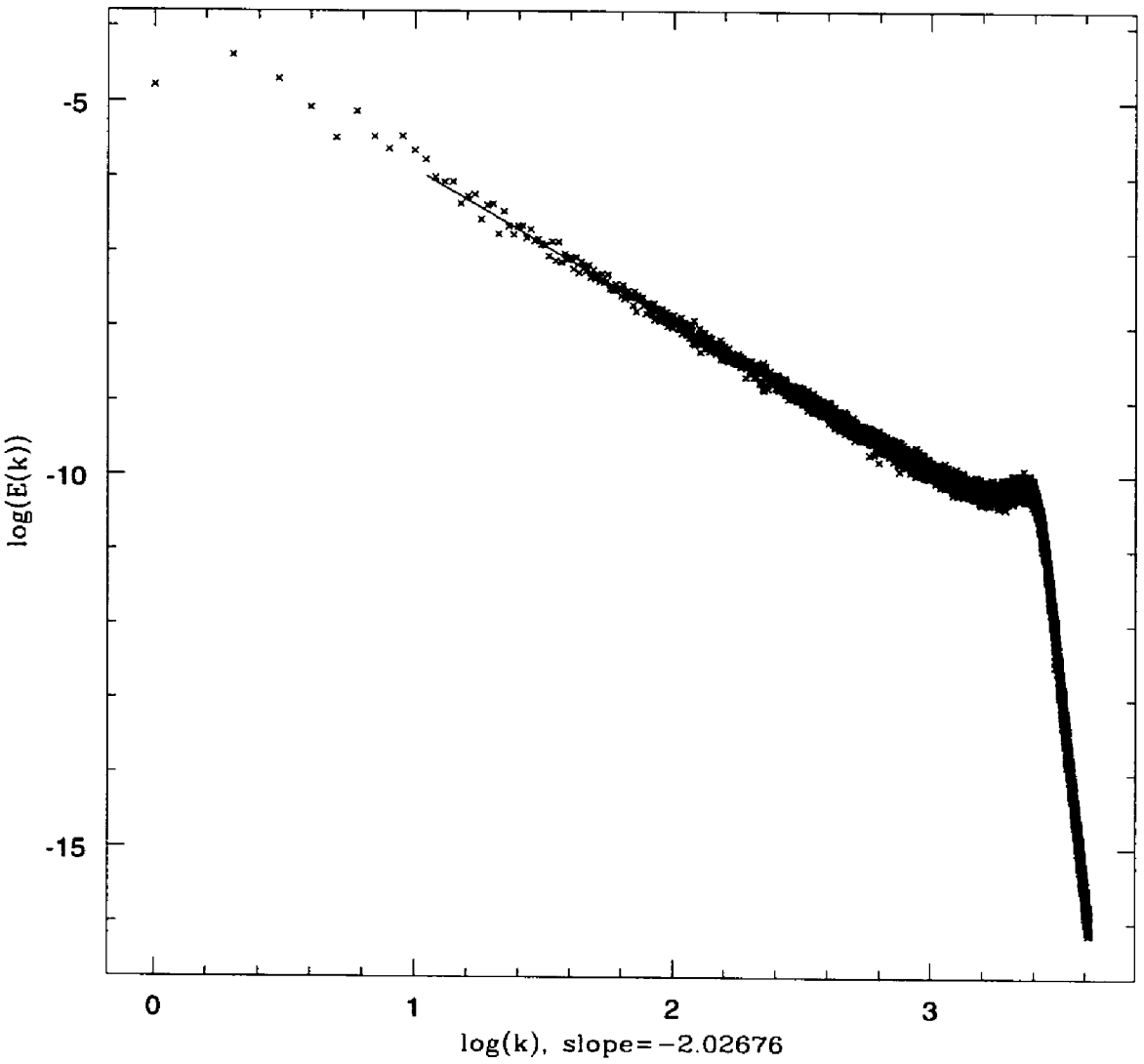


Figure 1.13: Energy spectrum in the large-scale forcing case. Slope of the linear least-square fit is approximately equal to $-2.03$.

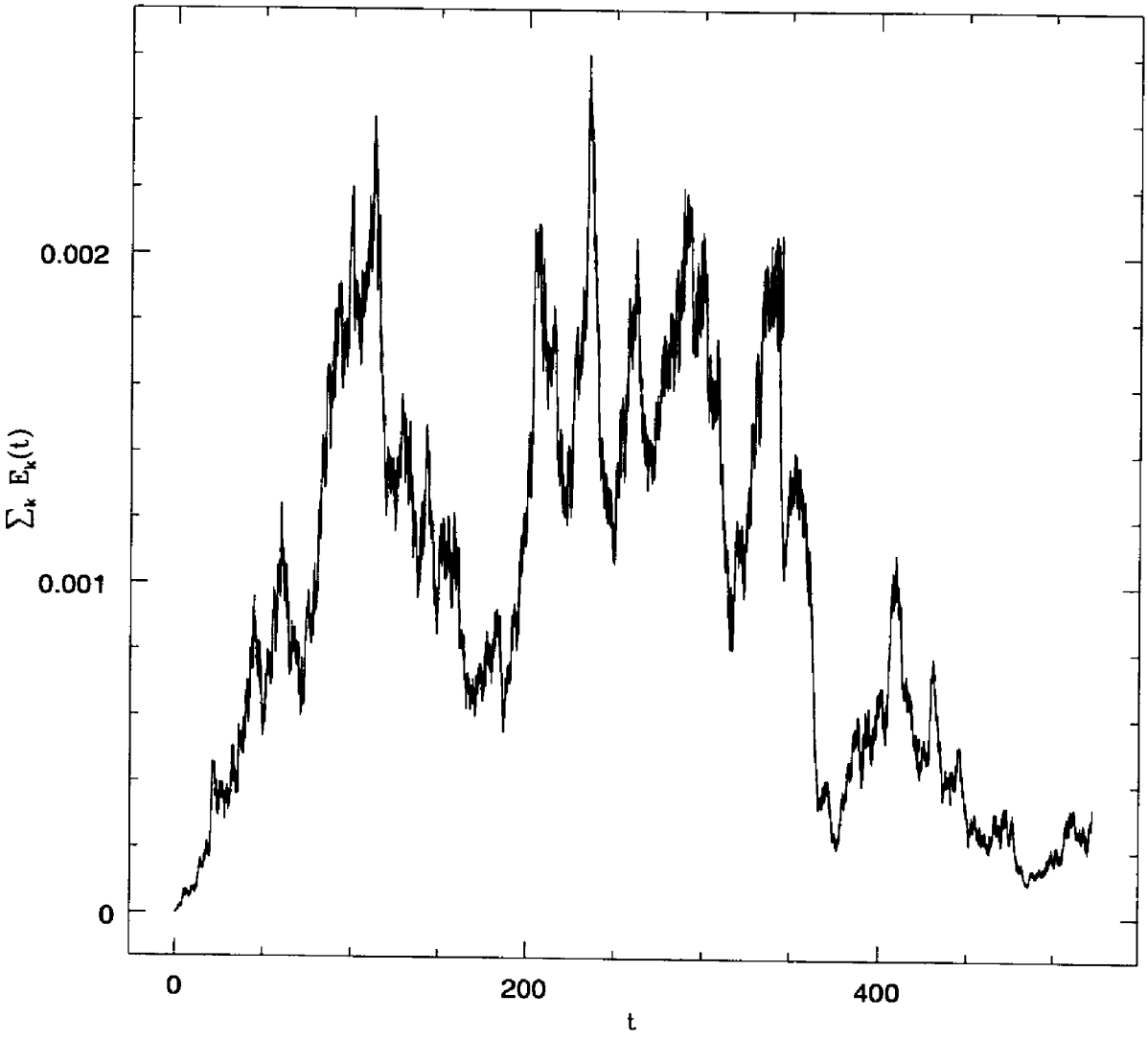


Figure 1.14: Total energy evolution in the large-scale forcing case.

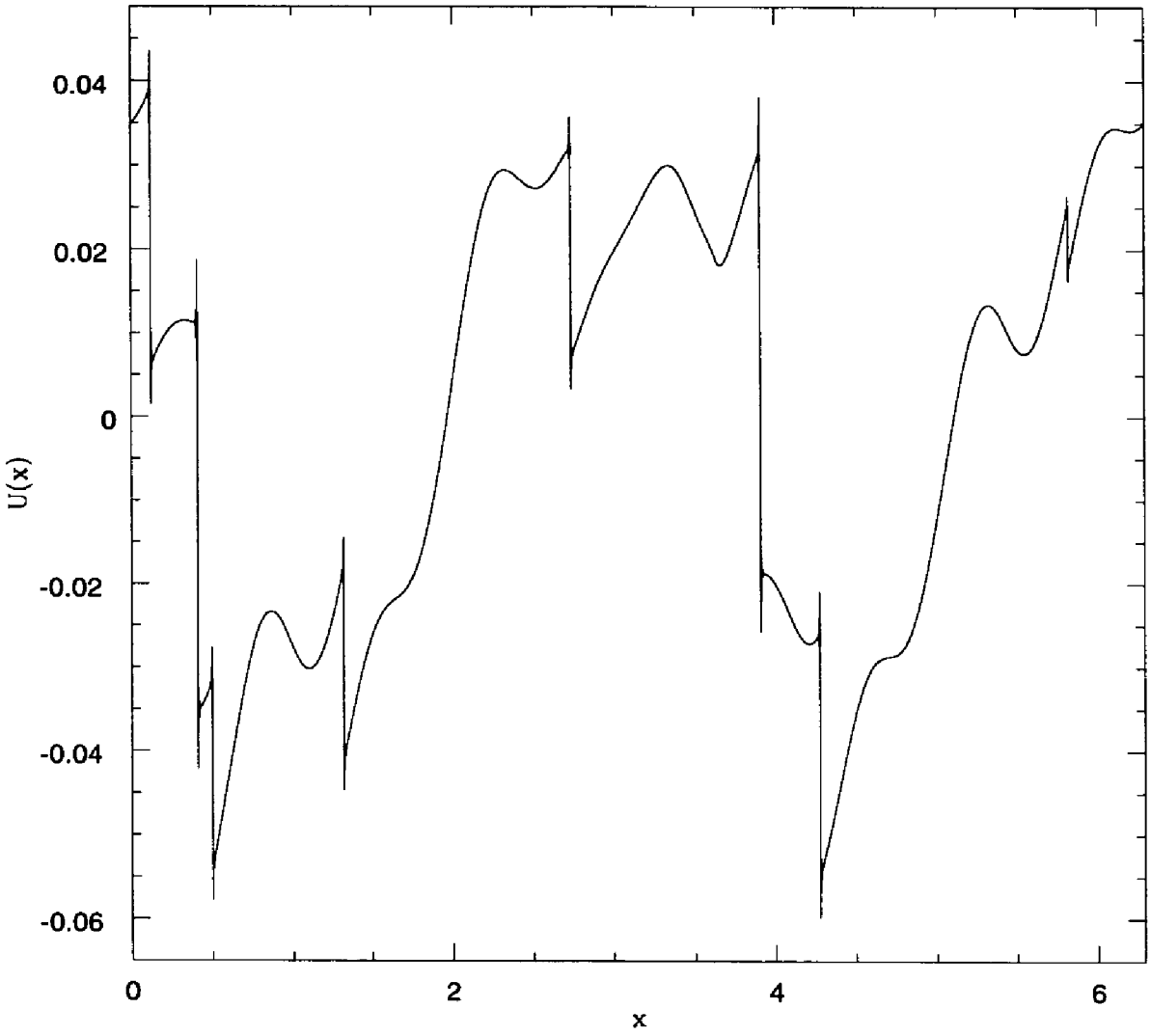


Figure 1.15: Physical space solution $u(x,t)$ at $t = 523$ in the large-scale forcing case.

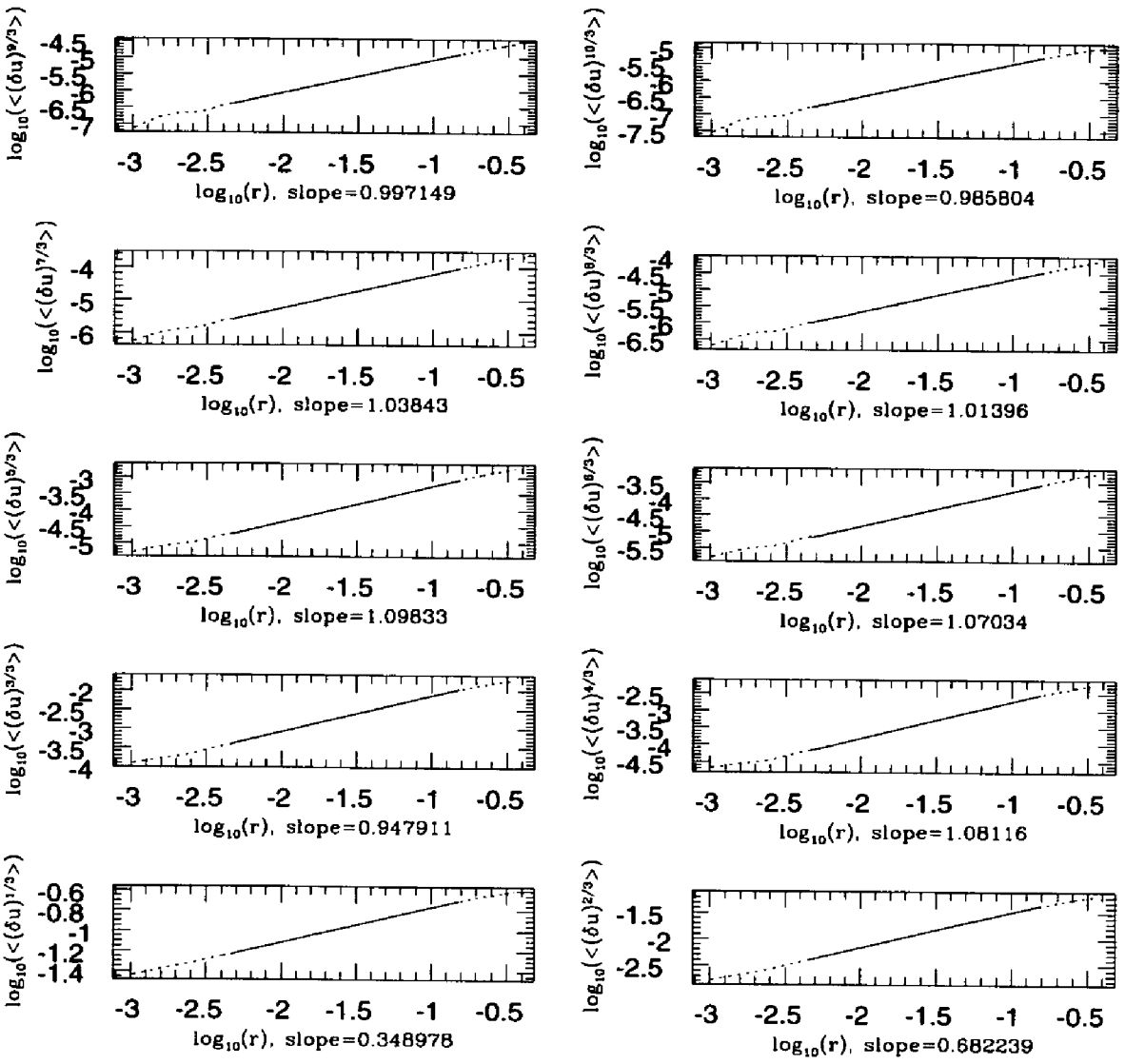


Figure 1.16: Velocity structure functions $\overline{|u(x+r,t)-u(x,t)|^p}$ for exponents $p = 1/3$, $2/3, \ldots, 10/3$ with least-square fits within the inertial range in the large-scale forcing case.

known (and we will show it in Section 1.6) that all cases with $y \leq -2$ are equivalent to the thermal equilibrium case $y = -2$ and thus form one universality class for this problem: $y \leq -2$ (which may be called *thermodynamic equilibrium turbulence*).

It is known that cases with $y \geq 2$ are statistically equivalent to the above considered case of the large-scale force (we have checked this, although we do not show the results of this here for brevity) and so forms a second universality class for this problem: $y \geq 2$ (which may be called *turbulence with strong large-scale structures*).

Also, as we have shown, the intermediate case with $y = 1$ is well described by the one-loop RG results and gives scaling in agreement with the prediction $\nu_E(y) = 1 - 2\epsilon/3 = -5/3$. It is of considerable interest whether this prediction also holds true for all other intermediate values of $y$: $y \in [-2, 2]$, for example for $1 < y < 2$. For example, the RG prediction gives $\nu_E(y = 3/2) = -2$. We compare this prediction here with the outcome of numerical simulation.

Results of calculations with resolution 12288, $Dt = 5 \times 10^{-5}$, $A_f = 2 \times 10^{-3}$, and $\nu_0 = 9 \times 10^{-4}$ are presented in Figs. 1.17 – 1.20. First, and most importantly, we observe from Fig. 1.17 that the energy spectrum exponent $\nu_E \neq -2$ but rather, is approximately $-1.88$, showing that, for forces with a correlation function steeper than $k^{-1}$, the exponent $\nu_E$ is smaller than the one given by the one-loop RG prediction. These and our other numerical results indicate that there may be no jump in the exponent at $y = 2$ at all, although this should be considered as a working hypothesis for now. Variations of the total energy with time presented in Fig. 1.18 for this case are different from the $y = 1$ case in that the amplitudes of fluctuations are larger, indicating that the effect of structures in the flow becomes even more pronounced. The physical space solution shown in Fig. 1.19, on the whole, resembles that in the $y = 1$ case with, possibly, greater contrast between the large-scale and random components. Scaling laws of velocity differences, depicted in Fig. 1.20, show that $\overline{U^p} \propto r^1$ starts approximately at $p \approx 2 - 2.3$.

The data presented here provides some evidence that the one-loop RG predictions are inapplicable to $y = 3/2$ and, possibly, for all $y > 1$ cases. Further numerical and theoretical studies of changes in the statistical properties of the system with variation

of $y$ are necessary.

## 1.5 One-Loop Renormalization Group (RG) Predictions

Further insight into the statistical properties of the Burgers equation may be obtained using the Renormalization Group (RG) approach. Although the validity of this approach is questionable even in higher dimensions, and it is even more questionable in one dimension, we feel necessary to present some results which complement the direct numerical simulations (DNS) and phenomenological theory discussed in Sections $1.1 - 1.4$.

### 1.5.1 Review of the RG Approach in Hydrodynamics

In this thesis the RG procedure will be used several times and we will review some of the basic philosophical issues of its application to hydrodynamics and the qualitative description of the necessary steps. Although in the next Section we will employ it for the Burgers equation, it should be understood that a similar philosophy is used in all other applications in Chapters $2, 3, 4$ and $5$.

Since the mid-60's, considerable progress has been achieved in the theory of critical phenomena through the use of the RG approach. The basis of the microscopic approach to the theory of phase transitions induced by large-scale fluctuations have been developed by K. Wilson [88]. Among the major features of his approach, which was given the name of the *renormalization group* approach, are: the subsequent reduction of the description to account for the large-scale fluctuations, scaling transformations of the field variables, a rather special diagrammatic technique, and an expansion in terms of a parameter $\epsilon$, where $d - \epsilon$ is a noninteger dimension [46]. At the present time, the RG approach is not only used in the theory of critical phenomena, but also successfully applied to many other physical problems. The fact that the behavior of a substance in the neighborhood of the phase transition (say, near the critical temper-

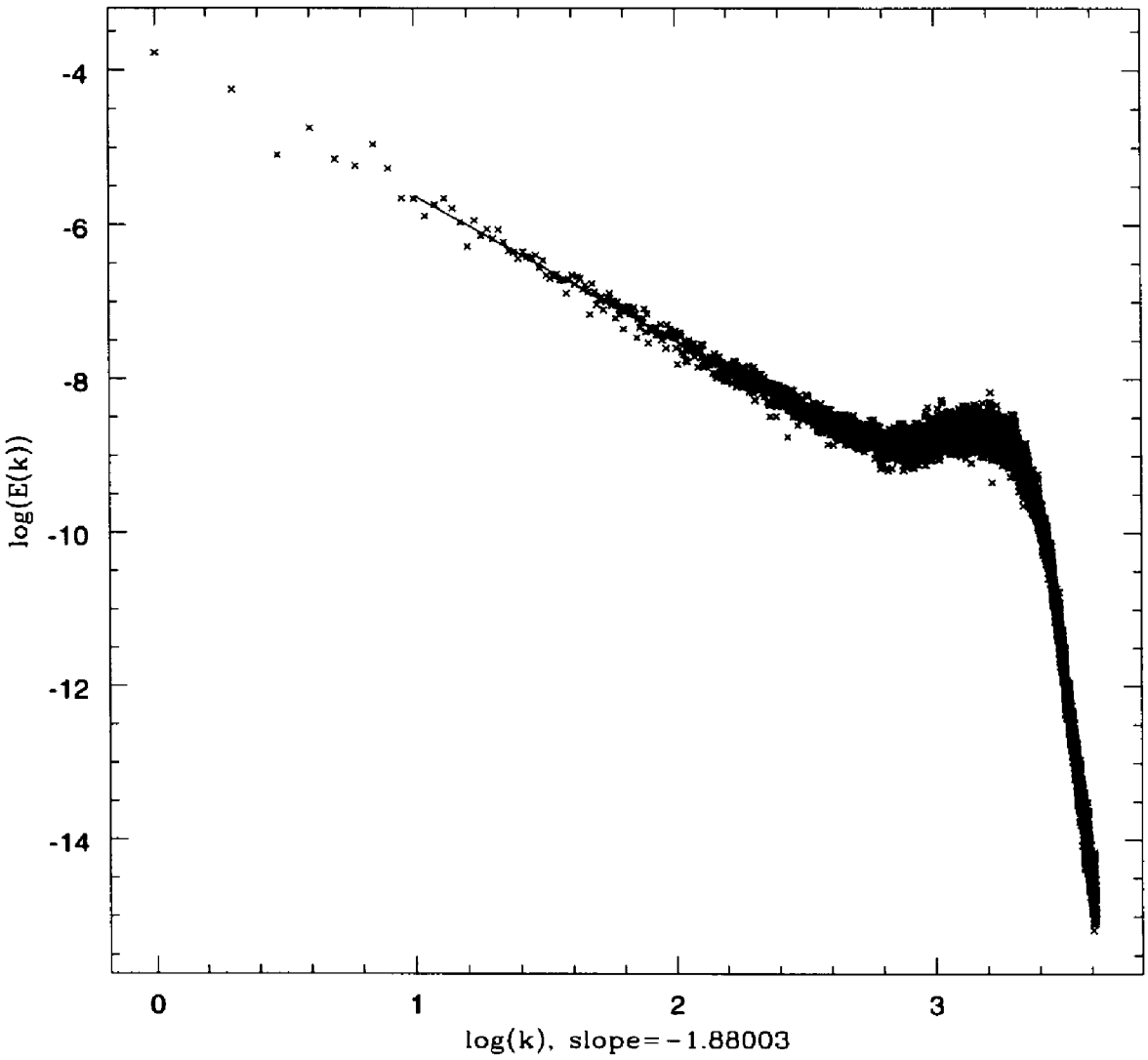


Figure 1.17: Energy spectrum in the case $y = 3/2$. Slope of the linear least-square fit is approximately equal to $-1.88$.

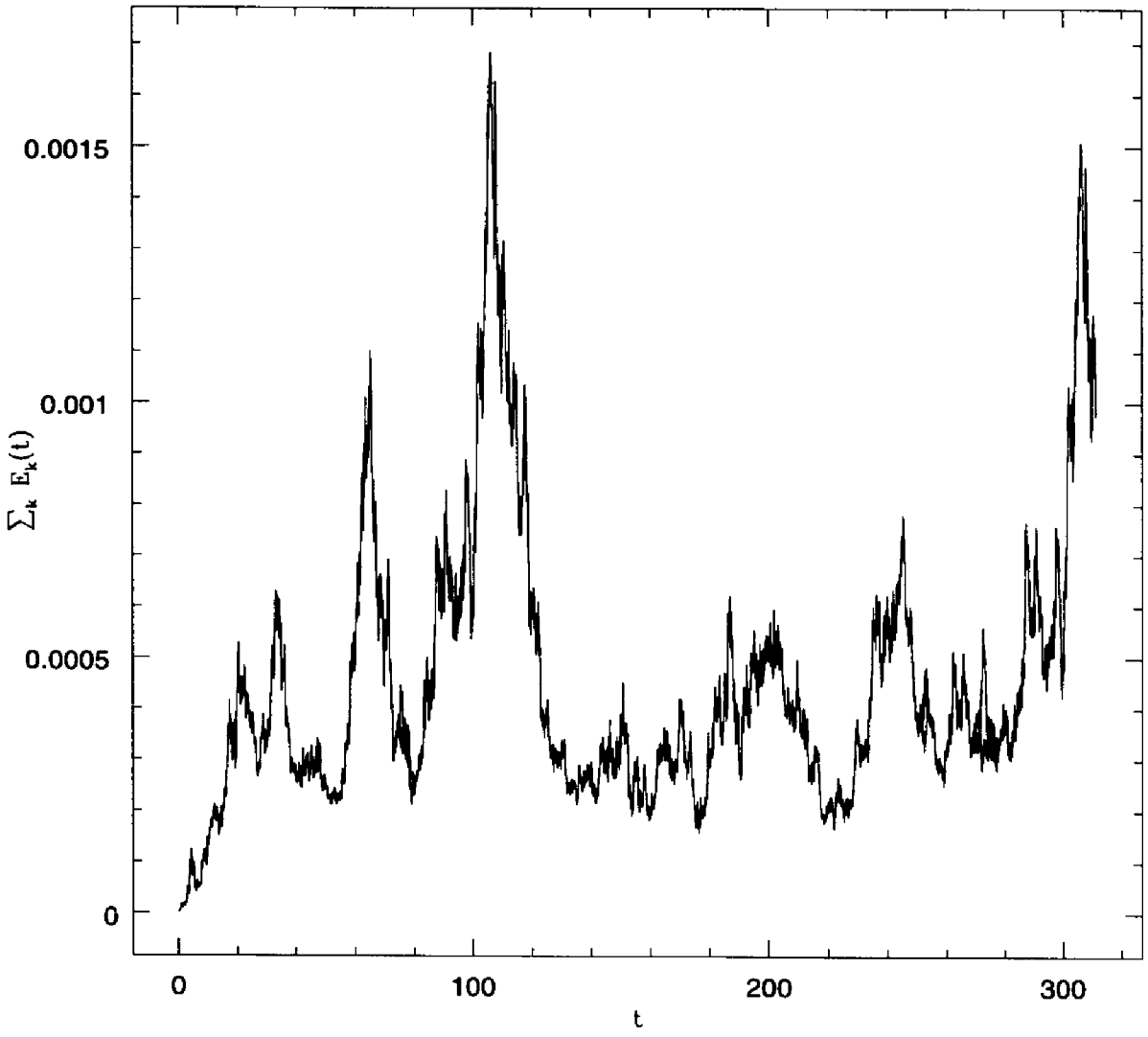


Figure 1.18: Total energy evolution in the case $y = 3/2$.

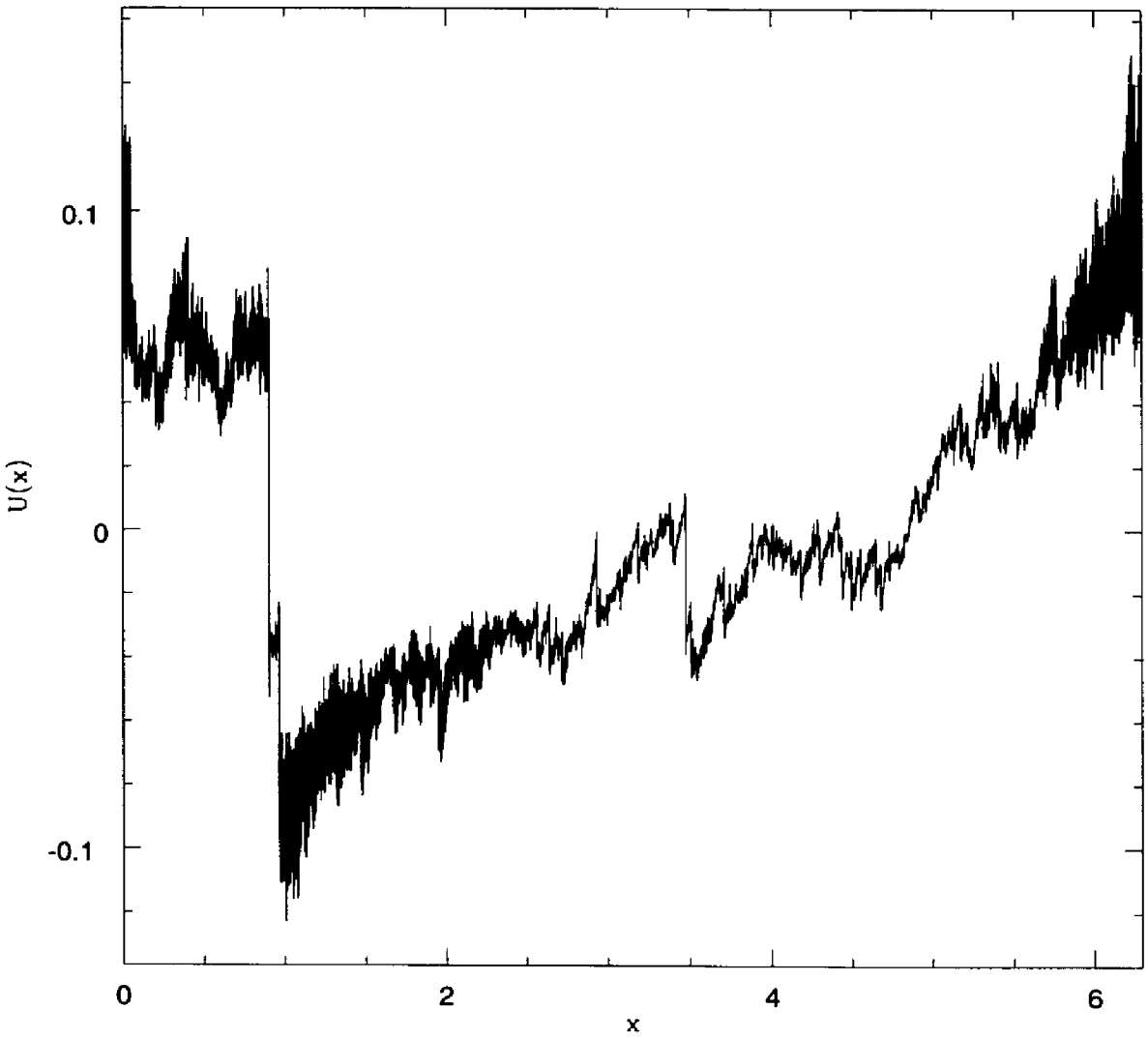


Figure 1.19: Physical space solution $u(x,t)$ at $t = 312$ for the case $y = 3/2$.

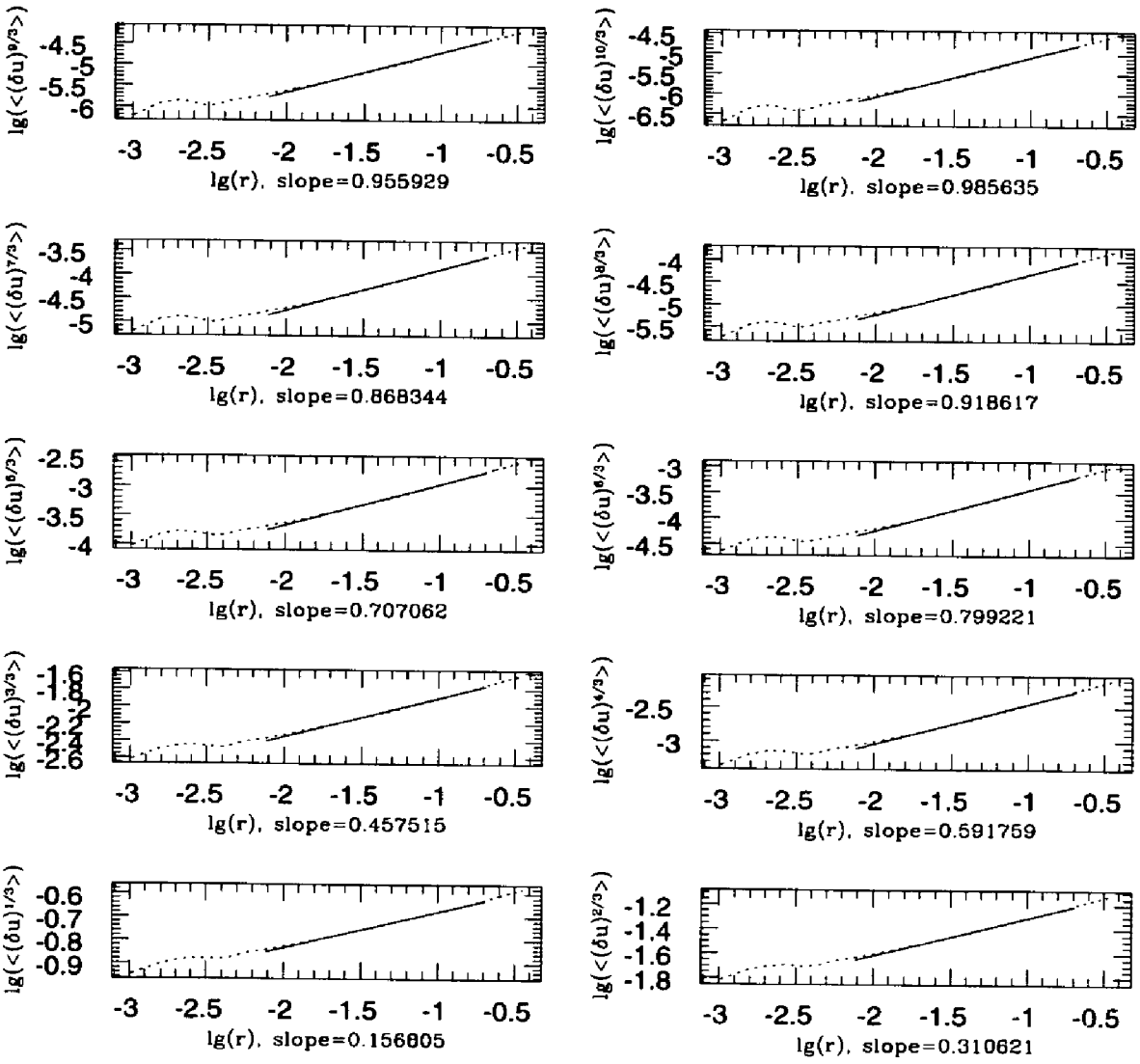


Figure 1.20: Velocity structure functions $\overline{|u(x+r,t)-u(x,t)|^p}$ for the powers $p = 1/3, 2/3, \ldots, 10/3$ with least square fits within the inertial range for the case $y = 3/2$.

ature) has many similarities to the behavior of a turbulent fluid has also been known for at least 20 years. These two classes of phenomena share at least one feature in common: their microscopic dynamics is very complicated and is governed by non-linear equations with an enormous number of degrees of freedom. At the same time in both cases the large-scale dynamics is considerably simpler; with good accuracy it may be described by the linear Langevin equation. Therefore, multiple attempts have been undertaken to apply a statistical theory such as RG to describe large-scale fluid turbulence properties.

It has come forward that the turbulence problem is more subtle and its dynamical effects are very important; whereas the dynamic version of the RG approach was not well established. Therefore it became obvious that the RG approach should evolve through substantial modifications and new developments in methodology to satisfy the needs specific to fluid turbulence. This may be one of the reasons why RG applications in hydrodynamics have been substantially less successful than in the theory of critical phenomena. At the same time it is understood that the RG approach may and does give new important information about turbulence properties. Multiple examples of this fact, which will be referenced in what follows, are provided in Refs. [16, 18, 95, 50, 93, 94, 13, 84, 20, 78, 79].

Here we will employ in detail only one particular version of the RG transformation, namely the one in wavenumber space.

First, one basic modification of conventional turbulence is necessary: the introduction of the stirring force [16]. This is a requirement of the theory which is not directly related with the concrete physical source of turbulence: we formally will study properties of turbulence induced by this force and not by some complicated boundary conditions or other sources. The basis for this is the so-called *correspondence principle* [16, 93] which may be expressed as the existence of a correspondence between real-life turbulent situations and situations with the force, if scales far removed from the largest (energy supplying) scale are considered. On such scales one can consider that the real cause of turbulence may be replaced with an effective large-scale force acting on the system. The relationship of the large-scale force with the power-law

correlation function considered here has been addressed in some detail in [51].

An important requirement of finiteness of energy in the system calls for the introduction of the *ultra-violet cut-off* wavenumber, which may be associated approximately with the inverse dissipative scale. At the initial step the governing system of equations (Navier-Stokes, for example) is called the *bare* system and all the entering parameters (like the viscosity coefficient) are called *bare* parameters. As in the theory of critical phenomena, the RG transformation should be defined in such a way that it gradually reduces the number of degrees of freedom in the system, leaving the most important ones which determine the dynamics. On physical grounds we assume that most practically interesting situations of strong turbulence are determined by the large-scale fluctuations.

The role of small-scale fluctuations is two-fold: averaging over them leads to the corrections to the parameters of the system (such as the viscosity or the force amplitude) and in this sense they are important. On the other hand, it is assumed that their action may totally be replaced with thus-altered parameters of the system, and in this sense they are irrelevant and may be fully eliminated from the system. This causes the RG transformation to gradually remove (average out) the fastest and the smallest modes from the system. Such procedure may be done in a variety of ways, one of which is employed in this thesis and in many other cited references. This process, which is called a wavenumber *shell-elimination*, may deal with a finite width shell or infinitesimally small width shell, depending on the particular situation. The shell is defined as a region in wavenumber space which is bounded by the ultra-violet cut-off wavenumber and another smaller *movable cut-off* wavenumber. Any field variable, such as velocity $u(\vec{k})$ or forcing $f(\vec{k})$, corresponding to the small-scale modes from within the shell is denoted as $u^{>}(\vec{k})$ or $f^{>}(\vec{k})$. The shell elimination itself is defined as averaging of the equation of motion, in which the fast and small-scale modes $u^{>}(\vec{k})$ have been totally eliminated, over the noise $f^{>}(\vec{k})$, the statistics of which is assumed known. Infinitesimal shell-elimination, as we will illustrate below, is analytically more attractive: it leads to differential recursion relations, which are easier to analyze. Finite-step shell-elimination is what one should expect normally

and it leads to difference recursion relations. Some particular details of the procedure will be described in several concrete applications below.

Each step of the shell-elimination in the nonlinear equation of the Navier-Stokes type leads to an infinite number of terms in the averaged equation. The RG procedure has a special language for the classification and accounting of the terms that arise, based on the diagrammatic technique [90] similar to the one developed by Feynman. This technique dramatically simplifies the analysis.

Another essential step in the original RG theory is the *stretching transformation*, which, after the shell has been eliminated, restores the size of the Fourier space to the original one. By means of this step the problem is formally almost reduced to the initial one, except for the changed (*clothed*) entering parameters (viscosity and others). Although in the first applications of the RG approach to the turbulence problem the stretching transformation has been unchanged, it was understood later [18, 93] that the elimination of this constraint will lead to the *clothed* viscosity having the well-known physical meaning associated with the *turbulent* or *eddy viscosity*.

The evolution of the governing system of equations under the RG transformation may be mapped into the *RG phase space* motion, that is, into the evolution of parameters like viscosity as the number of steps of applying the transformation grows.

The central point of the RG theory is a notion of a *fixed point*. As in the theory of critical phenomena, the basic assumption is that if the RG transformation is defined correctly, then the fixed points of the recursion relations should correspond to some physically relevant states of the system. To find the fixed points of a given system under thus-defined RG transformation is the goal of the RG theory. Knowing the fixed-points and the behavior of the solutions to the recursive relations in the neighborhood of the fixed-points for strongly turbulent situations turns out not to depend on such microscopic parameters as the bare viscosity but to be determined by the character of nonlinear interaction, which is in perfect agreement with what may be expected for real-life turbulence.

The notion of the fixed point naturally leads to the notion of *universality* and *universality classes*. Universality simply means that the physically relevant fixed-

points should not depend on the *bare* parameters of the system. Also, all the fixed-points may be classified into several classes which correspond to some completely different physical properties (such as the symmetry with respect to a transformation).

Another central notion in the RG approach which was first introduced by Wilson [88], is the notion of the *relevant* and *irrelevant* parameters. This notion forms a solid basis under any RG analysis. The definition of *irrelevant* parameter may be given as follows. Consider a parameter, say, fourth-order (hyper-) viscosity added to our system. Apply the RG approach to thus-extended system and solve for the fixed-points. If it turns out that the fixed-points do not depend on this new parameter, it is called *irrelevant* for this system. Any other parameters are called *relevant* and namely on their basis the major large-scale and long-time statistical properties of the system are determined. On the basis of several examples considered in what follows and results of [50, 16, 93], we can make conclusion that the normal viscosity coefficient, normal (nonthermal) force amplitude always are relevant parameters for the Navier-Stokes-type systems. Thermal noise may become relevant in two dimensions. It is always a requirement of any RG approach to check is there are no other relevant parameters in the system.

These are the essential notions and steps of the RG approach applied to fluid dynamics. The RG theory has been applied not only to the Navier-Stokes equations but to other physically important statements having relevance to fluid motions with extremely large number of degrees of freedom. For more details of the RG procedure we direct the reader to the cited literature.

Here we will use the dynamic RG transformation based upon perturbation theory and the $\epsilon$-expansion. We will consider one-dimensional and $d$-dimensional cases separately: the one-dimensional case is presented in detail, whereas results for the $d$-dimensional case are given concisely in the form of final results.

### 1.5.2 The One-Dimensional Burgers Equation

**General Statement and Notations.** We begin by stating the problem in the physical space. Consider the one-dimensional Burgers equation

$$u_t + u\,u_x = \nu_0\,u_{xx} + f \tag{1.18}$$

to be studied for all real $x$ and $t$. Consider the space-time Fourier transform defined as

$$\begin{aligned} u(k,\omega) &= \int_{-\infty}^{+\infty}\int_{-\infty}^{+\infty} u(x,t)\,e^{i(\omega t - k x)}\,dx\,dt, \\ u(x,t) &= \int_{-\infty}^{+\infty}\int_{-\infty}^{+\infty} u(k,\omega)\,e^{i(-\omega t + k x)}\,\frac{dk}{2\pi}\,\frac{d\omega}{2\pi}. \end{aligned} \tag{1.19}$$

We will use the Fourier-space $\delta$-function defined as

$$\int_p F(p)\,\delta(k-p)dp = F(k).$$

In Fourier space, the basic equation becomes

$$\begin{aligned} u(k,\omega)\,(-i\,\omega + \nu_0\,k^2) &= f(k,\omega) - \\ -\frac{i\,k}{2\,(2\pi)^2}\int\int u(p,\psi)\,u(k-p,\omega-\psi)\,dp\,d\psi. \end{aligned} \tag{1.20}$$

We begin by introducing convenient notations for 2-vectors: $\tilde{k} = \{k,\omega\}$, $\int\int dk\,d\omega = \int d\tilde{k}$; for the vertex operator: $A(k) = -i\,k/(2\,(2\pi)^2)$; and for the bare Green's function: $G^0(\tilde{k}) = (-i\,\omega + \nu_0\,k^2)^{-1}$. Sometimes, when it does not lead to misunderstanding, we will use $k$ instead of $\tilde{k}$ for simplicity. We further denote by $\_ \circ \_(\tilde{k})$ the convolution procedure $\int \_(\tilde{p})\_(\tilde{k}-\tilde{p})\,d\tilde{p}$.

The force is assumed to be white-noise in time and a Gaussian random function in space, specified by its second-order correlation function

$$\langle f(\tilde{p}) f(\tilde{q})\rangle = 2\,(2\pi)^2\,D(p)\,\delta(\tilde{p}+\tilde{q}). \tag{1.21}$$

In what follows, we assume

$$D(p) = D_0\,|p|^{-y} + T_0\,|p|^2\,, \tag{1.22}$$

where $D_0$ is the bare amplitude of the normal forcing and $T_0$ is the thermal noise amplitude, which is generated entirely by the RG-transformation, so that $T_0 = 0$.

Another parameter of interest, also generated through the application of the RG, is the coupling constant $\lambda$. We formally introduce it by inserting $\lambda_0 = 1$ into the basic equation

$$u = G^0 f + \lambda_0 G^0 A(u \circ u). \tag{1.23}$$

The parameter $\lambda_0$ carries no physical dimension and is introduced primarily to simplify accounting for the diagrams. We also introduce a cutoff wavenumber into our system: $\Lambda_d$, assuming that all variable quantities of the $u(\tilde{k})$-type will become zero whenever $k \geq \Lambda_d$. This parameter plays the role of the dissipative cutoff in real systems.

**Viscosity correction.** The term in the perturbation series which gives rise to a correction to the viscosity has the known [16, 93, 95] form

$$4\,\lambda_0^2\, G^0(k)\, A(k) \int_{\tilde{p}} G^0(p)\, A(p)\, G^0(k-p)\, f^>(k-p) \int_{\tilde{q}} u^<(q)\, G^0(p-q)\, f^>(p-q)\, d\tilde{q}\, d\tilde{p}. \tag{1.24}$$

Using it, the correction to the viscosity can be constructed

$$\delta\nu = -\frac{4\,2\,(2\pi)^2\,\lambda_0^2\,A(k)}{k^2} \int_{\tilde{p}} \left|G^0(p)\right|^2\, G^0(k-p)\, A(k-p)\, D(p)\, d\tilde{p}. \tag{1.25}$$

In the limit $\omega \to 0$ the frequency integration gives

$$\delta\nu = -\frac{4\,2\,(2\pi)^2\,\pi\,\lambda_0^2}{k^2\,\nu_0^2}\, A(k) \int_p \frac{D(p)\, A(k-p)}{p^2\,\left(p^2 + (k-p)^2\right)}\, dp. \tag{1.26}$$

Substitution for $A(k)$ and the change of variable $p \to p + k/2$ leads to

$$\delta\nu = -\frac{\lambda_0^2}{4\,\pi\,\nu_0^2}\,\frac{1}{k} \int_{p\in\Omega'} \frac{\left\{D_0\,\left|p+\frac{k}{2}\right|^{-y} + T_0\,\left(p+\frac{k}{2}\right)^2\right\}\,\left(p-\frac{k}{2}\right)}{\left(p+\frac{k}{2}\right)\,\left(p^2+\frac{k^2}{4}\right)}\, dp, \tag{1.27}$$

with the integration region

$$\Omega' = \left\{p : \Lambda \leq \left|p+\frac{k}{2}\right| \leq \Lambda - \delta\Lambda,\ \Lambda \leq \left|p-\frac{k}{2}\right| \leq \Lambda - \delta\Lambda\right\}. \tag{1.28}$$

Performing the integration in the limits $k \to 0+$, $\delta\Lambda \to 0-$ one obtains

$$\delta\nu = -\frac{\lambda_0^2}{4\,\pi\,\nu_0^2}\,\frac{(D_0\,\Lambda^{-y-2}\,(y+3)+T_0)}{\Lambda}\,\frac{\delta\Lambda}{\Lambda}. \tag{1.29}$$

**Force correction.** The term leading to the corrections $\delta D_0$ and $\delta T_0$ describes the zero-mean correction to the bare force

$$\delta f^<(k) = \lambda_0\,A(k)\int_{\tilde{p}} G^0(p)\,G^0(k-p)\,f^>(p)\,f^>(k-p)\,d\tilde{p}. \tag{1.30}$$

Its correlation function, using Wick's theorem and after integration over frequency, turns out to be

$$\langle\delta f^<(k_1)\,\delta f^<(k_2)\rangle = \frac{2\pi\,\lambda_0^2}{\nu_0^3}\,k_1^2\,\delta(k_1+k_2)\int_{p\in\Omega}\frac{D(p)\,D(k_1-p)}{p^2\,(k_1-p)^2\,(2p^2+k_1^2-2k_1p)}\,dp \tag{1.31}$$

with the integration region

$$\Omega = \{p : \Lambda \le |p| \le \Lambda-\delta\Lambda,\ \Lambda \le |p-k| \le \Lambda-\delta\Lambda\}. \tag{1.32}$$

Finally, taking the integral in (1.31) in the limits $k \to 0+$, $\delta\Lambda \to 0-$, yields

$$\langle\delta f^<(k_1)\,\delta f^<(k_2)\rangle = -\frac{2\pi\,\lambda_0^2}{\nu_0^3}\,k_1^2\,\delta(k_1+k_2)\,\frac{(D_0\,\Lambda^{-y-2}+T_0)^2}{\Lambda^2}\,\delta\Lambda. \tag{1.33}$$

This, in turn, leads to the following corrections to the force amplitudes

$$\begin{aligned}\delta D_0 &= 0,\\ \delta T_0 &= -\frac{\lambda_0^2}{4\pi\,\nu_0^3}\,\frac{(D_0\,\Lambda^{-y-2}+T_0)^2}{\Lambda^2}\,\delta\Lambda.\end{aligned} \tag{1.34}$$

This gives us the correction to the force correlation function amplitude: $\delta D(k) = \delta T_0\,k^2$.

**Stretching transformation.** Now, after the infinitely thin shell of wavenumbers has been removed, the intermediate Burgers equation becomes

$$\begin{aligned}u^<(k,\omega)\,\left(-i\,\omega+(\nu_0+\delta\nu_0)\,k^2\right) &= (f^<(k,\omega)+\delta f^<(k,\omega))+\\ &+A(k)\int_{\tilde{p}}(\lambda_0+\delta\lambda_0(p))\,u^<(p,\psi)\,u^<(k-p,\omega-\psi)\,dp\,d\psi+\\ +2\lambda_0^2A(k)\int_{\tilde{p}}u^<(\tilde{p})\,G^0(\tilde{k}-\tilde{p})\,A(k-p)\int_{\tilde{q}}u^<(\tilde{q})\,u^<(\tilde{k}-\tilde{p}-\tilde{q})\,d\tilde{q}\,d\tilde{p}&+\\ &O(\lambda_0^3),\end{aligned} \tag{1.35}$$

with the corrected force correlation function

$$\langle \left(f^<(\tilde{k_1}) + \delta f^<(\tilde{k_1})\right) \left(f^<(\tilde{k_2}) + \delta f^<(\tilde{k_2})\right) \rangle = \\ = 2\,(2\pi)^2\,\delta(\tilde{k_1} + \tilde{k_2})\,\left(D(k_1) + \delta D(k_1)\right). \tag{1.36}$$

For reasons discussed in detail in [16, 93], we disregard $\delta\lambda_0(k)$, using the fact that it actually is irrelevant in the limit $\Lambda \to 0+$, $k \to 0+$ (in the Wilson [88] and Ma [46] sense). The last term in (1.35) contains triple nonlinearity in $u^<$, the only term in the perturbation series of order $\lambda_0^2$.

We apply the following group of stretching transformations to the above problem (1.35) – (1.36)

$$k \to k\,e^{-r},\ \omega \to \omega\,e^{-\alpha r},\ u \to u\,e^{-\beta r},\ \text{with}: \\ r = -\frac{\delta\Lambda}{\Lambda},\ \alpha = \alpha(\epsilon),\ \beta = \beta(\epsilon). \tag{1.37}$$

Together with the averaging over $k \in [\Lambda, \Lambda - \delta\Lambda]$, this corresponds to the linear renormalization semi-group in the sense of Ma [46].

The variables of interest are then rescaled as follows

$$\nu \to \nu\,e^{(\alpha-2)r},\ f \to f\,e^{-(\alpha+\beta)r},\ \lambda \to \lambda\,e^{-(2+\beta)r}, \\ D_0 \to D_0\,e^{(3\alpha+2\beta+\epsilon-2)r},\ T_0 \to T_0\,e^{(3\alpha+2\beta-1)r}, \tag{1.38}$$

where we have introduced the parameter $\epsilon = 3 + y$.

Using these rescaling relations and the above corrections to the dimensional constants of our system, we can perform the above procedure an infinite number of times, yielding the following differential recursion relations for the dimensional parameters

$$-\frac{\partial \log \nu}{\partial \log \Lambda} = \epsilon g + h + \alpha - 2, \\ -\frac{\partial \log \lambda}{\partial \log \Lambda} = -2 - \beta, \\ -\frac{\partial \log D}{\partial \log \Lambda} = 3\,\alpha + 2\,\beta + \epsilon - 2, \\ -\frac{\partial \log T}{\partial \log \Lambda} = h\,\left(\frac{g}{h} + 1\right)^2 + 3\,\alpha + 2\,\beta - 1, \tag{1.39}$$

where we have used the following nondimensional combinations (Reynolds numbers)

$$g = \frac{D\,\lambda^2}{4\pi\,\nu^3\,\Lambda^\epsilon},\ h = \frac{T\,\lambda^2}{4\pi\,\nu^3\,\Lambda}. \tag{1.40}$$

From these equations, relations for the nondimensional coupling constants $g$ and $h$ can be constructed:

$$\begin{aligned} \frac{\partial \log g}{\partial \log \Lambda} &= 3\,(\epsilon\,g + h) - 2\,\epsilon, \\ \frac{\partial \log h}{\partial \log \Lambda} &= 3\,(\epsilon\,g + h) - 2 - \frac{1}{h}(g+h)^2. \end{aligned} \tag{1.41}$$

Simple analysis leads to the following statement for the above system: *for* $\forall\epsilon$ *the trivial fixed point of* (1.41) *is unstable to infinitesimal perturbations as* $\Lambda \to 0+$. Indeed, the solution of the linearized system (1.41) in this case is

$$\{g, h\} = C_1\,\vec{e}_1\,\Lambda^{-2\epsilon} + C_2\,\vec{e}_2\,\Lambda^{-2} \to \infty \text{ as } \Lambda \to 0+, \tag{1.42}$$

where $\vec{e}_1$ and $\vec{e}_2$ are eigenvectors. This leads to the conclusion that no stable basic solution exists upon which the $\epsilon$-expansion may be built. Exact solutions of (1.41) for two particular values of $\epsilon = 0, 1$ illustrate this. In the case $\epsilon = 0$

$$\epsilon\,g + h = \frac{2}{3 - C_1\,\Lambda^2} \to \frac{2}{3}, \tag{1.43}$$

and for the case $\epsilon = 1$ $(y = -2)$

$$g = \frac{C_2\,\Lambda}{(1 + C_1\,\Lambda^2)^{C_1 + \frac{1}{2}}},\quad g + h = \frac{1}{1 + C_1\,\Lambda^2} \to 1,\ \text{as } \Lambda \to 0+, \tag{1.44}$$

where $C_1$ and $C_2$ are arbitrary constants.

Now we can also consider the separate *universality classes* $y < -2$ and $y > -2$, where (1.41) can be simplified by letting $g = 0$ and $h = 0$, respectively.

In the case $y < -2$ (thermal noise dominates) we have a solution for $h$

$$h(\Lambda) = \frac{1}{1 + \frac{1 - h_0}{h_0}\left(\frac{\Lambda}{\Lambda_0}\right)^2}, \tag{1.45}$$

satisfying $h(\Lambda_d) = h_0$. It is easy to see that $\lim_{\Lambda \to 0+} h(\Lambda) = 1$.

If $y > -2$ (external force dominates), we similarly have

$$g(\Lambda) = \frac{2}{3 + \frac{2-3g_0}{g_0}\left(\frac{\Lambda}{\Lambda_0}\right)^{2\epsilon}}, \tag{1.46}$$

such that $g(\Lambda_d) = g_0$. It is also easy to see that $\lim_{\Lambda\to 0+} g(\Lambda) = 2/3$ in this case.

The conclusion which can be drawn from this analysis is as follows. *The truncation of the diagrammatic series is not justified by the smallness of the limiting couplings.* Therefore, strictly speaking, the whole diagrammatic series should be taken into account in the corrections.

**Use of the One-Loop Results.** Despite the fact that the limiting couplings are not small, we will try to employ the one-loop results as if they were obtained self-consistently, in the hope that summation of all the diagrammatic corrections will not change the scaling law predictions which follow from the one-loop approximation.

Assume now that the scale-elimination is performed without subsequent stretching. Then, from (1.39), we have $D(\Lambda) = D_0$, $\lambda(\Lambda) = \lambda_0$. For $y > -2$ we then obtain for the eddy-viscosity

$$\nu(\Lambda) = \left\{\nu_0^3 + \frac{3\,D_0\,\lambda_0^2}{4\,\pi}\left(\Lambda^{-\epsilon} - \Lambda_d^{-\epsilon}\right)\right\}^{\frac{1}{3}}. \tag{1.47}$$

This gives us the asymptotic $\Lambda \to 0+$ behavior

$$\nu(\Lambda) \propto \left(\frac{3\,D_0\,\lambda_0^2}{4\,\pi}\right)^{\frac{1}{3}} \Lambda^{-\frac{\epsilon}{3}}. \tag{1.48}$$

For $y \leq -2$ one accordingly has

$$\nu(\Lambda) = \left\{\nu_0^2 + \frac{T_0\,\lambda_0^2}{2\,\pi\,\nu_0}\left(\Lambda^{-1} - \Lambda_d^{-1}\right)\right\}^{\frac{1}{2}},$$
$$T(\Lambda) = \frac{T_0}{\nu_0}\,\nu(\Lambda), \tag{1.49}$$

with the asymptotic $\Lambda \to 0+$ behavior

$$\nu(\Lambda) \propto \left(\frac{T_0\,\lambda_0^2}{2\,\pi\,\nu_0}\right)^{\frac{1}{2}} \Lambda^{-\frac{1}{2}}. \tag{1.50}$$

The results (1.48), (1.50) may be physically motivated as follows. In the case when the energy is pumped into the system primarily at the large scales, the turbulent viscosity turns out not to depend on the bare viscosity, and the nontrivial scaling law is determined by the exponent of the correlation function of the applied force. In the case when the energy is supplied at small scales (at the "molecular" level), it appears that the turbulent viscosity strongly depends on the bare viscosity and is independent of $y$. The second formula in (1.49), which has been obtained by direct computation of the first-loop corrections, can be shown to hold to all orders in $\lambda$ and is a manifestation of the *fluctuation-dissipation theorem* [16]. The fact that there is no smooth match between (1.48) and (1.50) at $\epsilon = 1$ shows that a phase transition occurs.

Following [16, 95], we can introduce the full $(k, \omega)$-dependent correlation function and compute it in the lowest order in the limiting coupling:

$$C(k,\omega) \equiv \int_{-\infty}^{+\infty} \int_{-\infty}^{+\infty} \frac{\langle u(k,\omega) u(k',\omega') \rangle}{2} \frac{dk'}{2\pi} \frac{d\omega'}{2\pi} = |G(k,\omega)|^2 \, D_0 \, |k|^{-y} \qquad (1.51)$$

such that the energy spectrum, defined as $\int_k E(k)\, dk = E_{tot}$-total energy, can be computed [58, 16] as

$$E(k) \equiv 2 \int_{-\infty}^{+\infty} C(k,\omega) \frac{d\omega}{(2\pi)^2} = \frac{D_0 \, |k|^{-y}}{2\pi \, \nu(k) \, k^2}. \qquad (1.52)$$

As was pointed out in [16, 18], if one assumes that all the modes higher than $k$ are removed ($\Lambda \to k+$), then $\nu(\Lambda) \approx \nu(k)$. For $y > -2$ this gives

$$C(k,\omega) = \frac{D_0 \, k^{3-\epsilon}}{\omega^2 + \left(\frac{3 D_0 \lambda_0^2}{4\pi}\right)^{\frac{2}{3}} k^{4-\frac{2}{3}\epsilon}}, \qquad (1.53)$$

and for $y \leq -2$:

$$C(k,\omega) = \frac{2}{\sqrt{\pi}} \frac{E_0^{\frac{3}{2}} \lambda_0 \, k^{\frac{3}{2}}}{\omega^2 + \frac{E_0 \lambda_0^2}{\pi} k^3}. \qquad (1.54)$$

Note that the present results with $\epsilon = y + 3$ taken for $\epsilon = 1$ precisely coincide with those in [16], which are obtained on the basis of $\epsilon$-expansion with $\epsilon = 2 - d$ where $d$ is the number of space dimensions.

Corresponding energy spectra can now be obtained. The result for $y > -2$ is

$$E(k) = \left(\frac{D_0^2}{6\pi^2\,\lambda_0^2}\right)^{\frac{1}{3}}\, k^{1-\frac{2}{3}\epsilon}, \tag{1.55}$$

and for $y \leq -2$ it is

$$E(k) = E_0 = \frac{T_0}{2\,\nu_0}. \tag{1.56}$$

By employing these results one can get an estimate for the Kolmogorov constant (by analogy with three-dimensional case) as follows. Define the energy flux-function $\mathcal{P}(k)$ as

$$\frac{d\mathcal{P}(k)}{dk} \equiv \mathcal{T}(k) \equiv -\frac{k\,\lambda_0}{4\,\pi}\int_{p=-\infty}^{+\infty} Im\left\{\langle u(p,t)u(k-p,t)u(-k,t)\rangle\right\}\,dp. \tag{1.57}$$

Then the stationary equation of motion implies the following relation for $\mathcal{P}(k)$

$$\mathcal{P}(\Lambda) = -2\,\nu_0\int_{k=\Lambda_0}^{\Lambda} k^2\,E(k)\,dk + \int_{k=\Lambda_0}^{\Lambda} Re\left\{\langle f(k,t)\,u(-k,t)\rangle\right\}\,dk, \tag{1.58}$$

considered in the limit $\Lambda_0 \to 0+$ if this limit exists. Consider the second integral first. For a white-in-time force one can show that

$$\langle u(-k,t')f(k,t)\rangle = \begin{cases} 0 & \text{if } t > t' \\ \langle f(-k,t)f(k,t)\rangle & \text{if } t < t' \\ \frac{\langle f(-k,t)f(k,t)\rangle}{2} & \text{if } t = t'. \end{cases} \tag{1.59}$$

Using this the second integral in (1.58) for $y = 1$ is equal to

$$D_0\,\log\left(\frac{\Lambda}{\Lambda_0}\right), \tag{1.60}$$

which does not depend on the shape of the energy spectrum (1.55), but only on the force correlation function. If $\nu_0$ is small enough, then the first integral in (1.58) is much smaller than the second for some $1 \sim \Lambda_0 \leq \Lambda \ll \Lambda_d$. Then the energy spectrum follows:

$$E(k) = C_K\left(\frac{\mathcal{P}(k)}{\log(k)}\right)^{\frac{2}{3}} k^{-\frac{5}{3}}, \quad C_K = \left(\frac{1}{6\,\pi^2}\right)^{\frac{1}{3}} \approx 0.257. \tag{1.61}$$

### 1.5.3 $d$-Dimensional Case

Here we briefly consider some details of the $d$-dimensional RG for the randomly stirred Burgers equation

$$\frac{\partial \vec{u}}{\partial t} + \lambda_0 \, (\vec{u}, \nabla) \, \vec{u} = \nu_0 \, \Delta \vec{u} + \vec{f}. \tag{1.62}$$

Here all vectors are considered to have $d$ Cartesian coordinates, e.g., $\vec{x} = \{x_1, \ldots, x_d\}$. We will limit ourselves to consideration of potential flows, that is,

$$\exists \, \varphi : \quad u_i = \frac{\partial \varphi}{\partial x_i}, \; \forall \, i = 1, 2, \ldots, d, \tag{1.63}$$

which leads to a rotational symmetry of the diagrams because the governing equation may be presented in Fourier space as

$$u_j(k) = G^0(k) \, f_j(k) - \frac{i \, \lambda_0 \, k_j \, G^0(k)}{2 \, (2\pi)^{d+1}} \int_p u_l(p) \, u_l(k-p) \, dp, \tag{1.64}$$

where the bare propagator is defined as $G^0(k) = (-i\,\omega + \nu_0 \, k^2)^{-1}$. If one does not impose the potentiality condition, then the diagrammatic technique is more complicated and second-viscosity effects appear, which seems to be an undesirable complication in this study. Also, the introduction of the velocity potential allows one to avoid dealing with the *curl* operator in $d$-dimensions. For more information on the Navier-Stokes/Burgers equation statements in multiple dimensions and approaches other than RG, consider [17, 19].

From the potentiality of the solution $\vec{u}$ the potentiality of the force $\vec{f}$ follows. Therefore the force is defined as the white-in-time Gaussian random vector function with the second-order correlation function

$$\langle f_j(\vec{k}, \omega) \, f_l(\vec{k'}, \omega') \rangle = 2 \, D_0 \, (2\,\pi)^{d+1} \, k_j \, k_l \, \left|\vec{k}\right|^{-2-y} \, \delta(\vec{k} + \vec{k'}) \, \delta(\omega + \omega'). \tag{1.65}$$

As before, we will omit vector signs, using notations of the type $k = \{\vec{k}, \omega\}$ for brevity. Sometimes, when it does not lead to a misunderstanding, we use $k = \left|\vec{k}\right|$.

**$O(u^< u^<)$-diagrams.** Omitting the lengthy derivations, we will just show the final result of the lowest-order (first-loop) term in the perturbation series for $u_j^<(k)$. For

details, consult references [16, 93]. After the finite shell elimination the result is

$$-\frac{\lambda_0^2 D_0}{\nu_0^2}\frac{S_d}{(2\pi)^d}\frac{(4+y-d)}{4d}k_j\,k_m\,u_m^<(k)\frac{\left(\Lambda_d^{-4-y+d}-\Lambda^{-4-y+d}\right)}{-4-y+d}. \tag{1.66}$$

Here $S_d = 2\pi^{d/2}/\Gamma(d/2)$ is the surface area of $d$-dimensional sphere with unit radius. Using the identity $\nabla(\nabla,\vec{u}) = \Delta\vec{u}+[\nabla,[\nabla,\vec{u}]]$, which holds in $d$-dimensions, this leads to the viscosity correction. The resulting viscosity recursion relation is

$$\frac{\partial\log\nu}{\partial\log\Lambda} = -g\,\epsilon\,a(d), \tag{1.67}$$

where: $\epsilon = 4+y-d$, $a(d) = 1/(2^{d+1}\,d\,\pi^{d/2}\,\Gamma(d/2))$; and $g = \lambda^2 D/(\nu^3\,\Lambda^\epsilon)$ is a nondimensional coupling constant.

**$O(1)$-diagrams.** We recall that such terms lead to force amplitude corrections. Denoting the lowest-order correction to the force as $\tilde{f}$, the result of its correlation function calculation will be

$$\langle\tilde{f}_j(k)\,\tilde{f}_m(k')\rangle = -\frac{\lambda_0^2 D_0^2\,\pi}{\nu_0^3}\delta(k+k')\,S_d\,k_j\,k_m\,\delta\Lambda\,\Lambda^{-7-2y+d}. \tag{1.68}$$

In the case $y=-2$, this leads to the following recursion relation for the force amplitude

$$\frac{\partial\log D}{\partial\log\Lambda} = -g\,b(d), \tag{1.69}$$

where: $b(d) = 1/(2^{d+1}\,\pi^{d/2}\,\Gamma(d/2))$.

**Coupling constant in the case $y > -2$.** It easily follows from the preceding results that the exact solution of the recursion relation for nondimensional coupling will be

$$g(\Lambda) = \frac{g_1}{1-\left(1-\frac{g_1}{g_0}\right)\left(\frac{\Lambda}{\Lambda_d}\right)^\epsilon}, \tag{1.70}$$

where $g_0 = g(\Lambda_d)$ and $g_1 = 1/(3a) = d/2\,\Gamma(d/2)\,4/3\,2^d\,\pi^{d/2}$. For $\epsilon \geq 0$, the limiting value of the coupling constant as $\Lambda \to 0+$ is $g_1$, which may not be made small for any $d \geq 0$. Situations with $\epsilon < 0$ lead to a well-defined trivial fixed-point regime.

**Coupling constant in the case $y \leq -2$.** This case is identical to the one considered in [16, 95]. In our notation, the solution for the coupling constant is

$$g(\Lambda) = \frac{g_2}{1 - \left(1 - \frac{g_2}{g_0}\right)\left(\frac{\Lambda}{\Lambda_d}\right)^{\epsilon}}, \tag{1.71}$$

where: $g_2 = 2\epsilon(2-\epsilon)/(2\epsilon - 1)$. The limiting value for $\epsilon \geq 0$ is $g_2$ and the $\epsilon$-expansion can be formally organized. In fact, however, there are some difficulties: for $1.5 < d < 2$, coupling constant changes its sign as it moves towards $g_2$, and this region cannot be described by the one-loop theory. The region $0 \leq d \leq 1.5$ possesses a good nontrivial fixed point $g_2$. Region $d \geq 2$ gives trivial (Gaussian) fixed-point behavior. The point $d = 1$ corresponds to the nontrivial fixed point with $\epsilon = 1$. But this refers to thermal equilibrium cases only. As we have just shown, nonequilibrium cases do not seem to be rigorously accessible to the above one-loop theory because of the lack of a small expansion parameter.

# Chapter 2

# One-Dimensional Galilean-Noninvariant System: Effect Of Cubic Nonlinearity

In this Chapter we will consider an example of a forced-dissipative one-dimensional (1D) system which does not possess Galilean invariance, which is an essential property of both Burgers and Navier-Stokes equations considered in the rest of the thesis. From a formal point of view, the system under study here is characterized by a cubic nonlinearity in the governing equation of motion, which makes it treatable by the $\epsilon$-expansion methods even in the 1D-case, unlike its counterpart considered in Chapter 1.

It should be emphasized that such model 1D forced-dissipative systems have been under extensive investigation for quite a long time [8, 95]. This interest may be explained by the fact that they usually serve as simple toy models to understand such important global problems as turbulence in statistical systems with strong nonlinearity, whereas systems with quadratic nonlinearity have been studied in the first place due to their obvious similarity to the Navier-Stokes system. As a result, there have been some progress in understanding universal statistical properties in the forced-dissipative Burgers equation [8, 16, 95]. At the same time, there still remain some

principal theoretical difficulties in the strongly-coupled Burgers equation which are yet to be resolved [16, 95].

In this Chapter the statistical large-distance and long-time properties of the equation with a cubic nonlinearity of the mKdV-type

$$\frac{\partial u}{\partial t} + c_0 \frac{\partial u}{\partial x} + \lambda_0 u^2 \frac{\partial u}{\partial x} = \nu_0 \frac{\partial^2 u}{\partial x^2} + f \tag{2.1}$$

are investigated. A notable feature of this equation is its Galilean noninvariance. Such equations are known to serve as models in physical applications, such as nonlinear Rossby waves in geophysics [31, 52]. A cubic nonlinearity of this type also appears in the derivation of the equations for the long weakly nonlinear gravity surface waves. Third- and higher-order nonlinearities are usually neglected to obtain Burgers or KdV equations. As in the case of 1D forced-dissipative Burgers equation, the equation with cubic nonlinearity is of nontrivial mathematical interest as a prototype model for ocean and atmospheric turbulence. It may be considered also as a possible generalization of the forced-dissipative Burgers equation problem with a strong coupling which remains challenging. This problem provided an additional technical interest for us as a possible application of a finite-step RG transformation to systems of hydrodynamic type.

## 2.1 Finite-Step RG Transformation

Consider the following problem written in the Fourier space

$$\begin{aligned} G^{-1}(\hat{k})\, u(\hat{k}) &= f(\hat{k}) - \frac{i\, k\, \lambda_0}{3\,(2\pi)^4} \int_{\hat{p}} \int_{\hat{q}} u(\hat{p}) u(\hat{q}) u(\hat{k} - \hat{p} - \hat{q})\, dp\, dq, \\ G^{-1}(\hat{k}) &= -i\,(\omega - c_0\, k) + \nu_0\, k^2, \\ \langle f(\hat{k}) f(\hat{k}') \rangle &= D(k)\, \delta(\hat{k} + \hat{k}'), \quad D(k) = 2\,(2\pi)^2\, D_0\, |k|^{-y}. \end{aligned} \tag{2.2}$$

Here we use the notation $\hat{k} = \{k, \omega\}$, frequently omitting the hat when it does not lead to a misunderstanding.

We make the common assumption about the existence of the dissipative cutoff wavenumber $\Lambda_d$ such that all the Fourier-space functions are zero whenever $k > \Lambda_d$.

Also for some $0 < \Lambda < \Lambda_d$ let us use the notation $u^<(k) = u(k)$ if $0 \le k < \Lambda$, $u^<(k) = 0$ elsewhere and $u^>(k) = u(k)$ if $\Lambda \le k < \Lambda_d$, $u^>(k) = 0$ elsewhere. Here $u(k)$ can be any function of the wavenumber.

Following the classical work [46], we define a step of the dynamic RG transformation for some intermediate wavenumber $\Lambda$ as follows.

In equation (2.2) we eliminate all the $u^>$ by expressing them through $u^<$ and $f^>$, which leads to an infinite series in (2.2) (reversible part). The partial statistical averaging over $f^>$ leads to an infinite diagrammatic equation relating $u^<$ and $f^<$ (nonreversible part). The nondimensional coupling constant

$$g_0 = \frac{\lambda_0 D_0}{\nu_0^2 \Lambda^\epsilon}, \text{ with } \epsilon = 2 + y \tag{2.3}$$

is a formal expansion parameter in the resulting diagrammatic series. If by some reason it turns out to be infinitesimally small, then computing only the lowest order in $g_0$ nonvanishing diagrams will be sufficient and will lead to the corrections to dimensional constants of the system: $\{\lambda_0, \nu_0, c_0, D_0\}$. Finally, the stretching of the wavenumber space to its original size will give rise to a system formally coincident with the original one except for the changed dimensional constants and smaller "density" of degrees of freedom. The main assumption behind this procedure which is well established in the theory of critical phenomena is that *the major statistical properties of the system are preserved while applying the RG transformation* [46, 88].

To rephrase abstractly, the transformation thus defined may be expressed as an operator $\mathcal{R}_\delta$ dependent on one parameter $\delta = \Lambda_d/\Lambda$ acting on the point in the phase space $\vec{\mu}$. This RG operator can be by construction factored into an averaging (Kadanoff-like) operator $\mathcal{K}_\delta$ and a stretching operator $\mathcal{S}_\delta$. As a phase space for this problem we can consider the space spanned by the largest possible number of dimensionless combinations of all dimensional constants in the problem $\{\lambda_0, \nu_0, c_0, D_0, \Lambda\}$. It turns out that there are only two possible nondimensional combinations composed from these constants. One is the coupling (2.3), the other one contains the constant advection velocity $c_0$

$$h_0 = \frac{\lambda_0 D_0}{\nu_0 c_0 \Lambda^{\epsilon-1}}, \tag{2.4}$$

giving: $\vec{\mu} = \{g, h\}$. One can distinguish between finite ($1 < \delta < +\infty$) and infinitesimal ($0 < \delta - 1 \ll 1$) transformations. So, the application of the finite RG transformation corresponds to a discrete motion of point $\vec{\mu}$ in the phase space. That is if $\vec{\mu}_0$ is known, then the specification of the law $\vec{\mu}_{n+1} = \mathcal{R}_\delta[\vec{\mu_n}]$ fully defines this motion. If the infinitesimal transformation can be defined, the motion of the point in the phase space will be continuous.

It is common to call such a transformation a Renormalization Group (RG) transformation. In fact, such an infinite set of operators $\mathcal{K}_\delta$ is not a group at least due to a nonreversible part in its definition: averaging. That means that the inverse does not exist and $\mathcal{R}_\delta$ can form at most a semi-group. Another axiom in the definition of a group, namely that $\forall\delta_1, \delta_2\ \exists\delta_3$: $\mathcal{K}_{\delta_1}\mathcal{K}_{\delta_2} = \mathcal{K}_{\delta_3}$ also generally does not hold. In fact, as can be demonstrated, in the case of the infinitesimal RG transformation, a set of operators $\mathcal{K}_\delta$ does form an Abelian semi-group with the property $\mathcal{K}_{\delta_1}\mathcal{K}_{\delta_2} = \mathcal{K}_{\delta_1\delta_2}$. For a finite RG transformation this generally does not hold and the word *group* in the *Renormalization Group* here is not supposed to have the exact mathematical meaning of a group.

Below we will be dealing with the finite RG transformation in the case when $-\infty < \epsilon \ll 1$. We will classify a diagram according to how many $u^<$ it has.

## 2.2 Detailed Structure of the Diagrams

**Diagrams of the $O(u^<)$-Type.** There is one first-order in $\lambda$ diagram which leads to a correction to the bare advection speed

$$-\frac{i\,k\,\lambda}{(2\pi)^4}\,G(k)\,u^<(k)\int_p |G^>(p)|^2\,D(p)\,dq. \tag{2.5}$$

In the limit $k \to 0$, $\omega \to 0$ it gives

$$\delta c = \frac{D\,\lambda}{\pi\,\nu}\,\frac{\Lambda_d^{-y-1} - \Lambda^{-y-1}}{-y-1}. \tag{2.6}$$

The only nonzero second-order in $\lambda$ diagram which leads to a correction to the bare viscosity is

$$-\frac{2\,k\,\lambda^2}{(2\pi)^8}\,G(k)\,u^<(k)\left\{\int_p |G^>(p)|^2\,D(p)\,\times\right.$$

$$\times \left( \int_q |G^>(k-p-q)|^2 \; G^>(q)\, q\, D(k-p-q)\, dq \right) dp \Big\} \tag{2.7}$$

with the integration region $\Lambda < |p| < \Lambda_d$, $\Lambda < |q| < \Lambda_d$ and $\Lambda < |k-p-q| < \Lambda_d$. After the frequency integration it becomes

$$\frac{i\,k\,\lambda^2\,D^2}{2\,\pi^2\,\nu^2}\, G(k)\, u^<(k) \int_p \int_q \frac{|p|^{-y-2}\; q\; |k-p-q|^{-2-y}}{-\omega + c\,k - i\,\nu\,\left[p^2+q^2+(k-p-q)^2\right]}\, dp\, dq. \tag{2.8}$$

Integrals over such an integration region will be dealt with as follows. First, we make the rotation by $-\pi/4$ with stretching: $q \to p+q$ and $p \to p-q$, after which the integration region becomes symmetric with respect to the $p$-axis. Using this, we get (up to a factor)

$$\int_p \int_q \frac{\left\{(p-q)\;|p+q|^{-2-y} + (p+q)\;|p-q|^{-2-y}\right\}\;|k-2\,p|^{-2-y}}{-\omega + c\,k - i\,\nu\,\left[(k-2\,p)^2 + (p+q)^2 + (p-q)^2\right]}\, dp\, dq \tag{2.9}$$

with a new integration region: $\{q > 0,\ \Lambda < |p+q| < \Lambda_d,\ \Lambda < |p-q| < \Lambda_d,\ \Lambda < |k-2\,p| < \Lambda_d\}$, which in fact consists of 4 subregions

$$\begin{aligned}
\frac{-\Lambda_d + k}{2} \le p \le -\Lambda,\ 0 \le q \le -\Lambda - p; \\
\frac{-\Lambda_d + \Lambda}{2} \le p \le \frac{-\Lambda + k}{2},\ \Lambda - p \le q \le \Lambda_d + p; \\
\frac{\Lambda + k}{2} \le p \le \frac{\Lambda_d - \Lambda}{2},\ \Lambda + p \le q \le \Lambda_d - p; \\
\Lambda \le p \le \frac{\Lambda_d + k}{2},\ 0 \le q \le -\Lambda + p.
\end{aligned} \tag{2.10}$$

We are looking for an expansion of the integral depending on parameter $k$ for small values of $k$. After calculations up to terms of order $O(k^3)$ the result will be

$$-\frac{k^2\,\lambda^2\,D^2\,\Lambda^{-4-2y}}{(2\pi)^2\,\nu^3}\, G(k)\, u^<(k)\, \left(2^{-y-2}\,\{A_1 + A_2\} + \delta^{-2-y}\, B_1 + B_2\right). \tag{2.11}$$

Introducing the notation $\epsilon = y+2$, the nondimensional $A_1, A_2, B_1, B_2$ are given by the following quadratures

$$\begin{aligned}
A_1(\delta,\epsilon) = \int_{\xi=1}^{\frac{\delta}{2}} \int_{\eta=0}^{\xi-1} \left\{\epsilon(3\xi^2+\eta^2) + 4\xi^2\right\}\, \xi^{-\epsilon-1} \times \\
\times \frac{\{(\xi+\eta)(\xi-\eta)^{-\epsilon} + (\xi-\eta)(\xi+\eta)^{-\epsilon}\}}{(3\xi^2+\eta^2)^2}\, d\xi\, d\eta,
\end{aligned}$$

$$A_2(\delta,\epsilon) = \int_{\xi=\frac{1}{2}}^{\frac{\delta-1}{2}} \int_{\eta=1+\xi}^{\delta-\xi} \left\{\epsilon(3\xi^2+\eta^2)+4\xi^2\right\} \xi^{-\epsilon-1} \times$$
$$\times \frac{\{(\xi+\eta)(\eta-\xi)^{-\epsilon}+(\xi-\eta)(\xi+\eta)^{-\epsilon}\}}{(3\xi^2+\eta^2)^2}\, d\xi\, d\eta,$$
$$B_1(\delta,\epsilon) = \int_{\eta=0}^{-1+\frac{\delta}{2}} \frac{\left\{(\frac{\delta}{2}-\eta)(\frac{\delta}{2}+\eta)^{-\epsilon}+(\frac{\delta}{2}+\eta)(\frac{\delta}{2}-\eta)^{-\epsilon}\right\}}{\frac{3\delta^2}{4}+\eta^2}\, d\eta,$$
$$B_2(\delta,\epsilon) = \int_{\eta=\frac{3}{2}}^{\delta-\frac{1}{2}} \frac{\left\{(\eta-\frac{1}{2})(\eta+\frac{1}{2})^{-\epsilon}-(\eta+\frac{1}{2})(\eta-\frac{1}{2})^{-\epsilon}\right\}}{\frac{3}{4}+\eta^2}\, d\eta. \qquad (2.12)$$

For arbitrary $\delta$ and $\epsilon$ these integrals are to be computed numerically.

Additionally, denote

$$F(\delta;\epsilon) = 2^{-\epsilon}\,\{A_1(\delta;\epsilon)+A_2(\delta;\epsilon)\} + \delta^{-\epsilon}\,B_1(\delta;\epsilon)+B_2(\delta;\epsilon). \qquad (2.13)$$

Then the correction to the bare viscosity follows

$$\delta\nu = \frac{\lambda^2\,D^2}{(2\pi)^2\,\nu^3\,\Lambda^{2\epsilon}}\,F(\delta;\epsilon). \qquad (2.14)$$

For $\epsilon = 0$ and after some algebra, one can reduce the expression for this correction to

$$\delta\nu = \frac{\lambda^2\,D^2}{(2\pi)^2\,\nu^3}\,F(\delta), \qquad (2.15)$$

where

$$F(\delta) = \frac{4}{\sqrt{3}}\left\{\frac{\pi}{3}+\arctan\left(\frac{\delta-2}{\sqrt{3}\,\delta}\right)-\arctan\left(\frac{2\delta-1}{\sqrt{3}}\right)\right\}+$$
$$+\frac{4}{3\sqrt{3}}\left\{\int_1^{\frac{\delta}{2}}\frac{1}{x}\arctan\left(\frac{x-1}{\sqrt{3}\,x}\right)dx+\right.$$
$$\left.+\int_{\frac{1}{2}}^{\frac{\delta-1}{2}}\frac{1}{x}\arctan\left(\frac{\delta-x}{\sqrt{3}\,x}\right)dx-\int_{\frac{1}{2}}^{\frac{\delta-1}{2}}\frac{1}{x}\arctan\left(\frac{1+x}{\sqrt{3}\,x}\right)dx\right\}. \qquad (2.16)$$

Formula (2.15) defines $\delta\nu$ for $\delta > 2$. For $1 \le \delta \le 2$, $\delta\nu = 0$ is true, which may be easily seen considering the geometrical properties of the integration region in (2.9). A plot of the function $F(\delta)$ computed numerically is shown in Fig. 2.1. It is possible to show that the following asymptotic behavior as $\delta \to +\infty$ holds

$$F(\delta) \propto \frac{2\,\pi}{3\sqrt{3}}\,\log\delta + O(1). \qquad (2.17)$$

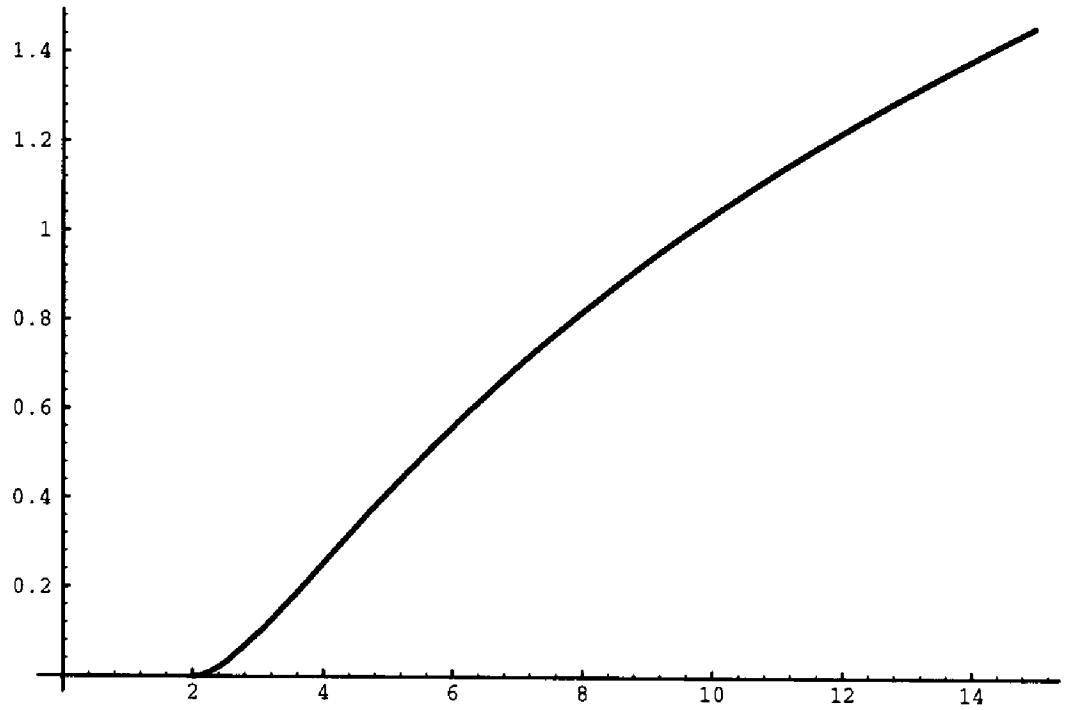


Figure 2.1: The function $F(\delta)$ which determines the correction to the viscosity $\nu$.

**Diagrams of the $O(1)$-Type.** Diagrams of such type lead to the bare force correction. Considering only the lowest order in $\lambda$ corrections, the expression for the correlation function of the resulting corrections to the force may be reduced to

$$\langle \delta f(k) \delta f(k') \rangle = \frac{2\,k^2\,\lambda^2\,\delta(k+k')}{3\,(2\pi)^8} \times$$
$$\times \int_p \int_q |G^>(p)|^2\,|G^>(q)|^2\,|G^>(k-p-q)|^2\,D(p)D(q)D(k-p-q)dpdq. \qquad (2.18)$$

The frequency integration in the limit $\omega \to 0$ results in

$$\langle \delta f(k) \delta f(k') \rangle = \frac{4k^2\lambda^2 D^3 \delta(k+k')}{3\nu^2} \int_p \int_q \left\{ p^2 + q^2 + (k-p-q)^2 \right\} \times$$
$$\times \frac{|p|^{-\epsilon}\,|q|^{-\epsilon}\,|k-p-q|^{-\epsilon}}{c^2\,k^2 + \nu^2\,\left(p^2+q^2+(k-p-q)^2\right)^2}\,dp\,dq. \qquad (2.19)$$

The integration region here is the same as in (2.9), therefore the same procedure for integration can be applied. After some algebra the result can be expressed as follows. Introduce the nondimensional function

$$J(\delta,\epsilon) = \int_{\xi=1}^{\frac{\delta}{2}} \int_{\eta=0}^{-1+\xi} \frac{\left(\xi^2-\eta^2\right)^{-\epsilon}\,\xi^{-\epsilon}}{3\xi^2+\eta^2}\,d\xi\,d\eta +$$
$$+ \int_{\xi=\frac{1}{2}}^{\frac{\delta-1}{2}} \int_{\eta=1+\xi}^{\delta-\xi} \frac{\left(\eta^2-\xi^2\right)^{-\epsilon}\,\xi^{-\epsilon}}{3\xi^2+\eta^2}\,d\xi\,d\eta. \qquad (2.20)$$

Then in the limit $k \to 0$ we get

$$\langle \delta f(k) \delta f(k') \rangle = \frac{2\,D^3\,\lambda^2\,k^2\,2^{-\epsilon}\,\Lambda^{-3\epsilon}}{3\,\nu^4}\,J(\delta;\epsilon), \qquad (2.21)$$

which shows that in the infra-red limit the bare force acquires a thermal noise correction with the correlation function proportional to $k^2$.

In the case $\epsilon = 0$ this result gives us the correction $\delta D$

$$\delta D = \frac{\lambda^2\,D^3}{3\,(2\,\pi)^2\,\nu^4}\,J(\delta), \qquad (2.22)$$

with

$$J(\delta) = \frac{1}{\sqrt{3}} \left\{ \int_1^{\frac{\delta}{2}} \frac{1}{x} \arctan\left(\frac{x-1}{\sqrt{3}x}\right) dx + \right.$$
$$\left. \int_{\frac{1}{2}}^{\frac{\delta-1}{2}} \frac{1}{x} \arctan\left(\frac{\delta-x}{\sqrt{3}x}\right) dx - \int_{\frac{1}{2}}^{\frac{\delta-1}{2}} \frac{1}{x} \arctan\left(\frac{1+x}{\sqrt{3}x}\right) dx \right\}. \qquad (2.23)$$

As in the case of $F(\delta)$, the large $\delta$ asymptotic behavior of $J(\delta)$ is also logarithmic

$$J(\delta) \propto \frac{\pi}{2\sqrt{3}} \log \delta + O(1). \tag{2.24}$$

The dependence $J(\delta)$ computed numerically is shown in Fig. 2.2.

**Diagrams of the $O(u^< u^< u^<)$-Type.** The only nonzero second-order diagram which contains a triple nonlinearity is

$$-\frac{\lambda^2 k}{(2\pi)^8} G^<(k) \int_p \int_q u^<(p)\, u^<(q)\, u^<(k-p-q) \times$$
$$\times \left( \int_r r\, G^>(r)\, |G^>(k-p-r)|^2\, D(k-p-r)\, dr \right) dp\, dq. \tag{2.25}$$

Denote for brevity here $\zeta = k - p$, $\Omega = \omega - \psi$. Then the integral

$$\int_r r\, G^>(r)\, |G^>(\zeta - r)|^2\, D(\zeta - r)\, dr \tag{2.26}$$

with the integration region $\Lambda < |\zeta - r| < \Lambda_d$, $\Lambda < |r| < \Lambda_d$ can be transformed into

$$\frac{8\, i\, D\, \pi^3}{\nu} \int_{r=\Lambda+\frac{|\zeta|}{2}}^{\Lambda_d - \frac{|\zeta|}{2}} \frac{\left(r^2 - \frac{\zeta^2}{4}\right) \left\{ \left(r - \frac{\zeta}{2}\right)^{-\epsilon-1} - \left(r + \frac{\zeta}{2}\right)^{-\epsilon-1} \right\}}{\Omega - c\zeta + 2\, i\, \nu \left(r^2 + \frac{\zeta^2}{2}\right)}. \tag{2.27}$$

For small $\Omega$ and $\zeta$ this expression is $O(\Omega, \zeta)$, which makes it an irrelevant correction. Therefore we conclude that $\delta\lambda = 0$.

## 2.3 Recurrence Relations in the Trivial Case

Consider the stretching transformation

$$k \to \frac{1}{\delta} k,\ \omega \to \frac{1}{\alpha} \omega,\ u^< \to \frac{1}{\beta} u^<. \tag{2.28}$$

Then an iterative application of the above averaging procedure together with such rescaling will lead to recurrence relations for dimensional and nondimensional parameters.

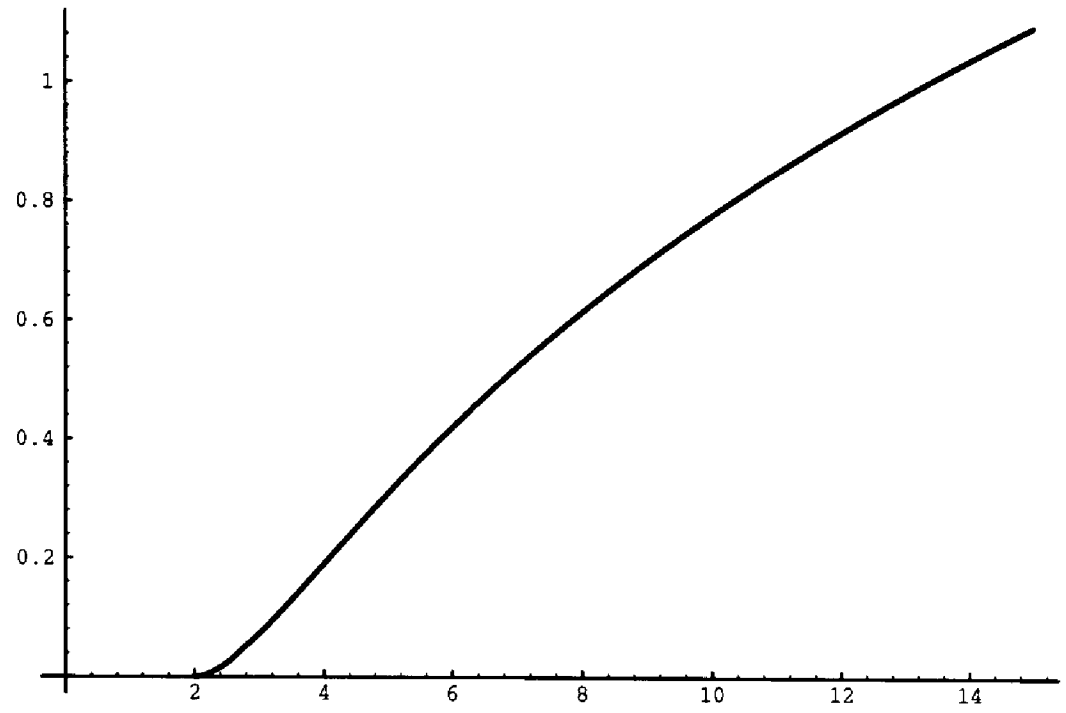


Figure 2.2: The function $J(\delta)$ which determines the correction to the force correlation function amplitude $D$.

Let us consider the case $\epsilon = 0$ first. Then the thermal noise is of the same order in $k$ as the bare force, which lead us above to $\delta D$ given by (2.22). Recurrence relations for the dimensional parameters in this case will be

$$\begin{aligned} c_{n+1} &= c_n \left(1 + \frac{D_n \lambda_n \Lambda}{\pi \nu_n c_n}(\delta - 1)\right) \frac{\alpha}{\delta}, \\ \nu_{n+1} &= \nu_n \left(1 + \frac{\lambda_n^2 D_n^2}{(2\pi)^2 \nu_n^4} F(\delta)\right) \frac{\alpha}{\delta^2}, \\ \lambda_{n+1} &= \lambda_n \frac{1}{\beta^2 \delta^3 \alpha}, \\ D_{n+1} &= D_n \left(1 + \frac{\lambda_n^2 D_n^2}{3(2\pi)^2 \nu^4} J(\delta)\right) \frac{\alpha^3 \beta^2}{\delta}. \end{aligned} \tag{2.29}$$

Introducing notations similar to (2.3), (2.4) for the nondimensional constants

$$g = \frac{\lambda D}{2\pi \nu^2}, \quad h = \frac{\lambda D \Lambda}{\pi \nu c}, \tag{2.30}$$

we derive the recurrence relations for them

$$\begin{aligned} g_{n+1} &= g_n \frac{1 + g_n^2 \frac{J(\delta)}{3}}{(1 + g_n^2 F(\delta))^2}, \\ h_{n+1} &= h_n \frac{1}{\delta} \frac{1 + g_n^2 \frac{J(\delta)}{3}}{(1 + g_n^2 F(\delta))(1 + h_n(\delta - 1))}. \end{aligned} \tag{2.31}$$

There is one real-valued fixed point of the first equation $g = 0$ and there are two $h_1 = 0$, $h_2 = -1/\delta$ for the second one. Linear stability analysis shows that $h_2$ is unstable. For $4F(\delta) - \frac{2}{3}J(\delta) > 0$ which is true for all $\delta > 2$, the leading asymptotic behavior as $n \to +\infty$ of the solution in the neighborhood of the trivial fixed point is

$$g_n \propto \pm \frac{1}{\sqrt{4F(\delta) - \frac{2}{3}J(\delta)}} \frac{1}{\sqrt{n}}, \quad h_n \propto h_0 \delta^{-n}, \tag{2.32}$$

which shows that the trivial fixed point is stable with respect to infinitesimally small perturbations. Convergence for the strong coupling ($g_0 \gg 1$) is very fast: $g_1 = O(1/g_0)$. Note that the positive sign in (2.32) corresponds to the $\lambda_0 > 0$ case and the negative sign to the $\lambda_0 < 0$ case.

Now consider the case $\epsilon < 0$. Here the thermal noise correction dominates the bare force as $k \to 0$; and, to be consistent, we need to consider the renormalization

of the thermal noise amplitude, $T$. Therefore let

$$D(k) = 2\,(2\pi)^2\,T_0\,|k|^2 \tag{2.33}$$

to be our bare force correlation function. Without repeating any of the calculations it is possible to write down all the results for this case using the ones already obtained. For this purpose, one needs to make a change $G \to T$ in the $\epsilon = 0$ case. From the fact that the thermal noise nondimensional constants

$$g_T = \frac{\lambda\,T}{2\pi\,\nu^2}, \quad h_T = \frac{\lambda\,T\,\Lambda}{\pi\,\nu\,c} \tag{2.34}$$

will obey exactly the same recurrence relations (2.31), it follows that the whole region $\epsilon \leq 0$ forms a unique universality class for this problem with the trivial (Gaussian) fixed-point behavior.

## 2.4 Recurrence Relations in the Nontrivial Case

In this case the thermal noise correction defined by (2.21) is irrelevant and we get $\delta D = 0$. For $\delta\nu$, we use formula (2.14). Again, averaging together with rescaling (2.28) will lead to the recurrence relations. If we use the notation

$$g = \frac{\lambda\,D}{2\pi\,\nu^2\,\Lambda^\epsilon}, \quad h = \frac{\lambda\,D}{\pi\,\nu\,c\,\Lambda^{\epsilon-1}}, \tag{2.35}$$

then for the dimensional parameters, we get

$$\begin{aligned} c_{n+1} &= c_n \left(1 + h\,\frac{\delta^{1-\epsilon} - 1}{1-\epsilon}\right)\frac{\alpha}{\delta}, \\ \nu_{n+1} &= \nu_n \left(1 + g^2\,F(\delta;\epsilon)\right)\frac{\alpha}{\delta^2}, \\ \lambda_{n+1} &= \lambda_n\,\frac{1}{\beta^2\,\delta^3\,\alpha}, \\ D_{n+1} &= D_n\,\delta^{\epsilon-1}\,\alpha^3\,\beta^2, \end{aligned} \tag{2.36}$$

and for the dimensionless parameters, we get

$$\begin{aligned} g_{n+1} &= g_n\,\delta^\epsilon\,\frac{1}{\left(1 + g_n^2\,F(\delta;\epsilon)\right)^2}, \\ h_{n+1} &= h_n\,\delta^{\epsilon-1}\,\frac{1}{\left(1 + g_n^2\,F(\delta;\epsilon)\right)\left(1 + h_n\,\frac{\delta^{1-\epsilon}-1}{1-\epsilon}\right)}. \end{aligned} \tag{2.37}$$

A study of the fixed points gives the following results.

There are two fixed points $g_1 = 0$ and $g_2 = \left(\delta^{\epsilon/2} - 1\right)/F(\delta;\epsilon)$. The solution in the neighborhood of the trivial fixed point can be found: $g_n = g_0\,\delta^{\epsilon n} \to +\infty$ as $n \to +\infty$ for any $g_0 \neq 0$, therefore $g_1$ is unstable. Performing the same kind of linear stability analysis around $g_2$, we assume $g_n = (\epsilon \log\delta/F(\delta))^{1/2} + G_n$ and get the solution for $G_n$ : $G_n = G_0\,\delta^{-2\epsilon n} \to 0$ as $n \to +\infty$. That proves that $g_2$ is a nontrivial fixed point which is stable with respect to infinitesimal perturbations. So, as $n \to +\infty$ the coupling constant $g$ tends to

$$g^2 = \epsilon\frac{\log\delta}{2\,F(\delta)} + O(\epsilon^2), \tag{2.38}$$

exponentially fast at large enough $n$.

For the nondimensional constant $h$ similarly we obtain that there are two fixed points $h_1 = 0$ and $h_2 = (\epsilon - 1)\,\delta^{\epsilon-1}$, of which $h_1$ is stable for $\epsilon < 1$ and $h_2$ is stable for $\epsilon > 1$.

## 2.5 The RG Operator $R_\delta$ as $\delta \to +\infty$

So far we have dealt with a purely mathematical procedure. One of the results of this procedure was formula (2.38), which says that $\forall\delta : 2 < \delta < +\infty$ there exists a unique $\mu$ weakly dependent on $\delta$ such that $\mathcal{R}_\delta\mu = \mu$. In fact we could hardly expect of $\mu$ not to depend on $\delta$ for the reason already noted at the beginning: a set of finite RG transformations considered here does not form a group. Particularly here we do not have: $\mathcal{R}_{\delta_1}\mathcal{R}_{\delta_2} = \mathcal{R}_{\delta_1\,\delta_2}$. That can be illustrated by considering the example of the correction to the viscosity $\delta\nu$, given by (2.15). The correction $\delta\nu(\delta)$ is a complicated nonlinear function of $\delta$ for which the property $\delta\nu(\delta_1)+\delta\nu(\delta_2) = \delta\nu(\delta_1\,\delta_2)$ does not hold true. A similar situation has been observed in the finite RG analysis of the diffusion of a passive scalar in a random velocity field [94]. This is always the case for the finite RG transformation in which second-loop corrections are important. In this problem, as we have determined above, the limit $\delta \to 1+$ does not exist, because corrections $\delta\nu$ and $\delta D$ vanish for all $1 \leq \delta \leq 2$, and the infinitesimal RG transformation is not

defined. Therefore a weak dependence of $\mu(\delta)$ is what we must expect. Does that mean that we cannot use the information obtained by the finite RG transformation?

We strongly believe that this is not true. In fact the finite RG transformation applies in more general cases than the infinitesimal one. To make use of the information it supplies we need to make use of the following physical postulate, which has already worked in the case of the static RG [46]. We claim that the physical statistically stationary states of the problem correspond mathematically to the taking of two limits $n \to +\infty$ and $\delta \to +\infty$. The first one guarantees that we are at a fixed-point. The second one guarantees that we are at a universal fixed-point. That is, if $\delta$ is not large enough we cannot "see" the universal behavior of the system, but as $\delta$ gets larger we start to "see" it. In other words this may be called a *microscope principle*. At a very high resolution we "see" a microstructure of the solution which is of no use to us. Then as we gradually decrease the resolution we notice that after some time the picture we "see" does not change any more. That corresponds to taking the limit $\delta \to +\infty$. Moreover, it is interesting that due to the logarithmic behavior at large $\delta$ (cf. (2.17) and (2.23)) of the corrections $\delta\nu$ and $\delta D$, the set $\{R_\delta\}$ acquires the semi-group property as $\delta \to +\infty$.

In the case of (2.37) the limit $\delta \to +\infty$ will lead to

$$g^* = \left(\epsilon \frac{3\sqrt{3}}{4\pi}\right)^{\frac{1}{2}} . \tag{2.39}$$

One of the ways to check the correctness of this postulate is by comparing the consequences of this with numerical simulations.

## 2.6 Critical Behavior

One can get the large-eddy description when Fourier-modes are eliminated without the subsequent stretching, as it was done in [93]. Consider $\epsilon > 0$ first. Then from the recursion relations (2.36) it follows that: $D_n = D_0$, $\lambda_n = \lambda_0$, $c_n = c_0$. As is derived in detail in Appendix A, the leading-order solution of the difference equations for $\nu_n$

and $c_n$, if $\epsilon \to 0+$ and $n \to +\infty$, lead to

$$\nu(\Lambda) = \frac{\sqrt{\lambda_0 D_0}}{\left(3\sqrt{3}\pi\,\epsilon\right)^{\frac{1}{4}}}\,\Lambda^{-\frac{\epsilon}{2}}, \quad c(\Lambda) = c_0. \tag{2.40}$$

Define the full $(k,\omega)$-dependent correlation function and energy spectrum as follows

$$C(k,\omega) = \int_{-\infty}^{+\infty}\int_{-\infty}^{+\infty} \frac{\langle u(k,\omega)\,u(k',\omega')\rangle}{2}\,\frac{dk'}{2\pi}\,\frac{d\omega'}{2\pi},$$

$$E(k) = \int_{-\infty}^{+\infty} C(k,\omega)\,\frac{d\omega}{2\pi}.$$

Then their evaluation near the fixed point for $\epsilon > 0$ can be readily performed

$$C(k,\omega) = \frac{D_0\,k^{2-\epsilon}}{(\omega - c_0\,k)^2 + \frac{\lambda_0 D_0}{\left(3\sqrt{3}\pi\epsilon\right)^{\frac{1}{2}}}\,k^{4-\epsilon}}, \quad E(k) = \frac{1}{2}\sqrt{\frac{D_0}{\lambda_0}}\,\left(3\sqrt{3}\pi\epsilon\right)^{\frac{1}{4}}\,k^{-\frac{\epsilon}{2}}. \tag{2.41}$$

The case $\epsilon \le 0$ gives

$$C(k,\omega) = \frac{D_0\,k^2}{(\omega - c_0\,k)^2 + \nu_0^2\,k^4}, \quad E(k) = \frac{D_0}{2\,\nu_0}\,k^0 \tag{2.42}$$

for $\epsilon = 0$, and

$$C(k,\omega) = \frac{T_0\,k^2}{(\omega - c_0\,k)^2 + \nu_0^2\,k^4}, \quad E(k) = \frac{T_0}{2\,\nu_0}\,k^0 \tag{2.43}$$

for $\epsilon < 0$.

In the spirit of the theory of critical phenomena [46], one can say that the stationary energy exponent $i_E = d\log(E(k))/d\log(k)$ in our problem exhibits a "phase transition" if the external parameter $y = \epsilon - 2$ changes from $-2-0$ to $-2+0$, corresponding to a change from $i_E = 0$ in the $\epsilon \le 0$ region to $i_E = -\epsilon/2$ in the $\epsilon > 0$ region. The force correlation function exponent $y$ here plays the role of the temperature for the second-order phase transition in a ferromagnetic substance. The large-eddy viscosity exponent exhibits the same critical behavior at $y = -2$.

Note that the above results are rigorous only for $-\infty < \epsilon \ll 1$. And strictly speaking, the whole sum of the diagrammatic corrections to $\nu$, $D$ and $\lambda$ should be considered for finite $\epsilon > 0$. Only when summation of diagrams up to all orders in $\lambda$ does not lead to any new "hidden" scaling laws, may the above predictions be used for finite $\epsilon > 0$ as well. The scaling laws derived here may still hold true for $-\infty < \epsilon \le \epsilon_{crit} \approx 0.83$, as is shown in Appendix A.

## 2.7 Irrelevance of Higher-Order Nonlinearities

Now let us return to recursion relations for $\epsilon > 0$ (2.36). One can fix the stretching parameters by requiring that $D_n = D_0$ and $\lambda_n = \lambda_0$; then we get

$$\alpha = \delta^{2-\frac{\epsilon}{2}}, \quad \beta = \delta^{-1-\frac{\epsilon}{4}}. \tag{2.44}$$

Now consider the higher-order nonlinearities which are generated in the process of scale-elimination. A property of our system is that all even-order nonlinear terms are fluctuating and having zero mean. The fifth-order nonlinearity is

$$-\frac{\mu\, k}{3(2\pi)^8} \int_p \int_q p\, G^>(p)\, u^<(q)\, u^<(k-p-q) \times$$
$$\times \int_r \int_s u^<(r)\, u^<(s)\, u^<(p-s-r)\, dp\, dq\, dr\, ds, \tag{2.45}$$

with constant $\mu$ parametrizing it. Consider $\mu$ as a new dimensional parameter in the system. It will be *irrelevant* in the sense of Wilson, if for $\mu_0 \neq 0$ the quintic coupling constant $g_5 = \mu\, D^2\, \nu^{-4}\, \Lambda^{-2\epsilon}$ associated with $\mu_0$ tends to a fixed point faster than the leading cubic coupling $g_3$ (see also [16]). Really, the rescaling transformation (2.28) and the scale-elimination will lead to a recursion relation of the form

$$\mu_{n+1} = \mu_n\, (1 + \text{“loops”})\, \delta^{2\epsilon-10}, \tag{2.46}$$

which gives a solution that decays exponentially to zero, if $\epsilon < 5$ and loop-corrections do not affect this behavior. Higher-order nonlinearities of this type can be treated in a similar way and are irrelevant if $\epsilon < 5$. Of course, we realize that this condition is correct only if the loop corrections do not change the exponent $2\,(\epsilon - 5)$; otherwise the condition of irrelevance will be different.

## 2.8 Relation to the Forced-Dissipative Burgers Equation

Consider the equation in the physical domain (2.1). The change of the unknown function $u \to u + C/2$ with $C = const$ leads to

$$u_t + \left(c_0 + \frac{\lambda_0 C^2}{4}\right) u_x + \lambda_0 C u u_x + \lambda_0 u^2 u_x = \nu_0 u_{xx} + f. \tag{2.47}$$

After Galilean transformation $x \to x - (c_0 + \lambda_0 C^2/4)\, t$ into a moving frame of reference, this equation becomes

$$u_t + \lambda_0 C u u_x + \lambda_0 u^2 u_x = \nu_0 u_{xx} + f. \tag{2.48}$$

If $C$ is large enough, this becomes a forced-dissipative problem for the Burgers equation with a strong coupling regularized by a small cubic nonlinearity. How large should $C$ be must be specified by comparing the bare coupling constants in front of the quadratic and cubic nonlinearities which respectively are

$$g_2 = \frac{C \lambda D^{\frac{1}{2}}}{\nu^{\frac{3}{2}} \Lambda_d^{\frac{\epsilon+1}{2}}}, \quad g_3 = \frac{\lambda D}{\nu^2 \Lambda_d^{\epsilon}}. \tag{2.49}$$

The requirement that $g_2 \gg g_3$ leads to the condition on $C$ given by

$$C^2 \gg \frac{D}{\nu \Lambda_d^{4(\epsilon-1)}}. \tag{2.50}$$

In fact in a lot of physical applications where the Burgers equation arises from the real physical problem via a series of simplifications, it appears in the form (2.47) – (2.48). For this reason it is very interesting to consider both similarities and differences in the following two problems: (i) 1D forced-dissipative Burgers equation and (ii) 1D forced-dissipative Burgers equation with a small cubic nonlinearity considered here.

The theoretical work for (i) based on the one-loop RG for any exponent $y$ and dimension $d = 1$ fails to lead to a small coupling and therefore does not verify the diagrammatic series truncation, as we have already seen in Chapter 1. Considering

a variable space dimension $d$ leads to nontrivial fixed point behavior for $0 \leq d \leq 1.5$ and $y \leq -2$ (thermal equilibrium) [16]. The most interesting cases $y > -2$ (nonequilibrium) remain inaccessible by such theories.

A comparison of $C(k,\omega)$ and $\nu(k)$ predicted by [16] for (i) with $d = 1$, $y = -2$ with our results shows that problems (i) and (ii) are substantially different: in (ii) nonlinearity is infinitesimal (trivial behavior) via RG whereas in (i) it is finite (nontrivial behavior). That is, taking the limit $g_3/g_2 \to 0+$ in (ii) gives a result that is different from (i); this may be attributed to the fact that this limit is being taken under the condition of broken symmetry (Galilean noninvariance). This probably means that the cubic nonlinearity forms a singular perturbation. At the same time we notice that the energy spectrum exponents for (i) and (ii) seem to be the same for all $y \leq -2$.

# Chapter 3

# Isotropic Two-Dimensional Navier-Stokes System

In the previous Chapters we dealt with one-dimensional systems and we now proceed to the discussion of two-dimensional forced-dissipative systems. Chapter 3 illustrates some analytical methods and provides direct numerical simulation verification of these methods as applied to the two-dimensional isotropic Navier-Stokes system. The methods of Chapter 3 will be extensively used in Chapters 4 and 5 for the analysis of other two-dimensional systems which are more complex and may be more relevant for practical applications.

Homogeneous and isotropic turbulence has been a traditional idealization of real turbulent flows, which are usually neither homogeneous nor isotropic. However, this idealization has provided a wealth of information on the physics of turbulence and it still remains one of the main tools of theoretical and numerical turbulence research [54]. The same can be said about the dimensionality of the problem; indeed, many natural flows that span a large number of scales possess features of both three- (3D) and two-dimensional (2D) turbulence and can be classified somewhere between the purely 3D and 2D extremes. Thus, even though the focus of the following three Chapters is 2D turbulence one should keep in mind that applications of the results to quasi-2D flows are intended. Quasi-2D turbulent flows are widely found in geophysics and engineering. Although, under normal circumstances, all flows are unstable to

three-dimensional instabilities [2], there exist natural situations when a flow may attain a quasi-2D configuration or even become quasi-two-dimensionalized on certain scales. There are two major factors that may cause a flow to become quasi-2D: geometry of the flow boundaries and/or certain body forces (or 'extra strains') whose action leads to smoothing of the velocity fluctuations in a preferred direction. While in the geophysical context both factors are equally important (i.e., the small aspect ratio, density stratification, rotation), in the engineering context the second factor usually predominates (for instance, the so-called mechanism of "magnetic friction" in magneto-hydrodynamic flows with low magnetic Reynolds number [76]).

## 3.1 $\epsilon$-Expansion Procedure Via One-Loop RG

This Section will review the RG and the $\epsilon$-expansion methods as applied to the Navier-Stokes system. We would like to give the most recent presentation of theory on which most of our further results are based. Due to their importance, our goal was to verify these recent analytical results by other possible means like alternative derivations and comparisons with spectral closures and DNS, the direction pursued in the subsequent Sections.

### 3.1.1 Statement of the Problem

Consider the two-dimensional incompressible Navier-Stokes system

$$\frac{\partial \vec{u}}{\partial t} + \left(\vec{u}, \vec{\nabla}\right) \vec{u} = -\nabla p + \nu \, \Delta \vec{u} + \vec{g}, \quad \left(\vec{\nabla}, \vec{u}\right) = 0.$$

Introducing the vorticity $\zeta \equiv [\vec{\nabla}, \vec{u}]_3 = \partial v/\partial x - \partial u/\partial y$, $f \equiv [\vec{\nabla}, \vec{g}]_3$ and a stream function defined by $\vec{u} \equiv \nabla^T \psi$ where $\nabla^T : (\nabla^T, \nabla) = 0$, one obtains the so-called vorticity-stream function formulation

$$\begin{aligned} \frac{\partial \zeta}{\partial t} + \frac{\partial(\zeta, \psi)}{\partial(x, y)} &= \nu \, \Delta \zeta + f, \\ \zeta &= -\Delta \psi. \end{aligned} \tag{3.1}$$

Here and in the following the notation $[\cdot,\cdot]_3$ means the third component of the three-dimensional vector product, and we also use the following notation for the determinant of the Jacobi matrix: $\partial(\zeta,\psi)/\partial(x,y) \equiv \partial\psi/\partial y\,\partial\zeta/\partial x - \partial\psi/\partial x\,\partial\zeta/\partial y$.

Below we will employ the following definitions of the backward and forward Fourier transforms

$$\zeta(\vec{x},t) \equiv \zeta(\vec{k},\omega)^{\vee} = \int_{\vec{k}}\int_{\omega} \zeta(\vec{k},\omega)\, e^{i\left(-\omega t+(\vec{k},\vec{x})\right)}\, \frac{d\vec{k}}{(2\pi)^2}\,\frac{d\omega}{2\pi}$$
$$\zeta(\vec{k},\omega) \equiv \zeta(\vec{x},t)^{\wedge} = \int_{\vec{x}}\int_{t} \zeta(\vec{x},t)\, e^{-i\left(-\omega t+(\vec{k},\vec{x})\right)}\, d\vec{k}\, d\omega$$

and the $\delta$-function

$$\delta(\vec{x},t) \equiv \delta(\vec{x})\,\delta(t) = \int_{\vec{k}}\int_{\omega} e^{-i\left(-\omega t+(\vec{k},\vec{x})\right)}\, \frac{d\vec{k}}{(2\pi)^2}\,\frac{d\omega}{2\pi}.$$

Using these definitions the convolution theorem, for example, will take the form

$$\left(f(\vec{x},t)\,g(\vec{x},t)\right)^{\wedge} = \frac{1}{(2\pi)^3}\int_{\psi}\int_{\vec{p}} f(\vec{p},\psi)\,g(\vec{k}-\vec{p},\omega-\psi)\,d\vec{p}\,d\psi.$$

Let us also introduce the so-called *bare Green's function* or *bare propagator* defined as the linear part of the Navier-Stokes operator in Fourier space

$$G(\vec{k},\omega) \equiv \left(-i\omega + \nu\, k^2\right)^{-1}. \tag{3.2}$$

It is customary to use the brief notation $\hat{k} \equiv \{\vec{k},\omega\}$ for the three-vectors $\hat{k}$. Using all these notations and definitions one can write down the governing equation in Fourier space as follows

$$\zeta(\hat{k}) = G(\hat{k})\,f(\hat{k}) + \frac{G(\hat{k})}{2}\int_{\hat{p}}\left[\vec{k},\vec{p}\right]_3\left\{\frac{1}{p^2} - \frac{1}{\left|\vec{k}-\vec{p}\right|^2}\right\}\zeta(\hat{p})\,\zeta(\hat{k}-\hat{p})\,\frac{d\hat{p}}{(2\pi)^3}. \tag{3.3}$$

Note that thus written the nonlinearity is symmetrized, i.e., invariant under the change $\hat{p} \to \hat{k}-\hat{p}$.

Now we also need to be more specific about the noise $f(\hat{k})$ entering the basic equation (3.3). Turbulence here is assumed to be generated by this noise and its definition is therefore very important. Below we will consider the force $f(\vec{x},t)$ to be

a zero-mean Gaussian white noise in time random function given by its two-point correlation function in Fourier-space

$$\overline{f(\hat{p})\,f(\hat{q})} = D(p)\,\delta(\hat{p}+\hat{q}),\ \text{where:}\quad D(p) \equiv 2\,(2\pi)^3\,\left(D_0\,|\vec{p}|^{-y+2} + T_0\,|\vec{p}|^4\right). \quad (3.4)$$

We note that in the above definition of the force we have simultaneously considered two types of possible forces: thermal noise with the bare amplitude $T_0$ and nonthermal part (if $y \neq -2$) with the bare amplitude $D_0$. In doing so we follow the Ref. [79] where this approach was used for the first time, to the best of our knowledge. It is a peculiarity of the two-dimensional case that initially negligibly small or even zero thermal noise is very strongly self-generated in the course of shell-elimination and its use is necessary for a correct description of the fixed-point properties. As it was first shown in [79], consideration of the thermal noise changes the properties of the fixed point in two dimensions, whereas it is an irrelevant variable for the nontrivial ($y > -2$) situations in all dimensions higher than two. Some of the details relevant to the two-dimensional case illustrating this are presented below.

### 3.1.2 Ultra-Violet Shell-Elimination

Now we will follow the prescriptions of the book [46] and papers [16, 93, 18] which deal with the dynamic RG approach, particularly applied to the fluid flow equations. As was outlined in [46] for quite general nonlinear Langevin equations, we will perform the infinitesimal ultraviolet shell-elimination in the Fourier space.

First, in order to treat the ultraviolet divergences, we introduce the ultra-violet cutoff wavenumber, that is, we assume that all Fourier-space $\vec{k}$-dependent functions become zero whenever $\left|\vec{k}\right| \geq \Lambda_d \equiv \Lambda_0$. This assumption may be understood as an oversimplified attempt to introduce a real-life dissipative cutoff wavenumber into the system. Although all the specific properties of the dissipative range are neglected in this approximation and a sharp cut-off is introduced instead of a smooth exponential fall-off, it is assumed that these approximations do not alter the infra-red and long-time properties of the system, in which we are primarily interested. The self-consistency of this assumption will be verified in the end.

Now, consider another wavenumber $\Lambda$ such that $\Lambda \leq \Lambda_d$ and let us write the governing equation for the region of $\vec{k}$-space defined over only the $k < \Lambda$-part. This requires averaging of our basic equation (3.3) over the force defined only in the band of wavenumbers $[\Lambda, \Lambda_d]$ (the small-scale part of the force), under the assumption that the large-scale quantities $\zeta$ and $f$ are statistically independent of the small-scale part of the force.

As explained in detail in the abovementioned references, averaging over the small-scale part of the force results in the infinite set of corrections to the governing equation (3.3). These corrections are most easily considered in the language of Feynman-type diagrams [90]. Without going into the details of this well-established technique, but just using its results below, we will consider the resulting relevant corrections and compute them in the infra-red and long-time limit. The level of the approximation of the resulting diagrammatic series will be one-loop, i.e., only one-vertex diagrams will be considered. For more details of the diagrammatic technique, see [46, 90, 94]. Corresponding results are used here as a well-known tool without much further discussion.

### 3.1.3 Correction to the Inverse Propagator

It is possible to show that the one-loop correction in the diagrammatic series for $\zeta(k)$ leading to the lowest-order viscosity correction has the form

$$-\frac{G(\hat{k})\,\zeta(\hat{k})}{(2\pi)^6}\int_p |G(\hat{p})|^2\, G(\hat{k}-\hat{p})\, D(p)\, \left[\vec{k},\vec{p}\right]^2 \left\{\frac{1}{p^2}-\frac{1}{\left|\vec{k}-\vec{p}\right|^2}\right\}\left\{\frac{1}{p^2}-\frac{1}{k^2}\right\} d\hat{p}. \quad (3.5)$$

The region of integration is over such $\vec{p}$ that: $\Lambda \leq |\vec{p}| \leq \Lambda_d$ and $\Lambda \leq \left|\vec{k}-\vec{p}\right| \leq \Lambda_d$ and over frequencies $-\infty < \psi < +\infty$, which is a region of intersection of two shells of width $-\delta\Lambda \equiv \Lambda_d - \Lambda \geq 0$. Note that from the geometric properties of the integration region it is obvious that if $k$ is kept constant while $\delta\Lambda \to 0-$ then the region becomes doubly-connected with the integration region area scaling as $\delta\Lambda^2$. To avoid dealing with these complications in the RG procedure, we consider cases when $k < -\delta\Lambda$ and this region is singly-connected and shrinks to the simple shell $\Lambda \leq |\vec{p}| \leq \Lambda_d$ as $k \to 0+$.

This corresponds to taking both limits $k \to 0+$ and $\delta\Lambda \to 0-$ simultaneously such that $k < -\delta\Lambda$ always.

Frequency integration may be done exactly using the residue theorem. Indeed, there are 3 poles: $\psi_{1,2} = \pm i\nu\, p^2$, and $\psi_3 = \omega + i\nu \left|\vec{k} - \vec{p}\right|^2$ and the contour of integration can be considered as a piece of the real-axis and a lower half-plane semi-circle of radius $R \to +\infty$. After the inner frequency $\psi$-integration the result in the leading order of external frequency $\omega$ is

$$-\frac{G(\hat{k})\,\zeta(\hat{k})}{2\,(2\pi)^5\,\nu^2}\int_p \frac{D(p)\,\left[\vec{k},\vec{p}\right]^2\left\{\frac{1}{p^2}-\frac{1}{\left|\vec{k}-\vec{p}\right|^2}\right\}\left\{\frac{1}{p^2}-\frac{1}{k^2}\right\}}{p^2\left(p^2+\left|\vec{k}-\vec{p}\right|^2\right)}\,d\vec{p}+O(\omega). \tag{3.6}$$

The problem of dealing with two noises may be considerably simplified by dealing with a single more general noise first and then reproducing the result for two noises taken together (the noise enters only linearly here).

The above integral may be performed exactly in all orders of a small parameter $k$ using the following procedure. First we perform a rotation through the angle $-\phi_k$: $\vec{p} \to T_{\phi_k}\,\vec{p}$, where $\phi_k$ is a polar angle of $\vec{k}$ and $T_{\phi_k} \equiv \{\{cos\ \phi_k, sin\ \phi_k\}, \{-sin\ \phi_k, cos\ \phi_k\}\}$ is a two-dimensional rotation matrix. The second transformation is the symmetrization of the integration region, that is, translation $\vec{p} \to \vec{p} + \vec{e}_1\, k/2$, where $\vec{e}_1 \equiv \{1,0\}$. After these transformations the resulting integral in polar coordinates $\vec{p} \equiv \{p,\psi\}$ will be

$$-\frac{D\,G(\hat{k})\,\zeta(\hat{k})\,k^2}{(2\pi)^2\,\nu^2}\int_{p,\psi}\frac{\left(p^2+k\,p\,cos\ \psi+\frac{k^2}{4}\right)^{-\frac{y}{2}}}{\left(2\,p^2+\frac{k^2}{2}\right)}\,p^3\,sin^2\ \psi\ \times$$

$$\left\{\frac{1}{p^2}-\frac{1}{\frac{k^2}{4}-k\,p\,cos\ \psi+p^2}\right\}\left\{\frac{1}{\frac{k^2}{4}+k\,p\,cos\ \psi+p^2}-\frac{1}{k^2}\right\}dp\,d\psi+O(\omega), \tag{3.7}$$

with the new integration region over $\vec{p}$ such that: $\Lambda \le |\vec{p}+k/2\,\vec{e}_1| \le \Lambda_d$ and $\Lambda \le |\vec{p}-k/2\,\vec{e}_1| \le \Lambda_d$. Note that the result is isotropic, i.e., $\phi_k$-independent, as one might expect for an isotropic original problem. Now we represent this double integral in the form of a repeated integral. Denote the integrand by $F(k,p,\psi)$. Then we have

$$\int_{\psi=-\frac{\pi}{2}}^{\frac{\pi}{2}} d\psi \int_{p=\frac{k}{2}\cos\psi+\sqrt{\Lambda^2-\frac{k^2}{4}\sin^2\psi}}^{-\frac{k}{2}\cos\psi+\sqrt{\Lambda_d^2-\frac{k^2}{4}\sin^2\psi}} F\,(k,p,\psi)\,dp\,+$$

$$+\int_{\psi=\frac{\pi}{2}}^{\frac{3\pi}{2}} d\psi \int_{p=-\frac{k}{2}\cos\psi+\sqrt{\Lambda^2-\frac{k^2}{4}\sin^2\psi}}^{\frac{k}{2}\cos\psi+\sqrt{\Lambda_d^2-\frac{k^2}{4}\sin^2\psi}} F(k,p,\psi)\, dp, \tag{3.8}$$

which, after a change of the integration variable $\psi \to \pi - \psi$ in the second integral, becomes

$$\int_{\psi=-\frac{\pi}{2}}^{\frac{\pi}{2}} d\psi \int_{p=\frac{k}{2}\cos\psi+\sqrt{\Lambda^2-\frac{k^2}{4}\sin^2\psi}}^{-\frac{k}{2}\cos\psi+\sqrt{\Lambda_d^2-\frac{k^2}{4}\sin^2\psi}} \times$$
$$\times \{F(k,p,\psi) + F(k,p,\pi-\psi)\}\, dp. \tag{3.9}$$

After these transformations have been done, the Taylor expansion of the integrand can be termwise integrated in $p$, the result expanded in $k$ again, and the result of this integrated in $\psi$, giving the answer. This may be easily done, for example, using available symbolic algebra software [89]. The result gives us the following correction to the inverse propagator

$$\delta G^{-1}(\hat{k}) = \frac{D\,k^2\left(\Lambda_d^{-2-y} - \Lambda^{-2-y}\right) y}{32\pi\,(2+y)} + O(k^3,\omega) \approx$$
$$\approx \frac{D\,k^2\,\delta\Lambda\,y\,\Lambda^{-3-y}}{32\pi} + O(k^3,\omega,\delta\Lambda^2), \tag{3.10}$$

the final approximation being done in the $\delta\Lambda \to 0-$ limit. This is the required answer which generates the lowest-order viscosity correction

$$\delta\nu = \frac{(y\,D\,\Lambda^{-2-y} - 2\,T)\,\delta\Lambda}{32\,\pi\,\nu^2\,\Lambda}. \tag{3.11}$$

As we proposed before, here we have already recovered the result for both noises taken together.

### 3.1.4 Correction to the Force Self-Correlation Function

In a way similar to that used in the case of the inverse propagator correction, we will obtain here the expression for the force self-correlation function correction. Consider the lowest-order bare force correction in Fourier space

$$\delta f(\hat{k}) \equiv \frac{1}{2\,(2\pi)^3}\int_{\hat{p}} \left[\vec{k},\vec{p}\right]_3 \left\{\frac{1}{p^2} - \frac{1}{\left|\vec{k}-\vec{p}\right|^2}\right\} G(\hat{p})\, f(\hat{p})\, G(\hat{k}-\hat{p})\, f(\hat{k}-\hat{p})\, d\hat{p}. \tag{3.12}$$

After applying Wick's theorem it is possible to show that it generates the following correlation function $\overline{\delta f(\hat{k})\,\delta f(\hat{k}')}$

$$\frac{\delta(\hat{k}+\hat{k}')}{2\,(2\pi)^6}\int_p \left[\vec{k},\vec{p}\right]_3^2 \left\{\frac{1}{p^2}-\frac{1}{\left|\vec{k}-\vec{p}\right|^2}\right\}^2 |G(\hat{p})|^2\,\left|G(\hat{k}-\hat{p})\right|^2\,D(p)\,D(k-p)\,d\hat{p}. \quad (3.13)$$

After exact frequency integration, the result to lowest-order in $\omega$ will be

$$\frac{2\pi\,\delta(\hat{k}+\hat{k}')}{\nu^3}\int_p \left[\vec{k},\vec{p}\right]_3^2 \left\{\frac{1}{p^2}-\frac{1}{\left|\vec{k}-\vec{p}\right|^2}\right\}^2 \times$$

$$\frac{(D\,p^{-y}+T\,p^2)\left(D\left|\vec{k}-\vec{p}\right|^{-y}+T\left|\vec{k}-\vec{p}\right|^2\right)}{p^2+\left|\vec{k}-\vec{p}\right|^2}\,d\vec{p}+O(\omega). \quad (3.14)$$

Applying the transformations from the previous Section, one gets

$$\frac{2\pi\,\delta(\hat{k}+\hat{k}')\,k^2}{\nu^3}\int_p \frac{p^3\,sin^2\,\psi}{\left(2p^2+\frac{k^2}{2}\right)} \times$$

$$\left\{\frac{1}{p^2+k\,p\,cos\,\psi+\frac{k^2}{4}}-\frac{1}{p^2-k\,p\,cos\,\psi+\frac{k^2}{4}}\right\}^2 \times$$

$$\left\{D\left(p^2+k\,p\,cos\,\psi+\frac{k^2}{4}\right)^{-\frac{y}{2}}+T\left(p^2+k\,p\,cos\,\psi+\frac{k^2}{4}\right)\right\} \times$$

$$\left\{D\left(p^2-k\,p\,cos\,\psi+\frac{k^2}{4}\right)^{-\frac{y}{2}}+T\left(p^2-k\,p\,cos\,\psi+\frac{k^2}{4}\right)\right\}\,dp\,d\psi+O(\omega). \quad (3.15)$$

In the limit $\delta\Lambda \to 0-$, the Taylor expansion and termwise integration give

$$-\frac{\pi\,k^4\,\delta(\hat{k}+\hat{k}')}{\nu^3}\,\frac{\left(D\,\Lambda^{-2-y}+T\right)^2}{\Lambda}\,\delta\Lambda+O(k^5,\omega,\delta\Lambda^2). \quad (3.16)$$

This leads to the following corrections to the force amplitudes ($y \neq -2$)

$$\delta T=-\frac{\left(D\,\Lambda^{-2-y}+T\right)^2\,\delta\Lambda}{16\pi\,\nu^3\,\Lambda},\quad \delta D=0. \quad (3.17)$$

### 3.1.5 Nonlinear Coupling (Nondimensionalization)

Consider the problem containing only the nonthermal noise first. Let us apply the following nondimensionalization transformation to our dimensional problem (3.1),(3.4)

$$\vec{x}\to X\,\vec{x},\quad \vec{k}\to\frac{\vec{k}}{X},\quad t\to T\,t,\quad \zeta\to W\,\zeta,\quad \psi\to P\,\psi,\quad f(\vec{x},t)\to F\,f(\vec{x},t), \quad (3.18)$$

with quantities $X, T, W, P, F$ carrying the appropriate dimensions. Choosing rescaling coefficients

$$T = \frac{X^2}{\nu}, \quad W = D^{\frac{1}{2}}\, T^{\frac{1}{2}}\, X^{\frac{y}{2}-2}, \quad F = \frac{D^{\frac{1}{2}}\, X^{\frac{y}{2}-2}}{T^{\frac{1}{2}}} \tag{3.19}$$

will put our dimensional problem (3.1),(3.4) into a nondimensional form

$$\begin{aligned} \frac{\partial \zeta}{\partial t} + \sqrt{g}\, \frac{\partial(\zeta, \psi)}{\partial(x, y)} &= \Delta \zeta + f, \\ \zeta &= -\Delta \psi, \quad \text{and} \\ \overline{f(p)\, f(q)} &= 2\,(2\pi)^3\, |\vec{p}|^{-y+2}\, \delta(p+q), \end{aligned} \tag{3.20}$$

where we have introduced the scale-dependent nondimensional coupling constant

$$g(X) \equiv \frac{D\, X^{y+2}}{\nu^3}. \tag{3.21}$$

As may be seen, we have succeeded via the nondimensionalization (3.18) and (3.19) in reducing the number of determining parameters from three $X, \nu, D$ to one $g$ in the problem without thermal noise. Introduction of the thermal noise will lead to another nondimensional parameter, one which may be expressed, for example, as

$$h(X) \equiv \frac{T}{D\, X^{y+2}}, \tag{3.22}$$

or as yet another (thermal) coupling constant

$$g_T(X) \equiv \frac{T}{\nu^3}, \quad \text{such that:} \quad g_T = g\, h. \tag{3.23}$$

As a scale of length in the following we will use $X = 1/\Lambda$.

### 3.1.6 Differential Recursive Relations

Now one can imagine that the scale-elimination procedure is done recursively an infinite number of times. This will lead to the following differential recursive relations obtained from the infinitesimal corrections (3.11), (3.17)

$$\begin{aligned} \frac{\delta log\ T}{\delta log\ \Lambda} &= -\frac{g}{16\pi}\, \frac{(1+h)^2}{h}, \\ \frac{\delta log\ \nu}{\delta log\ \Lambda} &= \frac{g}{32\pi}\, (y - 2\,h)\,. \end{aligned} \tag{3.24}$$

The closed system may be obtained in terms of nondimensional parameters $g, h$

$$\frac{\delta log\ g}{\delta log\ \Lambda} = -\frac{3\,g}{32\pi}\,(y-2\,h) - y - 2,$$
$$\frac{\delta log\ h}{\delta log\ \Lambda} = -\frac{g}{16\pi}\,\frac{(1+h)^2}{h} + y + 2, \tag{3.25}$$

or in terms of $g, g_T$

$$\frac{\delta log\ g}{\delta log\ \Lambda} = -\frac{3}{32\pi}\,(y\,g - 2\,g_T) - y - 2,$$
$$\frac{\delta log\ g_T}{\delta log\ \Lambda} = -\frac{1}{16\pi}\,\frac{(g+g_T)^2}{g_T} - \frac{3}{32\pi}\,(y\,g - 2\,g_T)\,. \tag{3.26}$$

Now we will proceed to study the properties of the solutions of this system. We are especially interested in the stable fixed-points, which, following the lines of the general RG idea [46], are *associated with some physically meaningful states of the system.*

The dynamics of $\{g, g_T\}$ in phase-space for all $\Lambda \in [0, \Lambda_d]$ will be specified completely by fixing the initial conditions: $g(\Lambda_d) = g_0$, $g_T(\Lambda_d) = h(\Lambda_d) = 0$. The last condition simply signifies that in the original system bare thermal noise was absent; it is completely generated in the course of shell-elimination. As was noted before, large-scale ($\Lambda \to 0+$) properties are expected to be universal in all "normal turbulent" situations, that is, not to depend on the initial data $(g_0, \nu_0)$ and to be determined by the properties of (3.3), (3.4) alone.

### 3.1.7 Logarithmic Theory

Note that in the above derivation the case $y = -2$ is somewhat special and requires separate consideration. If $y = -2$ then one needs to consider only one (thermal) input noise, and the force amplitude and viscosity corrections may be readily written down using (3.11) and (3.17)

$$\delta T = -\frac{T^2\,\delta\Lambda}{16\pi\,\nu^3\,\Lambda}, \quad \delta\nu = -\frac{T\,\delta\Lambda}{16\pi\,\nu^2\,\Lambda}, \tag{3.27}$$

from which the relations of the *fluctuation-dissipation* type [16, 18] may be derived

$$\frac{\partial log\ T}{\partial log\ \Lambda} = \frac{\partial log\ \nu}{\partial log\ \Lambda} = -\frac{g_T}{16\pi}. \tag{3.28}$$

The resulting equation for the thermal coupling in this case is

$$\frac{\partial log\ g_T}{\partial log\ \Lambda} = \frac{g_T}{8\pi} \tag{3.29}$$

with the exact solution

$$g_T(\Lambda) = \frac{1}{\frac{1}{g_0} - \frac{1}{8\pi} log\ \frac{\Lambda}{\Lambda_d}}. \tag{3.30}$$

Note that the same results (3.29) and (3.30) could have been obtained by omitting the first equation and by formally inserting $g = 0$ in (3.26).

We see that as $\Lambda \to 0+$ the coupling behaves as $g_T(\Lambda) \propto 8\pi/(-log\ (\Lambda/\Lambda_d))$, which verifies the fact that the truncation of the diagrammatic series (with effective expansion parameter $g_T$ in this case) was done legitimately because the expansion parameter is as small as necessary. The solution in terms of RG viscosity also follows

$$\nu(\Lambda) = \nu_0 \left(1 - \frac{g_0}{8\pi} log\ \frac{\Lambda}{\Lambda_d}\right)^{\frac{1}{2}} \propto \nu_0 \sqrt{\frac{g_0}{8\pi}} \left(-log\ \frac{\Lambda}{\Lambda_d}\right)^{\frac{1}{2}}, \quad \text{as} \quad \Lambda \to 0+. \tag{3.31}$$

It should be noted that in the thermal equilibrium case the bare viscosity $\nu_0$ and initial coupling $g_0$ remain in the results, which signifies that the amplitudes thus obtained in front of logarithmic dependencies are nonuniversal. This is what we would to expect in the thermal equilibrium case, however, because this situation simulates the noise made by the random molecular motion coming from the smallest scales (recall that the thermal noise amplitude is $\propto k^4$). For discussion of this phenomenon, see [16, 18].

### 3.1.8 Trivial Case

In this case, as we will see shortly, nonthermal noise, although formally present as a phase-space variable, is *irrelevant* in the Wilson and Ma sense [88, 46]; that is, the fixed-point behavior will be totally unchanged if it was removed from consideration.

We claim that the trivial fixed point of system (3.26) is the only stable fixed point in the region $y < -2$. The fact that (3.26) has a trivial fixed point is obvious. The stability of this fixed point may be also verified. Asymptotically, in the neighborhood of this fixed point we assume that solutions $g, g_T \to 0+$ as $\Lambda \to 0+$. Then from

the first equation in (3.26) it immediately follows that $g \propto (\Lambda/\Lambda_d)^{-y-2}$, which is consistent with the assumption $g \to 0+$ as $\Lambda \to 0+$ if $y < -2$, which is the case. The asymptotic solution for $g_T$ coincides with the one already obtained for the $y = -2$ case, namely $g_T \propto 8\pi/(-log\ (\Lambda/\Lambda_d))$, as is easy to see. From this we conclude that $g \ll g_T$ as $\Lambda \to 0+$, and in this sense $y < -2$ case is similar to the $y = -2$ case considered before.

### 3.1.9 Nontrivial Case and $\epsilon$-Expansion

Assume now that $y = -2 + \epsilon$, where $\epsilon \ll 1$ is a sufficiently small parameter. Then the following stable nontrivial fixed point of the system (3.25) may be found in the form of a series in $\epsilon$

$$h^* = \frac{1}{2} + \frac{\epsilon}{4} + O(\epsilon^2), \quad g^* = \frac{32\pi\,\epsilon}{9} + O(\epsilon^2). \tag{3.32}$$

Indeed, assume that some small perturbation $h = h^* + h'$, $g = g^* + g'$ arises. Then the linearized equation for perturbation in the leading order in $\epsilon$ is

$$\frac{\partial g'}{\partial log\ \Lambda} = \frac{3^4\,g'}{2^5\pi^2\,\epsilon}, \quad \frac{\partial h'}{\partial log\ \Lambda} = -\frac{3^2\,g'}{2^4\pi}, \tag{3.33}$$

solution of which is obviously decaying as $\Lambda \to 0+$.

Having in mind the truncation of the perturbation diagrammatic series, we now require $\epsilon$ to be as small as necessary for this truncation to be legitimate: higher-order diagrams are to be small compared with first-loop diagrams already considered. Mathematically this question is very subtle, and it is also believed that solutions arising in the form of power series in $\epsilon$ may have a zero radius of convergence, i.e. will be at most asymptotic expansions valid in the limit $\epsilon \to 0+$. There exists a great hope though, supported by extensive numerical evidence [11, 95] (in one dimension), [9] (in two dimensions), and [59] (in three dimensions), that results based on the lowest-order $\epsilon$-expansion give predictions very close to the unknown exact results valid, possibly, for finitely large $\epsilon > 0$ as well. This does not follow from the above derivations, however, and may be considered as a working hypothesis, the validity of which is to be verified in each particular case via accurate comparisons of the resulting

predictions with the numerical solution. This assumption, first proposed in [93], is being exploited throughout the thesis.

Now the asymptotic behavior of the RG-viscosity may be found in the neighborhood of the fixed point $g^* = 32\pi\epsilon/9$, $h^* = 1/2$ by substituting it into (3.24) giving the scaling law $\nu(\Lambda) \propto \Lambda^{-\epsilon/3}$. To get the amplitude factor we use the definition of the coupling constant (3.21); this results in

$$\nu(\Lambda) \propto \left(\frac{9\,D_0}{32\pi\,\epsilon}\right)^{\frac{1}{3}} \Lambda^{-\frac{\epsilon}{3}}. \tag{3.34}$$

Note that according to [93], if we completely ignore the thermal noise from the very beginning, which may be reproduced, for example, from (3.24) by setting $h = 0$; then the RG-viscosity solution is

$$\nu(\Lambda) \propto \left\{\nu_0^3 + \frac{3\,D_0}{16\pi\,\epsilon}\left(\Lambda^{-\epsilon} - \Lambda_d^{-\epsilon}\right)\right\}^{\frac{1}{3}} \propto \left(\frac{3\,D_0}{16\pi\,\epsilon}\right)^{\frac{1}{3}} \Lambda^{-\frac{\epsilon}{3}}, \tag{3.35}$$

which has the same scaling law but a different amplitude factor (difference is in the multiplicative factor $(3/2)^{1/3} \approx 1.145$). Indeed, we observe that considering the thermal noise renormalization leads to changed amplitudes in the fixed point. This proves that the thermal noise is a *relevant variable* in the two-dimensional case. As we observed, however, scaling laws remain unchanged. Moreover, we conclude that in all the nontrivial situations ($y > -2$) there is no dependence on the ultra-violet cutoff parameters $\nu_0$, $g_0$, which illustrates the *universality* of these results.

### 3.1.10 Energy Spectrum

The RG formulation considered above differs from the one originally proposed by Ma [46] in the fact that rescaling relations are absent, therefore allowing the region of Fourier space on which the RG equation is defined to shrink to zero. This "simplified" version of RG was first proposed by Forster, Nelson, and Stephen [16], and then used by Fournier and Frisch in [18]; it not only gave the same fixed points as its rescaled counterpart but also allowed the energy exponents and universal amplitudes to be calculated, which was finally done in complete and self-consistent form in [93]. Some alternative ways to get the same results may be found in [27]. For some background

material on the correspondence between flows with a large-scale and a power-law forces, see [51].

Consider now only the case $0 < \epsilon \ll 1$. In the previous Sections we have removed all the Fourier modes with wavevector $\vec{k}$ such that $\Lambda < \left|\vec{k}\right| < \Lambda_d$. Now, assume that the "external" wavenumber $k$ is fixed and sufficiently small lying within the universal range, and let us remove all the modes with wavenumber higher than this wavenumber $k$. This may be formally achieved by taking the limit $\Lambda \to k + 0$ in the preceding results.

Also, as an auxiliary necessary result, let us obtain the renormalization of the thermal noise amplitude $T$. Near the fixed point (3.32) let us put $\nu(\Lambda)$ and $g(\Lambda)$ equal to their asymptotic laws (3.32) and (3.34). Then from the first recursive relation (3.24) one may get

$$\frac{\partial log\ T}{\partial log\ \Lambda} \propto -\epsilon, \tag{3.36}$$

which gives the scaling law $T(\Lambda) \propto B\,\Lambda^{-\epsilon}$. The limiting amplitude $B$ may be found from the algebraic relation $g_T = g\,h$ taken near the fixed point. This leads to the following asymptotic relation

$$T(\Lambda) \propto \frac{D_0}{2}\,\Lambda^{-\epsilon}. \tag{3.37}$$

Introduce the Fourier space two-point vorticity correlation function $C(\vec{k},\omega)$, defined by

$$C(\vec{k},\omega) \equiv \int_{\vec{k}'}\int_{\omega'} \frac{\overline{\zeta(\vec{k},\omega)\,\zeta(\vec{k}',\omega')}}{2}\,\frac{d\vec{k}'}{(2\pi)^2}\,\frac{d\omega'}{2\pi}. \tag{3.38}$$

Near the fixed point (3.32), in the lowest order in the $\epsilon$-expansion (or, in the limiting coupling-expansion) one gets

$$C(\vec{k},\omega) = \frac{\frac{3\,D_0}{2}\,k^{4-\epsilon}}{\omega^2 + \left(\frac{9\,D_0}{32\,\pi\,\epsilon}\right)^{\frac{2}{3}}\,k^{4-\frac{2}{3}\epsilon}}. \tag{3.39}$$

The steady-state energy spectrum, which is normalized by the condition $\int E(k)\,dk = E_{tot}$-total energy, may be found from this correlation function as (see [54, 58, 16, 93])

$$E(k) = \frac{1}{k\,(2\pi)^2}\int_{\omega=-\infty}^{+\infty} C(\vec{k},\omega)\,d\omega, \tag{3.40}$$

which, with the use of (3.39) reduces exactly to

$$E(k) \propto \left(\frac{3\,D_0^2\epsilon}{16\,\pi^2}\right)^{\frac{1}{3}} k^{1-\frac{2}{3}\epsilon}. \tag{3.41}$$

Note the difference between the above result and the result based on the Yakhot-Orszag theory [93]: when formally applied to two dimensions without considering thermal noise renormalization, it will give the RG energy spectrum amplitude $(2/3)^{2/3}$ times smaller. This demonstrates once again that the thermal noise is a relevant variable in exactly two dimensions.

### 3.1.11 RG-Based Enstrophy Transfer Function

The aim of the following two Sections is to present a way of employing the results obtained above for computation of the energy (enstrophy) transfer function, thus "resolving" the arising closure problem via considering a small coupling limit. As we have seen from the above results, small coupling turns out to be a self-consistent assumption for the RG Navier-Stokes equation in the cases when $-\infty < \epsilon \ll 1$. But practically interesting cases of "strong" turbulence correspond to finitely large $\epsilon > 0$. Therefore, the direct application of the small coupling results for finitely large $\epsilon > 0$ may not be rigorously justified. Despite this, we will employ the small coupling assumption for the Kolmogorov $\epsilon = 4$ case, thus making the closure of moments equations. It is assumed, however, that a small-coupling condition in such cases is not associated with asymptotically small $\epsilon$.

Let us enumerate again what has been achieved in the previous Sections. In accordance with the tradition in the existing turbulence phenomenology, we will express all the results in the time-wavenumber domain. After all the wavenumbers higher than some sufficiently small $k$ were removed, the renormalized equation of motion and the definition of the force took the form

$$\left(\frac{\partial}{\partial t} + \nu_k\right) \zeta(\vec{k},t) = f(\vec{k},t) + \lambda_r \int_{\vec{p}} g(\vec{k},\vec{p})\,\zeta(\vec{p},t)\,\zeta(\vec{k}-\vec{p},t)\,d\vec{p} + O(\lambda_r^2),$$

$$\text{where:} \quad g(\vec{k},\vec{p}) \equiv \frac{1}{2(2\pi)^2}\left[\vec{k},\vec{p}\right]\left\{\frac{1}{p^2} - \frac{1}{\left|\vec{k}-\vec{p}\right|^2}\right\},$$

$$\overline{f(\vec{k},t)\,f(\vec{k}',t)} = 2\,(2\pi)^2\,D_r(k)\,\delta\left(\vec{k}+\vec{p}\right)\,\delta(t-t'),$$

$$D_r(k) = \frac{3\,D_0}{2}\,k^{4-\epsilon},\quad \nu_k \equiv \nu_r(k)\,k^2,\quad \nu_r(k) = \left(\frac{9\,D_0}{32\,\pi\,\epsilon}\right)^{\frac{1}{3}}\,k^{-\frac{\epsilon}{3}}. \qquad (3.42)$$

Here we have introduced the accounting nondimensional parameter $\lambda_r = 1$ which will be used to obtain the corresponding power of the coupling constant, arising after nondimensionalization of (3.42), which is assumed to be small. In what follows we will preserve equations in the dimensional form.

Let us outline briefly what we are planning to present in this Section. Using the assumption of small large-scale (renormalized) coupling we will close up the equation for the two-point covariance in Fourier space, considering perturbation theory in this coupling constant. The expression for the enstrophy transfer function will be derived in the lowest order in this coupling.

To proceed, first, we develop the perturbation theory in the small coupling limit in an analogous way to [90, 13]. Seek the fluctuating solution in the following form

$$\zeta(\vec{k},t) = \zeta^0(\vec{k},t) + \lambda_r\,\zeta^1(\vec{k},t) + \lambda_r^2\,\zeta^2(\vec{k},t) + O(\lambda_r^3). \qquad (3.43)$$

Then, from the renormalized equation of motion (3.42), equating the same powers of parameter $\lambda_r$, we obtain

$$\left(\frac{\partial}{\partial t}+\nu_k\right)\,\zeta^0(\vec{k},t) = f(\vec{k},t),$$

$$\left(\frac{\partial}{\partial t}+\nu_k\right)\,\zeta^1(\vec{k},t) = \int_{\vec{p}} g(\vec{k},\vec{p})\,\zeta^0(\vec{p},t)\,\zeta^0(\vec{k}-\vec{p},t)\,d\vec{p},$$

$$\left(\frac{\partial}{\partial t}+\nu_k\right)\,\zeta^2(\vec{k},t) = \int_{\vec{p}} g(\vec{k},\vec{p})\,\left(\zeta^1(\vec{p},t)\,\zeta^0(\vec{k}-\vec{p},t)+\zeta^0(\vec{p},t)\,\zeta^1(\vec{k}-\vec{p},t)\right)\,d\vec{p}, \qquad (3.44)$$

etc.,

with the first two resulting solutions in the limit $t \to +\infty$ (to completely "forget" dependence on initial data)

$$\zeta^0(\vec{k},t) = \int_{s=0}^{t} f(\vec{k},s)\,e^{\nu_k\,(s-t)}\,ds,$$

$$\zeta^1(\vec{k},t) = \int_{s=0}^{t}\int_{\vec{p}} g(\vec{k},\vec{p})\,\zeta^0(\vec{p},s)\,\zeta^0(\vec{k}-\vec{p},s)\,d\vec{p}\,e^{\nu_k\,(s-t)}\,ds. \qquad (3.45)$$

Now consider the equation for the Fourier-space two-point vorticity correlation function. From the RG equation of motion (3.42) one can derive

$$\left(\frac{\partial}{\partial t}+\frac{\partial}{\partial t}+2\,\nu_k\right)\,\overline{\zeta(\vec{k},t)\,\zeta(\vec{k}',t')}=\overline{f(\vec{k},t)\,\zeta(\vec{k}',t')}+\overline{f(\vec{k}',t')\,\zeta(\vec{k},t)}+ \tag{3.46}$$

$$+\lambda_r\int_{\vec{p}}\left\{g(\vec{k},\vec{p})\,\overline{\zeta(\vec{p},t)\,\zeta(\vec{k}-\vec{p},t)\,\zeta(\vec{k}',t')}+g(\vec{k}',\vec{p})\,\overline{\zeta(\vec{p},t')\,\zeta(\vec{k}-\vec{p},t')\,\zeta(\vec{k}',t)}\right\}\,d\vec{p}.$$

Under the assumptions of stationarity in time and homogeneity in space, one has [54]

$$\overline{\zeta(\vec{k},t)\,\zeta(\vec{k}',t')}=(2\pi)^2\,W(\vec{k},|t-t'|)\,\delta\left(\vec{k}+\vec{k}'\right),\quad\text{and}\quad\frac{\partial}{\partial t}+\frac{\partial}{\partial t'}=0. \tag{3.47}$$

A note about this stationarity property in the two-dimensional case should be made. In fact, for the inverse cascade situation, which is our primary interest here, taking the limit $t\to+\infty$ will create a condensate state at $k=0$ due to the flow of energy towards small wavenumbers (see [74, 75]). This condensate state is known to alter the properties of the inertial range owing to direct interactions with the mode $k=0$. Therefore, stationarity in the two-dimensional case has some special features. We will understand stationarity in the sense that our system is observed and measured over very large but yet finite times, thus avoiding the need to deal with a condensate.

Using the lowest-order solution $\zeta^0$ one can derive

$$\overline{\zeta^0(\vec{k},t)\,\zeta^0(\vec{k}',t')}=2\,(2\pi)^2\,D_r(k)\,\delta\left(\vec{k}+\vec{k}'\right)\,e^{-\nu_k\,(t+t')}\,\frac{e^{2\nu_k\,\min\{t,t'\}}-1}{2\nu_k}. \tag{3.48}$$

From this, in the limit $t\to+\infty$ the expression for the equal-time lowest-order correlation function is

$$\overline{\zeta^0(\vec{k},t)\,\zeta^0(\vec{k}',t)}=2\,(2\pi)^2\,D_r(k)\,\delta\left(\vec{k}+\vec{k}'\right)\,\frac{1}{2\nu_k}. \tag{3.49}$$

Let us introduce expressions for the enstrophy and the energy per-scalar-mode spectra respectively:

$$\Omega(k)=\frac{k}{4\pi}\,\overline{\left|\zeta(\vec{k},t)\right|^2},\quad E(k)=\frac{\Omega(k)}{k^2}. \tag{3.50}$$

They are normalized by the conditions $\int_{k=0}^{+\infty}\Omega(k)\,dk=\Omega_{tot}$ and $\int_{k=0}^{+\infty}E(k)\,dk=E_{tot}$. Using them one obtains

$$\overline{\zeta^0(\vec{k},t)\,\zeta^0(\vec{k}',t)}=\frac{2\,(2\pi)^3}{k}\,\Omega^0(k)\,\delta\left(\vec{k}+\vec{k}'\right). \tag{3.51}$$

From the nonlinear term in (3.46) we can introduce the equal-time covariance transfer function. As is easy to see, the first nonvanishing term in the series in $\lambda_r$ for it is given by

$$T(\vec{k},\vec{k}') = 2\,\lambda_r^2 \int_{\vec{p}} g(\vec{k},\vec{p}) \left\{ \overline{\zeta^0(\vec{p},t)\,\zeta^0(\vec{k}-\vec{p},t)\,\zeta^1(\vec{k}',t)} + \right.$$
$$\left. + \overline{\zeta^0(\vec{p},t)\,\zeta^1(\vec{k}-\vec{p},t)\,\zeta^0(\vec{k}',t)} + \overline{\zeta^1(\vec{p},t)\,\zeta^0(\vec{k}-\vec{p},t)\,\zeta^0(\vec{k}',t)} \right\} d\vec{p}. \qquad (3.52)$$

Note that in the equal-time case the terms in (3.46) become real-valued and all the $\vec{k}'$-terms are equal to the corresponding $\vec{k}$-terms, simplifying the resulting expression.

As one may see from the previous result, the computation of the lowest-order transfer function reduces to the computation of the triple correlation functions of the form

$$\overline{\zeta^0(\vec{p},t)\,\zeta^0(\vec{k}-\vec{p},t)\,\zeta^1(\vec{k}',t)}. \qquad (3.53)$$

After substituting for $\zeta^1$ and using Wick's theorem together with the above formulas (3.48) and (3.51), after some algebra, one derives that this triple correlation function (3.53) in the limit $t \to +\infty$ is equal to

$$\frac{2\,(2\pi)^4}{p\,\left|\vec{k}-\vec{p}\right|}\,\Omega^0(p)\,\Omega^0\left(\left|\vec{k}-\vec{p}\right|\right)\delta(\vec{k}-\vec{k}')\,\left\{g(-\vec{k},-\vec{p}) + g(-\vec{k},\vec{p}-\vec{k})\right\}\,\Theta\left(k,p,\left|\vec{k}-\vec{p}\right|\right),$$

$$\text{where we denoted}\quad \Theta\left(k,p,\left|\vec{k}-\vec{p}\right|\right) = \frac{1}{\nu_k + \nu_p + \nu_{|\vec{k}-\vec{p}|}} \qquad (3.54)$$

The quantity $\Theta$ thus defined has the dimension of time and is called eddy-relaxation time in the closure theories [58]. Without repeating similar calculations one obtains the other two triple correlation functions in (3.52) on the basis of simultaneous change: $\vec{p} \to \vec{k}'$, $\vec{k} \to \vec{k}' + \vec{p}$, $\vec{k}' \to \vec{k} - \vec{p}$ made in (3.53), (3.54) once and twice respectively.

Using these results we obtain the following expression for the lowest-order vorticity correlation function transfer:

$$T(\vec{k},\vec{k}') = 2\,(2\pi)^4\,\delta(\vec{k}+\vec{k}') \int_{\vec{p}} g(\vec{k},\vec{p})\,\frac{\Theta\left(k,p,\left|\vec{k}-\vec{p}\right|\right)}{k\,p\,\left|\vec{k}-\vec{p}\right|} \times$$
$$\times \left\{\Omega^0(p)\,\Omega^0\left(\left|\vec{k}-\vec{p}\right|\right) k\,\left[g(\vec{k},\vec{p}) + g(\vec{k},\vec{k}-\vec{p})\right] + \right.$$
$$+\Omega^0(k)\,\Omega^0(p)\,\left|\vec{k}-\vec{p}\right|\,\left[g(\vec{k}-\vec{p},\vec{k}) + g(\vec{k}-\vec{p},-\vec{p})\right] +$$
$$\left. +\Omega^0(k)\,\Omega^0\left(\left|\vec{k}-\vec{p}\right|\right) p\,\left[g(\vec{p},\vec{p}-\vec{k}) + g(\vec{p},\vec{k})\right]\right\}. \qquad (3.55)$$

Now one can write down the enstrophy equation following from (3.46) as:

$$2\nu_k\,\Omega(k) = \frac{2\,k\,D_r(k)}{\pi} + T(k), \tag{3.56}$$

where the enstrophy transfer function $T$ is introduced and after the expansion of the geometrical factors, $g$ may be presented in the form

$$\begin{aligned} T(k) = \frac{2}{(2\pi)^3}\int_{\vec{p}} d\vec{p}\left[\vec{k},\vec{p}\right]_3^2 \left\{\frac{1}{p^2} - \frac{1}{\left|\vec{k}-\vec{p}\right|^2}\right\} \frac{\Theta\left(k,p,\left|\vec{k}-\vec{p}\right|\right)}{p\left|\vec{k}-\vec{p}\right|} \times \\ \times\left\{k\left(\frac{1}{p^2} - \frac{1}{\left|\vec{k}-\vec{p}\right|^2}\right)\Omega^0(p)\,\Omega^0\left(\left|\vec{k}-\vec{p}\right|\right) + \right. \\ + \left|\vec{k}-\vec{p}\right|\left(\frac{1}{k^2} - \frac{1}{p^2}\right)\Omega^0(k)\,\Omega^0(p) + \\ \left. + p\left(\frac{1}{\left|\vec{k}-\vec{p}\right|^2} - \frac{1}{k^2}\right)\Omega^0(k)\,\Omega^0\left(\left|\vec{k}-\vec{p}\right|\right)\right\}. \end{aligned} \tag{3.57}$$

### 3.1.12 Kraichnan's Two-Parametric Eddy-Viscosity

Let us follow [39], and introduce the notion of effective eddy-viscosity. For this purpose, we choose some intermediate wavenumber $k_c$ and split up the transfer function discussed above into two parts as

$$T(k) = T^{<}(k,k_c) + T^{>}(k,k_c), \tag{3.58}$$

where

$$T^{>}(k,k_c) = \int_{\tilde{\Delta}} T(\vec{k},\vec{p},\vec{q})\,d\vec{p}d\vec{q}, \tag{3.59}$$

and the region of integration $\tilde{\Delta}$ includes only $\vec{p}$ and $\vec{q}$ such that $|\vec{p}|$ or $|\vec{q}|$ is $> k_c$, and $\vec{q} = \vec{k} - \vec{p}$. We are using the standard notation $T(\vec{k},\vec{p},\vec{q})$ [39] for the integrand in (3.57).

Now we define the two-parametric eddy-viscosity (TPEV), taken in the lowest order in $\epsilon$-expansion, as

$$\nu(k,k_c) = -\frac{T^{>}(k,k_c)}{2k^2\Omega^0(k)}. \tag{3.60}$$

These two-parametric quantities are thus fully defined and may be reduced to simpler quadratures and computed numerically, as has been first done on the basis of Test-Field Model (TFM) closure in [39], and, more recently, in [78] on the basis of RG. We will return to these results several more times in the following Sections and elaborate on some of the details of the transfer calculation in the last Chapter of the thesis. Let us just mention one principal result here.

The leading-order in $k \to 0+$ limit of the effective eddy-viscosity in the Kolmogorov case of $\epsilon = 4$ may be expressed through the RG viscosity as (for details, see Appendix B)

$$\nu(0, k_c) = -\frac{1}{3}\,\nu_r(k_c). \tag{3.61}$$

This result requires a special note. It means that the eddy-viscosity in 2D becomes negative in the limit $k \to 0+$, corresponding to the flow of energy to the large scales (inverse energy cascade). It also shows the important differences between the RG viscosity and the two-parametric one. The RG-based viscosity is a positive quantity which is unable to account for the inverse energy cascade, having the physical meaning of the response of the Navier-Stokes system to the finite band of wavenumbers elimination. Namely the two-parametric eddy-viscosity has the physical meaning of turbulent viscosity in two dimensions.

Eddy-viscosity may be expressed through the universal function $H(k/k_c)$ as follows:

$$\nu(k, k_c) = \nu(0, k_c) H(\frac{k}{k_c}). \tag{3.62}$$

As we will see in what follows, this sign-changing function tends to 1.8 as $k \to k_c$ and to $-1$ as $k \to 0$, crossing the $k/k_c$-axis at $k/k_c = 0.82$. Such a behavior agrees very well with Kraichnan's conclusions based on the TFM closure [38].

## 3.2 Direct Numerical Simulation (DNS) Tests Of Eddy Viscosity

It is well known that the existence of inviscid invariants $\int d^2x\zeta^{2n}$ of (3.1) results in the flux of energy towards the largest spatial scales. The presence of this inverse cascade complicates the large-scale description of 2D flows and requires a refinement of the classical hydrodynamic notion of "eddy viscosity." The concept of eddy viscosity is well defined for 3D turbulent flows, where energy cascades towards the smallest flow scales where it is dissipated. To achieve an adequate coarse-grained description of 3D flow, one can introduce an increased "effective" dissipation at large scales which accounts for the unresolved dissipation.

In 2D flows, the inverse flux of energy at large scales and the enstrophy dissipation at small scales make the eddy viscosity concept more subtle. It was argued by Kraichnan [39] that, in Fourier space, a 2D eddy viscosity should include two parameters: a cutoff wave number $k_c$ (which essentially determines the size of the coarse grain), and the wave number of a given mode, $k$. The two-parameter eddy viscosity (TPEV), denoted by $\nu(k|k_c)$, describes the energy exchange between a given resolved vorticity mode with the wave number $k$ and all sub-grid, or unresolved, modes with $k > k_c$; it accounts correctly for the energy and enstrophy fluxes between resolved and unresolved scales. The TPEV is derived from the evolution equation for the spectral enstrophy density $\Omega(k,t) \equiv \frac{k}{4\pi}\overline{\zeta(\mathbf{k},t)\zeta(-\mathbf{k},t)}$

$$\left(\partial_t + 2\nu k^2\right)\Omega(k,t) = T_\Omega(k,t). \tag{3.63}$$

Here, the enstrophy transfer function $T_\Omega(k,t)$ is given by

$$T_\Omega(k,t) = \frac{k}{4\pi}\int_{\mathbf{p}+\mathbf{q}=\mathbf{k}} \frac{\mathbf{p}\times\mathbf{q}}{p^2}\overline{\zeta(\mathbf{p},t)\zeta(\mathbf{q},t)\zeta(-\mathbf{k},t)}\frac{d\mathbf{p}\;d\mathbf{q}}{(2\pi)^2} \;+\; \text{c.c.}, \tag{3.64}$$

where c.c. stands for the complex conjugate term. Assuming that the system is in a statistical steady state and extending integration in (3.64) only over all triangles $(\mathbf{k},\ \mathbf{p},\ \mathbf{q})$ that $|k-p| < q < k+p$ and $p$ or $q$ is greater than $k_c$, one defines the

two-parametric transfer $T_\Omega(k|k_c)$ and TPEV [39]:

$$\nu(k|k_c) = -\frac{T_\Omega(k|k_c)}{2k^2\Omega(k)}. \tag{3.65}$$

In a wide class of quasi-normal approximations [49], the two-parametric transfer $T_\Omega(k|k_c)$ in two dimensions is given by

$$\begin{aligned} T_\Omega(k|k_c) \quad &= \int\int_\Delta \Theta_{-k,p,q}(p^2-q^2)\sin\alpha \left[\frac{p^2-q^2}{p^2q^2}\Omega(p)\Omega(q)\right. \\ &\left. - \frac{k^2-q^2}{k^2q^2}\Omega(q)\Omega(k) + \frac{k^2-p^2}{k^2p^2}\Omega(p)\Omega(k)\right] dpdq, \end{aligned} \tag{3.66}$$

where $\Theta_{-k,p,q}$ is the triad relaxation time. Here, the angle $\alpha$ is formed by the vectors $\mathbf{p}$ and $\mathbf{q}$, and $\int\int_\Delta$ denotes integration over the area defined above (3.65).

The main difference between various spectral closure models is in the specification of $\Theta_{-k,p,q}$. In [39], $T_\Omega(k|k_c)$ was evaluated using TFM. It was found that TPEV is a sign-changing function of the form $\nu(k|k_c) = |\nu(0|k_c)|N(k/k_c)$, with $\nu(0|k_c) < 0$, $N(0) = -1$, and $N(1) \approx 1.8$. The derivation of $\Theta_{-k,p,q}$ using the RG theory was given in [13] and adapted for 2D isotropic turbulence in [78]. In the present work, we compare $\nu(k|k_c)$ for the inverse energy cascade regime calculated from DNS data with those predicted by TFM and the RG theory.

We solve equation (3.1) numerically in a periodic box of the size $2\pi \times 2\pi$ using $512^2$ Fourier modes. The numerical scheme involves a Fourier-Galerkin pseudo-spectral spatial approximation with the implicit Adams-type second order stiffly stable time-stepping scheme [33]. In order to increase the effective inertial range, mode-selective hyperviscosity [44] of the form $\nu(k) = \nu_L(k) + \nu_S(k) = A_L k^{-10} + A_S k^{14}$ has been introduced in the vorticity equation (3.1) instead of the molecular viscosity. The constant coefficients $A_L$ and $A_S$ have been selected empirically so as to minimize the distortion of the energy inertial subrange.

To simulate the inverse energy cascade, high wave number forcing

$$f(k,t) = \frac{A_f}{\sqrt{\tau}}\left(\delta_{k,k_f-1} + \delta_{k,k_f} + \delta_{k,k_f+1}\right)\sigma_{\vec{k}}$$

is introduced in the vorticity equation; here, $\tau$ is the time-step, $A_f$ is the forcing amplitude, and the random variable $\sigma_{\vec{k}}$ is a Gaussian random function with unit

variance. It was assumed that no correlation in time exists, in such a way simulating the white-noise property of the force. The results are not sensitive to initial vorticity field distributions, including the extreme case of the zero field. A series of numerical experiments with various $k_f$ and other flow parameters have been performed. Here we shall report only the results with $k_f = 98$ since they gave the broadest inertial range. Other parameters used in these simulations were $A_f = 0.03244$, $A_L = 0.5$, and $A_S = 0.95 \times 10^{-34}$. The value of $A_S$ chosen is somewhat high, to ensure efficient enstrophy dissipation and to eliminate the need for the de-aliasing.

In Fig. 3.1 we plot the total energy $E_{tot}(t) = \int_0^{+\infty} \Omega(k,t)/k^2\, dk$ and the enstrophy $\Omega_{tot}(t) = \int_0^{+\infty} \Omega(k,t)\, dk$ as functions of time. In Fig. 3.1 one can see that the energy grows with time and eventually tends to reach a steady state. However, the drift towards the energy steady state is significantly slower than towards that of the enstrophy. Defining the rms velocity as $V_{\rm rms}^2 = \sum_{\mathbf{k}} |\mathbf{u}(\mathbf{k})|^2$ and the characteristic turnover time of the largest eddies as $\tau_{tu} = 2\pi/V_{\rm rms}$, we infer from Fig. 3.1 that a steady state for the total enstrophy was achieved after about $1.2\ \tau_{tu}$, while about $5\tau_{tu}$ were required to attain a steady state for the total energy. Note however, that all the modes with $k > 5$ have reached the steady state after $t \approx 2\tau_{tu}$, and only the largest modes were still developing. The results presented below pertain to the integration time $t \leq 10^4$ before the energy saturates at low wavenumbers.

In Fig. 3.2 we plot the time-averaged energy spectrum obtained after about $5\ \tau_{tu}$. The inertial range $E \propto k^{-x}$ extends over more than a decade in wave number space. Mean square line-fitting over the interval $k \in (12, 50)$ gives the scaling exponent close to the Kolmogorov value of 5/3. Note that a good agreement with the Kolmogorov scaling in the energy sub-range has been reported recently in [48] for $256^2$ simulations and in [74, 75] for very high resolution simulations with $2048^2$ Fourier modes. In Fig. 3.2 we also plot a compensated energy spectrum, $k^{5/3}\, \epsilon^{-2/3}\, E(k)$, where $\epsilon$ is the energy transfer rate. The value of the Kolmogorov constant calculated from this data is about $C_k = 6.2$, in reasonable agreement with the value 5.8 calculated from DNS in [47] using the $256^2$ resolution and 6.69 obtained analytically in [38] on the basis of TFM.

In Fig. 3.3 we plot the $k$-dependent energy and enstrophy flux functions defined as $\Pi_E(k) = \int_0^k T_\Omega(n)\, n^{-2}\, dn$ and $\Pi_\Omega(k) = \int_0^k T_\Omega(n) dn$, respectively. As expected, an inverse energy cascade with the constant energy transfer rate $\epsilon$ develops for $k < k_f = 98$, see Fig. 3.3. For $k > k_f$, $\Pi_E(k)$ and $\Pi_\Omega(k)$ both quickly fall to zero, due to the strong dissipation at wave numbers adjacent to $k_f$. In Fig. 3.3 we see that the flux of enstrophy in the energy sub-range $k < k_f$ is zero. A strong enstrophy flux is observed for $k > k_f$, until the enstrophy dissipation takes over and suppresses the flux of enstrophy into even smaller scales. The resolution employed in this study was insufficient to detect a well-defined enstrophy transfer range. The results plotted in Fig. 3.3 also indicate that the numerical scheme used conserves both total energy and enstrophy, since $\Pi_\Omega(0) = \Pi_\Omega(\infty) = 0$ and $\Pi_E(0) = \Pi_E(\infty) = 0$.

By computing the third-order vorticity correlation function in (3.64) we have calculated $k$- and $k_c$-dependent enstrophy transfer function $T_\Omega(k|k_c)$ employed in (3.65) extending the integration only over those $\mathbf{p}$ and $\mathbf{q}$ that either $p \geq k_c$ or $q \geq k_c$. We set $k_c = 50$, well inside the energy inertial subrange.

The DNS-inferred normalized TPEV [ viz., $N(k/k_c) = \nu(k|k_c)/|\nu(0|k_c)|$] is plotted in Fig. 3.4, along with the TFM-based [39] and the RG-based [78] analytical predictions. The agreement between the DNS-based results and the TFM and RG theories is very good over the entire energy transfer range, up to the wave numbers close to $k_c$, where the DNS data saturates, while TFM and RG curves exhibit sharp cusp. The physics leading to this cusp is as follows. As $k$ approaches $k_c$, more elongated triads with either $p$ or $q \ll k_c$ become involved in the energy exchange between the mode $k$ and the sub-grid scale modes. The contribution of these triads results in the cusp behavior of the theoretical TPEV. However, in finite box DNS with large-scale energy removal, the energy of small wave number modes is reduced (see Fig. 3.2), which implies that instead of the sharp growth, the TPEV should saturate at $k \to k_c$. To illustrate and quantify this explanation, we recalculated the RG-based TPEV with the enstrophy spectrum in (3.66) corrected at $k \leq 5$ according to Fig. 3.2. In Fig. 3.5, we compare the DNS- and the RG-based TPEV in their actual values, whereas the RG calculations were based upon the value of $\epsilon$ found from DNS. The agreement

between the two is very good. We have also calculated TPEV for $k_c = 35, 45$ and 55 and found that the DNS-inferred TPEV scales with $k_c^{-4/3}$, in full agreement with the Kolmogorov and the Richardson laws. At all values of $k_c$ tested an equally good agreement between the DNS data and the RG predictions was observed.

The good agreement demonstrated in Figs. 3.4 and 3.5 provides an indirect validation of the TFM and the RG results for isotropic 2D turbulence.

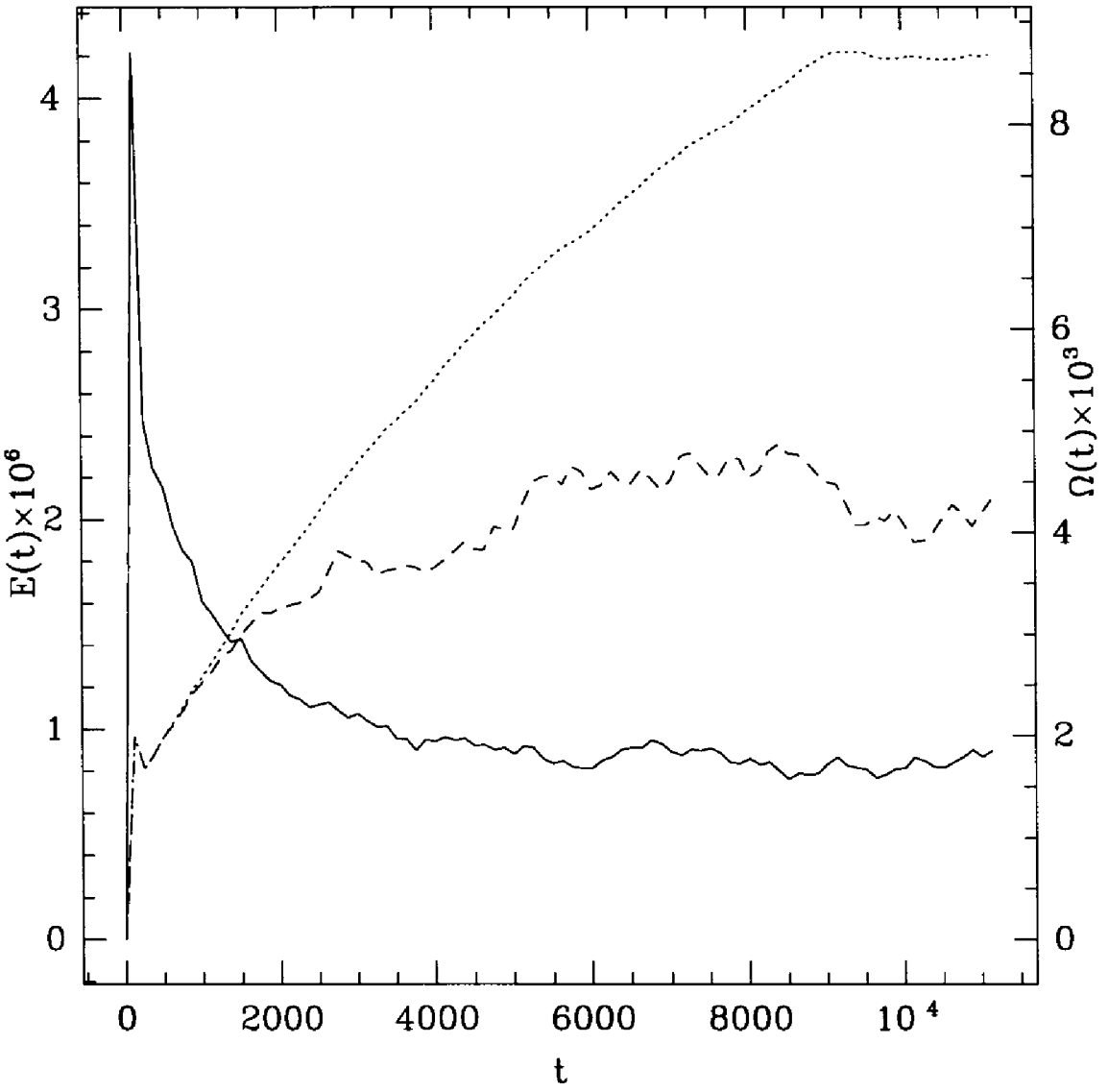


Figure 3.1: Evolution of the total energy $E(k)$ (dotted line) and enstrophy $\Omega(k)$ (solid line) towards the steady state. Dashed line denotes the total energy with the first six modes excluded.

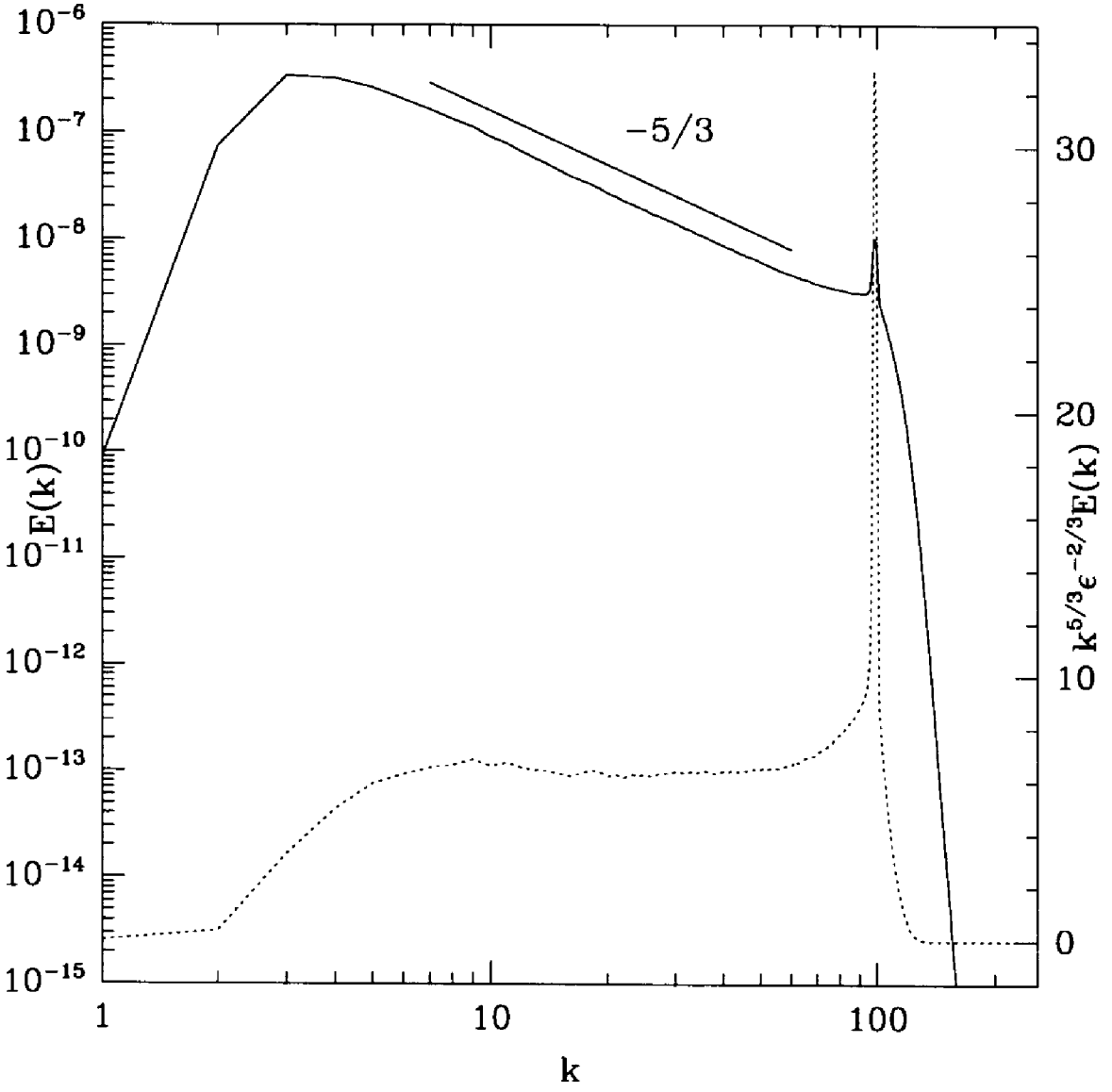


Figure 3.2: Energy spectrum $E(k)$ (solid line) and compensated energy spectrum $E(k)k^{5/3}\epsilon^{-2/3}$ (dotted line).

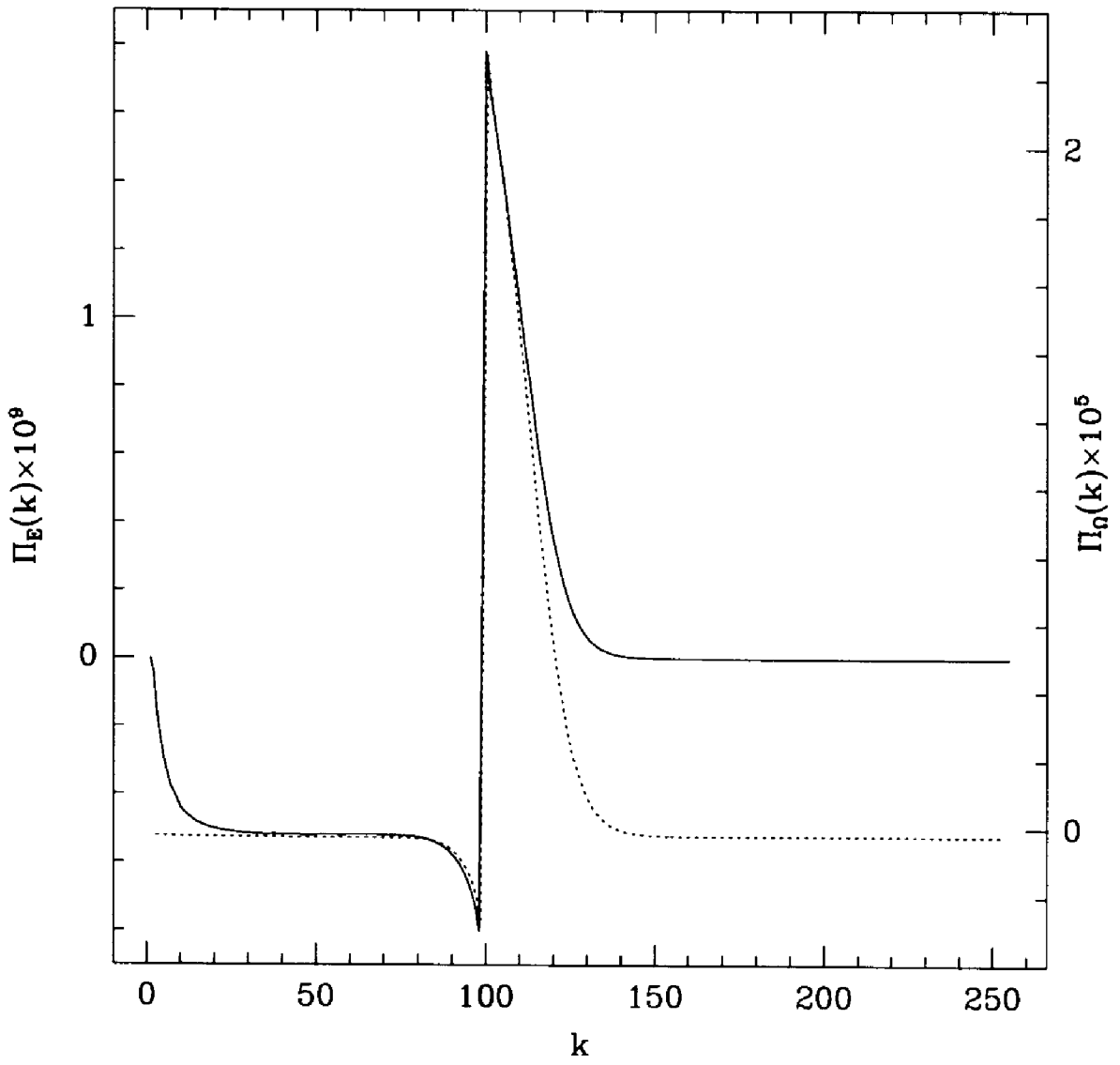


Figure 3.3: The energy flux $\Pi_E(k)$ (solid line) and the enstrophy flux $\Pi_\Omega(k)$ (dotted line).

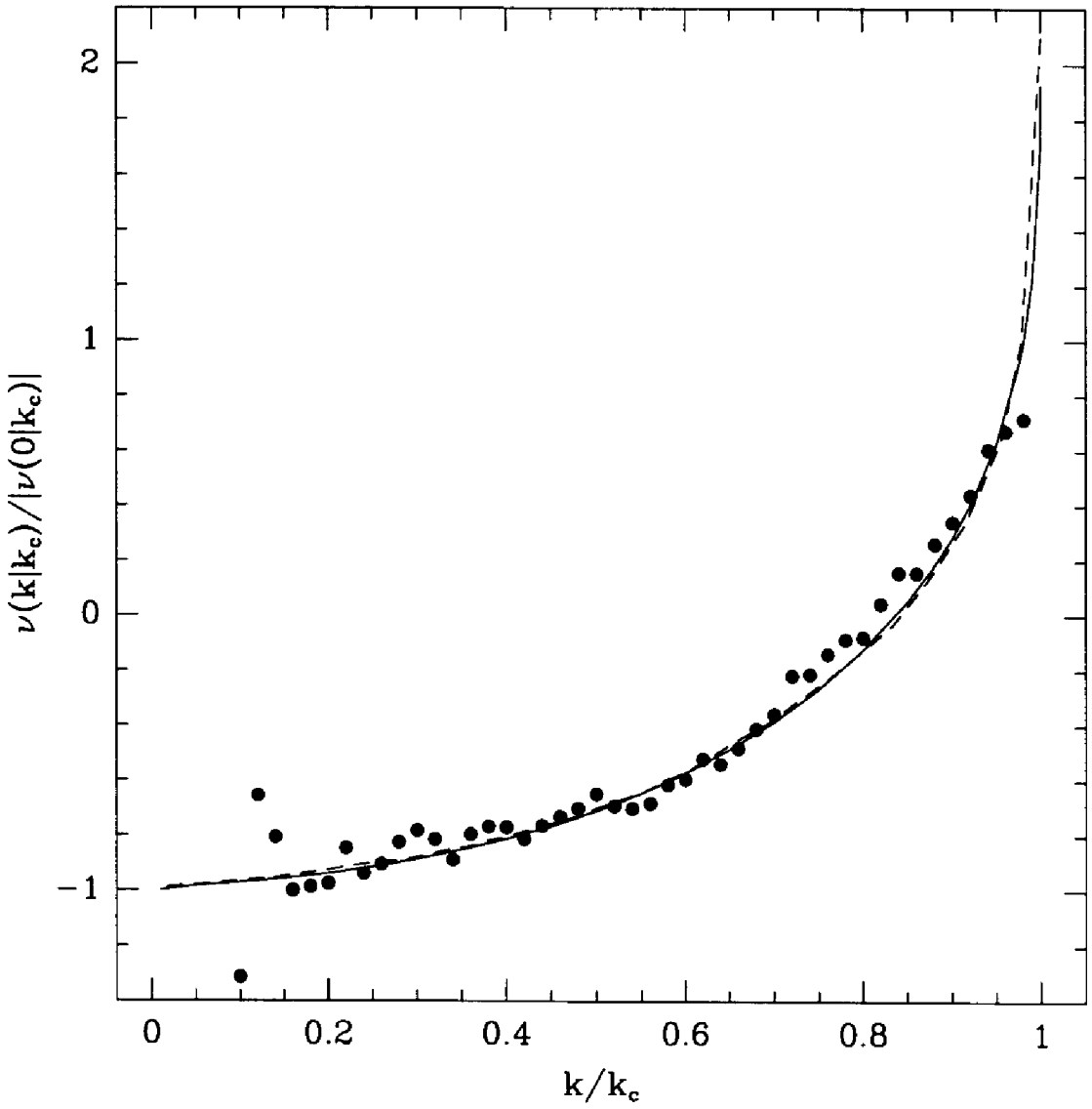


Figure 3.4: Normalized two-parametric eddy viscosity from DNS (dots), from TFM (dashed line), and from RG (solid line).

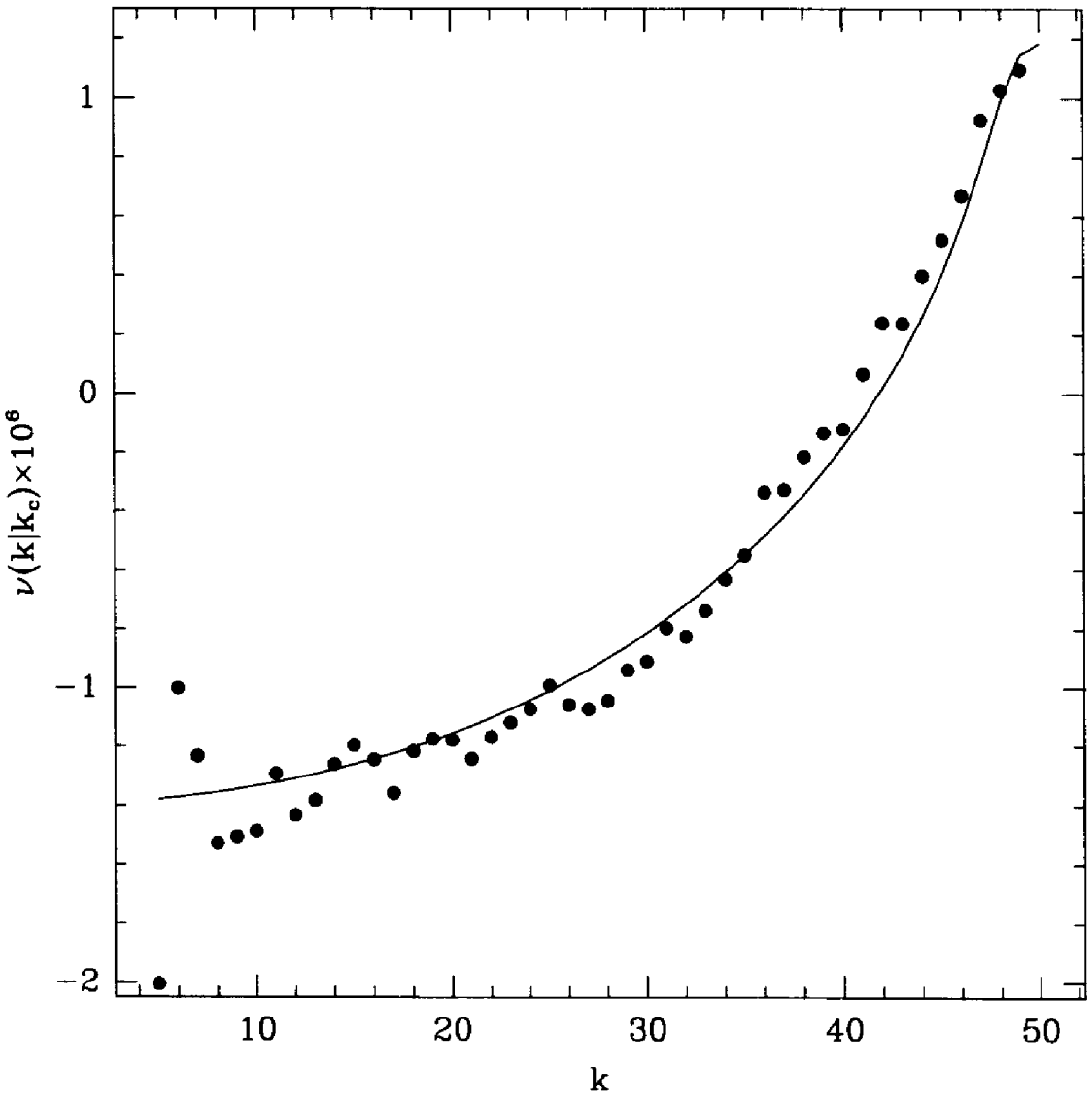


Figure 3.5: Actual two-parametric eddy viscosity from DNS (dots) and from RG (solid line). In RG calculations, the energy spectrum for $k < 5$ was corrected in accordance with the DNS results, Fig. 3.2.

# Chapter 4

# Anisotropic Two-Dimensional System: Turbulence on a $\beta$-Plane

Turbulent flows subjected to a differential rotation develop spectral anisotropy. Understanding and modeling of such flows present a major theoretical and experimental challenge, mainly because of their importance in geophysics, astrophysics and plasma physics. Here we study the simplest two-dimensional system of this kind which describes the flow of a thin layer of a homogeneous fluid on the surface of a rotating sphere. Techniques used in Chapter 3 will be applied to this anisotropic system along with long-time numerical simulations, thus bringing some new results.

We will study the long-time and large-distance statistical properties of the system described by

$$\frac{\partial \zeta}{\partial t} + \lambda_0 \left( \frac{\partial \psi}{\partial x} \frac{\partial \zeta}{\partial y} - \frac{\partial \psi}{\partial y} \frac{\partial \zeta}{\partial x} \right) + \beta_0 \frac{\partial \psi}{\partial x} = \nu_0 \Delta \zeta + f, \quad -\zeta = \Delta \psi. \tag{4.1}$$

Equation (4.1) combines features of isotropic 2D turbulence and planetary, or Rossby waves, and describes their interaction. The importance of this equation for understanding of the geophysical processes on a planetary scale and its relative simplicity have placed it in one of the focal points of theoretical geophysical fluid dynamics, and much was learned from this equation. However, its large-scale behavior still remains a realm of controversy; its spectral evolution laws have not been well established, while the spectral anisotropy and the importance of nonlinearity have received insufficient

attention in the literature. The relevance of equation (4.1) for geophysical applications will be explained in Section 4.1, whereas the theoretical and numerical analysis for it will be presented in Sections 4.2 and 4.3 respectively.

In the context of the earth's atmospheric turbulence, the experimental evidence suggests that the Kolmogorov inverse cascade persists on a variety of scales: from 500 km down to 100 m (mesoscale) [4, 72]. Similar data are obtained from the high-resolution "SKYHI" general circulation model simulations, see [81, 82]. The range of scales larger than 500 km and up to several thousand of km is called "geostrophic turbulence range" [72], to emphasize that in this range the effects of rotation may not be neglected and may even be dominant. Currently it is widely accepted that in this range the energy spectrum scales as $k^{-3}$, which fits well the available experimental data (see, for example, [72]). We need to note that in the real-life atmospheric turbulence the observed energy spectrum is a result of joint action of several important effects, such as stratification, surface friction, differential rotation, and others. In this Chapter we are only interested in studying the effects of the differential rotation, or the $\beta$-effects.

## 4.1 Geophysical Background

Here we will outline the derivation of equation (4.1) from the basic principles of geophysical fluid dynamics as well as some additional relevant issues.

**Geostrophic Motion.** Atmospheric and ocean dynamics normally deals with the motion of a stratified incompressible fluid on the surface of rotating sphere with or without effects of topography. Since the Rossby number $\epsilon \equiv U/(2\Omega L)$, where $U$ is the characteristic large-scale velocity, $\Omega$-angular velocity, and $L$-characteristic length scale, is small for large-scale motions, a series of approximations for the full equations of motion can be constructed [61]. The lowest order in this hierarchy describes the so-called *geostrophic motion.*

In the rotating coordinate frame with angular velocity $\Omega$ the three-dimensional

momentum equations read

$$\frac{\partial \vec{u}}{\partial t} + (\vec{u}, \nabla)\,\vec{u} + 2\,[\Omega, \vec{u}] = -\frac{\nabla p}{\rho} + \nabla\Phi + \nu\,\Delta\vec{u}, \tag{4.2}$$

where $\Phi$ is the potential of external forces including the centrifugal force. Assume now that the Ekman number $E \equiv \nu/(2\Omega\,L^2)$ and the Rossby number are small. Estimates for the atmosphere give $E \approx 10^{-14}$ and $\epsilon \approx 0.07$ if $U = 1\ m/sec$ and $L = 100\ km$.

Nondimensionalizing and neglecting terms relatively small in $\epsilon$ and $E$, one gets

$$2\,[\Omega, \vec{u}] = -\frac{\nabla p}{\rho} + \nabla\Phi. \tag{4.3}$$

In the spherical coordinates where $\phi$, $\theta$, $r$ denote longitude, latitude, and radius, this equation reads

$$\begin{gathered}\rho\,(-2\,\Omega\,v\,sin\theta + 2\,\Omega\,w\,cos\theta) = -\frac{1}{r\,cos\theta}\,\frac{\partial p}{\partial \phi} \\ \rho\,2\,\Omega\,u\,sin\theta = -\frac{1}{r}\,\frac{\partial p}{\partial \theta}, \quad -\rho\,2\,\Omega\,u\,cos\theta = -\frac{\partial p}{\partial r} - \rho\,g.\end{gathered} \tag{4.4}$$

A second approximation is to regard as small the thickness of the fluid layer on the earth's surface: $\delta \equiv D/L \ll 1$, where $D$ is the average thickness of the layer. Then using the smallness of $\delta$ and $z \equiv r - r_0 \ll r_0$, where $r_0$ is the earth's radius, we obtain

$$f\,v = \frac{1}{\rho_s\,r_0\,cos\theta}\,\frac{\partial p}{\partial \phi}, \quad f\,u = -\frac{1}{\rho_s\,r_0}\,\frac{\partial p}{\partial \theta}, \quad \rho\,g = -\frac{\partial p}{\partial z}. \tag{4.5}$$

Here $\rho_s$ is the static density, i.e. that is density if no motion were present at all, and $f \equiv 2\,\Omega\,sin\theta$ is the Coriolis parameter. The first two equations in this formula constitute the so-called *geostrophic approximation*. They define geostrophic velocity to be functions of the pressure field as $\vec{u}_H = 1/(f\rho_s)\,\left[\vec{k}, \vec{\nabla} p\right]$, where $\vec{u}_H$ denotes the horizontal velocity and $\vec{k}$ is the Cartesian unit vector in the vertical direction.

**Quasigeostrophic Approximation.** The systematic expansion in Rossby number $\epsilon$ leading to the geostrophic approximation in the lowest-order term may also be constructed [61]. The next-order correction, which is called *quasigeostrophic approximation*, will be discussed now.

Consider a plane shallow layer of fluid rotating with the angular velocity $\Omega$ [61]. Axes $x$ and $y$ are chosen in the layer's plane; the axis $z$ and $\vec{\Omega}$ are perpendicular to it. The Coriolis parameter is here simply $f = 2\Omega$. The rigid bottom is defined by the surface $z = h_B(x, y)$ and $h(x, y, t)$ denotes elevation of the upper layer boundary at the moment $t$. Then the depth of the fluid is $H \equiv h - h_B \approx D$, where $D$ gives the mean value of depth. We assume again that $\delta = D/L \ll 1$, where $L$ is a horizontal length scale of the motion considered.

Performing nondimensionalization of the three-dimensional incompressible inviscid Navier-Stokes equations and keeping the same-order in $\delta$ terms, one may arrive at the *shallow water approximation* [61]

$$\frac{\partial u}{\partial t} + u\frac{\partial u}{\partial x} + v\frac{\partial u}{\partial y} - f\,v = -g\frac{\partial h}{\partial x}, \quad \frac{\partial v}{\partial t} + u\frac{\partial v}{\partial x} + v\frac{\partial v}{\partial y} + f\,u = -g\frac{\partial h}{\partial y},$$
$$\frac{\partial H}{\partial t} + \frac{\partial}{\partial x}(u\,H) + \frac{\partial}{\partial y}(v\,H) = 0. \qquad (4.6)$$

As is clear, in the absence of rotation ($f = 0$) this system is equivalent to the two-dimensional compressible gas dynamics equations, where the height of the fluid layer acts as pressure.

Now we nondimensionalize this system again assuming the Rossby number $\epsilon$ to be small. Let $H = D + \eta - h_B$ be such that $\eta$ is the departure of the free surface from its rest level. Seeking solution in the asymptotic form $u = u_0 + \epsilon\,u_1 + \epsilon^2\,u_2 + O(\epsilon^3)$, and assuming similar expansions for $v, \eta$, from the $O(1)$-terms one may obtain a familiar geostrophic approximation: $v_0 = \partial\eta_0/\partial x$, $u_0 = -\partial\eta_0/\partial y$. Similarly, the $O(\epsilon)$-terms yield

$$\frac{\partial u_0}{\partial t} + u_0\frac{\partial u_0}{\partial x} + v_0\frac{\partial u_0}{\partial y} - v_1 = -\frac{\partial \eta_1}{\partial x}, \quad \frac{\partial v_0}{\partial t} + u_0\frac{\partial v_0}{\partial x} + v_0\frac{\partial v_0}{\partial y} + u_1 = -\frac{\partial \eta_1}{\partial y},$$
$$F\left\{\frac{\partial \eta_0}{\partial t} + u_0\frac{\partial \eta_0}{\partial x} + v_0\frac{\partial \eta_0}{\partial y}\right\} - u_0\frac{\partial \eta_B}{\partial x} - v_0\frac{\partial \eta_B}{\partial y} + \frac{\partial u_1}{\partial x} + \frac{\partial v_1}{\partial y} = 0, \quad (4.7)$$

where $F \equiv (L/R)^2$, $R = \sqrt{gD}/f$. It can be rewritten completely in terms of $\eta_0$ as

$$\left(\frac{\partial}{\partial t} + \frac{\partial \eta_0}{\partial x}\frac{\partial}{\partial y} - \frac{\partial \eta_0}{\partial y}\frac{\partial}{\partial x}\right)(\Delta\eta_0 - F\,\eta_0 + \eta_B) = 0. \qquad (4.8)$$

From this we see that despite the fact that the total $\vec{u}$ is a compressible field, its geostrophic part $\vec{u}_0$ is incompressible, which allows to introduce the stream-function

$\psi \equiv \eta_0$, leading to

$$\left(\frac{\partial}{\partial t} + \frac{\partial \psi}{\partial x}\frac{\partial}{\partial y} - \frac{\partial \psi}{\partial y}\frac{\partial}{\partial x}\right)(\Delta\psi - F\,\psi + \eta_B) = 0. \tag{4.9}$$

The case of our future interest is $R \gg L$, when the free surface is almost rigid.

**Rossby Waves.** For the case of a linearly changing topography $\eta_B = \beta\, y$ there exists an exact solution of (4.9) in the form of normal modes: $\psi = Re\left\{A\, e^{i(k x + l y - \omega t + \alpha)}\right\}$ with the dispersion relation: $\omega = -\beta\, k/(k^2 + l^2 + F)$. This solution is called *Rossby wave* (topographic in this context). Note that the sum of two such waves is already not an exact solution of the nonlinear equation (4.9) due to the interaction terms. At first glance, these waves exhibit "absurd" behavior following from the dispersion relation: the short waves are very slow, whereas the long waves are very fast.

**$\beta$-Plane.** As is shown in [61], the following claim holds: *the above-considered plane model with a topographic variation is dynamically totally equivalent to the differential rotation on the surface of the sphere.* Indeed, if for some nonzero latitude the local tangential plane coordinates on the sphere are $x$ in the east-west (longitudal) direction, and $y$ in the south-north direction, then a small variation of Coriolis parameter can be written as $f \equiv 2\,\Omega\, sin\theta = f_0 + \beta\, y, \quad \beta = 2\,\Omega\, cos\theta_0/r_0$. There exists a rigorous derivation of this equivalence between the variation of topography in the plane rotating layer and the variation of the Coriolis parameter due to the rotation on the sphere (see [61]).

**Linear Stability of Zonal Flows on a $\beta$-Plane.** Consider the shallow water system (4.6) in the $\beta$-plane approximation for $F \ll 1$-case:

$$\frac{\partial u}{\partial t} + u\frac{\partial u}{\partial x} + v\frac{\partial u}{\partial y} - f\,v = -\frac{\partial p}{\partial x}, \quad \frac{\partial v}{\partial t} + u\frac{\partial v}{\partial x} + v\frac{\partial v}{\partial y} + f\,u = -\frac{\partial p}{\partial y},$$
$$\frac{\partial u}{\partial x} + \frac{\partial v}{\partial y} = 0. \tag{4.10}$$

It is obvious that this system allows for exact solutions in the form of zonal currents:

$$u_0 = U(y), \quad v_0 = 0, \quad p_0 = P(y) = P(0) - \int_{y'=0}^{y} f(y')\,U(y')\,dy'. \tag{4.11}$$

Let us generalize the well-known Rayleigh linear stability condition [15] of the plane-parallel flow for the case of nonzero $\beta$-effect. Linearizing the basic equations in the neighborhood of the exact solution (4.11), and seeking perturbations in the form of normal modes in the $x$-direction, one can get the following generalization of Rayleigh's equation for the stream-function $\psi(y)$:

$$\psi'' + \psi \left\{ \frac{k\,(U'' - \beta)}{\omega - k\,U} - k^2 \right\} = 0. \tag{4.12}$$

For example, consider the vertically-periodic case $\psi(0) = \psi(2\pi)$. Then, multiplying (4.12) by $\psi^*$ and integrating over a period, one gets

$$\int_{y=0}^{2\pi} |\psi'|^2 \, dy = \int_{y=0}^{2\pi} |\psi|^2 \left\{ \frac{k\,(U'' - \beta)}{\omega - k\,U} - k^2 \right\} dy. \tag{4.13}$$

Taking the imaginary part, one obtains ($\omega = \omega_r + i\,\omega_i$):

$$k\,\omega_i \int_{y=0}^{2\pi} |\psi|^2 \, \frac{(U'' - \beta)}{(\omega_r - k\,U)^2 + \omega_i^2} \, dy = 0, \tag{4.14}$$

from which it follows that *if there exists* $\omega_i \neq 0$ *(=instability), then there exists* $z \in [0, 2\pi]$ *such that* $U''(z) = \beta$. Therefore, the necessary stability condition of the zonal flow is $U'' \neq \beta$.

## 4.2 One-Loop RG Approach

Here we will generalize the results already described in detail in Section 3.1 to account for the effects of differential rotation considered in the geostrophic approximation on a $\beta$-plane, described by (4.1). Without unnecessary repetition we will present only the final results of applying the one-loop RG-formalism described in Section 3.1.

One can write the statement in the Fourier-space as a single nonlinear integral equation

$$G_0^{-1}(\vec{k},\omega)\,\zeta(\vec{k},\omega) = f(\vec{k},\omega) - N(\vec{k},\omega), \text{ where denoted :}$$

$$G_0^{-1}(\vec{k},\omega) = -i\left(\omega + \frac{\beta_0\,k_1}{k^2}\right) + \nu_0\,k^2,$$

$$N(\vec{k},\omega) = \frac{\lambda_0}{2(2\pi)^3} \int_p \left[\vec{k},\vec{p}\right]_3 \left\{ \frac{1}{p^2} - \frac{1}{\left|\vec{k}-\vec{p}\right|^2} \right\} \zeta(\vec{p},\psi)\,\zeta(\vec{k}-\vec{p},\omega-\psi)\,d\vec{p}\,d\omega. \tag{4.15}$$

For simplicity, we omit the thermal part of the force and consider force to be a white-noise, Gaussian random function given by its second-order correlation function

$$\langle f(\vec{k},\omega)\, f(\vec{k}',\omega')\rangle = 2(2\pi)^3\, D_0\, k^{2-y}\, \delta\left(\vec{k}+\vec{k}'\right)\, \delta\left(\omega+\omega'\right). \tag{4.16}$$

It is possible to demonstrate that the one-loop correction for the propagator is

$$-\frac{\lambda_0^2}{(2\pi)^3}\, 2D_0\, G_0(\vec{k},\omega)\, \zeta(\vec{k},\omega) \int_p p^{2-y}\, \left[\vec{k},\vec{p}\right]_3^2 \left\{\frac{1}{p^2}-\frac{1}{\left|\vec{k}-\vec{p}\right|^2}\right\} \times$$
$$\times \left\{\frac{1}{p^2}-\frac{1}{k^2}\right\} \left|G_0(\vec{p},\psi)\right|^2\, G_0(\vec{k}-\vec{p},\omega-\psi)\, d\vec{p}\, d\psi, \tag{4.17}$$

with the same integration region as in Section 3.1.

Frequency integration can be performed exactly to give

$$-\frac{i\,\lambda_0^2\, D_0}{\nu_0\,(2\pi)^2}\, \zeta^{<}(\vec{k},\omega)\, G_0(\vec{k},\omega) \int_p p^{-y}\, \left(\vec{p},\vec{k}\right)^2 \times$$
$$\times \frac{\left\{\frac{1}{p^2}-\frac{1}{\left|\vec{p}-\vec{k}\right|^2}\right\} \left\{\frac{1}{p^2}-\frac{1}{k^2}\right\}\, d\vec{p}}{\omega+\beta_0\left[\frac{p_1}{p^2}+\frac{k_1-p_1}{\left|\vec{k}-\vec{p}\right|^2}\right]+i\nu_0\left[p^2+\left|\vec{p}-\vec{k}\right|^2\right]}. \tag{4.18}$$

The leading-order behavior in $k$ may be found to be exactly equal to the corresponding isotropic one

$$\frac{\lambda_0^2\, D_0\, k^2}{16\pi\,\nu_0^2}\, \Lambda^{-3-y}\, \delta\Lambda\, \zeta(\vec{k},\omega)\, G_0(\vec{k},\omega). \tag{4.19}$$

The one-loop correction to the force correlation function is

$$2\lambda_0^2\, D_0^2\, \delta\left(\vec{k}+\vec{k}'\right)\, \delta\left(\omega+\omega'\right) \int_p \left[\vec{k},\vec{p}\right]_3^2 \left\{\frac{1}{p^2}-\frac{1}{\left|\vec{k}-\vec{p}\right|^2}\right\}^2 \times$$
$$\times p^{2-y}\, \left|\vec{k}-\vec{p}\right|^{2-y} \left|G_0(\vec{p},\psi)\right|^2\, \left|G_0(\vec{k}-\vec{p},\omega-\psi)\right|^2\, d\vec{p}\, d\psi, \tag{4.20}$$

with its leading-order term

$$-\frac{\pi^2\,\lambda_0^2\, D_0^2}{\nu_0^3}\, \delta\left(\vec{k}+\vec{k}'\right)\, \delta\left(\omega+\omega'\right)\, k^4\, \Lambda^{-5-2y}\, \delta\Lambda. \tag{4.21}$$

We observe that the one-loop corrections remain unaffected by the $\beta$-term; the $\beta$-term itself does not gain a correction also (*does not renormalize*). This presents a significant difficulty in applying the RG results to the $\beta$-plane equation.

Thus a formal extension of the results of Section 3.1 would contradict known experimental and numerical data (including our data presented below), since the anisotropic term does alter the large-scale turbulence dynamics.

Here we will only propose several ways to resolve thus issue analytically. First, it may turn out that the one-loop RG results are insufficient to describe the effect of the $\beta$-term on large scales. In fact we have calculated the second loops which generate corresponding corrections to the inverse propagator and we did observe that *there exists a $\beta$-dependent viscosity correction arising from the second loops.* An accurate consideration of the two-loop RG, however algebraically complicated, may yield correct results. Second, it may happen that a RG is not applicable in this particular case, at least in the formulation used here. The third possibility may be that going one step back to the forced-dissipative shallow water equations with a varying Coriolis parameter will enrich the problem formulation sufficiently so that the RG theory may be regularized. We shall consider these objectives for future work. At this stage, however, one of the most straightforward and productive tools is DNS, the results of which will be presented in the next section.

## 4.3 Anisotropic Energy Spectrum in $\beta$-Plane Turbulence

The simplest system displaying effects of differential rotation due to surface sphericity, is the $\beta$-plane model for the relative vorticity, described by (4.1). As we have outlined above, equation (4.1) may be derived in the so-called quasigeostrophic approximation to describe the local properties of a thin fluid layer on the surface of the rotating sphere for small latitude variations, see e.g. [61, 3]. Here we consider only motions with scales $L \ll R$, where $R$ is the so-called Rossby deformation radius [61], so that in (4.6) the effects of the layer thickness variation are neglected and the flow becomes effectively incompressible. We have shown that in the inviscid case (4.1) is known to have a class of exact solutions (4.11) in the form of zonal currents determined by an arbitrary velocity profile $U(y)$, which simply describes a geostrophic velocity. There

exists strong experimental evidence that the zonal currents are actually observed in large-scale oceanic flows, see [60, 85]. The $\beta$-term in the equation for fluctuations (4.1) itself does not lead to a corresponding term in the energy equation, due to the fact that in the solution of the linearized problem (4.1) only its complex phase depends on $\beta$. But this does not mean that the energy spectrum resulting from (4.1) will be $\beta$-independent. It is namely the nonlinear term in (4.1) which makes the transformation of complex phases into complex amplitudes, thus leading to the $\beta$-dependence of the energy spectrum. In this section we shall report on some details of our numerical studies of this $\beta$-dependence. Some of the results presented here are reported in [10, 24].

As is commonly assumed in most geophysical applications, the forcing $f$ in the Fourier space is considered peaked at some high wavenumber $k_f$, and a zero-mean Gaussian white-in-time random function defined by

$$\overline{f(\vec{k},t)\,f(\vec{k'},t')} = 2\pi\,\overline{\eta}\,\delta(k-k_f)\,\delta(\vec{k}+\vec{k'})\,\delta(t-t'). \tag{4.22}$$

Thus defined, the force supplies the enstrophy $\Omega(t)$ with a rate $\int \left|f(\vec{k},t)\right|^2 d\vec{k} = \overline{\eta}$ and the energy $E(t)$ with a rate $\int \left|f(\vec{k},t)\right|^2/k^2\,d\vec{k} = \overline{\epsilon} = \overline{\eta}/k_f^2$ into the system and in the inviscid case $E(t) = E(0) + \overline{\epsilon}\,t$ and $\Omega(t) = \Omega(0) + \overline{\eta}\,t$.

Compared to the $\beta = 0$ case, the nonzero $\beta$ in (4.1) introduces a new scale into the system, which on a purely dimensional basis is

$$k_\beta = \left(\frac{\beta}{\nu}\right)^{\frac{1}{3}}, \quad \text{or} \quad k'_\beta = \left(\frac{\beta^3}{\overline{\epsilon}}\right)^{\frac{1}{6}}. \tag{4.23}$$

Superficially considered, the term $i\,\beta/k\,\cos\phi\,\zeta(\vec{k},t)$ vanishes as $k \to \infty$ and the large $k$ dynamics is not affected by the $\beta$-term. Intuitively, there should be a scale where the $\beta$-term becomes important and there are noticeable deviations from the isotropic dynamics. Therefore, we will define $k_\beta$ as a wavenumber at which the modulus of the $\beta$-term is of the same order as the corresponding viscous term, which leads to the first formula in (4.23). It follows from this definition that for $k \le k_\beta$ the solution of (4.1) becomes more and more dependent on $\beta$ and $\phi$. In the isotropic region $k \gg k_\beta$, the angular-dependent energy spectrum which we define as $E(\vec{k},t) = 2\pi\,\overline{\left|\zeta(\vec{k},t)\right|^2}/k$, such

that $\int dk \int_0^{2\pi} d\phi/(2\pi) E(\vec{k},t) = E(t)$ is the total energy, is nearly isotropic: $E(\vec{k},t) \approx E(k,t)$. Here the $\beta$-term by construction has a small effect and one can hope that the perturbation theory in $\beta^2$ may be developed resulting in the leading-order Kolmogorov energy spectrum

$$E_K(k) = C_K\, \bar{\epsilon}^{\frac{2}{3}}\, k^{-\frac{5}{3}} \tag{4.24}$$

and $O(\beta^2)$-corrections to it. Following Rhines [63], one can also assume that in the range $k \ll k_\beta$, the universal turbulence properties do not depend on parameters $\bar{\epsilon}$, $\nu$ but are determined by the inverse local eddy size $k$ and the parameter $\beta$ alone. The only dimensionally correct combination for the energy spectrum leads to the Rhines energy spectrum

$$E_R(k) = C_R\, \beta^2\, k^{-5}. \tag{4.25}$$

Now the second formula in (4.23) for $k'_\beta$ may be obtained from the matching condition of (4.24) with (4.25) at $k = k_\beta$. We will use formulas (4.23) with the understanding that they give only order of magnitude estimates for $k_\beta$.

There is yet another viscosity-free argument leading to the length scale determined by $\beta$. The effects of turbulence and waves become comparable when eddy turnover time of isotropic 2D turbulence is equal to the Rossby wave period; then a transitional wave number $k_t(\phi)$ can be defined

$$k_t(\phi) = k_\beta \cos^{3/5}\phi, \quad k_\beta = (\beta^3/\epsilon)^{1/5}. \tag{4.26}$$

Contour (4.26) was dubbed "the dumb-bell shape" by Vallis and Maltrud [86]. According to [63] and [86], as $k \to k_\beta$, the inverse energy cascade terminates, and the energy piles up at the boundary of the dumb-bell shape, which then acts as an impenetrable wall for turbulence energy. This would mean that the nonlinear transfer becomes ineffective, and that the flows inside the dumb-bell shape should be governed by linear dynamics. However, since the dumb-bell shape excludes the axis $k_x = 0$, the inverse cascade can continue in a small vicinity of $k_x = 0$; the resulting structures correspond to zonal flows. Rhines [63], Vallis and Maltrud [86], and Holloway

[29] note that the spectral anisotropy induced by the $\beta$-term can be associated with the mechanism of generation of zonal flows. The existence of zonal structures was a robust feature of simulations by Rhines [63], Vallis and Maltrud [86] and Panetta [60].

A numerical solution of (4.1) was performed with the hyperviscosity substituting the normal viscosity, that is with the change $\nu\Delta\zeta \to \nu_S\,(-1)^{p+1}\,\Delta^p\zeta + \nu_L\,(-1)^{q+1}\,\Delta^{-q}\zeta$, where $p, q > 0$ are integers. The specific choice of $p = 7, q = 6$ was primarily dictated by the sufficiently sharp energy removal from both small and large wavenumbers. The basic assumption behind this is that the infra-red and long-time statistical properties do not depend on the structure of the ultra-violet dissipation range. To exclude the nonlocal effects of the infra-red viscosity, the DNS are considered only until the flow reaches the largest scales where the infra-red viscosity is important. Equation (4.1) was numerically solved using the fully de-aliased pseudospectral Fourier method in a box $\{x, y\} \in [0, 2\pi] \times [0, 2\pi]$ with doubly periodic boundary conditions and zero initial data. The spatial resolution used was $512^2$ including de-aliased modes. The time-discretization was the same as in [9]. Discrete approximation for the white-noise force with property (4.22) was: $f(k,t) = A_f\,\sigma_k/\sqrt{\delta t}$ for $k \in [k_f - 2, k_f + 2]$ and zero otherwise, where $\sigma_k$ is the Gaussian random number with unit variance, $\delta t$ is the time step. For this particular resolution the forcing wavenumber $k_f = 102$ was found optimal. For a given $k_f$ we have performed a series of DNS with several different $k_\beta \in [0, 150]$, which covers the interval of the unforced modes. But our principal interest here is in studying the strongly anisotropic region $k \ll k_\beta$, thus leading to the choice $k_\beta \approx k_f$. Below we will present the results of the longest run corresponding to $k'_\beta = 140$ which was performed until the largest scales were saturated and the processes leading to the creation of condensate state [74, 75] appeared. For completeness we shall give all the parameter values for this run: $\delta t = 1.$, $\nu_L = 20.$, $\nu_S = 1. \times 10^{-36}$, $A_f = 0.1$, and $\beta = 0.3$. the integration time was approximately equal to $175\,\tau_{tu}$, where $\tau_{tu}$ is the largest eddy turn-over time, defined as $\tau_{tu} = 2\pi/\sqrt{2\,E(t)}$. For comparison, the beginning of the condensation time for the corresponding isotropic DNS on this resolution is approximately $5\,\tau_{tu}$. After the condensation features started to appear, the

run was interrupted. Such a long integration time may be explained by the following idealized estimate. If there is no energy dissipation at the large scales then using (4.24) and (4.25), $k_{\bar{\epsilon}}(t) = (3\,C_K/2)^{3/2}\,\bar{\epsilon}^{-1/2}\,t^{-3/2}$, and $k_\beta(t) = (C_R\beta^2/(4\bar{\epsilon}))^{1/4}\,t^{-1/4}$ give the minimal excited wavenumber depending on time for the Kolmogorov and Rhines spectrum respectively. From the examination of these formulas it follows that to go from $k_1 = 100$ to $k_2 = 10$ it will take 2154 times longer for the Rhines spectrum than for the Kolmogorov one.

The measurements of the averaged spectral characteristics are presented in Figs. $4.1 - 4.7$. The total energy and enstrophy evolution is presented in Fig. 4.1. One can see that the energy of the $k = 7$ and higher modes start to saturate at $t \approx 100\,\tau_{tu}$. To display the anisotropy in the resulting spectrum, the local angle averages of the energy spectrum over the angle $\pm\pi/12$ around $\phi = 0$ and $\phi = \pi/2$ are presented in Fig. 4.2 for the two well-separated moments of time. One can observe that the Rhines spectrum (4.25) in the $\pi/2$-direction and the Kolmogorov spectrum (4.24) in the $\phi = 0$-direction are established already after the time $7\,\tau_{tu}$. Note that, contrary to the conclusion of [86], it is obvious from Figs. 4.1, 4.2 that there is no impenetrable barrier for the energy in the wavenumber space at $k \approx k_\beta$ in any direction $\phi$. Energy keeps going to larger and larger scales as time grows. Cascade in the directions other than $\phi = \pi/2$ is simply much slower than in the $\pi/2$-direction. Figs. 4.3, 4.4 representing the time-averaged energy spectrum compensated by $k^{5/3}$ and $k^5$ before saturation illustrate the fact that (4.25) is observed only in the $\pi/2$-direction. Due to obvious symmetries with respect to the changes $\phi \to -\phi$ and $\phi \to \pi - \phi$ we consider region $\phi \in [0, \pi/2]$ only. The approximate values of Kolmogorov and Rhines constants following from these Figs are $C_K \approx 3$ and $C_R \approx 0.5$, but due to the large fluctuations the accuracy of the $C_R$ calculation is obviously quite low. The smearing observed in the $\pi/2$-direction may be due to the finite resolution effect but a careful study of the resolution refinement is complicated by a very long integration time required to obtain (4.25) in DNS. In any case, it is clear that the actual anisotropic energy spectrum is more complicated than the one observed in [86] and contains directions with the Rhines energy spectrum which to the best of our knowledge has never been

observed until now. The difficulties in the measurements include a long integration time and different scaling laws in different directions.

Fig. 4.5 shows the anisotropic energy transfer $T_E(\mathbf{k}|k_c)$ defined by analogy to that in [9]. Here, wavenumber $k_c$ was set $k_c = 50$, and $T_E(\mathbf{k}|k_c)$ describes energy transfer from all modes with $k > k_c$ to a mode with a given wave number $\mathbf{k}$, $k < k_c$. Consistently with the isotropic case, $T_E(\mathbf{k}|k_c)$ develops the cusp at $k \to k_c$. At $k \to 0$, strong anisotropy prevails, and most of the energy is funneled into the sectors adjacent to $\phi = \pm\pi/2$. A small but finite $k_x$ allows for a weak $x$-dependency of the flow field maintaining a nonzero nonlinearity which, in turn, sustains the anisotropic transfer. Flows with small $k_x$ correspond to nearly one-dimensional, zonal structures, or jets. Such structures are clearly seen in an instantaneous snapshot of the vorticity field in the physical space at $t = 115\tau_{tu}$ shown in Fig. 4.5; they have also been a robust feature of simulations [86, 60].

An instantaneous realization of the vorticity field corresponding to $t = 115.0\,\tau_{tu}$ is shown in Fig. 4.6. In agreement with the previous studies [86, 60, 85], the flow is composed of nearly one-dimensional zonal (in east-west direction) structures or jets [1]. These structures are not ideally one-dimensional but with some turbulent wave-like perturbations superimposed on them, illustrating the fact that this zonal flow is stable. These deviations from one-dimensionality create a nonzero nonlinearity thereby sustaining the flow of energy towards large scales. Main features of the flow can be seen from Fig. 4.7 where the zonally-averaged horizontal component of velocity $U(y,t)$ is shown at various moments of time during the run. It is obvious that the already anisotropic flow at $t = 58.5\,\tau_{tu}$, having the profile almost symmetric with respect to the change $y \to -y$ at $t = 175.0\,\tau_{tu}$, develops into a noticeably non-symmetric profile, which corresponds to sharp and narrow east-flowing jets and smooth and wide west-flowing jets. Although profile $U(y,t)$ is time-dependent, y-directional motion of jets is rather slow compared with the motion of fluid particles inside the jets. Under this condition, the generalization of the Rayleigh inviscid stability theorem for the case of $\beta \neq 0$ [1] locally in time states that if there are no inflection points in the $U(y,t) - \beta y^2/2$, then the flow is stable. In the second

column of Fig. 4.7, the second derivative $U_{yy}(y,t)$ is presented showing that the Rayleigh stability condition $U_{yy}(y,t) - \beta \neq 0$ does hold true. Moreover, with time, large negative peaks in the $U_{yy}(y,t)$ develop leaving such a flow linearly stable at later times. Until the large-scale drag effect remains small, the number of jets diminishes in time consistently with what was observed in other geophysical simulations [60, 85].

In conclusion, it is useful to highlight the importance of nonlinearity in the barotropic vorticity equation on the $\beta$-plane. Although the $\beta$-term does not enter the energy and enstrophy equation explicitly, it has a profound effect on the energy spectrum and spectral transfer. This effect is solely due to the nonlinearity of equation (4.1) that enables complex interaction between Rossby waves phases and vorticity modes amplitudes. As a result, the dumb-bell shape (4.26) does not become an impenetrable barrier for turbulence energy. Furthermore, inside the dumb-bell shape, where the $\beta$-effect is expected to prevail, the energy spectrum is determined by presumably irrelevant parameter $\epsilon$. On the other hand, in the small sectors around $\phi = \pm\pi/2$ outside the dumb-bell shape the $\beta$-effect is supposed to be small while the mechanism of anisotropic inverse transfer funnels energy into zonal jets. It was found that the zonal jets do form, but their spectrum is determined by the presumably irrelevant parameter $\beta$.

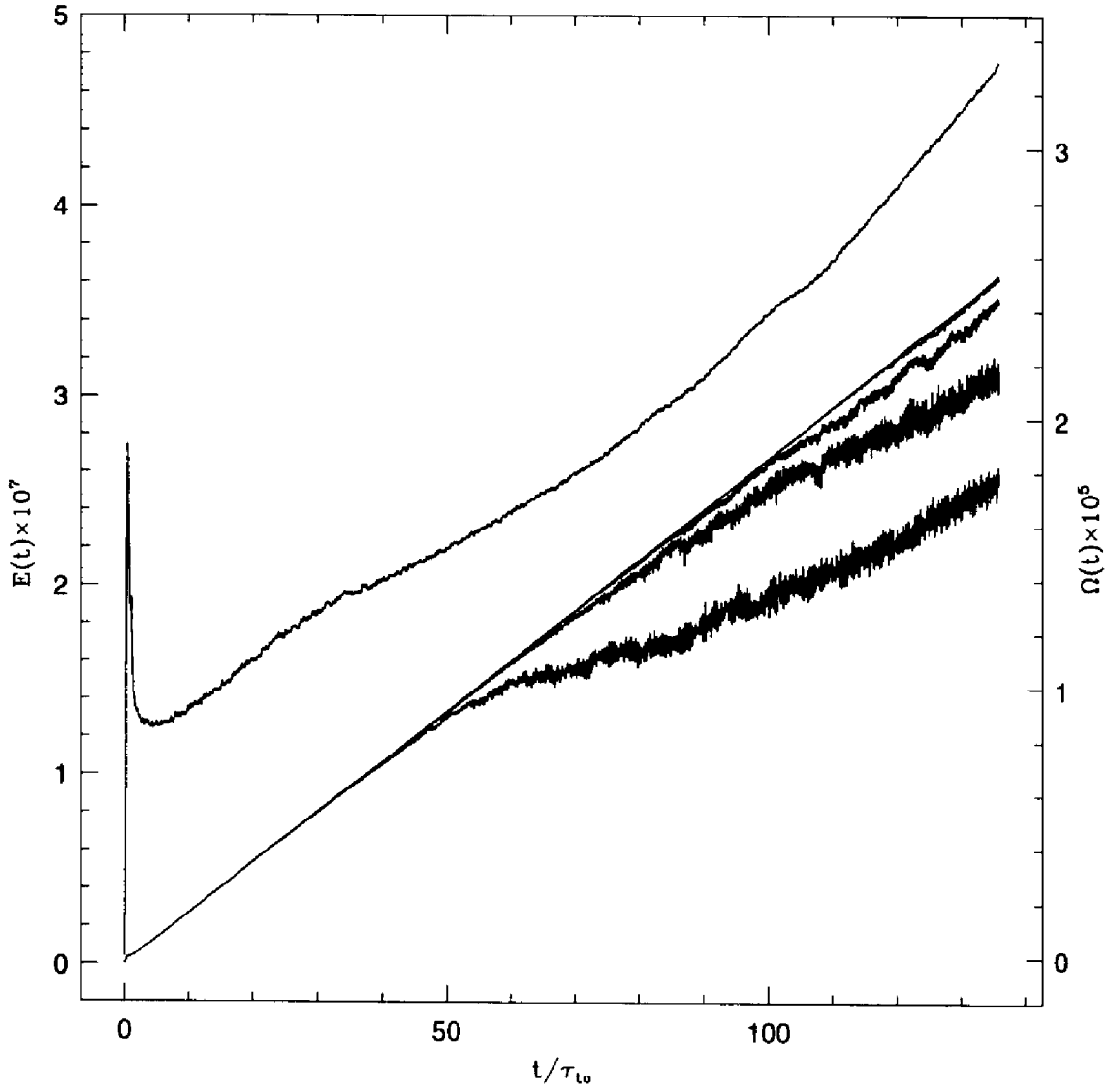


Figure 4.1: The evolution of total energy $E(t)$ (left axis) and enstrophy $\Omega(t)$ (right axis). Also shown is $E(t)$ with the energy of $1, 2, \ldots, 8$ modes subtracted.

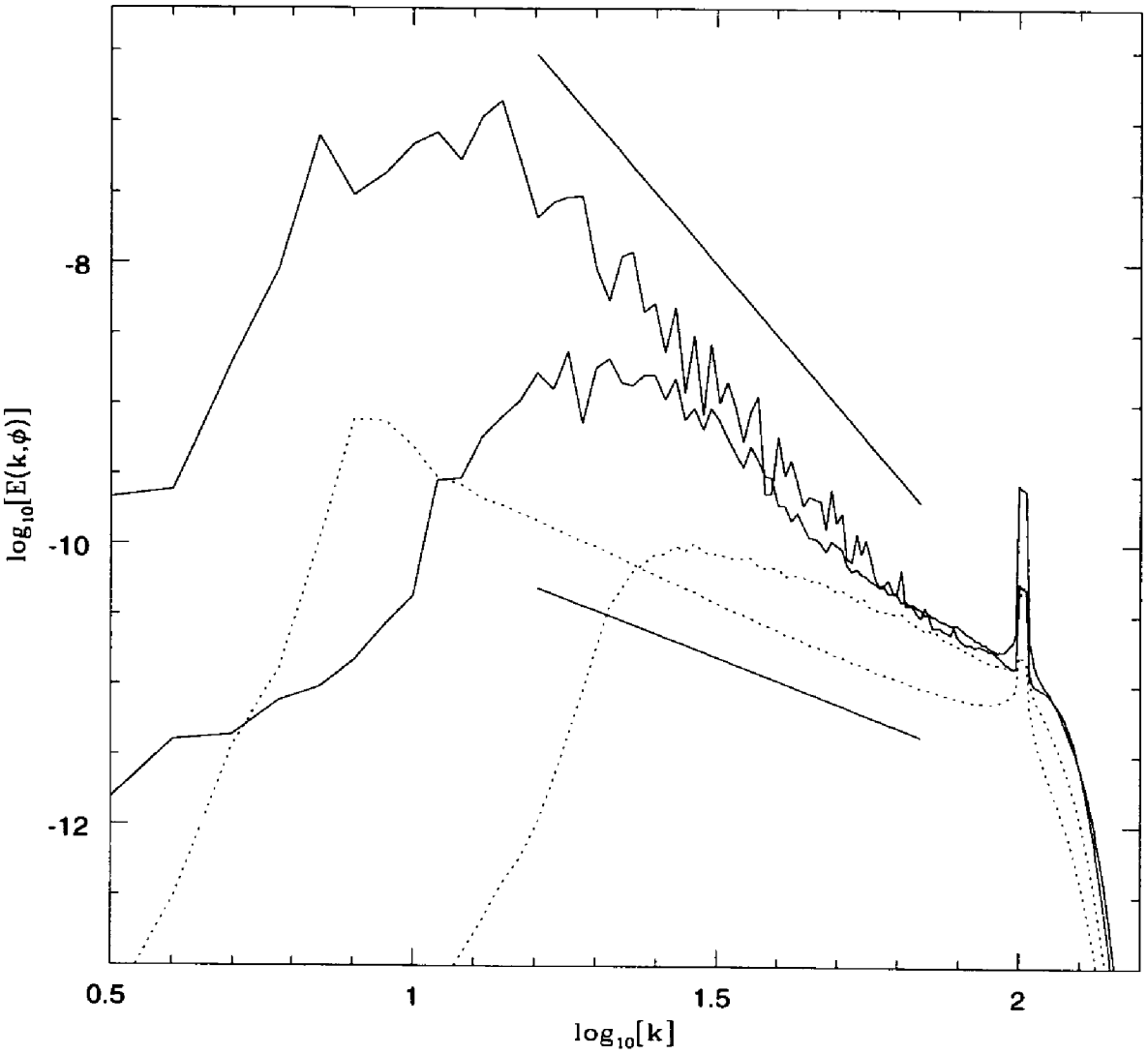


Figure 4.2: Energy spectra for $\phi = 0$ (dotted line) and $\phi = \pi/2$ (solid line) averaged in time and over small surrounding sector $\pm\pi/12$ for $t/\tau_{tu} = 7$ and 100. Straight lines have exact slopes $-5$ and $-5/3$.

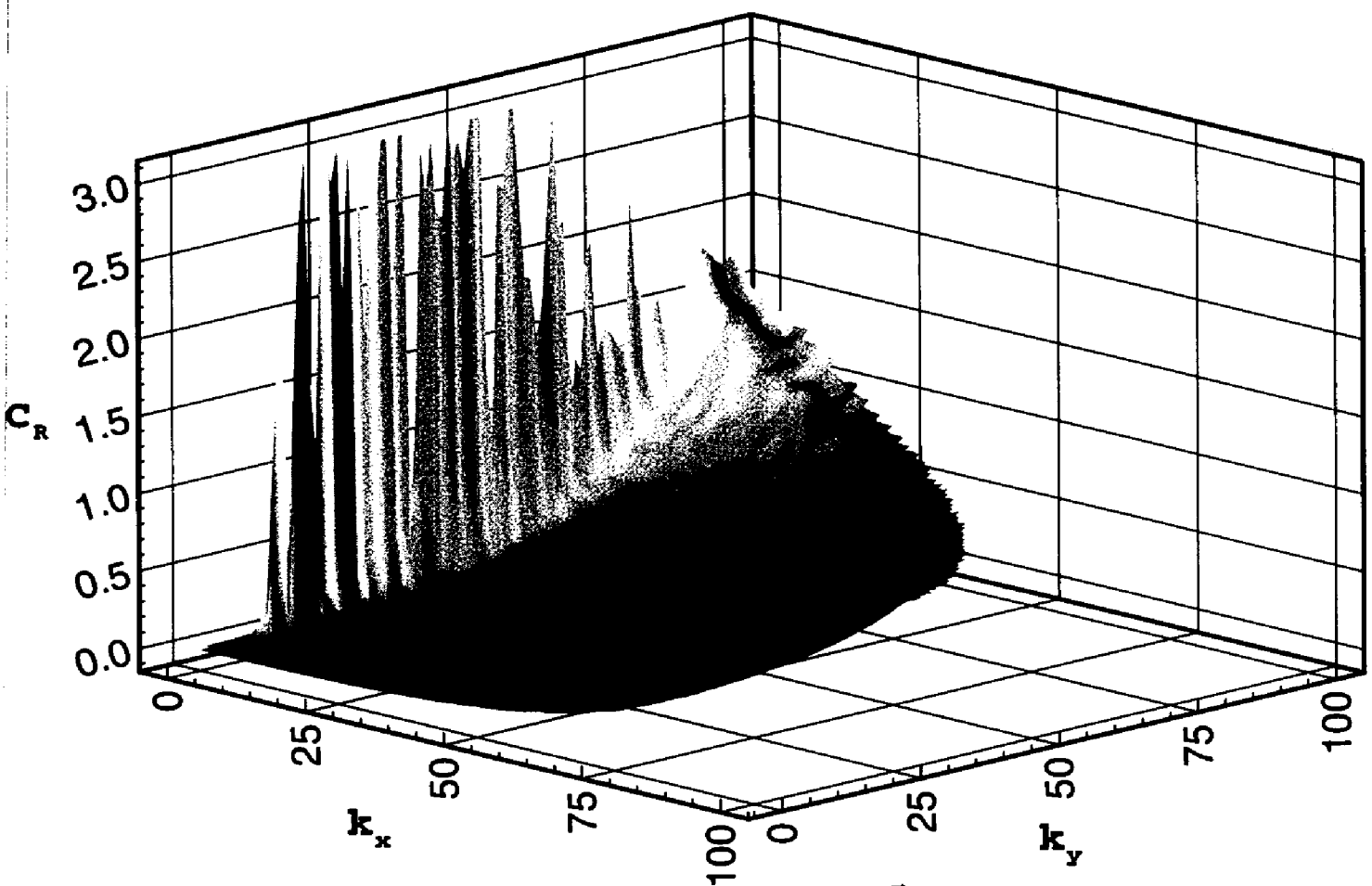


Figure 4.3: The compensated energy spectrum $C_R = E(\vec{k},t)\,\beta^{-2}\,k^5$ at $t = 81.9\,\tau_{tu}$ for $k < k_f$.

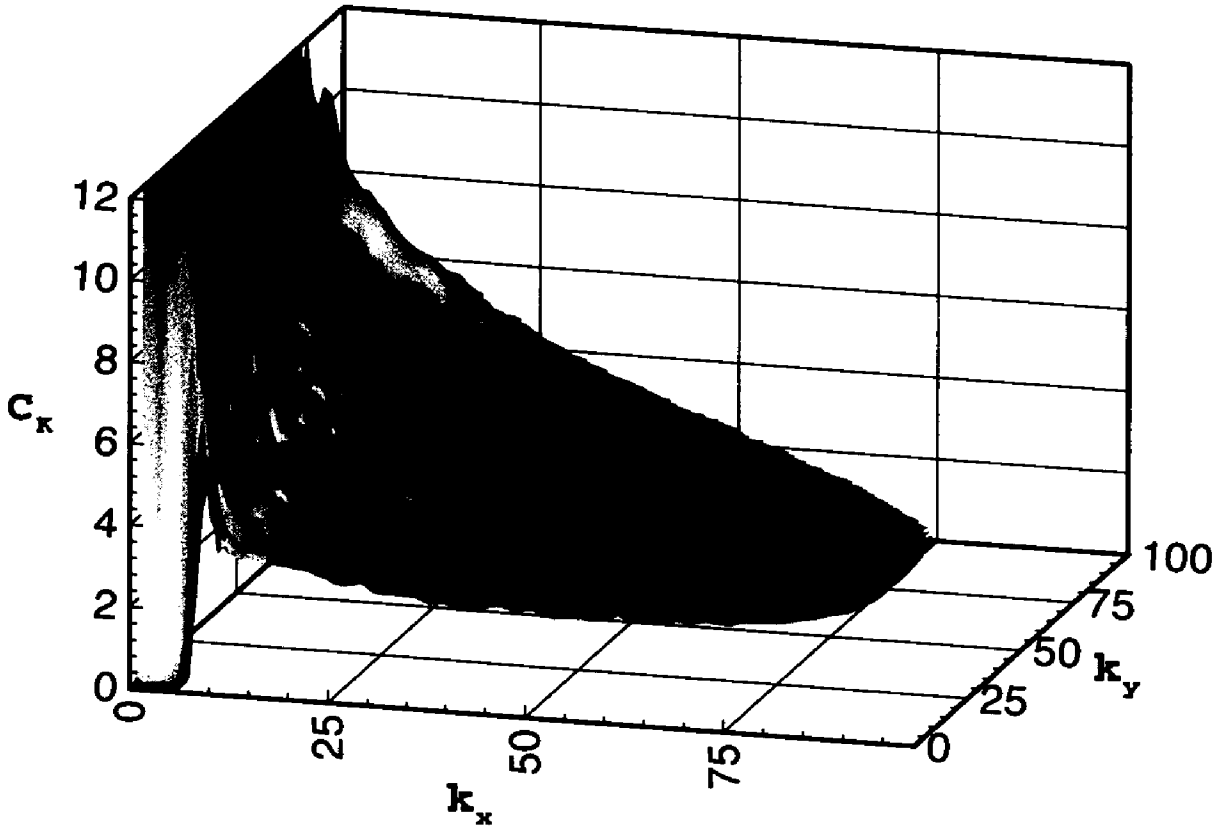


Figure 4.4: The compensated energy spectrum $C_K = E(\vec{k},t)\,\overline{\epsilon}^{-2/3}\,k^{5/3}$ at $t = 81.9\,\tau_{tu}$ for $k < k_f$.

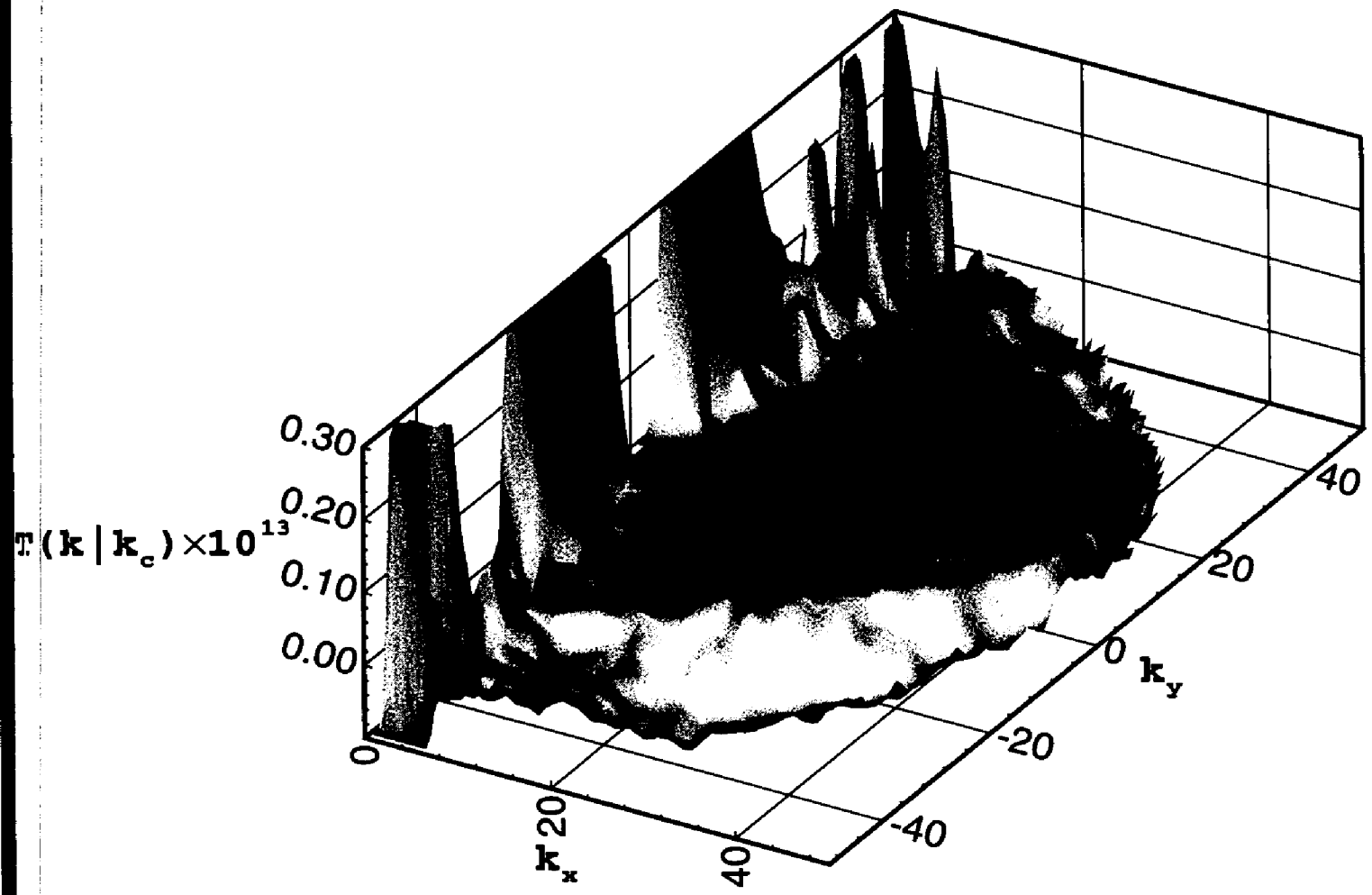


Figure 4.5: Spectral energy transfer, $T_E(\mathbf{k}|k_c)$, for $k_c = 50$ at $t = 115.0\,\tau_{tu}$.

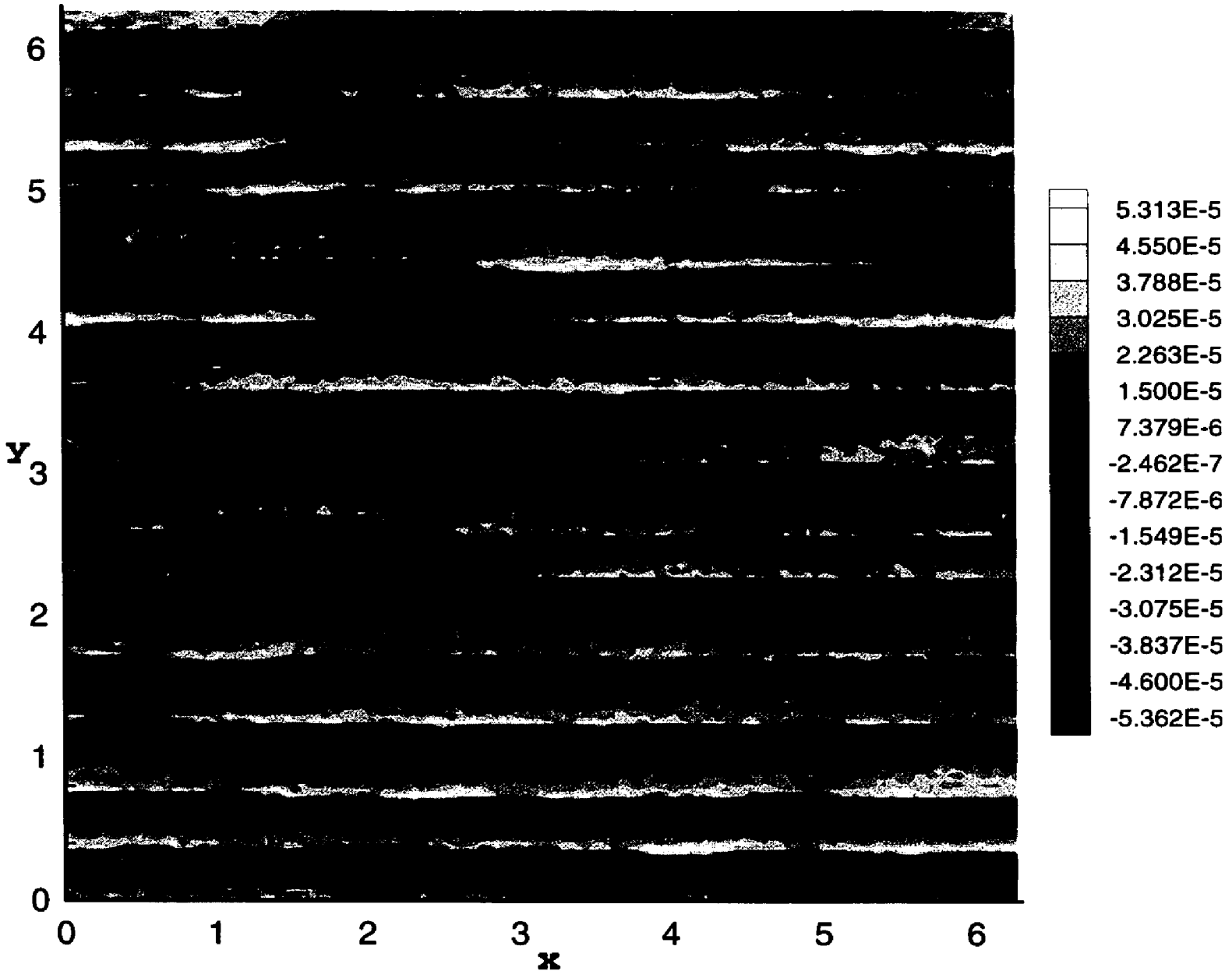


Figure 4.6: Instantaneous vorticity field $\zeta(\vec{x}, t)$ at $t = 115.0\,\tau_{tu}$.

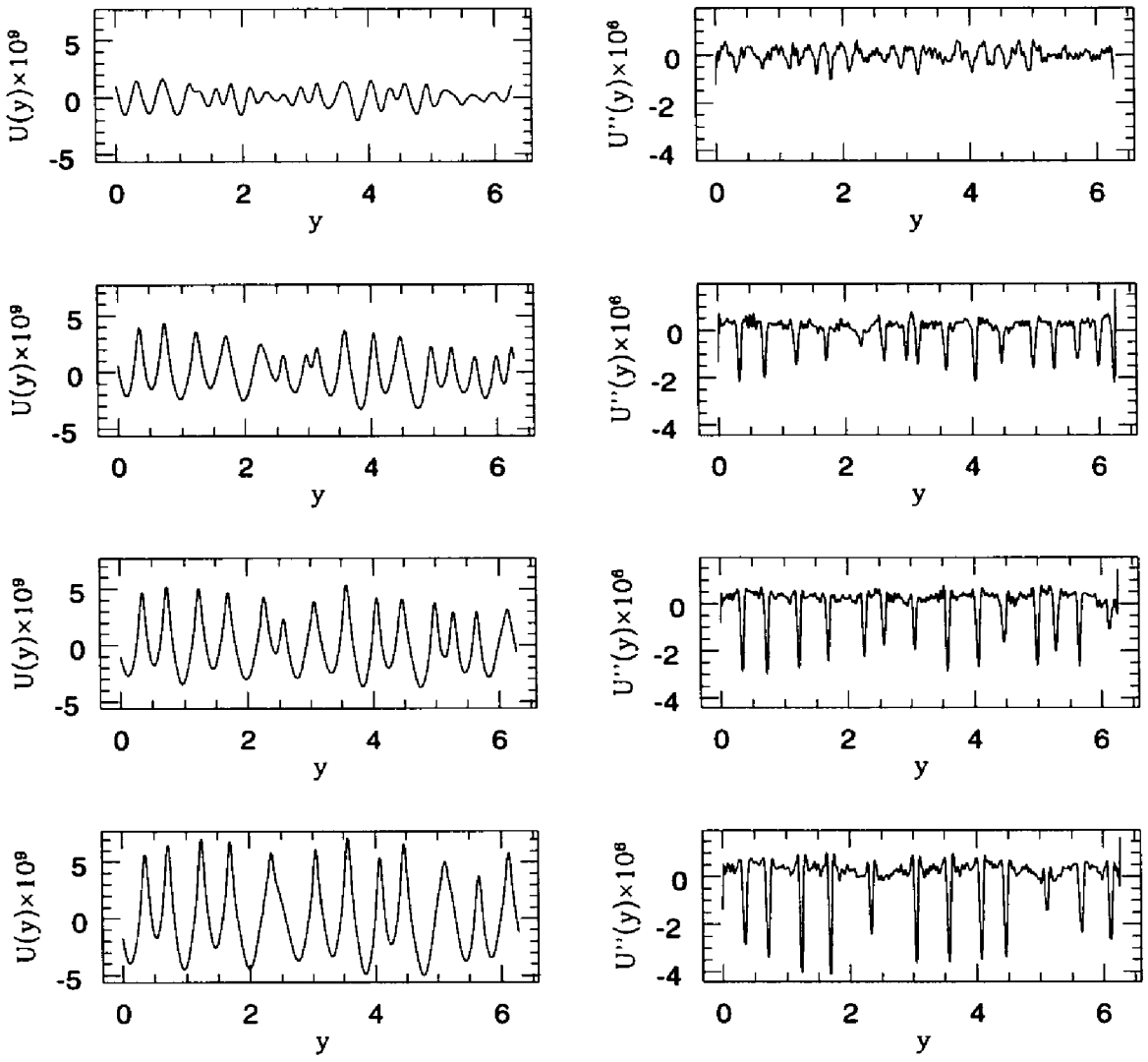


Figure 4.7: Zonally-averaged horizontal velocity profile $U(y,t)$ (first column) and its second derivative $U_{yy}(y,t)$ (second column) at $t = 58.5\,\tau_{tu}$, $t = 81.9\,\tau_{tu}$, $t = 115.0\,\tau_{tu}$, and $t = 175.4\,\tau_{tu}$ (from the top to the bottom).

# Chapter 5

# Large Eddy Simulation (LES) of Two-Dimensional Isotropic Turbulence

Although the mathematical modeling of quasi-2D flows has important practical applications, particularly in the atmospheric and oceanic sciences, it has not received as much attention in the literature as the modeling of the 3D flows. Partly, this can be explained by the fact that the quasi-2D problems are less computationally intense than their 3D counterparts. Thus there exists a hope that in the near future, practically important quasi-2D problems can be solved using Direct Numerical Simulation (DNS) in which all scales are resolved [45]. In addition, despite the specific peculiarities of quasi-2D flows related to the energy and vorticity dynamics, their sub-grid scale (SGS) representation has not received sufficient attention so far. There have been attempts to parameterize the SGS processes in quasi-2D flows similarly to those in 3D flows using Laplacian or biharmonic dissipation, the most advanced method being the anticipated potential vorticity method [64]. However, such methods can only perform well in the vorticity dissipation subrange when energy is injected on relatively large scales. Being applied in the energy transfer subrange, they will lead to energy dissipation, contradicting basic energy and vorticity transfer dynamics of quasi-2D turbulence. Moreover, Large Eddy Simulation (LES) of quasi-2D flows in

the energy transfer subrange has never been attempted, despite the fact that such flows would bear strong analogy to large scale oceanic and atmospheric circulation and that DNS of such flows cannot be expected in the foreseeable future. Thus, there exists a need to improve our understanding of the SGS processes in the energy transfer subrange of quasi-2D flows and to successfully simulate such flows when their energy sources reside in the SGS region. These both issues are addressed in the present Chapter. In the next Section, the basic difficulties of the SGS representation of the quasi-2D flows in the energy transfer subrange are discussed. Then, the following Section elaborates on the notion of the two-parametric viscosity and explains how this viscosity resolves the conflict between inverse transfer of energy and direct transfer of enstrophy. In Section 5.3, advantages and deficiencies of various implementations of the two-parametric viscosity for LES of 2D turbulence in the energy subrange are described. In Section 5.4, simplified SGS representations for LES of 2D turbulence are considered and the notion of the Stabilized Negative Viscosity (SNV) is introduced. Finally, Section 5.5 discusses the results of performed LES. Material presented in this Chapter is included in [83].

## 5.1 Basic Problems of the Sub-Grid Scale (SGS) Representation of Quasi-2D Flows in the Energy Transfer Subrange

Confined to two dimensions, turbulent flows become non-vortex-stretching and undergo dramatic structural changes [40]. The most profound modifications take place in the dynamics of energy and vorticity transfer. It is well known that in isotropic homogeneous 3D turbulence, the direct energy cascade from large to small scales facilitates efficient energy dissipation by molecular viscosity. This process is accompanied by and closely related to the production of enstrophy (mean square vorticity) through vortex stretching mechanism. Since in 2D flows vortex stretching cannot occur, the enstrophy then is conserved. Thus, 2D inviscid fluids possess two nontriv-

ial integrals of motion: the energy and the enstrophy. The enstrophy conservation prevents cascade of energy from large to small scales because such cascade would increase enstrophy [36, 38, 40].

Mathematically, this important feature is illustrated by the Fjørtoft theorem [45]. However, the direct cascade of enstrophy from large to small scales is possible. It results in molecular dissipation of large scale vorticity at small scales. Drawing analogy to eddy viscosity in 3D flows, one can infer that small scale processes in 2D flows generate an *effective*, or eddy viscosity for the *vorticity* of large scales. However, introducing an eddy viscosity concept in 2D flows seems to be intrinsically inconsistent and self-defeating because the dissipation of enstrophy will be accompanied by the dissipation of energy, which is physically incorrect. This controversy calls for modification of the eddy viscosity concept for quasi-2D flows; the issue in the focus of the present Section.

More detailed consideration of the transport processes in 2D turbulence reveals that they depend on the wave numbers of the energy injection, $k_f$. For $k < k_f$, the energy cascades up scales (inverse cascade), while the enstrophy flux is zero. For $k > k_f$, the energy flux is zero, but there exists the direct enstrophy flux [38]. If LES of a quasi-2D flow is thought of, the proper SGS parameterization should depend on the wave number of the energy source, $k_f$, i.e., whether $k_f$ belongs in the resolved (or explicit) or unresolved (or SGS) region. In the former case, a simple hyperviscous SGS representation may suffice, because it should only account for the enstrophy dissipation due to the direct cascade. However, if the forcing is located in the subgrid scales, then the hyperviscous SGS representation would lead to erroneous results since it will constitute energy dissipation in non-energy-dissipating flows. To sustain such flows, one would need to introduce a large scale energy source in the energy cascade subrange. A possible solution to this problem would be to replace an SGS forcing by a forcing located in the explicit region near $k_c$, where $k_c$ is the cutoff wave number corresponding to the grid resolution. However, this solution is not only quite cumbersome but it also significantly distorts the explicit scales near $k_c$. In addition, this approach is difficult for implementation in the physical space, particularly for

bounded systems and/or systems with spatially nonuniform energy sources.

Another solution would be to introduce a negative eddy viscosity, first extensively discussed by [80], as an SGS parameterization of the unresolved energy source. Studies of flows with negative viscosity were conducted in [25, 26] for 2D- and in [70, 96] for 3D-case. Although such an SGS representation could address the issue of the inverse energy cascade, it would not satisfy the constraint of the zero enstrophy flux. In addition, equations of motion with negative viscosity produce ill-posed problems. It appears therefore that addressing the issue of SGS representation for quasi-2D flows in self-consistent and comprehensive way would require full consideration of energy and enstrophy dynamics and should be based upon the corresponding transport equations. Such an approach was first outlined by Kraichnan [39] who introduced the notion of two-parametric viscosity. This approach and its implications will be elaborated in the next Section.

## 5.2 Two-Parametric Viscosity as SGS Representation of Quasi-2D Flows

In Chapter 3 we have demonstrated that for the two-dimensional incompressible turbulent flows described by the vorticity equation (3.1), the two-parametric eddy viscosity may be introduced via (3.64)-(3.66) and derived from the RG results.

The introduction of the classical eddy viscosity concept for LES with equation (3.1) implies that there is a distinct scale separation between the resolvable and SGS modes. Indeed, only if such a separation exists, the eddy viscosity would be $k$-independent and a function of the cutoff wave number $k_c$ only. However, the assumption of scale separation fails in all turbulent flows, particularly in 2D flows, such that, strictly speaking, an SGS representation should depend on two parameters, $k$ and $k_c$. Such two-parametric viscosity, denoted by $\nu(k|k_c)$, was first introduced by Kraichnan (1976). It describes the energy exchange between given resolved vorticity mode with the wave number $k$ and all SGS modes with $k > k_c$.

In Chapter 3 we have also compared $\nu(k|k_c)$ calculated from the DNS data with

those evaluated by Kraichnan (1976) using his Test Field Model (TFM) and obtained from the Renormalization Group (RG) theory (see Appendix B). The results of this comparison were presented in Figs. 3.4 and 3.5. Let us recall that Fig. 3.4 presents the DNS-inferred normalized two-parametric viscosity,

$$N(k/k_c) \equiv \frac{\nu(k|k_c)}{|\nu(0|k_c)|}, \tag{5.1}$$

along with the TFM- and RG-based analytical predictions. The results are in very good agreement with each other over the entire energy transfer range, up to the wave numbers close to $k_c$, where the DNS data saturates, while the TFM and RG curves exhibit sharp cusp. This theoretical cusp is due to the fact that as $k \to k_c$, more and more elongated triads with either $p$ or $q \ll k_c$ become involved in the energy exchange between the mode $k$ and the sub-grid scale modes. The contribution from these triads to the energy exchange near $k_c$ is very significant and results in the cusp behavior. However, in finite box DNS with large-scale energy removal, the energy of small wave number modes is reduced and $\nu(k|k_c)$ is expected to saturate near $k_c$. Indeed, when the RG-based $\nu(k|k_c)$ was re-calculated based upon the DNS energy spectrum, the unnormalized DNS- and RG-based two-parametric viscosities were found to be in very good agreement for all wave numbers, as was shown in Fig. 3.5.

Figs 3.4 and 3.5 show that for the large scale modes, for which $k \ll k_c$ and scale separation exists, the effect of the SGS modes is represented by a negative and constant viscosity, such that these modes *gain* energy from their SGS counterparts by means of the inverse transfer. On the other hand, $\nu(k|k_c) > 0$ for $k \to k_c$ such that the modes close to $k_c$ lose their energy to the SGS modes. The difference between the large scale gain and the small scale loss produces constant energy flux $\bar{\epsilon}$, the rate of the energy input due to the forcing $f$ in equation (3.1) and equation (5.8) below. If the enstrophy balance is considered, recall that the enstrophy transfer is most efficient at small scales, such that the resulting balance for the resolvable scales turns out to be zero (see [38], and (5.13) below), i.e. the enstrophy is conserved. This explains how the two-parametric viscosity resolves the controversy of the inverse cascade of energy and conservation of enstrophy in the energy subrange of 2D flows. It appears therefore that the only physically correct way to represent SGS processes

in 2D turbulence would be through the two-parametric viscosity. Such an approach has become quite popular in simulations of 3D flows, see [14] and review [23] but has not yet been fully explored for LES of quasi-2D flows. The implementation of the two-parametric viscosity for LES of 2D turbulent flows, the arising problems, their solutions and results are described in the following Sections.

## 5.3 Implementation of the Two-Parametric Eddy Viscosity for LES of 2D Turbulence

To test the two-parametric viscosity-based SGS parameterization in the energy transfer subrange, a series of LES of 2D turbulence in Fourier space was designed. These LES were based upon equation (3.1) in which all the sub-grid scale processes including the forcing were represented by the two-parametric viscosity $\nu(k|k_c)$,

$$\frac{\partial \zeta(\mathbf{k})}{\partial t} + \int_{|\mathbf{p}|,|\mathbf{k}-\mathbf{p}|<k_c} \frac{\mathbf{p}\times\mathbf{k}}{p^2}\zeta(\mathbf{p})\zeta(\mathbf{k}-\mathbf{p})\frac{d\mathbf{p}}{(2\pi)^2} = \nu(k|k_c)k^2\zeta(\mathbf{k}), \qquad 0<k<k_c. \quad (5.2)$$

It is important to reiterate that in LES of 2D turbulence in the energy subrange, the source of energy resides on the unresolved scales, such that equation (5.2) appears unforced. However, as was explained earlier, the negative part of $\nu(k|k_c)$ serves as the only energy source for the resolved modes. In the course of the present LES it was found that numerical results critically depend on the way $\nu(k|k_c)$ is introduced into the solver. Thus, a series of simulations was designed with the purposes of understanding the nature of the problems associated with the implementation of the two-parametric viscosity and of identifying the most viable and robust ways to use this viscosity in LES of 2D flows.

**Description of numerical method.** The numerical solver used in the present calculations was based upon Fourier-Galerkin pseudo-spectral formulation [57] the same as the one utilized in Chapter 3. The present LES employed $162^2$ resolution including aliased modes; the cutoff wave number was set at $k_c = 50$, which is about half of the resolution used in DNS of Chapter 3, see also [9]. The initial flow field

was set to zero everywhere except for a narrow band of wave numbers in the middle part of the spectrum where it was assigned random Gaussian distribution. The DNS inferred value of $\bar{\epsilon}$ was about $5.19 \times 10^{-10}$; the same $\bar{\epsilon}$ was used in LES. The time-step in LES was set to $\delta t = 0.5$ satisfying both convective and viscous necessary conditions for linear stability. Based upon the size of the largest energy containing eddy with the wave number $k_{\min}$, $2\pi/k_{\min}$, and the total energy of the steady-state $\overline{E}(t)$, the maximum large scale eddy turnover time defined as $\tau_{tu} = 2\pi/(k_{\min}\sqrt{2\overline{E}})$ was about $\tau_{tu} \simeq 3600$ for LES of cases 1 and 2 below, where $k_{\min} = 1$, and $\tau_{tu} \simeq 900$ for cases $3, 4, 5$, and 6 for which $k_{\min} = 4$.

**Case 1. Flow independent $\nu(k|k_c)$.** With $\nu(k|k_c)$ known and flow independent, equation (5.2) can be solved directly. According to Fig. 3.4, $\nu(k|k_c)$ can be obtained from DNS or from some statistical theory of turbulence. Thus, in the first LES numerical solver for equation (5.2) utilized $\nu(k|k_c)$ derived from the renormalization group (RG) theory of turbulence (see Appendix B for the details). As shown in the Appendix B,

$$\nu(k|k_c) = 0.327\bar{\epsilon}^{1/3}k_c^{-4/3}N(k/k_c), \tag{5.3}$$

where $N(k/k_c)$ is given by (5.1), and since $\bar{\epsilon}$ is a constant, $\nu(k|k_c)$ is a function of $k$ and $k_c$ only. It was assumed that thus defined $\nu(k|k_c)$ would be capable of supporting inverse energy cascade with constant SGS energy input $\bar{\epsilon}$. To verify this assumption, one needs to examine the evolution of total energy and enstrophy of the resolved modes, $\overline{E}(t)$ and $\overline{\Omega}(t)$, respectively. By definition, $\overline{E}(t) = \int_0^{k_c} E(k,t)dk$, where $E(k,t) \equiv (4\pi k)^{-1}\langle\zeta(\mathbf{k},t)\zeta(-\mathbf{k},t)\rangle$ is the spectral energy density, and $\overline{\Omega}(t) = \int_0^{k_c} \Omega(k,t)dk$. The basic requirement to LES would be that $\overline{E}(t)$ and $\overline{\Omega}(t)$ of LES have the same behavior as those derived from (3.1) for which the evolution laws are $\overline{E}(t) \propto \bar{\epsilon}t$ and $\overline{\Omega}(t) = \text{const}$, due to the conservation of the inviscid integrals for $\overline{E}(t)$ and $\overline{\Omega}(t)$ (recall that in the energy subrange of 2D turbulence the rate of the enstrophy flux $\eta = 0$). Figs 5.1(a,b) show that in the first LES, both $\overline{E}(t)$ and $\overline{\Omega}(t)$ exhibit nonlinear growth indicating that not only the rate of the energy transfer to the resolvable scales $\bar{\epsilon}_{les} \neq \text{const}$, but also the rate of the enstrophy transfer $\overline{\eta}_{les} \neq 0$.

Fig. 5.2 shows that instantaneous spectrum $E(k,t)$ also reveals tendency to growing up with time without stabilizing around any universal distribution. At some point of its evolution, $E(k,t)$ passed through the Kolmogorov law

$$E(k) = C_K \, \bar{\epsilon}^{\frac{2}{3}} \, k^{-\frac{5}{3}}, \tag{5.4}$$

where $C_K \approx 6$ is the Kolmogorov constant, and $\bar{\epsilon}$ was close to its prescribed DNS value. However, at larger times the Kolmogorov scaling (5.4) was lost, while $\bar{\epsilon}_{les}$ kept growing. The roots of the problem are revealed when one calculates the rate of the energy input into all resolved modes, $\bar{\epsilon}_{les}$. The energy equation derived from the definition of spectral energy density and (5.2) yields

$$\bar{\epsilon}_{les}(t) \equiv \frac{\partial \overline{E}(t)}{\partial t} = -2 \int_0^{k_c} \nu(k|k_c) E(k,t) k^2 dk. \tag{5.5}$$

Since in the first series of LES, $\nu(k|k_c)$ depends on $k$ and $k_c$ only, and $E(k,t)$ is a dynamic variable that depends on the evolution of the flow field, $\bar{\epsilon}_{les}(t)$ also turns out to be time dependent. This is not only in direct conflict with the requirement that $\bar{\epsilon}_{les} = \bar{\epsilon}$ =const, but also leads to a positive feedback between the energy input and total energy of the system, which results in numerical instability. To correct this problem, one must ensure that $\bar{\epsilon}_{les} = \text{const}$. This can be achieved by allowing $\nu(k|k_c)$ to become time dependent and related to resolved variables. The philosophy of using actual flow field characteristics to determine energy input and dissipation would be analogous to a standard practice of 3D LES.

Inspection of equation (5.5) reveals that $\bar{\epsilon}_{les}(t)$ is proportional to the total enstrophy of the resolvable field, such that stipulating $\bar{\epsilon}_{les} = \text{const}$ would require $\nu(k|k_c)$ to become time dependent and inversely proportional to $\overline{\Omega}(t)$ (the time dependency of $\nu(k|k_c)$ will be implied in the following discussion but suppressed in notations). To find the explicit dependency of $\nu(k|k_c)$ on $\overline{\Omega}(t)$, let us assume that $\nu(k|k_c)$ can be represented by

$$\nu(k|k_c) = F(\overline{\Omega}) N(k/k_c), \tag{5.6}$$

where $F(\cdot)$ is some function of $\overline{\Omega}(t)$ and $N(k/k_c)$ is still determined by (5.1). Accord-

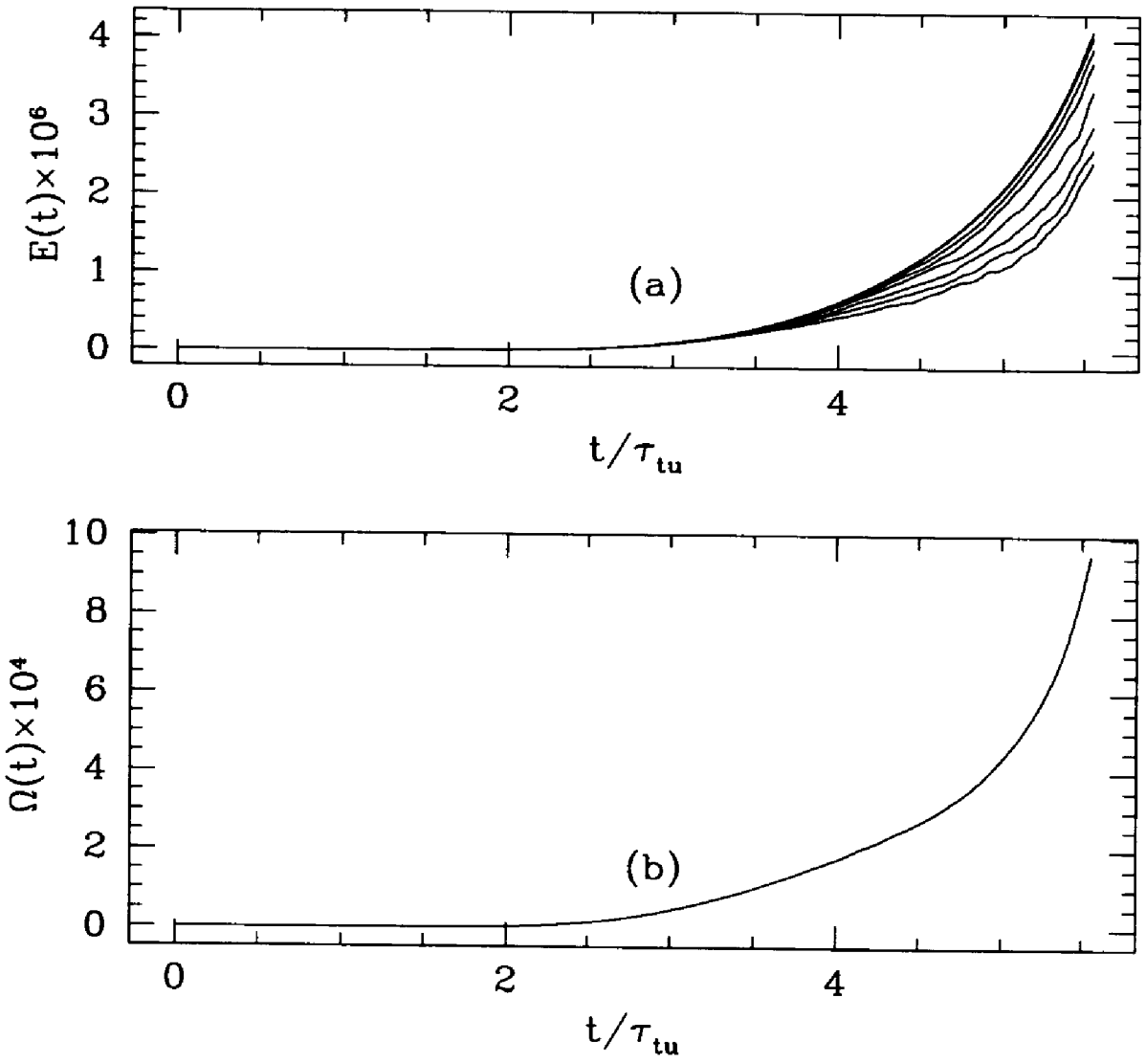


Figure 5.1: The evolution of the total energy $\overline{E}(t)$ (a) and total enstrophy $\overline{\Omega}(t)$ in Case 1 LES. Fig. 5.1(a) also shows the evolution of $\overline{E}(t)$ with the energy of the 1st, 2nd, 3rd, 4th, 5th, 6th and 7th modes removed.

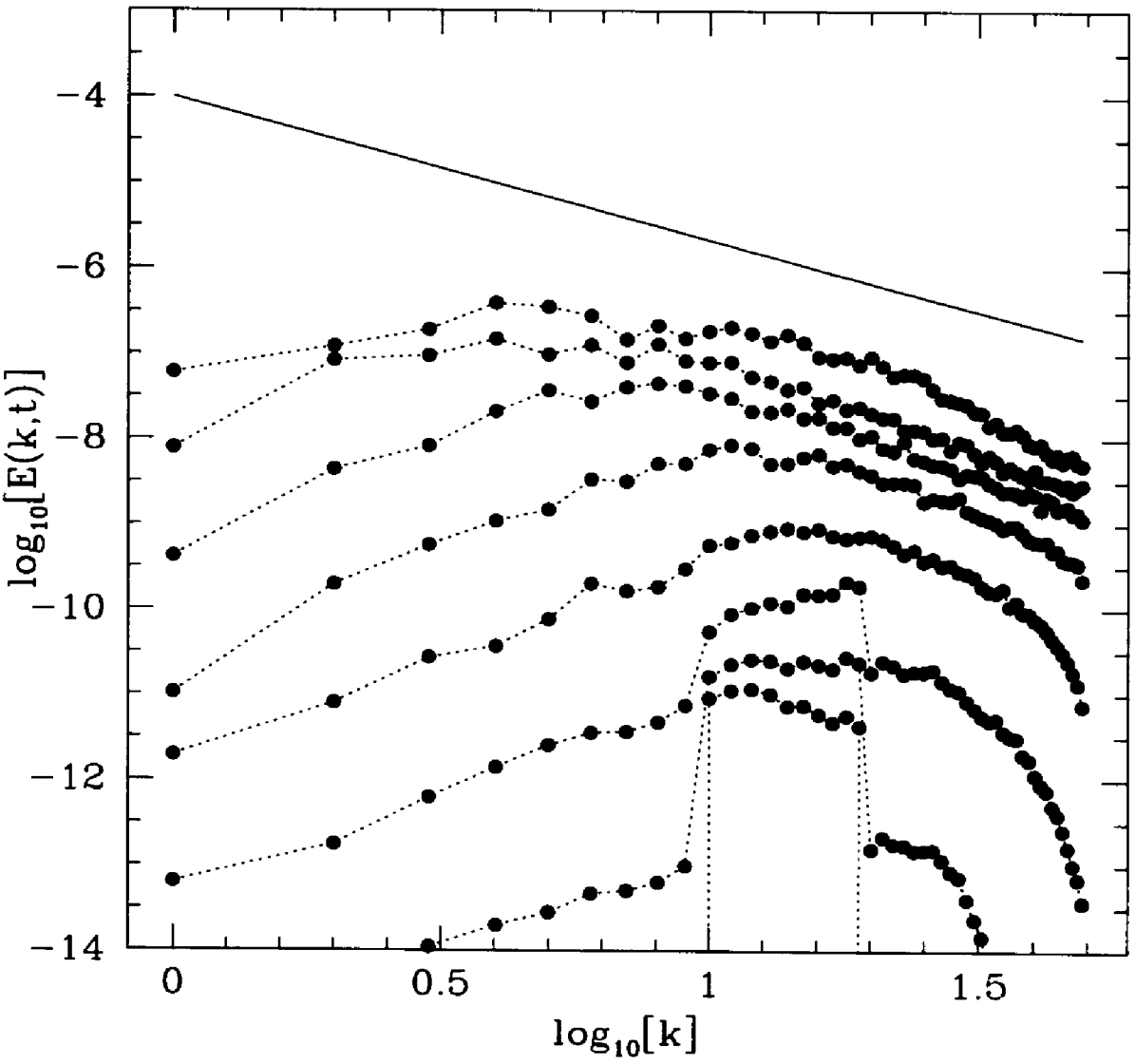


Figure 5.2: The evolution of the instantaneous energy spectrum for $t/\tau_{tu} = \{0.56, 1.11, 1.67, 2.78\}$ in Case 1 LES. The solid line shows the Kolmogorov $-5/3$ slope.

ing to Fig. 3.4, $N(k/k_c)$ can be split into negative and positive terms,

$$N(k/k_c) = -1 + \phi(k/k_c), \quad \phi(k/k_c) > 0, \quad 0 \leq k/\ k_c \leq 1. \tag{5.7}$$

One can now calculate integral in (5.5) using equations (5.6) and (5.7)

$$\begin{aligned}\bar{\epsilon}_{les} &= 2F(\overline{\Omega})\int_0^{k_c} E(k,t)k^2dk - 2F(\overline{\Omega})\int_0^{k_c}\phi(k/k_c)E(k,t)k^2dk \\ &= 2F(\overline{\Omega})\overline{\Omega}(t) - 2F(\overline{\Omega})\int_0^{k_c}\phi(k/k_c)E(k,t)k^2dk.\end{aligned} \tag{5.8}$$

Integration of (5.8) for the Kolmogorov spectrum with $\phi(k/k_c)$ evaluated from the RG theory (see Appendix B) yields

$$\bar{\epsilon}_{les} \simeq 0.8F(\overline{\Omega})\overline{\Omega}(t). \tag{5.9}$$

Equation (5.9) shows that to satisfy the requirement $\bar{\epsilon}_{les} = \bar{\epsilon} = \text{const}$, one has to impose

$$F(\overline{\Omega}) = \frac{\bar{\epsilon}}{0.8\,\overline{\Omega}(t)}, \tag{5.10}$$

such that the two-parametric viscosity (5.6) becomes

$$\nu(k|k_c) = \frac{\bar{\epsilon}}{0.8\overline{\Omega}(t)}N(k/k_c) = -\frac{\bar{\epsilon}}{0.8\overline{\Omega}(t)} + \frac{\bar{\epsilon}}{0.8\overline{\Omega}(t)}\phi(k/k_c). \tag{5.11}$$

The first term in the right hand side of (5.11) accounts for the SGS energy input while the second term represents the high wave number dissipation as $k \to k_c$. As was argued earlier, to ensure $\bar{\epsilon}_{les} = \text{const}$, the energy source term must be time dependent and inversely proportional to $\overline{\Omega}(t)$. Thus, the negative feedback between energy input and enstrophy of the resolved modes is the mechanism that stabilizes numerical process. Note that the SGS formulation based upon (5.11) complicates equation (5.2) because its right hand side now depends on the functional of the solution, $\overline{\Omega}(t)$. However, on the one hand, it is clear from the presented analysis that LES of 2D turbulence based upon (5.2) is impossible if $\nu(k|k_c)$ depends on $k$ and $k_c$ only. On the other, the SGS representation (5.11), though complicated, is in line with the eddy viscosity approach, in which the eddy viscosity coefficient is usually solution-dependent, see, for example, in [71, 73, 72, 93, 91].

**Case 2. Flow dependent $\nu(k|k_c)$ with no large scale drag.** The SGS formulation (5.11) was used in the second LES and considerable improvement over Case 1 was observed. Figs 5.3(a,b) show that up to the simulated time $t = 3\tau_{tu}$, $\overline{E}(t)$ grows linearly, while $\overline{\Omega}(t)$ attains a constant value. Fig. 5.4 shows that during the same time, $E(k,t)$ quickly approaches steady-state Kolmogorov distribution (5.4). However, for $t > 3\tau_{tu}$ the flow field undergoes irreversible modifications; the behavior of $\overline{E}(t)$ and $\overline{\Omega}(t)$ changes, while $E(k,t)$ begins to deviate from the Kolmogorov law. All these changes reflect the basic problem of the present LES that simulates the behavior of an infinite system in a finite computational box [74, 75]. In this box, the smallest wave number modes become energy saturated at $t \simeq 3\tau_{tu}$, and, if the energy of these modes is not removed, they begin to alter the behavior of the entire flow field. Therefore, to extend LES beyond $t \simeq 3\tau_{tu}$, one needs to prevent the accumulation of energy at the lowest modes, which was accomplished in LES of Case 3. Note however that by the time $t \simeq 3\tau_{tu}$ the inverse cascade swept through all the resolved modes such that they became energy saturated and attained the steady state. Therefore, one should expect that in LES with $t > 3\tau_{tu}$ both $\overline{E}(t)$ and $\overline{\Omega}(t)$ remain nearly constant.

**Case 3. Flow dependent $\nu(k|k_c)$ with large scale drag.** The simplest way to withdraw energy from the lowest modes would be simply to set to zero the amplitudes of those modes. However, such a "chopping" alone is known to produce unsatisfactory results [7]. Therefore, in addition to the chopping, one needs to introduce a mechanism that would account for the energy exchange between the resolved modes and the low wave number modes excluded in LES. Such a mechanism, the large scale drag, was introduced in this study in direct analogy to the two-parametric viscosity and we will not dwell on its description here.

The large scale drag was implemented in the third LES, whereas the amplitudes of all modes with $k < k_{\min} = 4$ were set to zero. As was explained in Chapter 3 and shown in Fig. 3.5, such a chopping results in flattening of the cusp in $N(k/k_c)$ as $k \to k_c$, such that this function had to be recalculated which in turn led to modification of the coefficient in (5.9) from 0.8 to 0.87. The results of the third LES

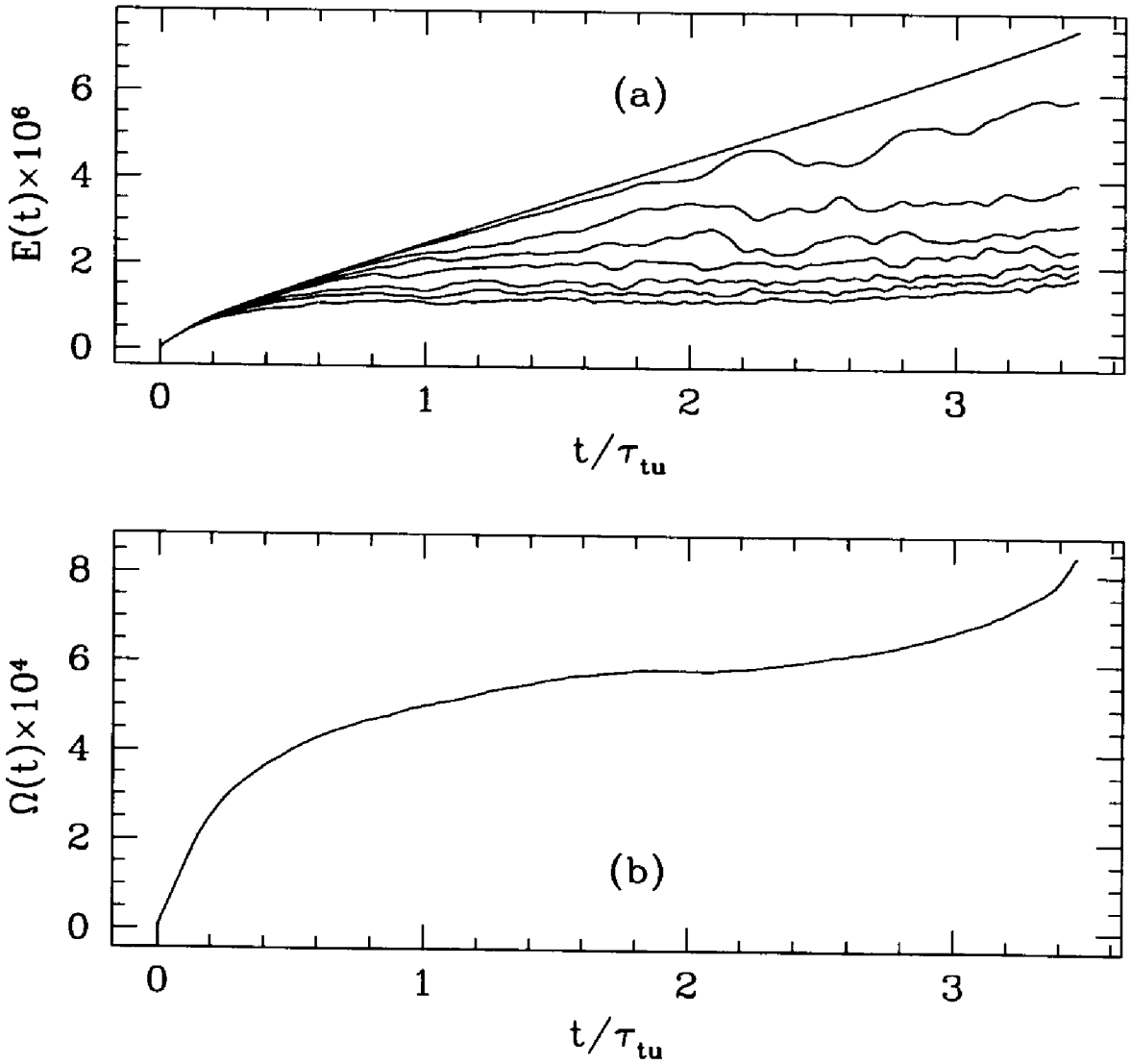


Figure 5.3: Same as Fig. 5.1 but for Case 2 LES.

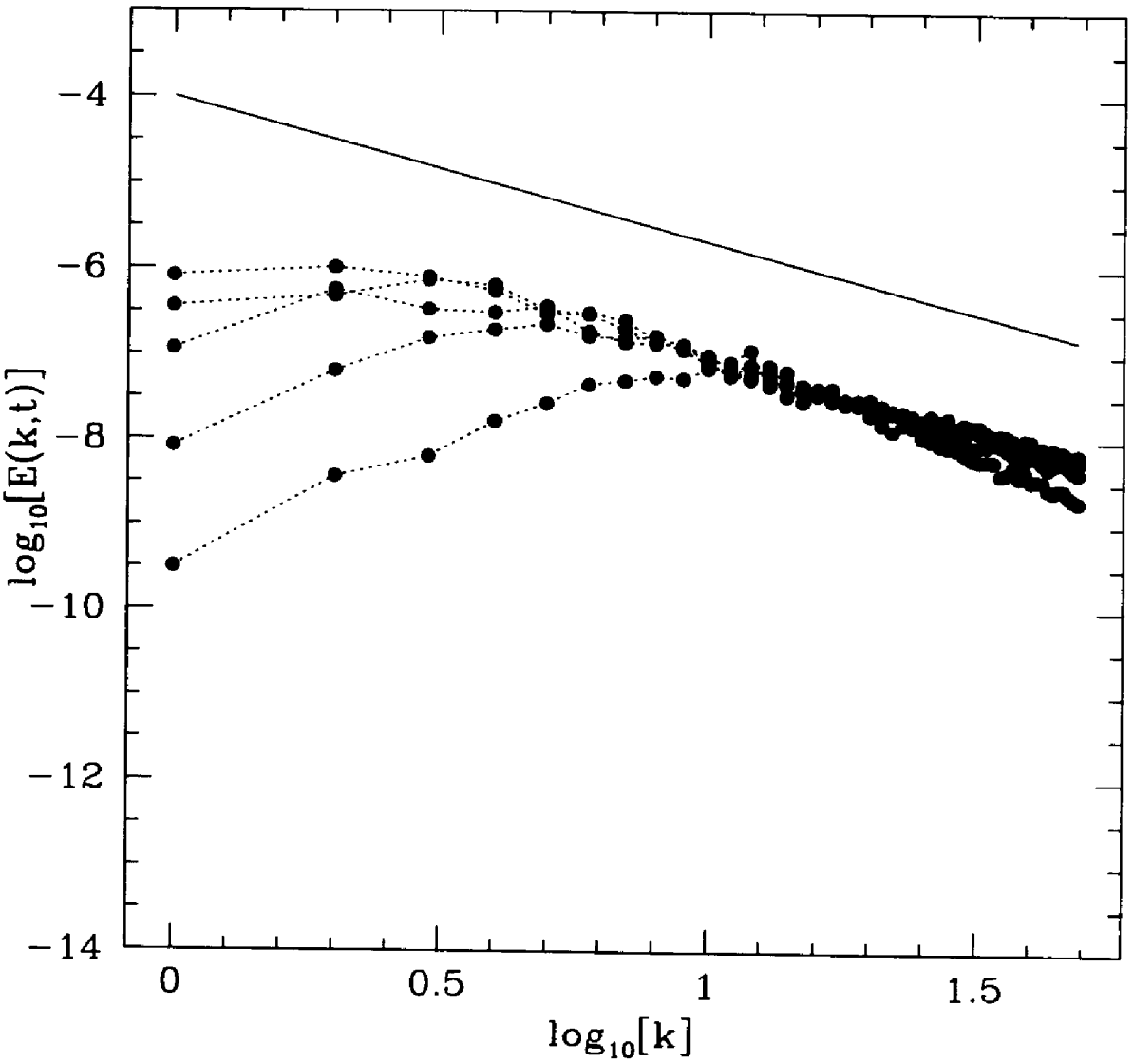


Figure 5.4: Same as Fig. 5.2 but for Case 2 LES. Note that after $t/\tau_{tu} \approx 2$ all instantaneous profiles $E(k,t)$ become close to Kolmogorov law (5.4).

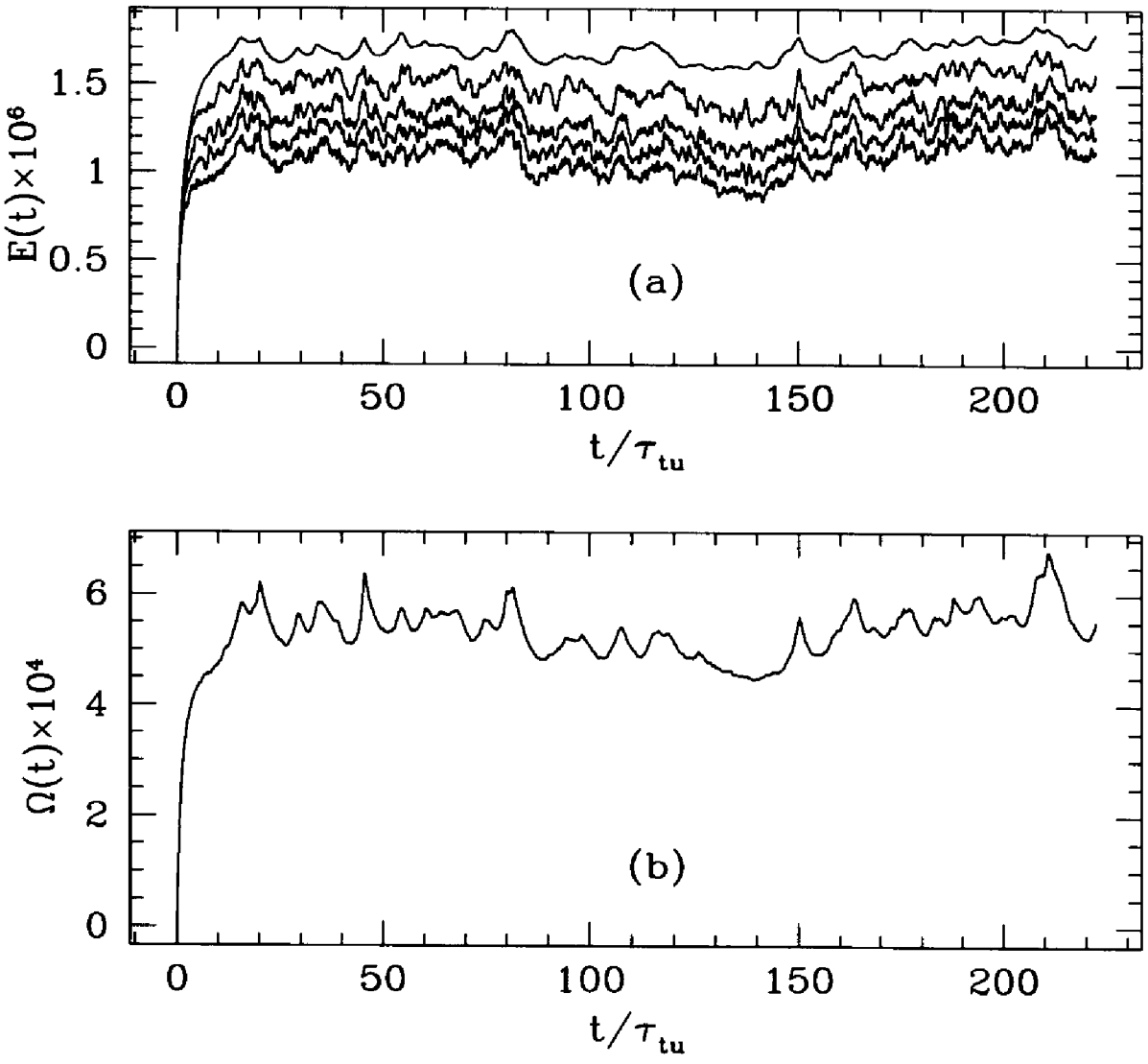


Figure 5.5: Same as Fig. 5.1 but for Case 3 LES. Because the amplitudes of the first four modes are set to zero, only the evolution of $\overline{E}(t)$ with the energy of the 4th, 5th, 6th and 7th modes removed is shown.

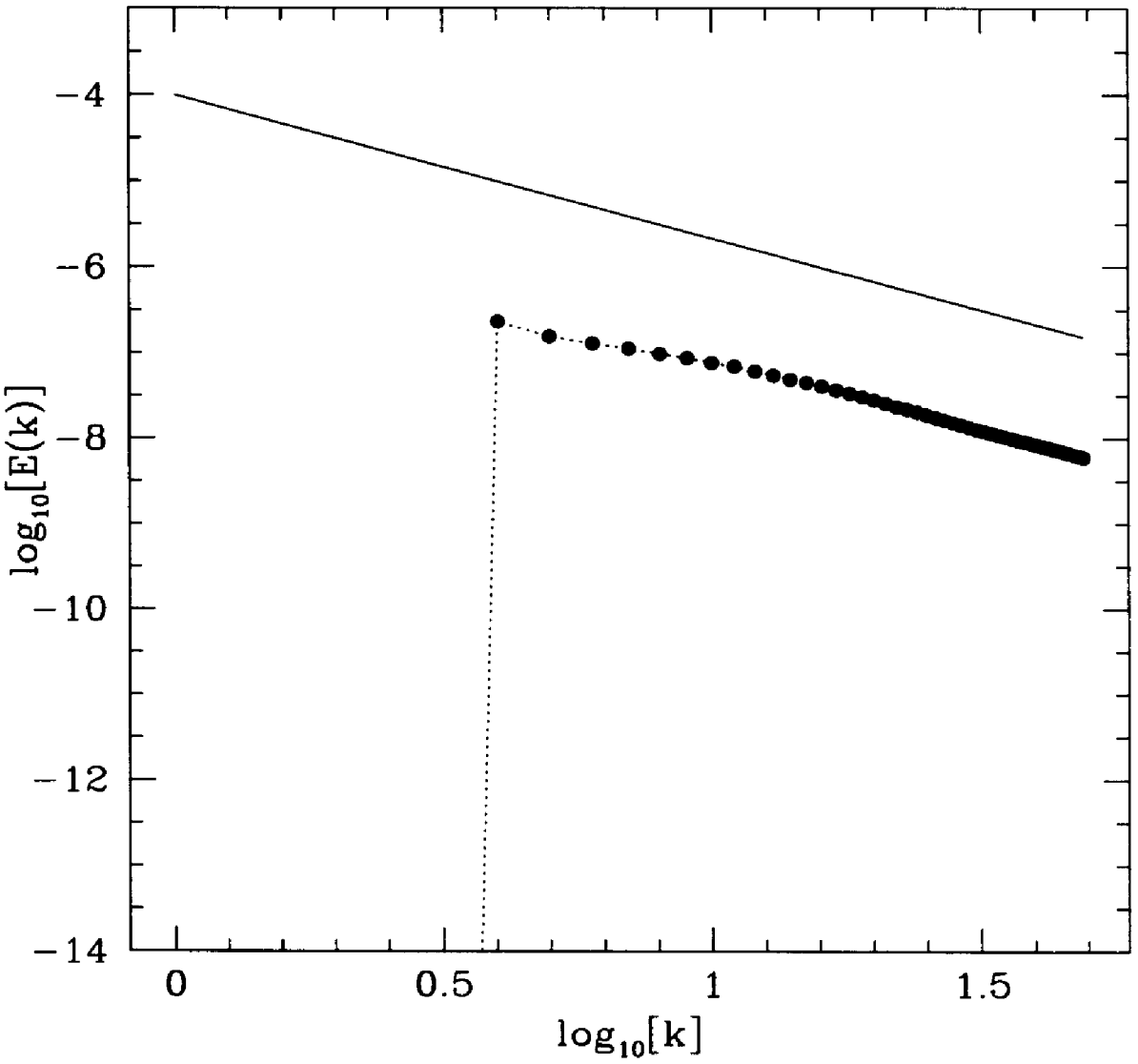


Figure 5.6: Same as Fig. 5.4 but for Case 3 LES. Note that the Kolmogorov scaling is attained after $t/\tau_{tu} \approx 2$, only the time-averaged spectrum is shown due to existence of the steady-state.

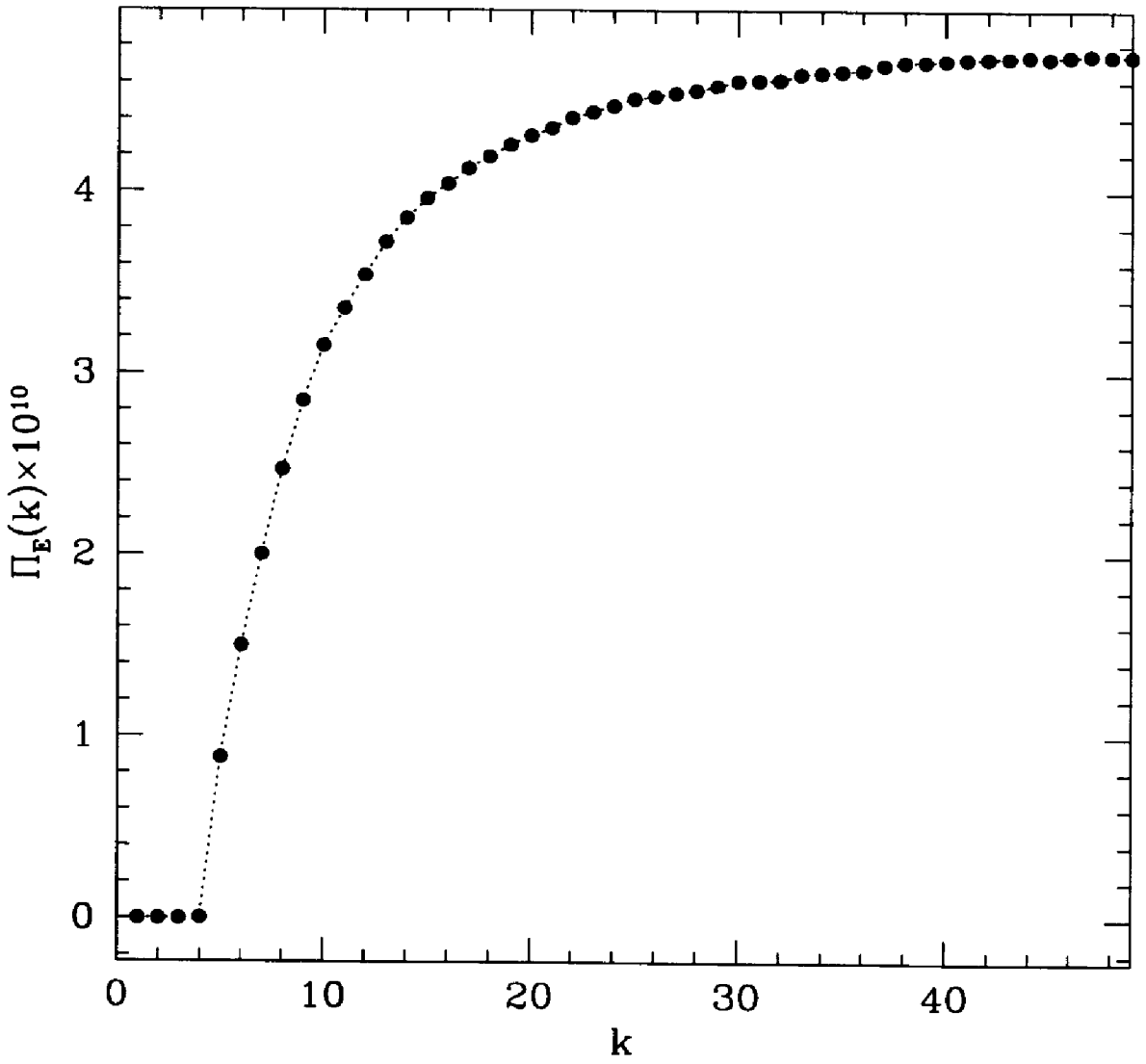


Figure 5.7: The energy flux $\Pi_E(k)$ for Case 3 LES.

are shown in Figs. 5.5(a,b), 5.6 and 5.7. One can see that this simulation could virtually be extended indefinitely, with $\overline{E}(t)$ and $\overline{\Omega}(t)$ slightly oscillating around their steady state values (the source of these oscillations is probably the self-adjustment of the numerical scheme to the mismatch between the small scale energy forcing and large scale withdrawal). The instantaneous energy spectrum, Fig. 5.6, exhibits steady and nearly perfect Kolmogorov scaling. Since the large scale drag enables one to dramatically increase the integration time in LES, it will be retained in all further simulations. Note however that these simulations will pertain to steady state rather than time developing flows. Figure 5.7 shows that the energy flux, $\Pi_E(k)$, is nearly constant for $k > 15$ and equal to $-5 \times 10^{-10}$ approximately, in good agreement with the corresponding DNS results (see Fig. 3 in [9]).

**Case 4. Flow dependent energy input with flow independent dissipation.** It would be tempting to simplify (5.11) by relaxing the time-dependency in the dissipation term. It is not clear a priori whether or not this time-dependency is critical, and to find out about it a fourth LES was conceived in which SGS representation (5.11) was modified by replacing $\overline{\epsilon}/0.8\ \overline{\Omega}(t)$ in the dissipation term by the RG derived expression $0.327\overline{\epsilon}^{1/3}k_c^{-4/3}$. Figs 5.8(a,b) and 5.9 show that this simplified SGS scheme performs in a very robust way with no oscillations at all for a relatively long time, $t \simeq 30\tau_{tu}$. Similarly to Case 3, there exists a mismatch between the small scale forcing and large scale energy removal, but since the dissipation in Case 4 cannot self-adjust, the solution begins to deteriorate when this mismatch accumulates significantly. Still, Case 4 LES could be extended to many more turnover times than the corresponding DNS, the result quite remarkable for its own sake. During this time, the instantaneous energy spectrum, Fig 5.9, exhibits steady and nearly perfect Kolmogorov scaling almost indistinguishable from that in Fig. 5.6. Figure 5.10 shows that the compensated energy spectrum gives Kolmogorov constant $C_K \approx 5$, in good agreement with the RG derived value of 5.12, see Appendix B for details. As in Case 3, the energy flux $\Pi_E(k)$ shown in Figure 5.11 is almost constant for $k > 15$ and is about $-5 \times 10^{-10}$.

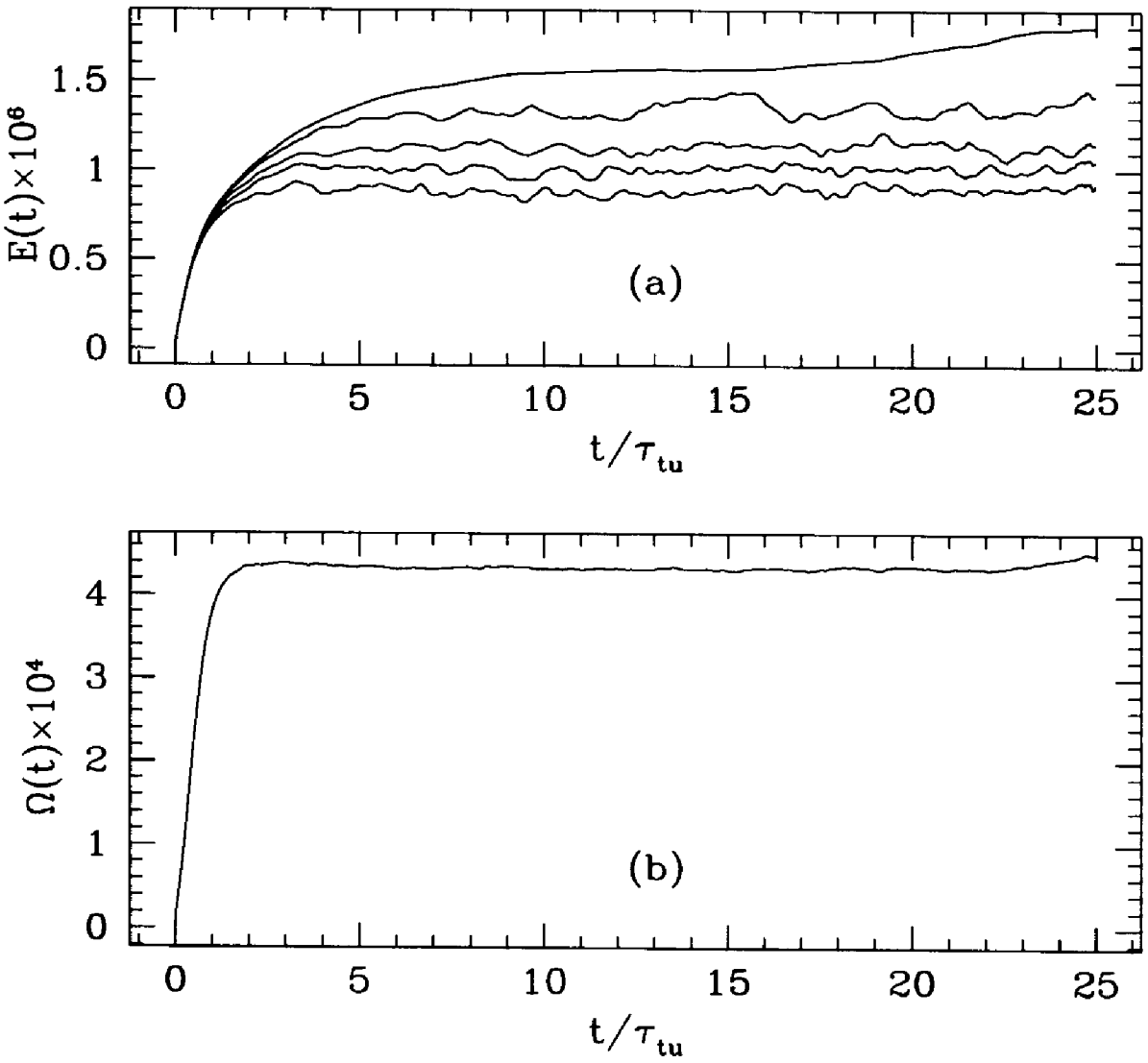


Figure 5.8: Same as Fig. 5.5 but for Case 4 LES.

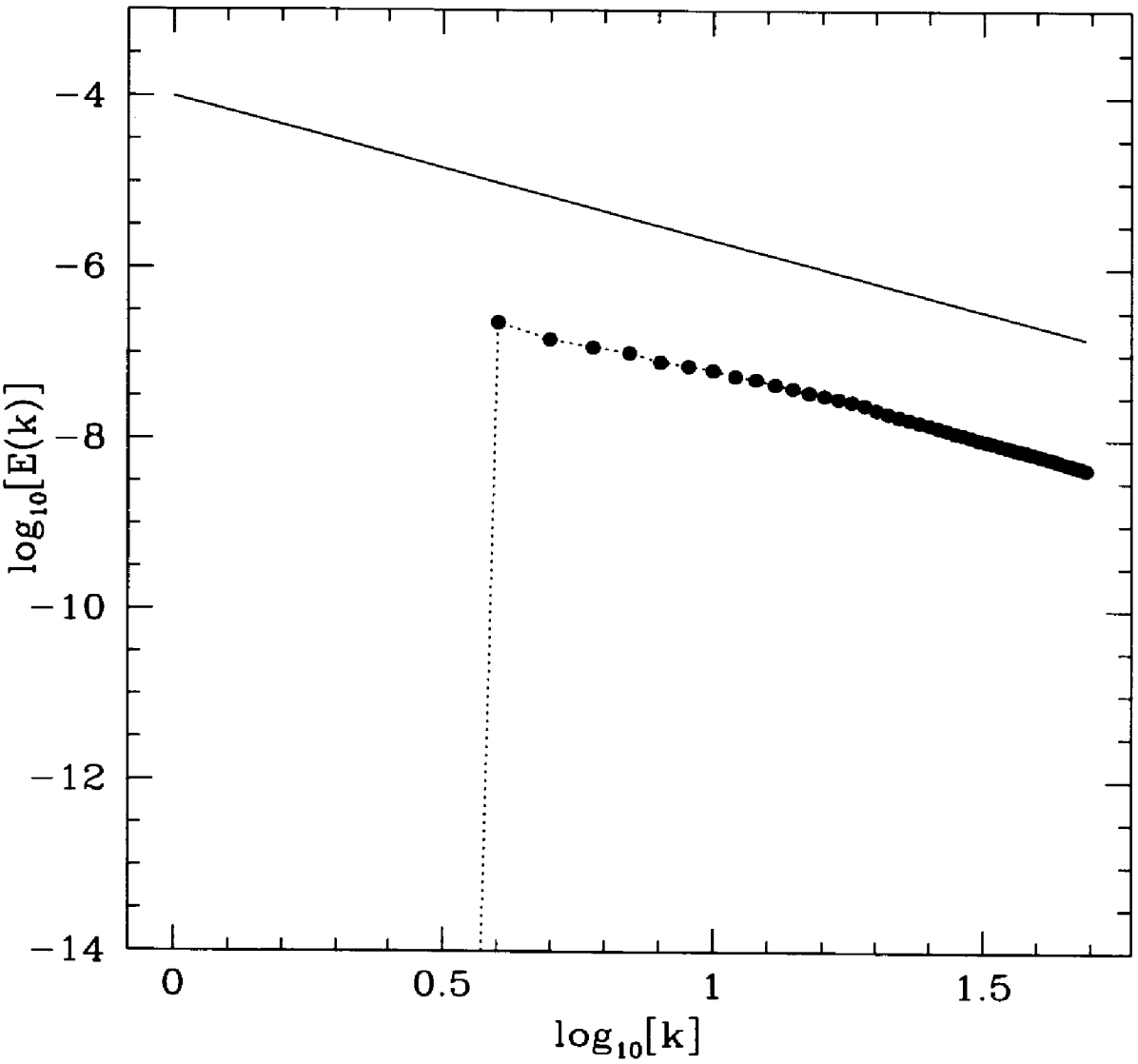


Figure 5.9: Same as Fig. 5.6 but for Case 4 LES.

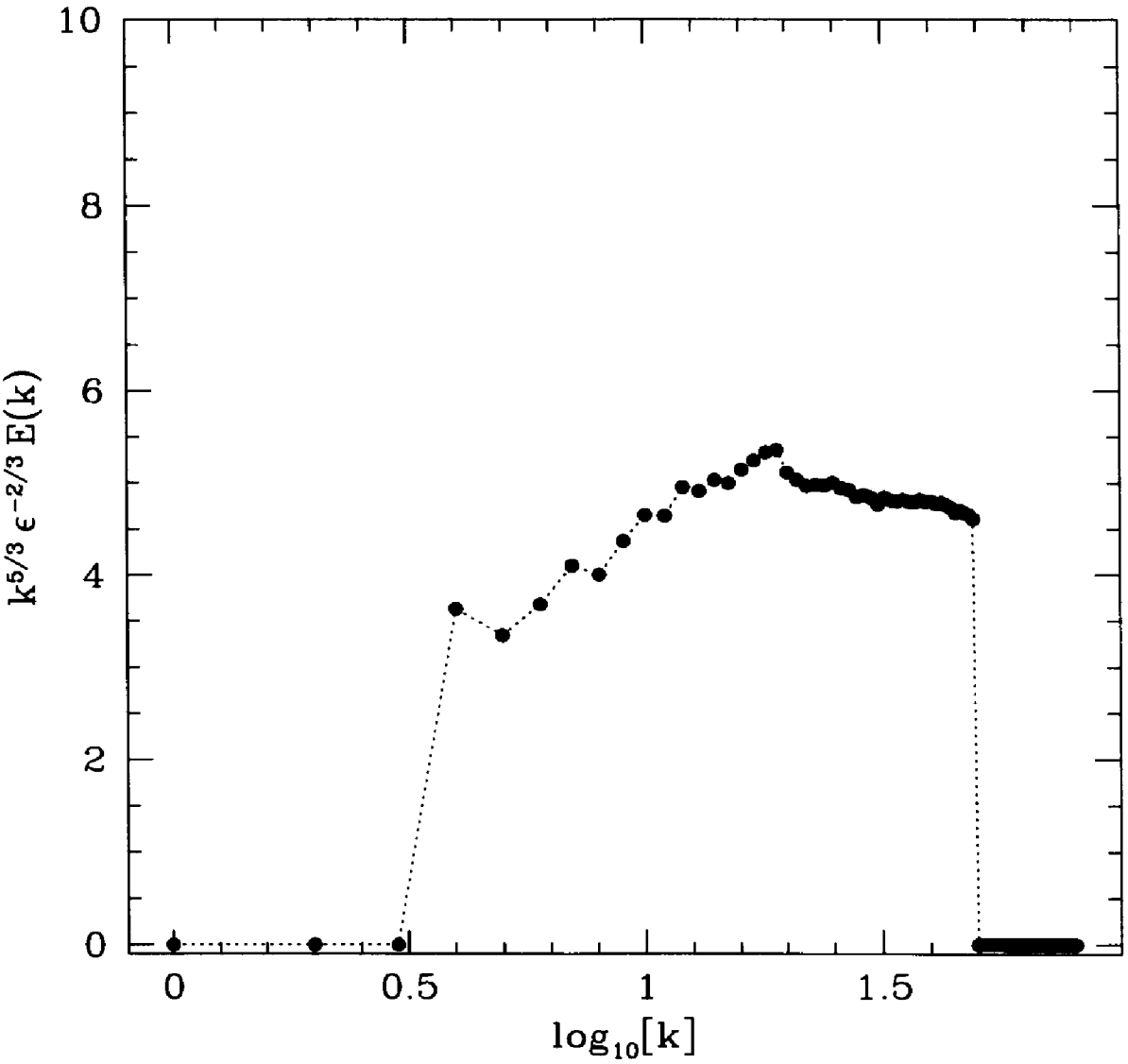


Figure 5.10: The time-averaged compensated energy spectrum $C_K$ for Case 4 LES.

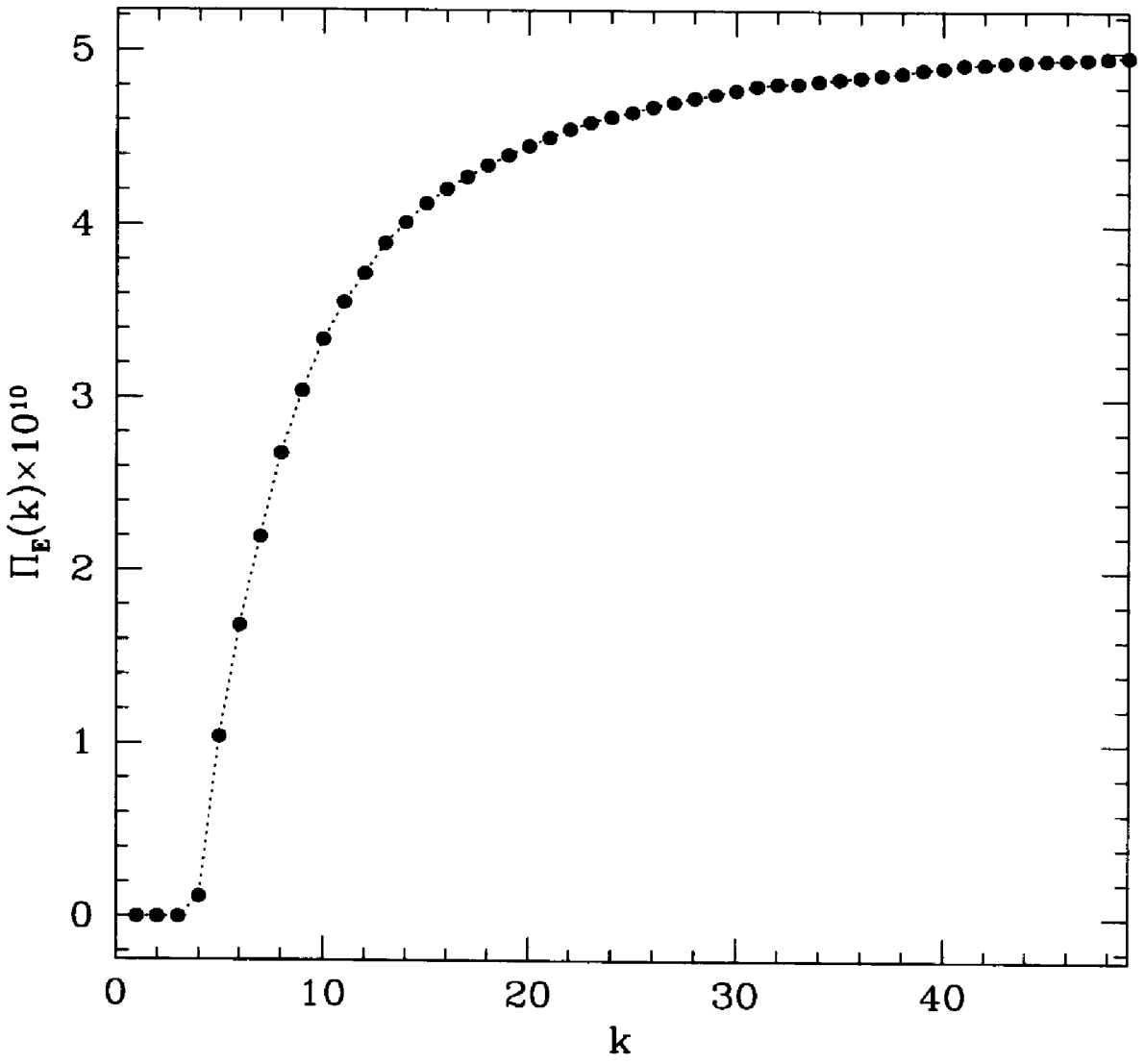


Figure 5.11: The energy flux $\Pi_E(k)$ for Case 4 LES.

Although the SGS formulation (5.11) is relatively easy to implement in spectral LES, in practical applications, particularly in the physical space, it would be far more useful to approximate $N(k/k_c)$ analytically. An additional benefit of such an approach would be a possibility to carry out further analytical studies of this SGS representation; the direction pursued in the next Section.

## 5.4 Stabilized Negative Viscosity (SNV) Formulation

For practical implementation of SGS formulation (5.11) it is convenient to approximate $N(k/k_c)$ in (5.1) by a series in powers of $k^2$. It was found that even the first two terms of this series,

$$N(k/k_c) \simeq -1 + \alpha(k/k_c)^2, \tag{5.12}$$

where $\alpha$ is a constant, are sufficient to perform successful LES of 2D turbulence. To find $\alpha$ recall that representation (5.12) must ensure zero enstrophy transfer in the energy subrange,

$$\overline{\eta}_{les} = 2\int_0^{k_c} \nu(k|k_c)E(k,t)k^4dk = 2F(\overline{\Omega})\int_0^{k_c} N(k/k_c)E(k,t)k^4dk = 0. \tag{5.13}$$

Substituting (5.12) into (5.13) and assuming that $E(k,t)$ is Kolmogorovian, one finds that $\alpha = \frac{8}{5}$ such that (5.13) becomes

$$\begin{aligned}\overline{\epsilon}_{les} = -2\,F(\overline{\Omega})\int_0^{k_c}\left[-1+\frac{8}{5}\left(\frac{k}{k_c}\right)^2\right]E(k,t)\,k^2\,dk = \\ = 2\,F(\overline{\Omega})\,\overline{\Omega}(t) - \frac{16}{5}\,F(\overline{\Omega})\,k_c^{-2}\,\overline{P}(t),\end{aligned} \tag{5.14}$$

where $\overline{P}(t) \equiv \int_0^{k_c} E(k,t)\,k^4\,dk$ is the total palinstrophy of the resolved modes. For Kolmogorovian $E(k,t)$, (5.14) can be integrated to yield $\overline{P}(t) = \frac{2}{5}\overline{\Omega}(t)k_c^2$ and

$$F(\overline{\Omega}) = \frac{25}{18}\,\frac{\overline{\epsilon}}{\overline{\Omega}(t)}. \tag{5.15}$$

Equation (5.15) completes the two-term SGS parameterization for LES of 2D turbulence in which the right hand side of (5.2) takes the form

$$\nu(k|k_c)k^2\zeta(\mathbf{k}) = \frac{25}{18}\frac{\overline{\epsilon}}{\overline{\Omega}(t)}\left[-1+\frac{8}{5}\left(\frac{k}{k_c}\right)^2\right]k^2\zeta(\mathbf{k}). \tag{5.16}$$

As in (5.11), the first term in the right hand side of (5.16) accounts for the energy flux from the unresolved modes and the inverse cascade of this energy, while the second term represents the energy dissipation near the cutoff. Using (5.16) and following the philosophy of Cases 3 and 4 LES, two more simulations were designed, with flow dependent and independent dissipation term in (5.16).

**Case 5. Two-term LES with flow dependent dissipation.** Simulations performed with the formulation (5.16) slightly adjusted to account for the finiteness of the computational domain are shown in Figs. 5.12(a,b) and 5.13. They exhibit very little difference compared to the third LES that employed the full curve $N(k/k_c)$ given by (5.1) and shown in Figs. 5.5(a,b) and 5.6. One infers therefore that (5.16) is a viable two term SGS representation for LES of 2D turbulence; obviously, (5.16) is significantly simpler than (5.11).

**Case 6. Two-term LES with flow independent dissipation.** For practical purposes, it would be most appealing to use formulation (5.16) with the dissipation term constant. A numerical experiment analogous to that of Case 4 LES was conducted with the energy source in (5.16) not changed but in the dissipation term, $\overline{\Omega}(t)$ was replaced by its value calculated for the Kolmogorov spectrum (5.4). Such an approach yields the dissipation term in (5.16) in the form

$$Ak^4\zeta(\mathbf{k}), \tag{5.17}$$

where $A$ is a constant given by

$$A = 0.511\overline{\epsilon}^{1/3}k_c^{-10/3}, \tag{5.18}$$

which corresponds to $C_K$=5.8. The results of this case 5 LES are presented in Figs. 5.14(a,b), 5.15 and 5.16; there is a very good agreement with the corresponding results

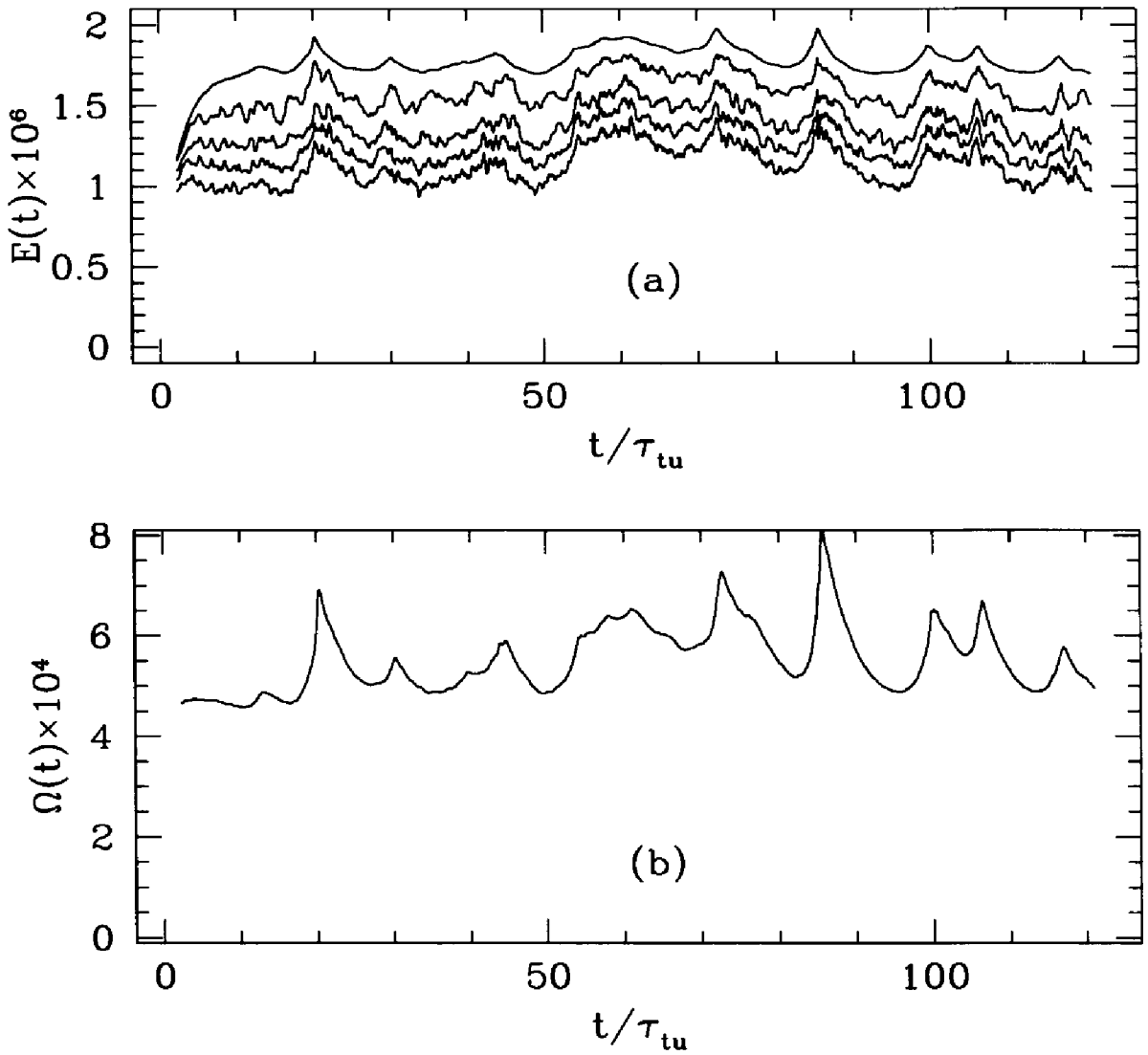


Figure 5.12: Same as Fig. 5.5 but for Case 5 LES.

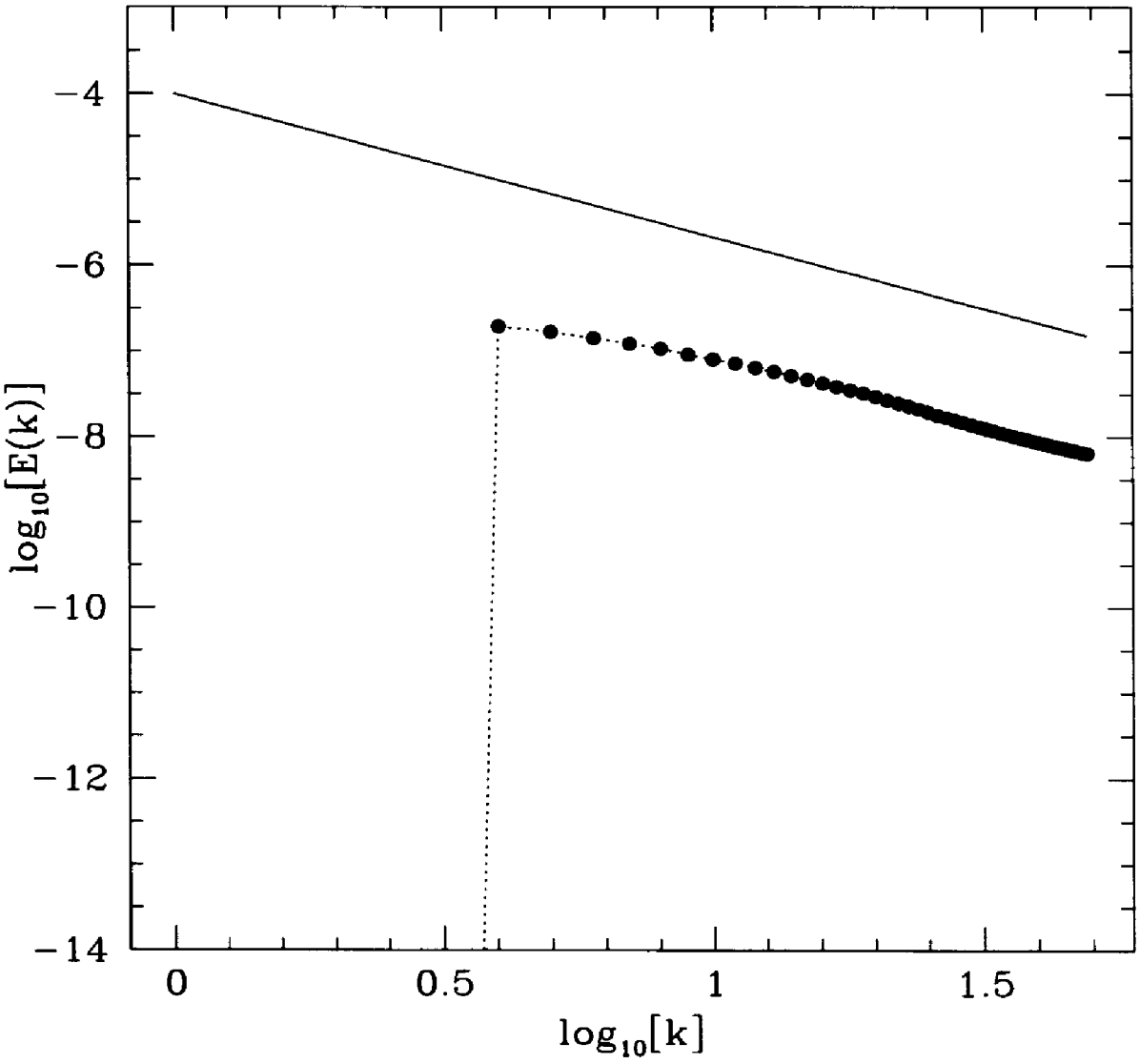


Figure 5.13: Same as Fig. 5.6 but for Case 5 LES.

obtained with the full curve $N(k/k_c)$ up to $t \simeq 40\tau_{tu}$ after which, similarly to Case 4, the solution begins to deteriorate. The compensated energy spectrum leads to the Kolmogorov constant $C_K \approx 5.8$, which is consistent with the derivation of (5.18). One can therefore infer that (5.16), (5.18) is probably the simplest SGS representation for LES of 2D turbulence possible.

Further advantages of the SGS representation (5.18) are revealed when LES of quasi-2D turbulence is sought in the physical space, where (5.16) combined with (5.18) leads to the following SGS representation

$$-\frac{\partial}{\partial x_i}\left(A_2\frac{\partial}{\partial x_i}\zeta(\mathbf{x})\right) - A_4\frac{\partial^4}{\partial x_i^2\partial x_j^2}\zeta(\mathbf{x}), \tag{5.19}$$

where

$$A_2 = \frac{25}{18}\frac{\overline{\epsilon}}{\overline{\Omega}(\mathbf{x})}, \quad A_4 = A = 0.511\,\overline{\epsilon}^{\frac{1}{3}}\left(\frac{\Delta}{2\pi}\right)^{\frac{10}{3}} = \text{const}, \tag{5.20}$$

and where $\overline{\Omega}(\mathbf{x})$ denotes the enstrophy averaged over a grid cell, and $\Delta$ is the grid resolution (note that the Laplacian term in (5.19) is written in the conservative form). Equation (5.19) thus includes two terms, the *negative* Laplacian and positive (in the sense of dissipation) biharmonic, and structurally resembles the Kuramoto–Sivashinsky equation widely known from combustion theory [69] and flows with chemical reactions [43, 42]. However, the SGS representation (5.19)-(5.21) combined with the explicit equation for the resolved scales produces far more complicated equation than the Kuramoto–Sivashinsky equation because generally its coefficients are not constant but, as in the eddy viscosity approach, are functions of the flow. There have been previous attempts to use formulation similar to (5.19)-(5.21) but with constant coefficients (dubbed the Kuramoto–Sivashinsky–Navier–Stokes equation, see [25]) to perform LES of 2D turbulence. However, they were not overly successful even in reproducing the Kolmogorov spectrum, mostly because they used constant "eddy viscosity" coefficients. Since, on the one hand, SGS representation (5.19)-(5.21) includes a negative Laplacian viscosity term and a positive, stabilizing, dissipation term, but, on the other hand, it is quite different from the Kuramoto–Sivashinsky equation in which "viscosity" coefficients are constant, it will be referred to as the

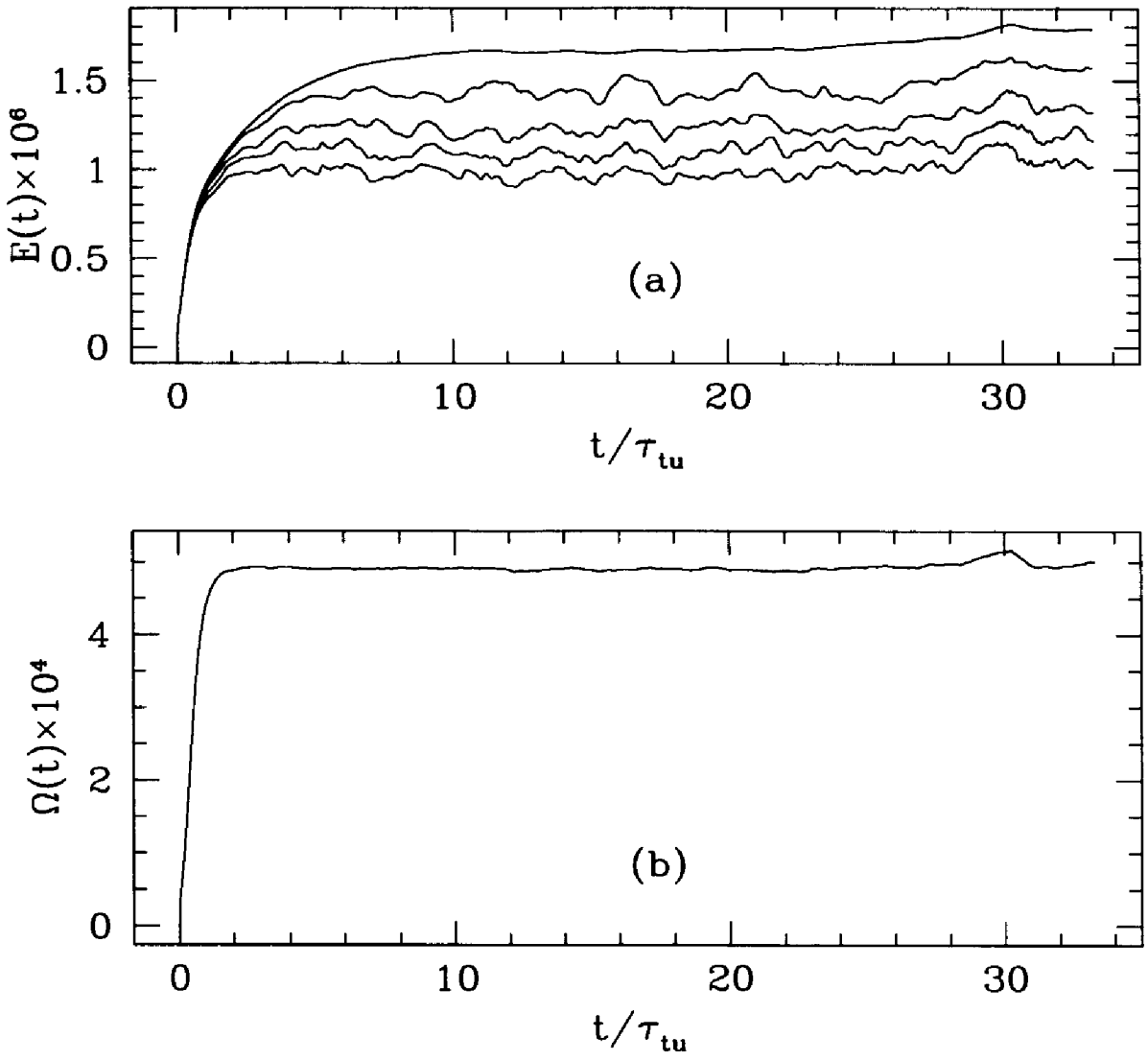


Figure 5.14: Same as Fig. 5.5 but for Case 6 LES.

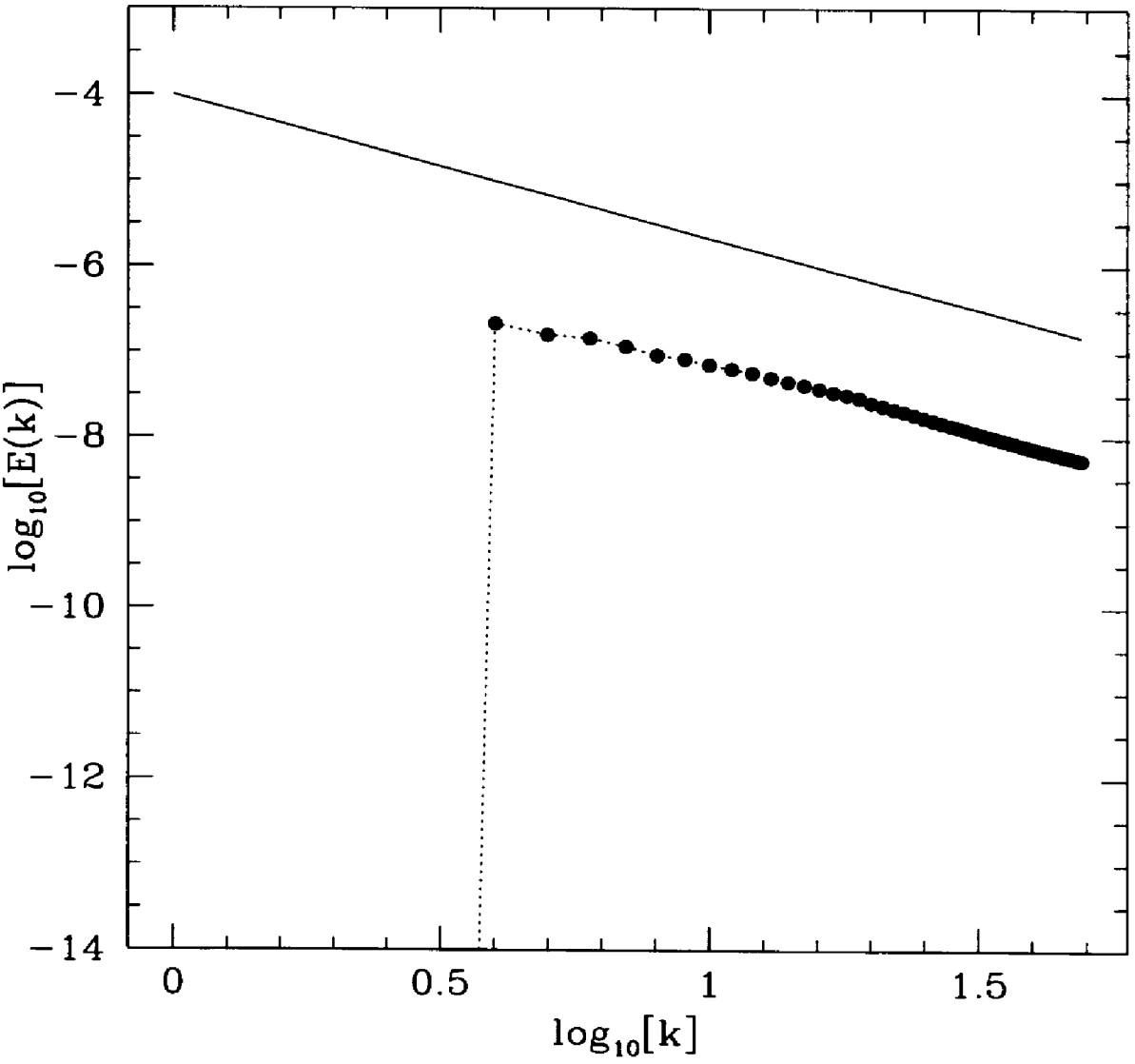


Figure 5.15: Same as Fig. 5.6 but for Case 6 LES.

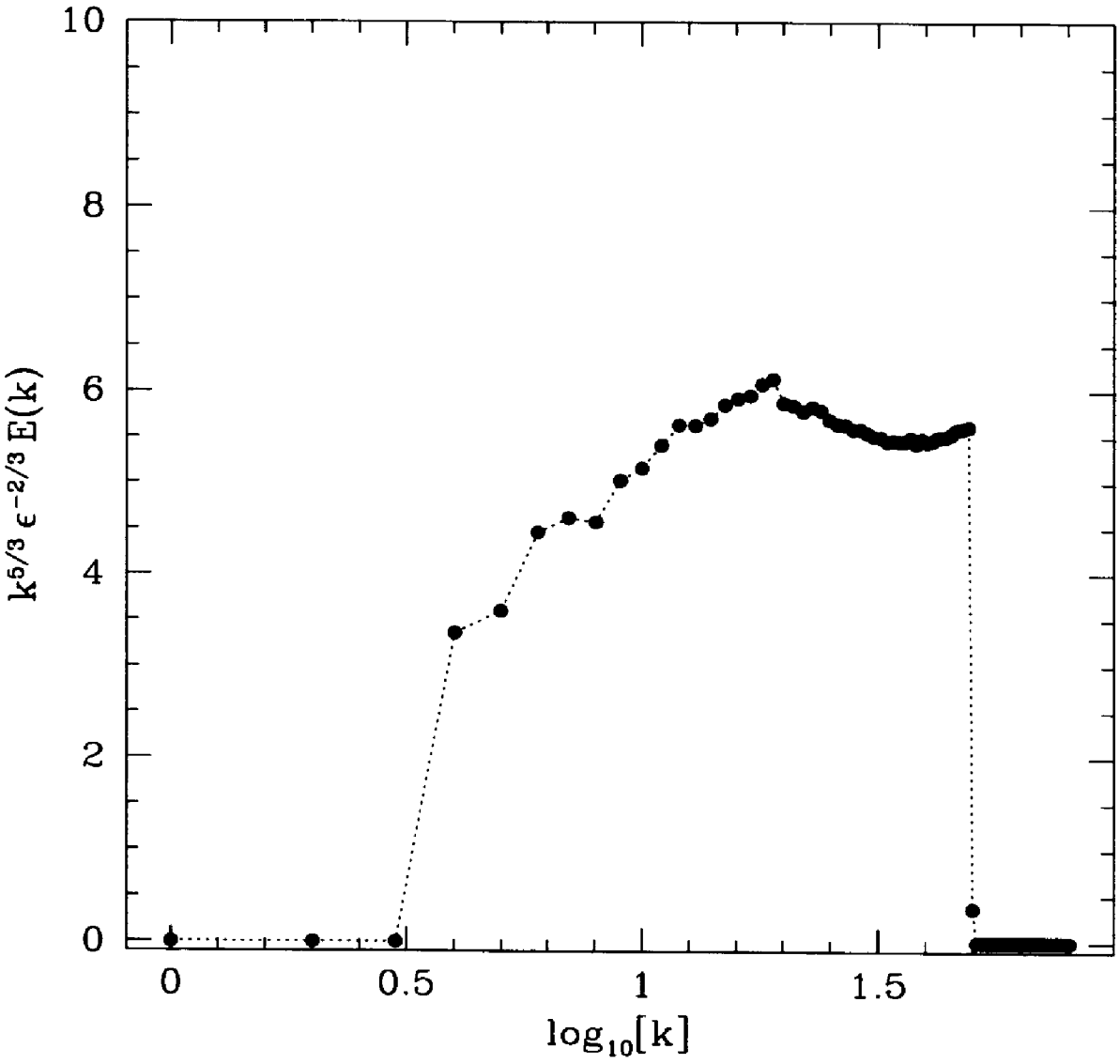


Figure 5.16: The time-averaged compensated energy spectrum $C_K$ for Case 6 LES.

Stabilized Negative Viscosity (SNV) formulation. The SNV formulation is expected to be particularly useful in simulations of atmospheric and oceanic flows where large scale motions are quasi-two-dimensional by their nature while small scale forcing is significant [53].

## 5.5 Discussion of the LES Approach

LES of homogeneous and isotropic 2D turbulence in the energy transfer subrange and appropriate SGS representation have been the central subject of this Chapter. Conservation of energy and enstrophy in 2D turbulent flows leads to coexistence of two spectral transfer processes, upscale for energy and downscale for enstrophy. Conventional eddy viscosity formulations are purely dissipative and fail to accommodate both transfers simultaneously. It was argued that proper SGS parameterization for LES of 2D flows is given by the two-parametric viscosity $\nu(k|k_c)$ introduced by Kraichnan (1976) that accounts for the energy (or enstrophy) exchange between given resolved and all SGS modes and which includes negative and positive branches; the negative branch of $\nu(k|k_c)$ represents the unresolved, small scale forcing and inverse cascade of energy, while the positive one represents the dissipation. It was shown that the negative and positive parts of the two-parametric viscosity play vital role in ensuring that all conservation and spectral transfer laws of 2D turbulence are satisfied. Then, $\nu(k|k_c)$ was used in LES of 2D turbulence in the energy transfer subrange where the negative part of $\nu(k|k_c)$ was the only energy source. The sensitivity of numerical results to the way of implementation of $\nu(k|k_c)$ in numerical schemes was studied. It was found that if $\nu(k|k_c)$ is specified as a flow independent parameter then a positive feedback is established between the forcing and the total energy of the system leading to numerical instability. Thus, another scheme was designed in which $\nu(k|k_c)$ was flow dependent but the rate of the energy input was kept constant. This LES exhibited a very stable behavior consistent with analytical theories and DNS; Kolmogorov scaling was evident and robust, and all conservation and spectral transfer laws were fulfilled. Then, a simplified SGS representation was advanced, in which only two terms were

retained: one negative and proportional to $k^2$, and one positive and proportional to $k^4$. The viscosity coefficient in the negative term served as the energy source and had to be flow dependent, to ensure that the energy input remains constant. However, since the $k^4$ term is mostly active at high wave number region near the cutoff wave number $k_c$, and its main role is energy and enstrophy dissipation at $k \rightarrow k_c$, this term did not need to be flow dependent and could essentially be kept constant and evaluated from analytical theories of 2D turbulence. Indeed, LES with constant and flow dependent $k^4$ terms gave very similar results.

The application of the two term parameterization to simulations in physical space results in the so called Stabilized Negative Viscosity (SNV) representation which includes negative Laplacian and positive biharmonic viscosities. Numerical implementation of the scheme with the constant biharmonic viscosity is obviously much simpler than that with the flow dependent viscosity.

On the one hand, the negative viscosity term is essential in SNV scheme; on the other, this scheme substantially differs from the Kuramoto-Sivashinsky equation with its constant viscosity because in SNV, the negative viscosity not only is not constant but is a nonlinear functional of the solution. In fact, the SNV representation is a peculiar case of the eddy viscosity approach; one normally expects that if all scales of a turbulent flow are resolved then eddy viscosity would become equal to the molecular viscosity which is true in 3D turbulence. In 2D turbulence, however, resolution of all scales must be accompanied by restoration of the explicit small scale forcing which would result in disappearance of both negative Laplacian and positive biharmonic viscosities and appearance of a single positive molecular viscosity.

It is believed that the SNV representation should be especially useful in quasi-2D flows in which considerable amount of energy resides on the unresolved scales. Such flows are typical in geophysical fluid dynamics where, due to the topographic and other constraints, flows are quasi-2D and where the small scale forcing is the predominant source of energy.

# Appendix A

# Details of the Asymptotic Solution of the Finite-Step Recursive Relation of Chapter 2

Here we will present the leading-order asymptotic solution of difference equation:

$$\nu_{n+1} = \nu_n \left(1 + \frac{\alpha^2}{\nu_n^4}\,\delta^{2n\epsilon}\right), \quad \text{for } \epsilon > 0. \tag{A.1}$$

First of all we concentrate on only power-law solutions, that is $\nu_n \propto \delta^{pn}$. Seeking the solution in the form: $\nu_n = \sqrt{\alpha}\,\delta^{n\epsilon/2}\,a_n$ one can find the solution for $a_n$ in the form: $a_n = a^* + f_n$ such that $f_n \to 0$ as $n \to \infty$. That leads to the following leading asymptotic behavior for $\nu_n$:

$$\nu_n \sim \sqrt{\alpha}\,\delta^{\frac{n\epsilon}{2}} \left\{\left(\delta^{\frac{\epsilon}{2}} - 1\right)^{-\frac{1}{4}} + f_0\left(4\,\delta^{-\frac{\epsilon}{2}} - 3\right)^n + \text{l.o.t}\right\}, \tag{A.2}$$

where l.o.t. denotes lower-order than the last term, $f_0$ is a constant which cannot be determined from this large $n$ formula and this expression makes sense only if $1 < \delta < (4/3)^{2/\epsilon}$ is satisfied, which is definitely true if $\epsilon \to 0$ is satisfied. For $\epsilon = 3$, for example, it gives $1 < \delta < 1.21$, which lies outside of the interval of validity of $(A.2)$: $\delta > 2$ (we remember that $\delta\nu$ vanishes if $1 < \delta < 2$). So, there is a hope to find this asymptotic behavior to be true only for those $\epsilon$ which give a nonempty

intersection of these two conditions. That puts the following restriction on $\epsilon$:

$$0 < \epsilon < \epsilon_{crit} = 2\,(2 - \log\ 3/\log\ 2) \approx 0.83. \tag{A.3}$$

Certainly after such a conclusion there arises a suspicion that asymptotic behavior $(A.3)$ may not be unique for sufficiently large $\epsilon$. In fact it is possible to show that this is not true. Really, one can rewrite $(A.2)$ in the form:

$$\nu_n = \nu_0 + \alpha^2 \sum_{j=0}^{n-1} \frac{\delta^{2j\epsilon}}{\nu_j^3}. \tag{A.4}$$

Using anzatz $\nu_n = A\,\delta^{2np\epsilon}$ for $p > 0$ one can show by exact summation of geometric progression that $p = 1/4$ is a unique exponent for all $\epsilon$. We would like to note that equation $(A.4)$ may not be true for large enough $\epsilon$ because of the infinite number of diagrams summation.

Now substituting for $\alpha = \lambda\, D\, \sqrt{F}/(2\pi\, \Lambda_d^{\epsilon})$ one can get the following asymptotic behavior for eddy-viscosity:

$$\nu(\Lambda) \propto \sqrt{\frac{\lambda_0\, D_0}{2\pi}}\, \left(\frac{F(\delta;\epsilon)}{\delta^{\frac{\epsilon}{2}} - 1}\right)^{\frac{1}{4}}\, \Lambda^{-\frac{\epsilon}{2}}. \tag{A.5}$$

Taking leading-order behavior if $\epsilon \to 0+$ of this expression gives:

$$\nu(\Lambda) \propto \frac{\sqrt{\lambda_0\, D_0}}{\left(3\sqrt{3}\pi\,\epsilon\right)^{\frac{1}{4}}}\, \Lambda^{-\frac{\epsilon}{2}}, \tag{A.6}$$

which does not depend neither on mode-elimination parameter $\delta$ nor on bare viscosity $\nu_0$. Note again the limited to small $\epsilon$ region of applicability of these results, given by formula $(A.3)$.

Now consider the advection speed difference equation at large enough values of $n$ and in the limit $\epsilon \to 0+$ when $(A.5)$ holds true. With the notation $\beta = \sqrt{\lambda_0\, D_0}\, \left(3\sqrt{3}\pi\epsilon\right)^{1/4}\, (\delta^{1-\epsilon} - 1)\, /\, \left(\pi\, \Lambda^{1-\epsilon/2}\, (1-\epsilon)\right)$, it will become:

$$c_{n+1} = c_n \left(1 + \frac{\beta\, \delta^{n\left(\frac{\epsilon}{2}-1\right)}}{c_n}\right). \tag{A.7}$$

The exact solution of this equation may be obtained:

$$c_n = c_0 + \beta\, \frac{1 - \delta^{n\left(\frac{\epsilon}{2}-1\right)}}{1 - \delta^{\left(\frac{\epsilon}{2}-1\right)}}. \tag{A.8}$$

If $\epsilon < 2$ the large-$n$ asymptotic behavior of this solution is a constant, which in the lowest order in $\epsilon$-expansion is $c_0$, that is:

$$c_n = c_0 + O\left(\epsilon^{\frac{1}{4}}\right). \tag{A.9}$$

# Appendix B

# Technical Details Relevant for Chapter 5: Derivation of Flow Parameters Based on RG Theory

Subsequent results serve as a continuation of the RG theory developed in Chapter 3, Section 3.1. Some of important formulas of the formalism reviewed in Section 3.1 will be also recalled here.

In 3.1 it was argued (see also [16, 93]) the RG procedure of small scale elimination, when iterated indefinitely, converges to a fixed point solution whereas $\zeta(k)$ is described by the Langevin equation:

$$\zeta(\mathbf{k},\omega) = G(\mathbf{k},\omega)\, f(\mathbf{k},\omega), \tag{B.1}$$

where $G(\mathbf{k},\omega) \equiv [i\omega + \nu(k)k^2]^{-1}$ is the renormalized propagator. The existence of the fixed point for RG procedure in 2D was demonstrated in Chapter 3 (for first reference, see [79]) for $\epsilon \ll 1$. Although the feasibility of continuation of these results into the region of large $\epsilon$ is still an open question, it is assumed here that the fixed point solution $(B.1)$ exists at $\epsilon = 4$.

As we have noted in Section 3.1, equation $(B.1)$ allows one to calculate the vorticity correlation function, $U(\mathbf{k},\omega) \equiv \langle \zeta(\mathbf{k},t)\zeta(-\mathbf{k},t)\rangle$, as well as the kinetic energy

spectrum,

$$E(k) = \frac{1}{4\pi} k^{-1} \int \frac{d\omega}{(2\pi)} U(k,\omega) = (3\pi^2)^{-1/3} D_0^{2/3} k^{-5/3}. \tag{B.2}$$

Although $\nu(k)$, given by (3.34) describes renormalization of the bare viscosity $\nu_0$, it is not what is often comprehended as an eddy viscosity. This is merely a response function of the nonlinear dynamical system described by the renormalized $(B.1)$. As such, it allows for calculating vorticity correlation function and energy spectrum but does not directly relate to enstrophy and energy transfer and dissipation. Furthermore, $[\nu(k)k^2]^{-1}$ can be viewed as a characteristic time scale of information loss at given $\mathbf{k}$ caused by nonlinear scrambling of all other modes [13]. Therefore, $\nu(k)$ has a meaning of an eddy damping parameter and is substantially one-point turbulence characteristic.

To analyze energy and enstrophy transfer, one needs to consider two-point characteristics that account for interaction between a given explicit mode $k < k_c$ and all modes $k > k_c$; $k_c$ is identified with the moving dissipation cutoff. For this purpose, as it was done in Chapter 3, the energy evolution equation should be derived at lowest nontrivial order of nonlinear coupling using fully renormalized propagator $G(k)$. The resulting dynamical closure is similar to the Eddy-Damped, Quasi-Normal, Markovian (EDQNM) approximation [58] where the lowest order RG analysis is invoked to obtain the eddy damping function. The energy equation then reads

$$(\partial_t + 2\nu_k)E(k,t) = \int\int_\Delta T(k,p,q,t)dpdq, \tag{B.3}$$

where

$$T(k,p,q,t) \equiv \frac{2}{\pi k}\theta_{kpq}(t)(p^2-q^2)\left[\frac{p^2-q^2}{pq}E(p)E(q)\right.$$
$$\left.-\frac{k^2-q^2}{kq}E(q)E(k)+\frac{k^2-p^2}{kp}E(p)E(k)\right]\sin\alpha, \tag{B.4}$$

and where $\nu_k \equiv \nu(k)k^2$, $\alpha$ is an angle opposite to the vector $\mathbf{k}$ in the triangle $\mathbf{k}+\mathbf{p}+\mathbf{q}=0$, and the integration domain $\Delta$ is defined by the triangular inequalities $|k-p| < q < k+p$. The function $\nu(k)$ given by (3.34) is used to compute the relaxation time $\theta_{kpq}(t) \equiv (1-e^{(\nu_k+\nu_p+\nu_q)t})/(\nu_k+\nu_p+\nu_q)$ in $(B.4)$.

In Section 3.1 we defined the two-parametric, or effective, eddy viscosity at wavenumber $k$ in terms of the energy transfer from all sub-grid scale modes with $k > k_c$ to the given explicit mode $k$,

$$\nu(k|k_c) = -T(k|k_c)/[2k^2E(k)], \tag{B.5}$$

where:

$$T(k|k_c) \equiv \int\int_{\Delta}' T(k,p,q)dpdq, \quad k < k_c, \tag{B.6}$$

and where the integration is extended over all $p$ and $k$ such that $p$ and/or $q > k_c$. Assuming that the limit $t \to \infty$ in $(B.10)$ is considered the time argument in $T(k,p,q)$ has been omitted. In that limit, $\theta_{kpq} = (\nu_k + \nu_p + \nu_q)^{-1}$.

For $k \ll k_c$ the two-parametric viscosity $\nu(k|k_c)$ can be calculated analytically [39]. In this case, the triangular inequality becomes $|p-q| \leq k \ll q$. Therefore, all the quantities that enter $T(k,p,q)$ can be expanded in powers of $p-q$. Then, the $p$ integration can be performed resulting in

$$\nu(k|k_c) = \frac{1}{4}\int_{k_c}^{\infty} \theta_{kqq}\frac{d}{dq}[qE(q)]dq, \qquad k \ll k_c. \tag{B.7}$$

Substitution of (3.34) and $(B.2)$ into $(B.7)$ gives the asymptotic eddy viscosity for the largest scales:

$$\nu(0|k_c) = -\frac{1}{3}\left(\frac{3D_o}{64\pi}\right)^{1/3} k_c^{-4/3}. \tag{B.8}$$

For arbitrary $k$, $\nu(k|k_c)$ was calculated via numerical integration of $(B.4)$; the resulting normalized two-parametric viscosity $N(k/k_c)$, see equation (5.1), was shown in Fig. 3.4. This function is negative for $k \ll k_c$ and positive for $k \to k_c$.

Noting that in the energy transfer subrange the energy injection rate $\bar{\epsilon}$ is equal to the rate of energy transfer from all the sub-grid modes $k > k_c$ to all explicit modes $k < k_c$, one can find the relation between the forcing amplitude $D_0$ and $\bar{\epsilon}$. Indeed, as follows from $(B.5)$ and $(B.6)$,

$$\bar{\epsilon} = -2\int_0^{k_c} \nu(k|k_c)E(k)k^2dk. \tag{B.9}$$

Substituting ($B$.2) and ($B$.8) into ($B$.9) and performing numerical integration one finds:

$$D_0 \simeq 63\,\bar{\epsilon}. \tag{B.10}$$

Using ($B$.10) one can now calculate the Kolmogorov constant $C_K$ in ($B$.8) and the numerical factor in ($B$.8) which leads to:

$$E(k) = C_K\,\bar{\epsilon}^{2/3}k^{-5/3}, \qquad C_K \simeq 5.12, \tag{B.11}$$

and

$$\nu(0|k_c) = -0.327\,\bar{\epsilon}^{1/3}k_c^{-4/3}. \tag{B.12}$$

These results have been used in equations (5.3) and (5.9) in Chapter 5.

# Bibliography


[1] L. Armi. Hydraulic Control of Zonal Currents on a $\beta$-Plane. *J. Fluid Mech.*, **69**:357–377, 1989.

[2] G. K. Batchelor. Computation of the Energy Spectrum in Homogeneous Two-Dimensional Turbulence. *Phys. Fluids Suppl. II*, **12**:233, 1969.

[3] G. K. Batchelor. *An Introduction to Fluid Dynamics.* Cambridge University Press, Cambridge, 1991.

[4] G. J. Boer and T. G. Shepherd. Large-Scale Two-Dimensional Turbulence in the Atmosphere. *J. Atmos. Sci.*, **40**:164, 1982.

[5] V. Borue and S. A. Orszag. Self-Similar Decay of Three-Dimensional Homogeneous Turbulence with Hyperviscosity. *Phys. Rev. E*, **51**, 1995. (in press).

[6] J. P. Boyd. Hyperviscous Shock Layers and Diffusion Zones: Monotonicity, Spectral Viscosity, and Pseudospectral Methods for Very High Order Differential Equations. *J. Sci. Comput.*, **9**:81–106, 1994.

[7] G. L. Browning and H.-O. Kreiss. Comparison of Numerical Methods for the Calculation of Two-Dimensional Turbulence. *J. Math. Comput.*, **52**:369, 1989.

[8] J. M. Burgers. *The Nonlinear Diffusion Equation. Asymptotic Solutions and Statistical Problems.* Reidel, Dordrecht, 1974.

[9] A. Chekhlov, S. A. Orszag, S. Sukoriansky, B. Galperin, and I. Staroselsky. Direct Numerical Simulation Tests of Eddy Viscosity in Two Dimensions. *Phys. Fluids*, **6**:2548–2550, 1994.

[10] A. Chekhlov, S. A. Orszag, S. Sukoriansky, B. Galperin, and I. Staroselsky. Evolution and Anisotropic Scaling Laws of $\beta$-Plane Turbulence. *Phys. Fluids*, 1995. (submitted).

[11] A. Chekhlov and V. Yakhot. Kolmogorov Turbulence in a Random-Force-Driven Burgers Equation. *Phys. Rev. E*, **51**, 1995. (in press).

[12] A. Chekhlov and V. Yakhot. Kolmogorov Turbulence in a Random-Force-Driven Burgers Equation: Anomalous Scaling and Probability Density Functions. *Phys. Rev. E*, 1995. (submitted).

[13] W. P. Dannevik, V. Yakhot, and S. A. Orszag. Analytical Theories of Turbulence and the $\epsilon$-Expansion. *Phys. Fluids*, **30**:2021–2029, 1987.

[14] J. A. Domaradzki, R. W. Metcalfe, R. S. Rogallo, and J. J. Riley. Analysis of Subgrid-Scale Eddy Viscosity with Use of Results from Direct Numerical Simulations. *Phys. Rev. Lett.*, **58**:547–550, 1987.

[15] P. G. Drazin and W. H. Reid. *Hydrodynamic Stability*. Cambridge University Press, Cambridge, 1991.

[16] D. Forster, D. Nelson, and M. J. Stephen. Large-Distance and Long-Time Properties of a Randomly Stirred Fluid. *Phys. Rev. A*, **16**:732–749, 1977.

[17] J.-D. Fournier and U. Frisch. $d$-Dimensional Turbulence. *Phys. Rev. A*, **17**:747–762, 1978.

[18] J.-D. Fournier and U. Frisch. Remarks on the Renormalization Group in Statistical Fluid dynamics. *Phys. Rev. A*, **28**:1000–1002, 1983.

[19] J.-D. Fournier, U. Frisch, and H. A. Rose. Infinite Dimensional Turbulence. *J. Phys. A: Math. Gen.*, **11**:187–198, 1978.

[20] E. Frey and U. C. Tauber. Two-Loop Renormalization-Group Analysis of the Burgers-Kardar-Parisi-Zhang Equation. *Phys. Rev. E*, **50**:1024–1045, 1994.

[21] U. Frisch and R. Morf. Intermittency in Nonlinear Dynamics and Singularities at Complex Times. *Phys. Rev. A*, **23**:2673–2705, 1981.

[22] U. Frisch, P.-L. Sulem, and M. Nelkin. A Simple Dynamical Model of Intermittent Fully Developed Turbulence. *J. Fluid Mech.*, **87**:719–736, 1978.

[23] B. Galperin and S. A. Orszag, editors. *Large Eddy Simulation of Complex Engineering and Geophysical Flows.* Cambridge University Press, New York, 1993.

[24] B. Galperin, S. Sukoriansky, A. Chekhlov, and I. Staroselsky. Subgrid-Scale Parameterization of Turbulence and Waves on the $\beta$-Plane. In *Bulletin of the APS, Series II*, volume **38**, page 2215, 1993. Annual Meeting of the APS Division of Fluid Dynamics.

[25] S. Gama, U. Frisch, and H. Scholl. The Two-Dimensional Navier-Stokes Equations with a Large-Scale Instability of the Kuramoto-Sivashinsky Type: Numerical Exploration on the Connection Machine. *J. Sci. Comput.*, **6**:425–452, 1991.

[26] S. Gama, M. Vergassola, and U. Frisch. Negative Eddy Viscosity in Isotropically Forced Two-Dimensional Flow: Linear and Nonlinear Dynamics. *J. Fluid Mech.*, **260**:95–126, 1994.

[27] M. J. Giles. Turbulence Renormalization Group Calculations Using Statistical Mechanics Methods. *Phys. Fluids*, **6**:595–604, 1994.

[28] A. V. Gruzinov. Decaying Burgers Turbulence: Exact Long-Time Asymptotics. (unpublished), 1994.

[29] G. Holloway. Eddies, Waves, Circulation, and Mixing: Statistical Geofluid Mechanics. *Ann. Rev. Fluid Mech.*, **18**:91, 1986.

[30] E. Hopf. The Partial Differential Equation $u_t + u\,u_x = \mu\,u_{xx}$. *Comm. Pure Appl. Math.*, **3**:201–230, 1950.

[31] H. Hukuda. Solitary Rossby Waves in a Two-Layer System. *Tellus*, **31**:161–169, 1979.

[32] M. Kardar, G. Parisi, and T.-C. Zhang. Dynamic Scaling of Growing Interfaces. *Phys. Rev. Lett.*, **56**:889–892, 1986.

[33] G. E. Karniadakis, M. Israely, and S. A. Orszag. High-Order Splitting Methods for the Incompressible Navier-Stokes Equations. *J. Comput. Phys.*, **97**:414–443, 1991.

[34] A. Kolmogoroff. The Local Structure of Turbulence in Incompressible Viscous Fluid for Very Large Reynolds' Numbers. *C. R. (Doklady) de l'Acad. des Sci. de l'URSS*, **30**:301–305, 1941.

[35] A. N. Kolmogoroff. Dissipation of Energy in the Locally Isotropic Turbulence. *C. R. (Doklady) de l'Acad. des Sci. de l'URSS*, **32**:16–18, 1941.

[36] R. H. Kraichnan. Inertial Ranges in Two-Dimensional Turbulence. *Phys. Fluids*, **10**:1417, 1967.

[37] R. H. Kraichnan. Lagrangian-History Statistical Theory for Burgers' Equation. *Phys. Fluids*, **11**:265–277, 1968.

[38] R. H. Kraichnan. Inertial-Range Transfer in Two- and Three-Dimensional Turbulence. *J. Fluid Mech.*, **47**:525–535, 1971.

[39] R. H. Kraichnan. Eddy Viscosity in Two and Three Dimensions. *J. Atmos. Sci.*, **33**:1521–1536, 1976.

[40] R. H. Kraichnan and D. Montgomery. Two-Dimensional Turbulence. *Rep. Prog. Phys.*, **43**:547–619, 1980.

[41] J. Krug and H. Spohn. Kinetic roughening of growing surfaces. In C. Godrich, editor, *Solids Far From Equilibrium: Growth, Morphology and Defects.* Cambridge University Press, Cambridge, England, 1992.

[42] Y. Kuramoto. *Chemical Oscillations, Waves, and Turbulence.* Springer-Verlag, 1984.

[43] Y. Kuramoto and T. Tsuzuki. Persistent Propagation of Concentration Waves in Dissipative Media Far From Thermal Equilibrium. *Progr. Theoret. Phys.*, **55**:365, 1976.

[44] B. Legras, P. Santangelo, and R. Benzi. High-Resolution Numerical Experiments for Forced Two-Dimensional Turbulence. *Europhys. Lett.*, **5**:37–42, 1988.

[45] M. Lesieur. *Turbulence in Fluids.* Kluwer, 2nd edition, 1990.

[46] S.-K. Ma. *Modern Theory of Critical Phenomena.* W. A. Benjamin, Advanced Book Program, Reading, Massachusetts, 1976.

[47] M. E. Maltrud and G. K. Vallis. Energy Spectra and Coherent Structures in Forced Two-Dimensional and $\beta$-Plane Turbulence. *J. Fluid Mech.*, **228**:321–342, 1991.

[48] M. E. Maltrud and G. K. Vallis. Energy and Enstrophy Transfer in Numerical Simulations of Two-Dimensional Turbulence. *Phys. Fluids A*, **5**:1760, 1993.

[49] W. D. McComb. *The Physics of Fluid Turbulence.* Oxford Science Pub., 1991.

[50] E. Medina, T. Hwa, M. Kardar, and Y.-C. Zhang. Burgers Equation with Correlated Noise: Renormalization-Group Analysis and Applications to Directed Polymers and Interface Growth. *Phys. Rev. A*, **39**:3053–3075, 1989.

[51] A. A. Migdal, S. A. Orszag, and V. Yakhot. Intrinsic Stirring Force in Turbulence and the $\epsilon$-Expansion. (unpublished), 1990.

[52] J. W. Miles. On Internal Solitary Waves. *Tellus*, **31**:456–462, 1979.

[53] A. S. Monin. Stratification and Circulation in the Ocean. In V. M. Kamenkovich, M. N. Koshlyakov, and A. S. Monin, editors, *Synoptic Eddies in the Ocean*, pages 1–33. D. Reidel Pub. Co., 1986.

[54] A. S. Monin and A. M. Yaglom. *Statistical Fluid Mechanics.* MIT Press, Cambridge, 1975.

[55] M. Nelkin. Do the Dissipation Fluctuations in High Reynolds Number Turbulence Define a Universal Exponent? *Phys. Fluids*, **24**:556–557, 1981.

[56] M. Nelkin. Universality and Scaling in Fully Developed Turbulence. *Adv. Phys.*, **43**:143–181, 1994.

[57] S. A. Orszag. High-Speed Computing in Fluid Dynamics. *Phys. Fluids Suppl. II*, **12**:250, 1969.

[58] S. A. Orszag. Lectures on the Statistical Theory of Turbulence. In R. Balian and J.-L. Peube, editors, *Fluid Dynamics*, pages 235–374. Gordon & Breach, 1977. Les Houches Summer School in Theoretical Physics, July 1973.

[59] R. Panda, V. Sonnad, E. Clementy, S. A. Orszag, and V. Yakhot. Turbulence in a Randomly Stirred Fluid. *Phys. Fluids A*, **1**:1045–1053, 1989.

[60] R. L. Panetta. Zonal Jets in Wide Baroclinically Unstable Regions: Persistence and Scale Selection. *J. Atmos. Sci.*, **50**:2073–2105, 1993.

[61] J. Pedlosky. *Geophysical Fluid Dynamics.* Springer-Verlag, New-York, Heidelberg, Berlin, 1979.

[62] A. Polyakov. private communication. 1995.

[63] P. B. Rhines. Waves and Turbulence on a Beta-Plane. *J. Fluid Mech.*, **69**:417–443, 1975.

[64] R. Sadourny and C. Basdevant. Parameterization of Subgrid Scale Barotropic and Baroclinic Eddies in Quasi-Geostrophic Models: Anticipated Potential Vorticity Method. *J. Atmos. Sci.*, **42**:1353, 1985.

[65] Z.-S. She, E. Aurell, and U. Frisch. The Inviscid Burgers Equation with Initial Data of Brownian Type. *Commun. Math. Phys.*, **148**:623–641, 1992.

[66] Z.-S. She, E. Jackson, and S. A. Orszag. Structure and Dynamics of Homogeneous Turbulence: Models and Simulations. *Proc. Royal Soc. London Ser. A*, **434**:101–124, 1991.

[67] Y. G. Sinai. Two Results Concerning Asymptotic Behavior of Solutions of the Burgers Equation with Force. *J. Stat. Phys.*, **64**:1–12, 1991.

[68] Y. G. Sinai. Statistics of Shocks in Solutions of Inviscid Burgers Equation. *Commun. Math. Phys.*, **148**:601–621, 1992.

[69] G. I. Sivashinsky. Nonlinear Analysis of Hydrodynamic Instability in Laminar Flames-I. Derivation of Basic Equations. *Acta Astr.*, **4**:1177, 1977.

[70] G. I. Sivashinsky and V. Yakhot. Negative Viscosity Effect in Large-Scale Flows. *Phys. Fluids*, **28**:1040–1042, 1985.

[71] J. Smagorinsky. General Circulation Experiments with the Primitive Equations. *Mont. Weather Rev.*, **91**:99–165, 1963.

[72] J. Smagorinsky. Some Historical Remarks on the Use of Nonlinear Viscosities. In B. Galperin and S. A. Orszag, editors, *Large Eddy Simulation of Complex Engineering and Geophysical Flows*, pages 3–36. Cambridge University Press, Cambridge, 1993.

[73] J. Smagorinsky, S. Manabe, and L. Holloway. Numerical Results from a Nine-Level General Circulation Model of the Atmosphere. *Mont. Weather Rev.*, **93**:727–799, 1965.

[74] L. M. Smith and V. Yakhot. Bose Condensation and Small-Scale Structure Generation in a Random Force Driven 2D Turbulence. *Phys. Rev. Lett.*, **71**:352–355, 1993.

[75] L. M. Smith and V. Yakhot. Finite Size Effects in Forced Two-Dimensional Turbulence. *J. Fluid Mech.*, **274**:115–138, 1994.

[76] J. Sommeria and R. Moreau. Why, How and When, MHD Turbulence Becomes Two-Dimensional. *J. Fluid Mech.*, **118**:507, 1982.

[77] K. R. Sreenivasan and P. Kailasnath. An Update on the Intermittency Exponent in Turbulence. *Phys. Fluids A*, **5**:512–515, 1993.

[78] I. Staroselsky and S. Sukoriansky. Renormalization Group Approach to Two-Dimensional Turbulence and the $\epsilon$-Expansion for the Vorticity Equation. In H. Branover and Y. Unger, editors, *Advances in Turbulence Studies*, volume **149**, pages 159–164. American Institute of Aeronautics and Astronautics, Inc., 1993.

[79] I. Staroselsky, S. Sukoriansky, and S. A. Orszag. The $\epsilon$-Expansion Procedure for Nearly-Equilibrium Two-Dimensional Randomly Stirred Fluids. *Phys. Rev. E*, 1995. (submitted).

[80] V. P. Starr. *Physics of Negative Viscosity Phenomena.* McGraw-Hill, 1968.

[81] S. E. Strahan and J. D. Mahlman. Evaluation of the "SKYHI" General-Circulation Model Using Aircraft $N_2O$ Measurements. 1. Polar Winter Stratospheric Meteorology and Tracer Morphology. *J. Geophys. Res.-Atmospheres*, **99**:10305–10318, 1994.

[82] S. E. Strahan and J. D. Mahlman. Evaluation of the "SKYHI" General-Circulation Model Using Aircraft $N_2O$ Measurements. 2. Tracer Variability and Diabatic Meridional Circulation. *J. Geophys. Res.-Atmospheres*, **99**:10319–10332, 1994.

[83] S. Sukoriansky, A. Chekhlov, B. Galperin, and S. A. Orszag. Large-Eddy Simulations of Two-Dimensional Isotropic Turbulence. *J. Sci. Comput.*, 1995. (submitted).

[84] T. Sun and M. Plischke. Field-Theory Renormalization Approach to the Kardar-Parisi-Zhang Equation. *Phys. Rev. E*, **49**:5046–5057, 1994.

[85] A. M. Treguier and R. L. Panetta. Multiple Zonal Jets in a Quasigeostrophic Model of the Antarctic Circumpolar Current. *J. Phys. Oceanogr.*, **24**:2263–2277, 1994.

[86] G. K. Vallis and M. E. Maltrud. Generation of Mean Flows and Jets on a $\beta$-Plane and over Topography. *J. Phys. Oceanogr.*, **23**:1346–1362, 1993.

[87] M. Vergassola. private communication. 1994.

[88] K. G. Wilson and J. Kogut. The Renormalization Group and the $\epsilon$-Expansion. *Phys. Rep. (Section C of Phys. Lett.)*, **12**:76–199, 1974.

[89] S. Wolfram. *Mathematica. A System for Doing Mathematics by Computer.* Addison-Wesley Pub. Co., Reading, Massachusetts, 2nd edition, 1992.

[90] W. Wyld. Formulation of the Theory of Turbulence in an Incompressible Fluid. *Ann. Physics*, **14**:143–165, 1961.

[91] A. Yakhot, S. A. Orszag, V. Yakhot, and M. Israeli. Renormalization Group Formulation of Large-Eddy Simulations. *J. Sci. Comput.*, **4**:139–158, 1989.

[92] V. Yakhot. private communication. 1995.

[93] V. Yakhot and S. A. Orszag. Renormalization Group Analysis of Turbulence. I. Basic Theory. *J. Sci. Comput.*, **1**:3–51, 1986.

[94] V. Yakhot and S. A. Orszag. Analysis of the $\epsilon$-Expansion in Turbulence Theory: Approximate Renormalization Group for Diffusion of a Passive Scalar in a Random Velocity Field. (unpublished), 1990.

[95] V. Yakhot and Z.-S. She. Long-Time, Large-Scale Properties of the Random-Force-Driven Burgers Equation. *Phys. Rev. Lett.*, **60**:1840–1843, 1988.

[96] V. Yakhot and G. Sivashinsky. Negative Viscosity Phenomena in Three-Dimensional Flows. *Phys. Rev. A*, **35**:815–820, 1987.

[97] Y.-C. Zhang. Directed Polymers in Hartree-Fock Approximation. *J. Stat. Phys.*, **57**:1123–1128, 1989.